Cardiovascular Magnetic Resonance Imaging

Beek, A.M.

2009

document version
Publisher's PDF, also known as Version of record

Cardiovascular Magnetic Resonance Imaging:
Applications in Patients with Myocardial Infarction and Ischemic Cardiomyopathy

Cardiovascular Magnetic Resonance Imaging: Applications in Patients with Myocardial Infarction and Ischemic Cardiomyopathy

ISBN: 9789086593958
Cover design: Anton Vos, Dedato Ontwerpers en Architecten, Amsterdam
Printed by: Ipskamp Drukkers BV, Enschede

VRIJE UNIVERSITEIT

Cardiovascular Magnetic Resonance Imaging:
Applications in Patients with Myocardial Infarction and Ischemic Cardiomyopathy

ACADEMISCH PROEFSCHRIFT

ter verkrijging van de graad Doctor aan
de Vrije Universiteit Amsterdam,
op gezag van de rector magnificus
prof. dr. L.M. Bouter,
in het openbaar te verdedigen
ten overstaan van de promotiecommissie
van de faculteit der Geneeskunde
op donderdag 5 november 2009 om 15.45 uur
in de aula van de universiteit,
De Boelelaan 1105

door
Aernout Michiel Beek
geboren te ’s-Gravenhage

promotor: prof.dr. A.C. van Rossum

Financial support by the Netherlands Heart Foundation for the publication of this thesis is gratefully acknowledged. The research described in this thesis was supported by grants of the Netherlands Heart Foundation (NHF-2001.158; NHF-2003B126).

Overige leden van de promotiecommissie:

Dr. C.P. Allaart

Prof.dr. E.F.I. Comans

Dr. F. Nijland

Dr. J. Schwitter

Prof.dr. E.E. van der Wall

Financial support for the publication of this thesis was kindly provided by: AstraZeneca BV, Biotronik Nederland BV, Bayer Schering Pharma, Daiichi Sankyo Nederland BV, Eli Lilly Nederland BV, Guerbet Nederland BV, Medis medical imaging systems BV, Pfizer BV, sanofi-aventis Nederland BV, Siemens Nederland BV.

CONTENTS

INTRODUCTION

Although progress in medical and surgical care has caused a considerable improvement in infarction-related mortality, coronary heart disease remains the principal cause of death in the western world. In the last decade, Cardiovascular Magnetic Resonance imaging (CMR) has transformed from a promising research technique into an established and valuable diagnostic tool in the daily practice of the clinical cardiologist.[1 2] Technical advances in hardware and development of new software have led to major improvements in image quality, spatial and temporal resolution, and imaging speed, allowing the detailed assessment of the whole spectrum of cardiovascular disease.[3] This thesis addresses the clinical application of CMR in patients with myocardial infarction.

Chapter 1 provides an overview of the CMR techniques used in patients with myocardial infarction, their latest developments, as well as their application in both the acute and the chronic phase of myocardial infarction. The theory of MR data acquisition and image reconstruction is beyond the scope of this thesis, and the interested reader is kindly referred to one of many available textbooks.

Chapters 2-4 focus on the use of CMR in patients with acute myocardial infarction. In Chapter 2, delayed contrast-enhanced (DCE) imaging is used to predict functional recovery of stunned myocardium. Chapter 3 compares DCE and first-pass CMR to angiographic and electrocardiographic measures of microvascular injury and their ability to predict functional outcome in reperfused myocardial infarction. In Chapter 4, non-enhanced T2-weighted imaging is used to assess the presence and impact of infarct-related haemorrhage in revascularised patients.

Chapters 5 and 6 focus on the use of DCE CMR in patients with chronic ischemic heart disease. In Chapter 5, DCE imaging is compared to the current reference imaging standard of viability, ^{18}F-fluorodeoxyglucose positron emission tomography. Chapter 6 studies the relation between DCE imaging, long term functional outcome and the time course of improvement after revascularisation.

The studies presented in Chapters 7 and 8 address the quantitative analysis of CMR images. In Chapter 7, normal values for regional wall thickness and wall thickening are provided using cine imaging and the centerline method in healthy volunteers. Chapter 8 studies the impact of DCE quantification methods on regional and global infarct extent, and on the ability of DCE CMR to predict functional outcome after revascularisation in chronic ischemic heart disease.

(References see Chapter 1)

Chapter 1

Cardiovascular Magnetic Resonance Imaging: Applications in patients with acute and chronic myocardial infarction – an overview

Aernout M. Beek

Beek AM, van Rossum AC. Cardiovascular Magnetic Resonance Imaging in Patients with Acute Myocardial Infarction (Adapted from Paragraph 1.2 and 1.3). In press, Heart 2009.

Beek AM, van Rossum AC. Cardiovascular Magnetic Resonance Imaging in Patients with Ischemic Cardiomyopathy and Chronic Myocardial Infarction (Paragraph 1.4). Provisionally accepted, Heart 2009.

1.1 GENERAL CONSIDERATIONS IN CARDIOVASCULAR MAGNETIC RESONANCE IMAGING

The MR scanner hardware is formed by a large bore magnet that creates a strong magnetic field, a radiofrequency transmitter, a radiofrequency receiver coil, and a computer to reconstruct the raw data into images. The strength of the magnet in most current MR systems is 1.5 Tesla (T), although commercial high field (3 T) scanners are becoming increasingly available. Cardiovascular Magnetic Resonance imaging (CMR) at high field strength has theoretical advantages related to the higher signal-to-noise, that can be translated into improved spatial or temporal resolution, or reduced scan time.[4] Although high field imaging of the heart is promising, it comes with considerable challenges and is currently still under development.

CMR is very safe, without harmful biological effects, and with relatively few absolute contra-indications. Patients with mechanical valves and newly implanted coronary stents can be safely scanned without specific precautions. CMR is potentially hazardous to patients with implanted (electronic) devices and all patients should be meticulously screened prior to the examination. Regularly updated lists of MR compatibility of numerous devices and other implanted structures can be found in the literature.[5 6]

To acquire the data, the user selects a software program, the pulse sequence. Signal intensity on MR images is defined by the interplay between the magnetic properties of the tissues and the characteristics of the pulse sequences. Each pulse sequence results in a typical image appearance. The selection of pulse sequence and the parameter setting is defined by the diagnostic question, and, in cardiac imaging, also by the clinical condition and the heart rate and rhythm of the patient. In all sequences, there is interdependence between spatial resolution, temporal resolution, scan duration, patient cooperation and resulting image quality. Since the majority of cardiac pulse sequences require breath-holding for optimal result, in some patients, spatial or temporal resolution has to be sacrificed to reduce scan duration to ensure images of diagnostic quality. In others, parameter setting within a pulse sequence needs adjusting because of an irregular heart rhythm or very fast or slow rates. In general, expiration breath-holding is advocated because of higher reproducibility. Because of the extra difficulties imposed by heart rate and rhythm, patient condition, the non-orthogonal, oblique imaging views, and the use of stress imaging, CMR is challenging to both physicians and technologists, and dedicated training is warranted.[7]

1.2 CMR PULSE SEQUENCES

The following paragraphs contain an overview of the CMR pulse sequences that may be used in patients with myocardial infarction. It focuses on function, the visualization of infarction and its complications, and the assessment of myocardial viability.

Cine imaging

Cine imaging forms the backbone of the cardiac examination, and is used for the qualitative and quantitative assessment of myocardial and valvular anatomy and function (table 1). When used with dobutamine stress, it can be used to detect myocardial ischemia (high dose) and viability (low dose). The typical pulse sequence used in cardiac cine imaging is a breath-hold, segmented, steady-state free precession (SSFP) sequence with retrospective ECG-gating. In comparison to the previously used gradient-echo sequence, SSFP cine imaging provides superior contrast between the high signal intensity of blood and the low-intermediate signal intensity of myocardium (figure 1). The raw data of each image frame of the cine loop are divided in parts (segments), and acquired in 8-10 successive cardiac cycles (segmented data acquisition). The degree of segmentation defines the temporal resolution of the cine loop and the number of cardiac cycles necessary to acquire all data: larger segments lower the temporal resolution but reduce the number of required cardiac cycles, and vice versa. The breath-hold duration is ultimately defined by the heart rate, and averages 8-10 seconds at 60-80 beats/minute, resulting in a high-resolution (average voxel size 1.5x1.8x5-6 mm) cine loop with temporal resolution 40-50 ms. The temporal resolution should not exceed 50 ms in order to capture the fast wall motion during systole and detect wall thickening abnormalities.

The efficiency of data acquisition can be considerably improved by using parallel imaging.[8 9] This technique has recently been introduced and is based on undersampling of the raw data and subsequent image reconstruction by using the spatial sensitivity profiles of the radiofrequency receiver coils. Dependent on coil configuration, scan efficiency may be increased up to 4 times, which may be translated into reduced scan time or improved resolution, at the small cost of a clinically non-relevant loss in signal-to-noise.[10] Even higher degrees of acceleration can be accomplished by more advanced undersampling methods that exploit the considerable amount of static, redundant information in cine imaging.[11 12] These so-called k-t methods (undersampling along *k*-space (the raw MRI data) and *t*ime) further reduce scan time (to 2-3 seconds per slice), and allow the acquisition of an entire 3D data set in one breath-hold as well as 4D (real-time 3D) scanning.[13] However, they can only be used in combination with cine imaging, and are not yet widely available.[13] Temporal resolution can also be improved by phase sharing, a technique that uses the raw

data of adjacent time frames to calculate additional frames.[14] The improved resolution can be used to reduce acquisition time or to optimize the timing of cardiac events like the isovolumetric relaxation time.

If the heart rhythm is mildly irregular (e.g. infrequent premature ventricular complexes), arrhythmia detection tools may still allow retrospective gating by discarding the extra beats according to a predefined time window. In more advanced irregularity (e.g. atrial fibrillation with continuously changing RR-intervals), prospective gating usually provides better results, and will adequately show the systolic phase but with the disadvantage that the final part of diastole is not visualized. In patients with poor breath-holding or with extremely irregular heart rhythm, real-time imaging is a good alternative. Using the SSFP sequence in combination with advanced image acceleration techniques, these now provide image quality that approaches the quality of 2D segmented sequences, with an average temporal resolution of 50-70 ms and voxel size of 2.9x3.5x8 mm.[10]

Table 1 Indications CMR cine imaging

Quantitative assessment of left and right ventricular volumes and mass
Regional left and right ventricular function
Detection of coronary artery disease using high-dose dobutamine stress
Detection of myocardial viability using low-dose dobutamine stress
Infarct-related complications (thrombus, (pseudo-)aneurysm)

Scan protocol. In a standard left ventricular study, the long axis (4-, 3-, and 2-chamber) views are acquired first. These allow a global assessment of left and right ventricular function and of the valves (except the pulmonary valve). Using the 4- and 2-chamber view for localisation, a continuous stack of (8-10) short axis slices is then planned, with acquisition generally every 10 mm, beginning at the base of the heart and covering the entire left ventricle (figure 2). This allows a more detailed assessment of regional function and the quantification of volumes and mass.

Quantitative analysis of global volumes and mass. Using dedicated software programs, endocardial and epicardial contours are semi-automatically or manually drawn on all short axis slices. Trabeculations and papillary muscles are generally excluded for the quantification of volumes and wall thickening (figure 3).[15] When papillary muscles are well defined they may be included for the calculation of left ventricular mass. End-diastolic volume, end-systolic volumes, ejection fraction and mass are then calculated using the disk-area summation method (Simpson's) and indexed to body surface area or length. With experienced technicians, total acquisition and analysis time is less than 15 minutes under normal circumstances. The same short axis data set can also be used for the quantification

of right ventricular function and mass, which is considerably more challenging because of the difficulty in identifying the right ventricular cavity during through-plane motion of the base of the heart, the prominent trabeculations and the relative lack of compact myocardium in the right ventricle.[16 17] An additional right ventricular long axis view is often required to facilitate differentiation between right atrium and the basal right ventricle. Right ventricular volumes can also be analysed on a transverse set of cines, which has higher reproducibility, but results in slightly different values and prolongs examination time because left ventricular analysis still requires a short axis set.[18] Normal values for global indices for both left and right ventricle have recently been updated.[17 19]

Quantitative analysis may be influenced by various factors such as the ECG gating method (prospective versus retrospective), the sequence type (SSFP versus older gradient-echo sequences), or the use of real-time imaging or phase sharing.[16] Although the differences in calculated volumes are generally small and clinically non-relevant, identical techniques should therefore be used in comparisons within or between subjects.

Regional analysis. Regional analysis of left ventricular function is generally done qualitatively, using the standard 17-segment model.[20] The high quality of the SSFP cine images and the reliable detection of endocardial and epicardial borders also allow the quantification of regional wall thickening by using the modified centerline method.[21 22] This method is based on the concept that systolic wall motion and thickening proceed in a multicentric fashion rather than directed at a single central point or axis in the left ventricular chamber. Systolic wall thickening is calculated as: (segmental end-systolic wall thickness – segmental end-diastolic wall thickness)/diastolic wall thickness, and expressed as a percentage of end-diastolic wall thickness or in mm's. Quantification of wall thickening is done using the short axis views. The apex is discarded and to translate the data into the 16-segment model, generally, one representative short axis slice is chosen for the basal, mid and distal position, respectively. Alternatively, data of 2-3 slices can be averaged.[23] With both methods, information is necessarily lost and, for research, other segmentation methods have been described that omit only the (1-2) most basal and most distal slices since the left ventricular outflow tract and small diameter preclude reliable quantitative analysis at these positions.

Studies providing the normal range of regional wall thickening are scarce, outdated, and used older techniques with inferior image quality and resolution. We recently analyzed the cine data of 38 healthy volunteers without cardiovascular risk factors and with normal ECG's using state-of-the-art SSFP cine CMR with retrospective gating (this thesis, chapter 7). We found a mean myocardial wall thickening of 89±29%, which results in a lower limit of normal wall thickening of 30% (defined as mean – 2SD). In line with previous reports, we found regional variation in wall thickening, demonstrating higher values in the lateral

and inferolateral segments, and lower values in the septum.[24-30] Although it is an easy and quick quantification tool, the centerline method is challenged by through-plane motion and does not take into account myocardial deformation in other than radial directions (longitudinal, circumferential, torsion).[31] Regional function is therefore ideally quantified with CMR myocardial tagging. With this technique, a saturation grid placed in one of several possible orientations allows the exact characterization of intramural deformation by the calculation of both 2D- and 3D-strain parameters.[31] The more advanced tagging techniques provide high-temporal resolution images (up to 14 ms), that can also be used to assess the fast changes in early diastole.[32 33] However, acquisition of these techniques is more elaborate, and the know-how and time required for off-line analysis largely limits its current use to research. An extensive description is therefore beyond the scope of this clinical review.

T2-weighted spin-echo imaging

The spin-echo sequence is widely used for a large diversity of indications. It provides static images with high soft tissue contrast, and, importantly, may be modified to accentuate or suppress specific tissue components such as fat, blood, or oedema. Acute coronary occlusion leads to intra- and extracellular oedema and causes a prolongation of a tissue-specific magnetic property, the T2-relaxation time.[34 35] On T2-weighted (T2W) spin-echo imaging, these regions appear bright, and T2W imaging can therefore be used to visualize acutely ischemic regions without the use of contrast agents (figure 4).[36 37] T2W imaging can also be used to visualize oedema in other (acute) myocardial disease states (table 2). Additional prepulses to suppress signal of blood and fat are usually included in T2W imaging.[38] Optimum image quality is ensured by breath-holding, segmentation of the image data over several heartbeats, and diastolic data acquisition.[38]

Table 2 Indications T2-weighted spinecho imaging

Infarct-related edema
Myocarditis
Transplant rejection

Scan protocol. T2W images should be acquired prior to contrast injection, in the standard long axis and short axis views in the same slice position as the cines to allow a side-by-side comparison.

Analysis. T2W images are generally analysed qualitatively by reporting the segmental presence of high signal intensity. The regions can be quantified after thresholding the image window setting at a predefined cut-off using the signal intensity of a remote normal region (e.g. > mean + 2SD), and expressed in absolute grams or as a percentage of total left ventricular mass.[39]

Contrast-enhanced imaging

Gadolinium chelates (Gd) are extracellular contrast agents that are administered intravenously and distribute rapidly from the intravascular space into the interstitium. Clearance from the myocardium is fast under normal circumstances, but may be considerably delayed in pathological conditions.[40 41] Gd affects the magnetic properties of surrounding protons, and special sequences can be used to differentiate between tissues with high and low Gd content. Using T1-weighted imaging, tissues with high Gd content typically appear bright.[42-44] Contrast-enhanced CMR can be used in a variety of cardiac conditions, including ischemic heart disease, non-ischemic myocardial disease and (intra-) myocardial tumors and thrombi (table 3 and 4).[40 41] Gd compounds have always been considered very safe in comparison to the potentially more harmful iodine-containing X-ray contrast agents. In recent years, however, concern has risen about their safety in patients with advanced renal failure because of a possible association with the development of nephrogenic systemic fibrosis. Despite the rarity of this disorder, preventive measures are now advocated in patients with glomerular filtration rate < 30 ml/min/1.73 m^2.[45 46]

Table 3 Indications first-pass myocardial perfusion CMR

Detection of coronary artery disease using adenosine stress
Microvascular obstruction (no-reflow)

Three techniques are used in combination with contrast. MR angiography is an important tool in the diagnosis and follow-up of vascular disease and congenital heart disease, but it has no specific value in the evaluation of the patient with myocardial infarction.[47] First pass myocardial perfusion imaging and delayed contrast-enhanced imaging will be discussed in the following paragraphs.

Table 4 Indications delayed contrast-enhaced CMR

a. Ischemic heart disease
Visualization of acute and chronic myocardial infarction
Quantification of regional and global infarct extent
Microvascular obstruction (no-reflow)
Myocardial viability
Detection of underlying coronary artery disease in patients with congestive heart failure
Differentiation between ischemic and non-ischemic cardiac disease
Intracavitary thrombus
b. Non-ischemic heart disease
Myocarditis
Hypertrophic cardiomyopathy
Dilated cardiomyopathy
Arrhythmogenic right ventricular cardiomyopathy
Cardiac sarcoidosis
Cardiac amyloidosis
Other secondary cardiomyopathies (e.g. Gaucher, Fabry, hypereosinophilic syndrome)
Intracardiac tumor
Pulmonary hypertension

First pass myocardial perfusion imaging

First pass (FP) myocardial perfusion imaging can be used to monitor the changes in myocardial signal intensity resulting from the (first) passage of a Gd-based contrast agent. The signal intensity is directly related to the concentration of the contrast agent, which in turn corresponds to regional myocardial perfusion.[48] FP imaging can be used to detect stress-induced myocardial ischemia in patients with suspected coronary artery disease and to visualize areas of microvascular obstruction in patients with acute myocardial infarction (table 3).[49 50]

Several sequence types can be used, and these are often combined with advanced acceleration techniques to improve scan efficiency.[51-53] Accurate monitoring of the changes in signal intensity is ensured by a single shot mode, which allows the acquisition of one entire image per heartbeat at every slice position. The acquisition time of one image is approximately 150 (50-200) ms, so that 3-4 slices can be acquired per heartbeat with heart rates ≤100/minute. The spatial resolution of FP (2-3 mm in-plane) compares favorably to nuclear techniques and allows transmural evaluation of myocardial perfusion.[48] Contrast dose for optimal myocardial enhancement is 0.1 mmol/kg, injected at 3-7 ml/sec, and

followed by a 15 ml saline flush.[48 54] Because of non-linearity of the relation between contrast dose and signal intensity at higher doses, lower contrast doses (0.025-0.05 mmol/kg) are generally used when (semi-)quantitative analysis of myocardial perfusion is performed. Imaging is started within 5 seconds after contrast injection, and is continued for 50 heart beats while the patient is asked to hold his breath for as long as possible, and if necessary take shallow breaths towards the end. This ensures the acquisition of pre-contrast baseline images and the full visualization of contrast passage through the left ventricular myocardium.

Scan protocol. To evaluate regional stress-induced myocardial perfusion defects, images are acquired during continuous adenosine infusion. Adenosine is a vasodilator with very short half-life (< 10 seconds) that is also used in nuclear perfusion imaging. FP imaging is started after 3 minutes of continuous adenosine infusion, with 3 slices acquired every heart beat, in basal, mid and apical short axis position (figure 5). The slices are positioned on end-systolic long axis views to facilitate exclusion of the left ventricular outflow tract. After 10-15 minutes (dependent on contrast dose), a rest series may be acquired to evaluate reversibility of the defects, although this can also be assessed with delayed contrast-enhanced imaging (see below).

For the assessment of microvascular obstruction in patients with recent myocardial infarction, only rest FP images are acquired, and one slice positioned at the infarct core is preferably added. Alternatively, since temporal resolution is less crucial for this indication, spatial coverage may be doubled by acquiring 6-8 slices over 2 heart beats, with slice positions matching the short axis cines.

Analysis. FP images are usually analysed qualitatively by assessing the enhancement pattern using a 16-segment model, discarding the apex that is not visible on the short axis views (figure 6). Quantitative FP analysis of perfusion-related parameters and absolute perfusion is feasible, but requires modifications of contrast dose and acquisition scheme, and complex off-line analysis of the signal-intensity-versus-time curve.[55 56]

Abbreviations and terms used for delayed contrast-enhanced CMR

DCE CMR	delayed contrast-enhanced CMR
CE CMR	contrast enhanced CMR
DE (CMR)	delayed enhancement (CMR)
LE (CMR)	late enhancement (CMR)
LGE (CMR)	late gadolinium enhancement (CMR)

Delayed contrast-enhanced imaging

Delayed contrast-enhanced imaging (DCE; see list for other abbreviations and terms used in the literature) is used for the detailed visualization of regional myocardial disease (table 4). Under normal circumstances, the extracellular agent Gd does not enter the myocardial cell and is rapidly cleared from the myocardium. Both in acute and chronic myocardial infarction, Gd distribution volume is increased and myocardial clearance is delayed.[57-62] In acute myocardial infarction, the expansion of the extracellular space is caused by myocardial cell lysis.[57 58] It has been suggested that oedema in the peri-infarct region also increases Gd distribution volume, which could cause an overestimation of the actual infarct area during contrast-enhanced imaging.[63] However, ischemia related tissue oedema leads to simultaneous expansion of both the intracellular and the extracellular compartment, which does not affect the Gd-mediated change in magnetic tissue properties required for signal enhancement.[64] In the chronic phase of infarction, Gd distribution volume is increased by regional collagenous scar that has replaced the normal myocardial cells.[59] Other, non-ischemic, acute or chronic, congenital or acquired myocardial diseases may also affect regional Gd distribution volume and lead to contrast enhancement (table 4).

Although CMR is capable of detecting ischemic myocardium without the use of contrast agents by using T2W imaging, visualization is considerably improved after Gd.[65 66] The high Gd-concentration in infarcted regions was first evaluated with non-breath-hold spin-echo sequences.[65 67] However, because of long acquisition times, image quality was suboptimal and chronic infarcts could not be reliably detected.[68-70] A new sequence was introduced at the end of the last century which marked a turning point in contrast-enhanced CMR imaging.[59] A series of experimental studies using in- and ex-vivo scanning provided the definitive evidence that DCE imaging was extremely accurate in detecting irreversible ischemic damage in any stage of the disease and irrespective of patency of the infarct related artery.[59 62 71] DCE imaging is now considered the non-invasive reference imaging technique for the depiction of both acute and chronic myocardial infarction.

Contrary to first pass imaging, DCE is postponed until Gd has reached a steady state, with image acquisition typically 5-30 minutes after injection of 0.1-0.2 mmol/kg Gd. Higher contrast doses (0.2 mmol/kg) provide better contrast-to-noise but the higher blood Gd concentration at the time of imaging may interfere with the detection of subendocardial infarcts, which can be solved by prolonging the minimum time between contrast injection and data acquisition to 10 minutes. DCE uses a breath-hold segmented gradient-echo pulse sequence that is designed to effectively suppress the signal of non-infarcted myocardium with low Gd concentration by the use of an inversion recovery prepulse.[72] The acquisition window is placed in diastole to avoid artefacts due to systolic motion. Ultimately, one high-quality image is generated, with high contrast between the suppressed signal in non-

infarcted myocardium and the hyperenhanced infarcted regions (figure 7).[72] Average in-plane spatial resolution is 1.5x1.7 mm allowing the transmural evaluation of infarction, and a maximum slice thickness of 5-6 mm helps to avoid partial volume effects in the apical slices. DCE is typically designed to visualize regional disease, and may have difficulty in the detection of diffuse, global heart disease. However, some regional variation is often seen, allowing the detection of typical enhancement patterns even in conditions with a more diffuse cardiac involvement.[41]

DCE imaging is robust and highly reproducible.[73 74] The region of hyperenhancement does not change between 5 and 30 minutes after contrast injection as long as timing of the inversion recovery prepulse (inversion time) is properly adjusted.[75] The inversion time is influenced by a number of factors such as heart rate, contrast dose and time after contrast injection, and with incorrect setting, suppression of the signal of non-injured myocardium may be insufficient. Inversion time after 10 minutes is generally around 250 msec, but, with ongoing contrast wash-out from non-injured myocardium, it increases to 300-350 msec after 20-30 minutes. Most vendors provide inversion time-scouts to estimate the inversion time although fine-tuning is often required.[76] An alternative reconstruction mode (phase-sensitive reconstruction) of the inversion recovery data does not require the delicate setting of inversion time, and provides a more consistent contrast between infarcted and non-infarcted regions which does not depend on the inversion time.[77]

New sequences are becoming available as alternatives to the standard segmented inversion recovery technique. With single shot inversion recovery SSFP imaging, one entire image is acquired every heartbeat. Single shot SSFP DCE imaging can even be used without ECG-gating and breath-holding, albeit at the price of reduced sensitivity and contrast-to-noise.[78] 3D sequences are also available, with comparable results as the standard 2D sequence, although with longer breath-hold duration.[79] A recently introduced 3D-sequence with respiratory navigator-gating offered shorter acquisition times with higher signal-to-noise and contrast-to-noise and may become the ideal technique in patients not capable of reproducible breath-holding.[80] Both the single shot and the 3D-sequence require adjustments of the inversion time for optimal signal suppression of remote myocardium.

Scan protocol. Both long and short axis views are acquired in the same slice positions as the cines. The imaging protocol should be tailored to the condition of the patient and the required clinical information. A detailed exploration of viability is best done with the high resolution, segmented sequence. In patients with very irregular heart rates or suboptimal breath-holding, or as a quick survey, single shot SSFP DCE imaging is a good and fast alternative.

Analysis. DCE images are assessed side-by-side with the cines. In the clinical setting, analysis is mostly done qualitatively, by reporting the visually estimated segmental extent

of hyperenhancement (<25%: no/minimal/subendocardial, 25-75% moderate, >75%: transmural) in the 17-segment model.

Using dedicated software, both global and segmental extent of hyperenhancement can be quantified. Endocardial and epicardial contours are drawn manually on all short axis views. After thresholding the window setting of the images, total infarct size and segmental extent are automatically calculated, and expressed in grams or as a percentage of total left ventricular mass or segmental area (figure 8). In viability studies, segmental extent of hyperenhancement is typically expressed on a 5-point scale: 1 – no hyperenhancement, 2 – 1-25%, 3 – 26-50%, 4 – 51-75% and 5 – 76-100% hyperenhancement.[81]

The size of the hyperenhanced regions is influenced by the image window setting (centre and width) that is critically dependent on the observer's personal preference. Although most studies have used a non-standardized, visual threshold setting, standardization of analysis is warranted to increase reproducibility and allow reliable follow-up studies and comparison between different centres. Simple standardization methods use either the (low) signal of a non-enhanced, remote region or the (high) signal of the infarcted region. Commonly, hyperenhancement is defined as a number of standard deviations above the signal of a normal, remote region. Because of the large difference in signal intensity between the hyperenhanced infarcted region and the (purposely) suppressed signal of remote myocardium (almost 500%, or 6 SD), defining hyperenhancement with the generally accepted cut-off of >2 SD above remote was found to grossly overestimate infarct size in comparison to visual thresholding.[72 81 82] The full-width-at-half-maximum method (FWHM) uses the (50% of the maximum) signal within the hyperenhanced region to define hyperenhancement. In an animal model, FWHM better correlated to histological infarct size than 1-6 SD above remote.[83]

We recently evaluated quantification of DCE in relation to functional outcome after revascularization, which is the clinical standard of viability (this thesis, chapter 8).[84] Thirty-eight patients with chronic ischemic myocardial dysfunction were scanned at baseline and 6 months after revascularization, and hyperenhancement was quantified by thresholding window setting at 2-6 SD above mean signal intensity of a remote normal region, and according to the FWHM method. Quantification methods had a strong influence on segmental extent of hyperenhancement and total infarct size, and multilevel analysis showed that thresholding contrast images at 6 SD best predicted segmental functional outcome after revascularization, but the difference with other methods was small and non-significant. The lack of a detectable difference between these quantification methods may be explained by the fact that, regardless of the method, the inverse relation between outcome and degree of hyperenhancement was always present. One might speculate that, although standardization is required for follow-up studies, it may not have major impact on

overall predictive value of the techniques. More complex quantification methods have been described, but clinical experience is still limited.[85 86] Further study is needed to define the optimal standardization method and its clinical relevance.

1.3 CMR IN PATIENTS WITH ACUTE MYOCARDIAL INFARCTION

The following paragraph will address the clinical application of CMR in patients with acute myocardial infarction (AMI). A basic protocol in patients after acute myocardial infarction includes cine imaging and delayed contrast-enhanced imaging. It allows the evaluation of ventricular and valvular function, infarct extent and microvascular obstruction, and can be acquired easily within 30 minutes. The protocol may be extended by T2-weighted spin-echo imaging and first pass imaging for a complete characterization of the ischemic region by visualizing infarct related oedema, intramyocardial haemorrhage and (rest) myocardial perfusion. The detection of coronary artery disease using high-dose dobutamine stress cine CMR or adenosine stress first pass myocardial perfusion imaging is beyond the scope of this overview. CMR scanning after AMI is optimally scheduled between 2 and 9 days after admission. CMR is a safe technique, even in the first days after percutaneous angioplasty and stent implantation.[87 88] An artefact related to the stent may be noted but generally does not interfere with image analysis.

Function

Global ventricular function. Left ventricular ejection fraction and end-systolic volume are strong predictors of prognosis after AMI.[89] Cine CMR is the gold standard for the quantification of global left and right ventricular volumes, ejection fraction and mass. The high reproducibility of cine CMR ensures the reliable detection of any significant change at follow-up, which makes it the ideal and most cost-effective technique for serial evaluation in clinical trials.[90-92] In successfully reperfused AMI, recovery of stunned myocardium often leads to functional improvement after discharge. Contrary, patients who received late or no reperfusion therapy are at risk of remodeling. Of interest, the cut-off that is generally used to define significant remodeling (an increase in end-diastolic volume ≥20%) is derived from left ventricular invasive contrast angiography, which might not be appropriate when using cine CMR.[93] Current guidelines state that an implantable cardioverter-defibrillator device (ICD) is indicated when ejection fraction is <30% (<35% in patients in New York Heart Association class II-III) 40 days after the acute event.[94 95] The selection of patients for this expensive therapy requires a technique that provides this information with the highest reproducibility and accuracy possible. In our institution, cine CMR is therefore routinely performed in every ICD candidate.

Regional function. Although the assessment of regional function does not play a major role in risk stratification and prognosis, it may provide the first indication of ischemic heart disease by showing subtle wall motion abnormalities in the territory of a coronary artery when global volumes and function are still well within normal limits. Right ventricular infarction may complicate inferior infarction and may be detected as regional dysfunction of the diaphragmatic right ventricular wall on the basal short axis cines. However, global function is usually not severely affected, and delayed contrast-enhanced imaging may be more sensitive.[96]

Infarct-related complications

The large field of view of cine CMR allows the accurate assessment of infarct-related complications, such as (pseudo-) aneurysms and pericardial effusion. Mitral regurgitation can be detected with cine CMR, and its mechanism can be further evaluated using contrast-enhanced imaging by showing the infarcted area or papillary muscle involvement. Left ventricular thrombi may develop early after infarction and can be seen as low-intermediate intensity intracavitary structures that may be difficult to differentiate from myocardium on cine images. Thrombi are avascular structures that do not take up contrast and delayed contrast-enhanced imaging was shown to be the most sensitive technique for their detection (figure 9).[97 98] The visualization of thrombi may be optimized by using a longer inversion time or an inversion time scout to allow differentiation from non-enhancing myocardial regions.

Infarct-related oedema

The morphological characterization of acute infarctions by unenhanced T2-weighted (T2W) imaging allows further insight in the pathophysiology of acute coronary syndromes. The reduced cardiomyocyte adenosine triphosphate (ATP) formation that immediately follows acute coronary occlusion inhibits Na^+/K^+-ATPase, and the resulting increased Na^+-and Cl^--concentration leads to intracellular oedema.[34] Inflammation and changes in endothelial permeability further increase myocardial water content. T2W imaging allows the visualization of infarct-related oedema without the use of contrast agents, and regions of high signal intensity have been demonstrated as early as 24 hours after infarction.[36 37 99]

Oedema is typically related to the acute phase and generally disappears between 3 and 12 weeks after the event and T2W imaging may therefore be used to differentiate new and old ischemic disease.[88 100 101] Adding T2W imaging to a protocol that already included cine imaging, rest first pass perfusion and DE improved the diagnostic accuracy of CMR in

patients with suspected acute coronary syndrome by allowing a better distinction between new and old ischemic disease.[100] T2W imaging can also be used to detect procedure-related myocardial injury after percutaneous or surgical revascularization in patients with old myocardial infarction. However, at a very early stage (within hours of the event), DE has been shown to be more sensitive than T2W imaging.[99]

Regional increased myocardial water content and high T2W signal intensity is not restricted to acute coronary syndromes but can also be found in other (acute) myocardial disease states, like myocarditis, transplant rejection or Tako Tsubo cardiomyopathy.[102 103] The fact that myocardial oedema is one of the earliest manifestations of ischemia and occurs prior to the development of definitive, irreversible damage has led to the use of T2W imaging to visualize the ischemic area at risk.[104] Both experimental and human research has shown that the ischemic region on T2W imaging is consistently larger than the infarcted region at DCE imaging (figure 10).[105 106] In a canine occlusion-reperfusion model, the area at risk as measured by microspheres showed good correlation with the T2W hyperintense region.[107] The possibility of visualizing both the area at risk and the final infarct size in a single (CMR) examination would allow the definition of the amount of salvaged myocardium in patients with reperfused infarction. This would be the ideal end point in studies evaluating new therapeutic strategies to reduce infarct size.[108] However, further evidence for the relation between area at risk and T2W imaging is needed, and it should be noted that the current T2W imaging technique is not robust and prone to artefacts that may interfere with diagnostic accuracy.[109] In our experience, up to 10-20% of T2W images may be of non-diagnostic quality, although new developments may improve its performance.[110 111] In addition, intramyocardial haemorrhage may attenuate the high T2W signal seen in acute infarction (see below). Therefore, the exact role of T2W imaging in the assessment of a patient with recent (acute) myocardial infarction remains to be established.

Infarct visualization

Delayed contrast-enhanced (DCE) imaging is the most sensitive technique for the detection and visualization of myocardial infarction (figure 11). Regional myocardial injury has been demonstrated as early as 1 hour after septal ablation in patients with hypertrophic cardiomyopathy, whereas T2W imaging showed regional high signal intensity only after 24 hours.[99] DCE can visualize micro-infarcts related to revascularization procedures and detects small subendocardial infarcts that are missed by single photon emission computed tomography (figure 11).[112 113] Right ventricular involvement in inferior infarction is demonstrated with higher accuracy than ECG or echocardiography (figure 12).[96]

DCE total infarct size and infarct transmurality are related to time-to-treatment, Thrombolysis-In-Myocardial-Infarction (TIMI)-flow, ST-segment resolution and enzymatic

infarct size after percutaneous coronary intervention in ST-elevation myocardial infarction.[114-116]

In line with the wave front theory, regional extent and transmurality of hyperenhancement may indicate the pathophysiological mechanism of the infarction. Proximal occlusion of a coronary artery followed by timely recanalisation will lead to subendocardial hyperenhancement in a relatively large area corresponding to the coronary artery distribution (figure 11b), whereas permanent occlusion of a smaller or distal side branch that is not accessible to percutaneous revascularization will cause a smaller, circumscript but more transmural infarction (figure 11c).

The location and transmural extent may also be used to differentiate acute coronary syndromes from myocarditis, which can closely mimic infarction in clinical presentation, enzyme release and ECG.[117 118] In its typical form, myocarditis shows subepicardial hyperenhancement in the lateral wall or midwall involvement of the septum, contrary to the subendocardial or transmural patterns seen in ischemic heart disease (figure 13).[119-121] In addition, DE may provide prognostic information and may be used to guide myocardial biopsy.[120 121] Tako Tsubo or stress-related cardiomyopathy mimics acute antero-apical infarction, and may show regional high T2W signal intensity related to oedema, but, as a rule, does not show hyperenhancement despite extensive functional impairment.[122]

Prognosis after acute myocardial infarction is closely related to infarct size. Early after acute infarction, functional parameters may overestimate the actual infarct size because of myocardial stunning. The incremental prognostic value of DCE was recently demonstrated in a study that evaluated 122 patients with ST-elevation myocardial infarction.[123] Although left ventricular volumes, ejection fraction and total infarct size were all associated with outcome, total infarct size was the only predictor at multivariate analysis.

Viability

Myocardial stunning refers to the prolonged post-ischemic contractile impairment that can be seen in acute ischemic syndromes after restoration of flow.[124] The likelihood of functional recovery of stunned myocardium depends on the degree of irreversible damage, and several studies have shown that it is predicted by the segmental extent of hyperenhancement (SEH).[115 125 126] We evaluated 30 patients after acute myocardial infarction and found a strong inverse relation between the likelihood of improvement and segmental infarct extent: dysfunctional segments without hyperenhancement were 3, 14 and 20 more likely to improve than segments with 1-25%, 26-50%, 51-75% and 76-100% segmental extent of hyperenhancement, respectively (figure 14)(this thesis, chapter 2).[125] In this study we used multilevel analysis, which is the statistical method of choice when assessing segmental functional changes, since it accounts for the fact that myocardial

segments cannot be regarded as independent units but, instead, are related at several levels (within patients and within slices).[127] Using the transmural infarct extent to predict functional outcome also acknowledges the fact that viability is a gradual rather than a binary phenomenon. Although the use of a single cut-off to separate viable from non-viable facilitates the traditional description of diagnostic accuracy (sensitivity, specificity), it underestimates the full potential of DCE imaging.

Low-dose dobutamine stress (LDDS) echocardiography has been used extensively for risk assessment and prediction of functional outcome after acute myocardial infarction.[128-130] Most authors found a positive relation between the presence of viability and a favourable outcome, although reports were not unanimous and the major part of the studies stems from the thrombolytic era. Several studies have shown that LDDS cine CMR is feasible and produces comparable results.[131-133] There are no studies comparing LDDS and DCE after acute infarction. However, DE imaging is simpler since it requires no stress and is therefore the preferred technique in our institution.

Microvascular obstruction

No-reflow refers to the lack of adequate restoration of flow despite successful revascularization of the occluded infarct related epicardial coronary artery.[134 135] It is characterized by regions of ultrastructural damage to the myocardial microvascular bed (reperfusion injury) with severely impaired tissue perfusion. Although the exact pathophysiology underlying no-reflow is incompletely understood, both ischemia and reperfusion are considered to be involved, and potential mechanisms include ischemia related endothelial damage, mechanical capillary plugging by platelets, erythrocytes or leukocytes, micro-embolization of atherosclerotic debris and compression by extravascular oedema.[135] No-reflow can be detected after angioplasty by assessing coronary flow according to the TIMI-classification or the TIMI-frame count, the Doppler intra-coronary flow pattern, the myocardial blush grade and by assessing electrocardiographic resolution of ST-segment elevation in the first 60-90 minutes after revascularization. The tissue equivalent of no-reflow is termed microvascular obstruction (MVO) or microvascular injury, which can be directly visualized with contrast-echocardiography, contrast-enhanced CMR or nuclear scintigraphic techniques.

Experimental studies using contrast-enhanced CMR have demonstrated that regions that are hypo-enhanced in the first 2 minutes after contrast injection correspond to no-reflow regions as defined by thioflavin S staining, and are characterized by severely impaired microsphere myocardial blood flow.[57] Serial contrast-enhanced CMR has been used to evaluate the dynamic nature of MVO and its close relation to reperfusion. Very early after reperfusion, blood flow is high, even in thioflavine S-negative (no-reflow) areas, but this is

followed by a progressive decrease in flow and an increase in size of MVO up to 3-fold during the first 48 hours after reperfusion.[136] MVO extent subsequently remains stable between 2 and 9 days after reperfusion, which is therefore considered the optimal window to detect and quantify MVO.[137]

Although these studies all provided insight into the mechanism and pathophysiology of acute myocardial infarction and MVO, current contrast-enhanced sequences may be more sensitive in the detection of MVO. Both dynamic first-pass imaging and steady state DCE imaging can be used to visualize MVO. First-pass images reflect myocardial perfusion, which is profoundly impaired in MVO and therefore results in hypo-enhanced regions of varying transmurality (figure 15).[138] Signal intensity continues to change in the first 5-10 minutes after contrast injection. Normal regions show a quick increase in signal intensity within 1 minute followed by a gradual decline.[57] Signal intensity in infarcted regions shows the same increase as in normal regions, but it continues to increase up to 5 minutes, remaining high for at least 30 minutes and resulting in the hyperenhancement typical for infarction ('bright is dead').[57 75] The injury in the MVO region is not homogeneous, and gadolinium continues to diffuse slowly into areas with less profound damage.[125] With subsequent delayed contrast-enhanced imaging, acquired 10-15 minutes after contrast injection, MVO can then be detected as (persistent) areas of hypo-enhancement, often with a patchy, heterogeneous character and located central and mostly subendocardial, but always spatially confined within the hyperenhanced, infarcted zone (figure 15).[116 125] Although infarct size remains unchanged on DCE images between 5 and 30 minutes after contrast injection, MVO size changes by on-going Gd-diffusion up to 45 minutes after injection (figure 15). MVO is typically related to the acute phase, and myocardial perfusion generally improves at follow-up although impaired perfusion may persist in some regions with the most severe microvascular damage.[138-140]

First-pass imaging is the most sensitive technique, and current sequences detect MVO in 65-87% of patients with reperfused acute myocardial infarction.[49 141 142] A recent study used semi-quantitative analysis of the first pass images and found impaired contrast wash-in in 19 of 20 patients.[138] There is high concordance between the presence of MVO on first pass and DCE images, although it follows from the gadolinium kinetics that prevalence at DCE imaging is lower with a reported 28-58%.[49 140 141 143]

Several studies using a variety of techniques have shown that MVO is a major prognostic factor after reperfused acute myocardial infarction.[114 140 144-147] We recently compared the prognostic value of first pass (early MVO) and DCE (persistent MVO, infarct size, infarct transmurality) to TIMI flow grade, myocardial blush grade and ST-segment resolution in a group of 60 patients with optimal treatment for AMI including primary percutaneous coronary intervention plus stenting, triple platelet inhibition (aspirin,

clopidogrel, abciximab), heparin and statins (this thesis, chapter 3).[49] Despite this optimal treatment, MVO was found in the majority of the patients: early MVO was found in 41 (68%) patients, and late MVO was found in 34 (57%) patients. Both early and late MVO were related to incomplete ST-resolution, but not to TIMI grade or myocardial blush grade. In a direct comparison between all parameters, late MVO was the most powerful predictor of left ventricular functional outcome. In addition, late MVO had diagnostic value beyond infarct transmurality for the prediction of regional outcome. Thus, although DCE imaging is less sensitive for the detection of MVO, it appears to have greater clinical significance.

Contrast-echocardiography may also be used to visualize microvascular damage. In a recent study, contrast-echocardiography proved a better predictor of remodeling than angiographic and electrocardiographic parameters.[148] A previous experimental study showed a fair correlation between both techniques, but they have not yet been compared in the clinical setting.[137]

DCE imaging may be the ideal technique to evaluate new strategies to reduce reperfusion injury. MVO can be quantified and expressed as absolute quantity or as a percentage of total infarct mass. For the quantification and comparison of MVO extent, a strict methodology is essential with respect to the time between contrast injection and data acquisition, because the MVO area may shrink with time due to on-going contrast wash-in.

Intramyocardial haemorrhage

The endothelial disruption that accompanies microvascular injury may lead to extravasation of eryhtrocytes and intramyocardial haemorrhage.[149] Myocardial haemorrhage was rare in the pre-reperfusion era, and it is considered to be closely related to the (microvascular) ischemia-reperfusion injury cascade.[150] [151] CMR is the only non-invasive technique that allows the visualization of haemorrhage because hemoglobin breakdown products alter regional magnetic tissue properties.[152] Both T2*('star')-weighted gradient-echo imaging and T2W imaging have been used to visualize haemorrhage, but T2W spin-echo imaging is the preferred technique because it also visualizes infarct related oedema.[150] [152] Signal intensity in acute infarction is normally increased on T2W images but it is attenuated by the presence of haemorrhage, which results in a patchy appearance or an averaged low to intermediate signal intensity especially at the core of the infarct (figure 16).[151] The T2W signal attenuation by haemorrhage has been validated in experimental models and, in a recent case report, by using ex-vivo imaging in two patients that died after recent acute myocardial infarction.[151] [154]

To assess the relation between haemorrhage and MVO and their clinical significance, we recently evaluated 45 patients after primary angioplasty for first acute myocardial infarction (this thesis, chapter 4).[155] Attenuated T2W signal was found in 22 of 29 patients

with MVO whereas homogenous (non-attenuated) signal was found in the 16 patients without MVO. Contrast-to-noise ratio between the attenuated T2W infarct core signal and the high signal in the infarct periphery was closely related to infarct size, MVO and ejection fraction both at baseline and at follow-up. However, haemorrhage did not have clinical significance beyond MVO since, in a multivariable analysis, only baseline ejection fraction and MVO were predictive of functional changes at follow-up.

CMR may thus provide additional insight in the pathophysiological changes after myocardial infarction and reperfusion. However, the significance of these findings is not yet clear and further study is needed to explore the relation of reperfusion-related haemorrhage to infarction, microvascular obstruction and clinical outcome.

1.4 CMR IN PATIENTS WITH ISCHEMIC CARDIOMYOPATHY AND CHRONIC MYOCARDIAL INFARCTION

This part will address the use of CMR in the chronic phase of infarction, focusing on patients with ischemic cardiomyopathy or (suspected) prior infarction. A basic imaging protocol in patients with ischemic cardiomyopathy or (suspected) old myocardial infarction includes cine imaging for the assessment of ventricular and valvular function, and delayed contrast-enhanced (DCE) imaging for the assessment of regional scar and viability. If a detailed evaluation of myocardial viability is required it is recommended to acquire the cines prior to contrast injection to achieve optimal contrast between blood and endocardium, with a total examination time of less than 30 minutes. If less detail is required, contrast can be given prior to the start of the exam, which reduces examination time to less than 20 minutes. If presence and distribution of scar is the only clinical question, single shot DCE imaging may provide the answer within 5 minutes. Low dose dobutamine cine is good alternative method to assess viability in patients with (relative) contra-indications to gadolinium-based contrast agents, e.g. in advanced renal failure. Depending on the clinical situation, adenosine first-pass imaging or high-dose dobutamine stress cine can be added to detect ischemia related perfusion defects or wall motion abnormalities, respectively. An extensive description of these techniques is beyond the scope of this review.

Function

Global ventricular function. Global left ventricular function strongly influences prognosis and management and its assessment is an essential part of the work-up in a patient with prior myocardial infarction. As in acute infarction, the selection of candidates for implantable cardioverter-defibrillator or cardiac resynchronization devices heavily relies on

left ventricular ejection fraction. Cine imaging ensures the quantification of global function with the highest reproducibility and accuracy possible, thus avoiding both unnecessary implantations and deaths.

Right ventricular dysfunction is a well-known risk factor of adverse outcome in patients with ischemic heart disease.[156] Quantified with cine CMR and defined as ejection fraction <40%, it was a significant predictor of mortality in a group of 147 patients with prior (>30 days) myocardial infarction, and remained so after adjustment for age, infarct size and left ventricular ejection fraction.[157] Only 16% of the patients with right ventricular dysfunction had right ventricular hyperenhancement, suggesting that other than ischemic mechanisms play a role in its pathogenesis.[157]

Regional function. The high-resolution SSFP cine sequence allows the detailed evaluation of regional wall thickness and thickening. Chronic scarring leads to regional thinning which may be extreme in remodeled ventricles (<4 mm). Decreased end-diastolic wall thickness is one of the parameters that can be used in the evaluation of myocardial viability (see below).

Infarct-related complications

The unrestricted access to the heart and the chest allows the full assessment of severely deformed and remodeled ventricles or (pseudo-)aneurysms prior to reconstructive surgery (figure 17).[158] Cine imaging is generally sufficient to show the deformation in detail and also provides geometric information on mitral annular size and papillary muscles which may play a role in the pre-operative evaluation of functional mitral regurgitation.[158] Delayed contrast-enhanced (DCE) imaging may help to diagnose and delineate (pseudo-)aneurysms by highlighting the borders of the scarred region and is highly sensitive for the detection of left ventricular thrombi, both in the acute and the chronic phase of infarction (fig 17; also see 1.3 Infarct-related complications).

Regional low signal intensity may be seen within chronically infarcted regions on SSFP cines (figure 18). These correspond to lipomatous metaplasia, which refers to the transformation of fibrotic scars into fat. Although fat normally has high signal intensity on SSFP images, the intravoxel presence of myocytes and fat may cause phase cancellation and signal loss. T1-weighted spinecho imaging with and without fat-suppression, or inversion recovery imaging (DCE) befóre contrast injection (with adjusted inversion time) can be used to confirm this diagnosis (figure 18).[159] [160] The clinical significance of this finding that may also be detected with CT is unknown, although an association with remodeling and aneurysm formation has been suggested.[161]

Infarct visualization

DCE CMR can be considered the current gold standard for in-vivo infarct visualization at every stage of myocardial infarction. Serial DCE imaging has shown that infarct size decreases by 19-31% in the first months after the acute event (figure 19).[59 116 162] Infarct regression is the result from the healing process and the replacement of inflammation, haemorrhage, oedema and necrotic myocytes by collagenous scar.[163] It is more pronounced in patients with larger infarct size and microvascular obstruction, and in patients with remodeling at follow-up.[164]

Chronic myocardial infarction is depicted as regional areas of hyperenhancement of varying extent, ranging from small and subendocardial with preserved wall thickness to completely transmural with advanced wall thinning (figures 11,12). Often, several degrees of transmural extent can be found within one infarction, and the enhancement pattern may be irregular and patchy in patients with chronic coronary artery disease and a history of multiple infarctions or revascularizations (figure 20). Not surprisingly, ECG-markers of transmurality (Q-, non-Q-wave) are poorly related to the actual extent of hyperenhancement.[165] Q-waves have low sensitivity for the detection of chronic infarction, especially of the (infero-)lateral wall, and their presence reflect the total size of the infarct rather than infarct transmurality.[166] When Q-waves are present, their location correlates well with the distribution according to DCE.[167]

The high sensitivity of DCE for the detection of chronic scar facilitates the non-invasive diagnosis of unsuspected or previously non-diagnosed coronary artery disease.[168] Although regional hyperenhancement per se is not specific for ischemic heart disease, location and extent generally allow the reliable differentiation from non-ischemic myocardial disease.[169] Ischemic scar has a transmural or subendocardial distribution, whereas non-ischemic disease can be found in the supepicardial or mid part of the left ventricular wall, outside the usual coronary artery territories.

Several studies have now shown that regional scar is strongly related to outcome and has prognostic value beyond global volumes and ejection fraction as well as other, commonly used clinical markers.[170-172] The size of the scarred region might be less relevant in terms of prognosis than its presence. One study evaluated 195 patients without known prior MI but with known or suspected coronary artery disease, and found that the presence of any hyperenhancement was the strongest multivariable predictor of major adverse cardiovascular endpoints during a 16 months follow-up period.[170]

In addition to presence, transmural extent and total size of the hyperenhanced region, recent studies have focused on the heterogeneity of signal in the infarct and its direct border zone.[173 174] DCE can visualize and quantify this ‘peri-infarct’ or ‘grey’ zone, which is thought to represent a mixture of viable myocytes and collagen fibers and a potential

substrate of ventricular arrhythmia (figure 21). The extent of tissue heterogeneity has been related to mortality and increased inducibility of ventricular arrhythmia in patients with previous myocardial infarction.[173 174] Also, papillary muscles with heterogeneous contrast uptake have been suggested as a possible origin of ventricular arrhythmia in patients with old myocardial infarction.[175] However, a uniform approach to the assessment of signal heterogeneity on DCE images is lacking and further study is needed to define its significance.

Viability

There is general agreement that patients with ischemic cardiomyopathy (defined as ejection fraction <40% with evidence of prior infarction or hibernation, and ≥2-vessel coronary artery disease) should undergo revascularization if there is significant potential for recovery of function.[176 177] CMR has several ways to assess the presence of viability in dysfunctional myocardium: morphological evaluation of end-diastolic wall thickness (EDWT) using cine imaging; functional evaluation of inotropic reserve using low-dose dobutamine stress cine imaging; evaluation of myocyte integrity and regional scar by DCE imaging. Although first pass perfusion imaging may be used to demonstrate impaired resting blood flow in hibernating myocardium, it is not used for the prediction of functional outcome and is therefore not routinely included in the CMR imaging protocol of myocardial viability.[178]

End-diastolic wall thickness

Both echocardiographic and CMR studies have demonstrated a low likelihood of functional recovery after successful revascularization in segments with chronically scarred, thinned myocardium.[179-181] Using cine CMR imaging, it was shown that segmental EDWT <5.5 mm (based on a mean – 2.5 SD in normal individuals) had a 92% sensitivity and a 56% specificity for the prediction of functional improvement.[179] Echocardiographic studies have used similar cut-offs with comparable results, confirming the high negative predictive value of EDWT, with <6mm virtually excluding functional recovery.[181] However, current SSFP cine sequences allow a considerably better delineation of the blood-endocardial and epicardial border. We recently evaluated 36 healthy volunteers and found a mean (SD) EDWT of 5.2 (1.3) mm, which illustrates the need for a new (and lower) cut-off to identify chronic scar (this thesis, chapter 5). Further more, we have seen on several occasions that wall thinning, even when extreme, did not preclude functional recovery, as long as there was no or minimal regional scarring at DCE imaging (figure 22). Although extensive literature data are lacking, others have reported similar findings, which is why we currently consider severely thinned (<4 mm) segments viable if there is no or minimal hyperenhancement.[182]

Low-dose dobutamine stress cine

Low-dose dobutamine (LDDS) (5-10 μg/kg/min) can be used to assess the contractile reserve of dysfunctional but viable myocardium, and its clinical use has been demonstrated in a large number of studies using both echocardiography and cine CMR.[183 184] A positive response (detectable increase in wall motion or thickening) requires both a significant amount of intact myofibrillar units as well as sufficient perfusion reserve, which is why LDDS techniques typically have lower sensitivity but higher specificity when compared to other (nuclear) techniques.[185]

Delayed contrast-enhanced imaging

The use of DCE in viability assessment has several advantages compared to other techniques. DCE offers superior spatial resolution (1-2 mm in-plane, slice thickness 4-6 mm) and high contrast between hyperenhanced scarred regions and non-enhanced viable regions. This allows the transmural evaluation of scar even in segments with marked wall thinning. DCE CMR is quick, reproducible and robust, and safer and less dependent on technician and observer skills than dobutamine stress imaging. Finally, it is the only technique that provides side-by-side visualization of viable and non-viable parts. Thus, it allows the assessment of viability as a gradual rather than a binary (present – non-present) phenomenon.

Functional improvement after revascularization. Kim et al were the first to show that the transmural extent of scar strongly predicted functional outcome after revascularization.[81] The likelihood of segmental functional recovery was inversely related to the segmental extent of hyperenhancement (SEH): 78% of dysfunctional segments without hyperenhancement improved, whereas only one segment with >75% hyperenhancement improved. Using a cut-off value of ≤ 25% SEH to define viability, positive and negative predictive values were 71% and 79% for segments with any baseline dysfunction, and 88% and 89% for segments with akinesia or dyskinesia. Further more, the total number of viable segments was strongly related to the degree of improvement of left ventricular ejection fraction. Other studies have since then confirmed the potential of DCE in viability assessment, although the total amount of evidence is still limited compared to other techniques.[23 186-193]

Comparison to other techniques. Several studies have shown that DCE has good correlation with 18F fluorodeoxyglucose positron emission tomography (FDG PET) which has since long been the reference imaging standard of viability.[194 195] In 26 patients with chronic ischemic cardiomyopathy, we showed that SEH was 9±14, 33±25 and 80±23% in severely dysfunctional segments with normal FDG uptake/perfusion, FDG/perfusion mismatch and matched defects, respectively (this thesis, chapter 5).[195] A cut-off value of 37% SEH

predicted PET viability with sensitivity 96% and specificity 84%. Two studies so far have compared FDG PET and DCE to the clinical reference standard functional outcome after revascularization.[191] [193] Both found comparable overall diagnostic accuracy, with one suggesting a higher negative predictive accuracy for FDG PET and the other for DCE at a 17 days and 6 months follow-up period, respectively. Knuesel et al postulated that functional improvement would only occur if a residual viable rim of sufficient wall thickness was present.[190] Both DCE and FDG PET were acquired in 10 patients with ischemic cardiomyopathy. After 11 months, 85% of dysfunctional segments with both a thick viable rim (defined as >4.5 mm) and preserved FDG-uptake improved, whereas all other segments (including thin segments with preserved FDG uptake and thick metabolically non-viable segments) had low improvement rates. However, the number of patients in this study was low, and, as stated above, wall thickness may be less relevant if there is no or little hyperenhancement (figure 22).

Although the ease, the robustness and the safety of DCE imaging strongly favour its use over LDDS cine imaging, two studies have recently suggested that adding LDDS cine imaging to the protocol might increase the prediction of functional improvement in segments with intermediate ranges of segmental extent of hyperenhancement (1-75%).[189] [192] However, the differences were only small and further study is needed to resolve this issue.

Lack of improvement despite viability. The use of DCE imaging may help to understand why left ventricular function does not always improve after revascularization despite the presence of viability. First, its high spatial resolution allows the identification of subendocardial scar, which may preclude functional improvement despite subepicardial viability. Second, DCE imaging may help to identify new, clinically undetected areas of necrosis between the baseline study and the follow-up study. Procedure-related myocardial necrosis may be substantial and has been shown an important negative predictor of functional outcome.[186] Finally, the timing of the follow-up study to assess recovery of function may play an important role. We recently reported on the relation between long-term functional outcome after revascularization and baseline segmental extent of hyperenhancement (this thesis, chapter 6).[23] Thirty-five patients with ischemic cardiomyopathy (ejection fraction 39±11%) underwent cine and DCE imaging 1 month before and 3, 6 and 24±12 months after revascularization. Throughout the entire study period, likelihood of improvement was strongly and inversely related to SEH (figure 23). Interestingly, segments from all SEH groups continued to improve throughout the whole study and, at the end of the study period, improvement rate was higher than previously reported in all SEH groups except in the 76-100% SEH. For example, at 3 months, 56% of segments without hyperenhancement had improved, which is relatively low compared to Kim et al.[81] At long-term follow-up however, practically all (93%) had improved, and

segments with 1-25, 26-50, 51-75 and 76-100% SEH were 2, 5, 11 and 86 times less likely to improve (multilevel analysis, $p<0.001$). The time course of improvement was considerably more delayed in segments with more extensive hyperenhancement at baseline (multilevel analysis, $p<0.001$) (figure 23). These results demonstrate that DCE imaging strongly predicts functional outcome even at long-term follow-up, that the time course of improvement may be considerably delayed, and that both likelihood and time course are related to the baseline amount of scar. The delayed time course suggests that long follow-up periods may be required to assess the full potential of recovery of dysfunctional but viable myocardium.

Device therapy

CMR cine imaging is the current gold standard for the quantification of ventricular function, which is the critical step in the selection of patients for implantable cardioverter-defibrillator (ICD) or cardiac resynchronisation therapy (CRT). The timing of ICD implantation may be difficult in patients with significant viability who have undergone revascularisation, since functional recovery may be considerably delayed.

Significant mechanical dyssynchronous contraction between the septal and the lateral wall is usually easily recognised on a regular 4-chamber or midventricular short axis SSFP cine. MRI tagging allows the detailed 3D-assessment of intramural deformation including strain, velocity and torsion. Although myocardial tagging is the ideal technique to assess the process of mechanical dyssynchrony, its current use is largely limited to research because postprocessing requires considerable know-how and is still relatively time consuming. Several quantitative measures of dyssynchrony have recently been proposed for both (plain) SSFP cine imaging as well as for myocardial tagging, all awaiting further clinical validation. [196 197]

DCE imaging may be of value in the selection of CRT candidates by identifying potential non-responders by demonstrating regional transmural scar in the posterolateral segments or a large amount of total scar.[198 199] Signal heterogeneity in the infarct zone may identify patients at increased risk of ventricular arrhythmia, however, as mentioned above, it is currently not clear whether these patients would benefit from a more aggressive approach and early ICD-implantation (see also *Infarct visualization*).[173 174]

FIGURES

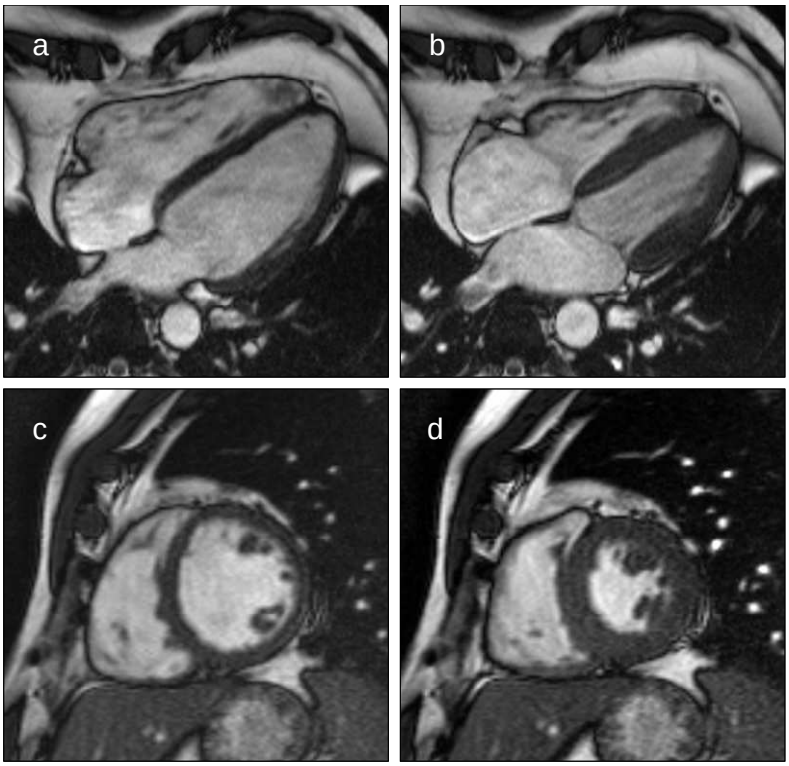

Figure 1. End-diastolic (a,c) and end-systolic (b,d) still-frames acquired with steady state free precession cine sequence in 4-chamber (a,b) and midventricular short-axis (c,d) position.

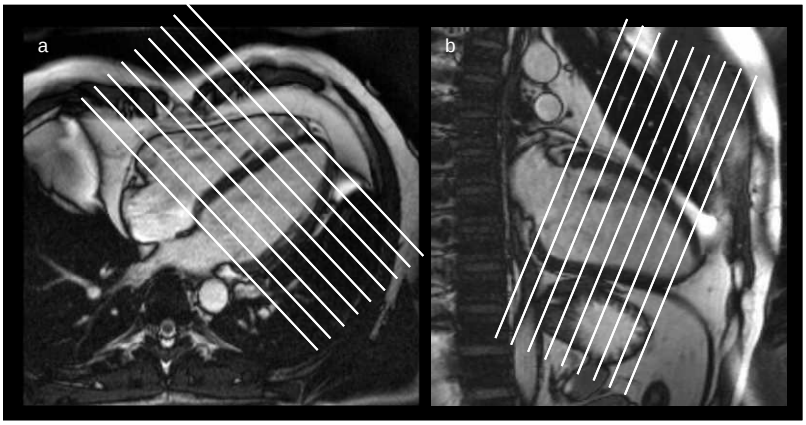

Figure 2. End-diastolic 4-chamber (a) and 2-chamber (b) still-frames showing the position of the short axis stack.

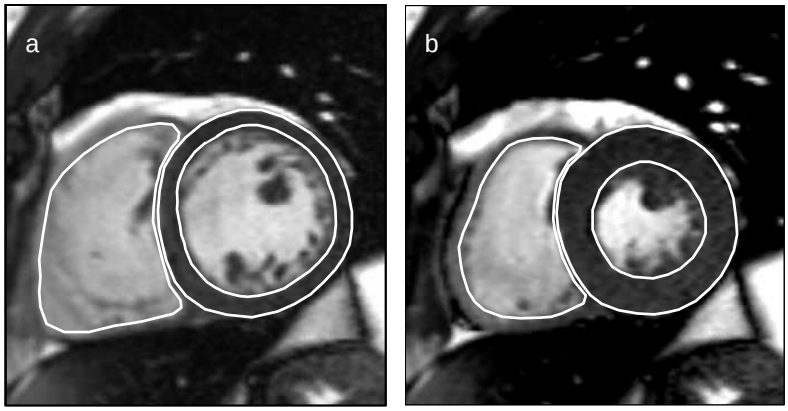

Figure 3. Left ventricular epicardial, endocardial and right ventricular endocardial contours on end-diastolic (a) and end-systolic (b) still-frames.

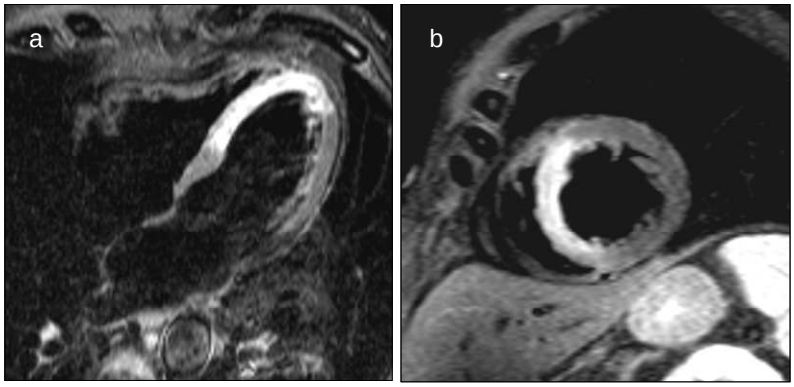

Figure 4. Four-chamber (a) and short axis (b) view acquired with dark-blood, T2-weighted spinecho imaging with fat-suppression in a patient with 5-day old reperfused anteroseptal myocardial infarction.

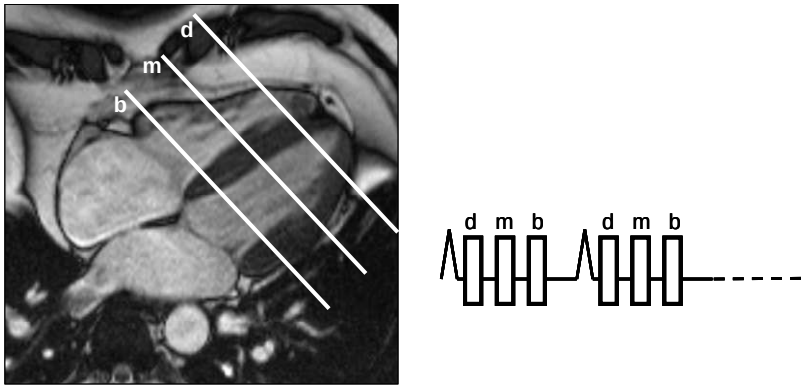

Figure 5. End-systolic 4-chamber still-frame showing the basal (b), mid (m) and distal (d) short axis position during first pass myocardial perfusion imaging and position of the 3 slices in relation to the QRS-complex.

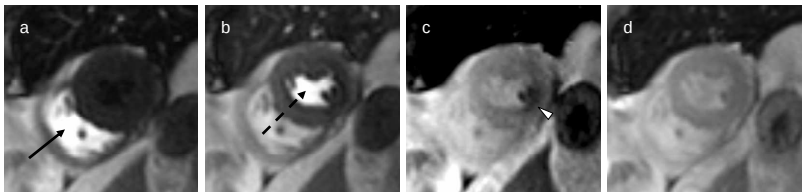

Figure 6. First pass myocardial perfusion imaging. Still-frames in midventricular position showing contrast arrival in the right ventricle (a, arrow), left ventricle (b, dashed arrow) and myocardium during adenosine stress (c) and rest (d). A reversible perfusion defect is visible in the subendocardial inferior wall and the posterior papillary muscle (marker).

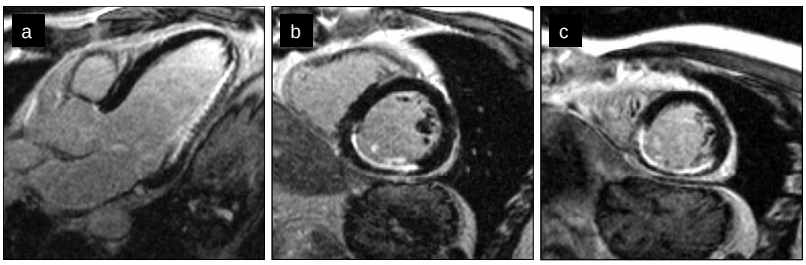

Figure 7. Delayed-contrast-enhanced images showing subendocardial infarction of the inferior and inferolateral wall in the 3-chamber view (a) and in a midventricular (b) and distal (c) short axis view.

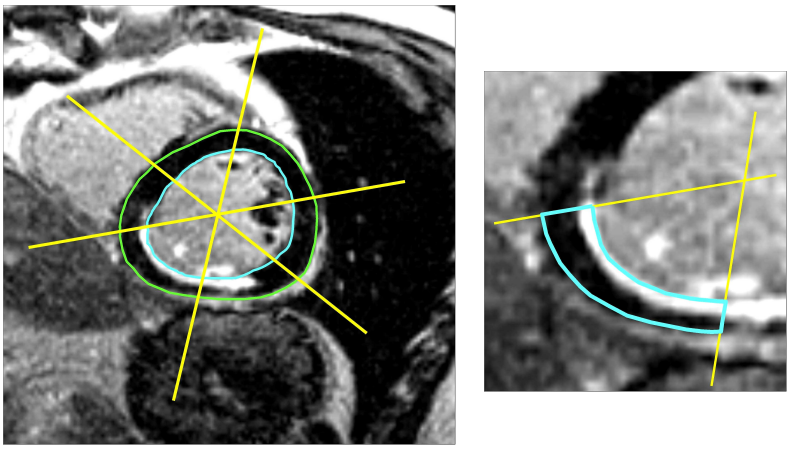

Figure 8. Delayed-contrast-enhanced imaging: segmental extent of hyperenhancement.

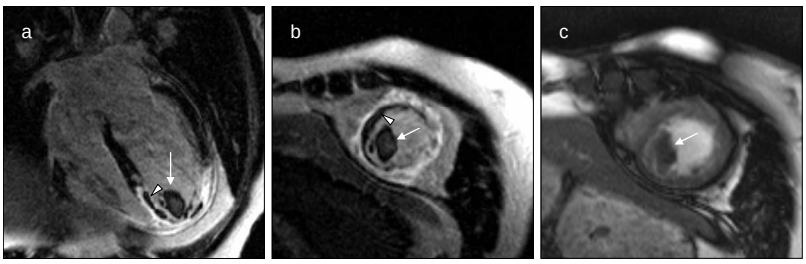

Figure 9. Four-chamber and short axis delayed-contrast-enhanced views (a,b) in a patient with 4-day old reperfused antero-apical infarction, showing transmural hyperenhancement with extensive microvascular obstruction (marker) and a large left ventricular thrombus (arrow). A short axis cine still frame (c) shows the low-intermediate signal intensity of the thrombus in comparison to the intermediate myocardial signal.

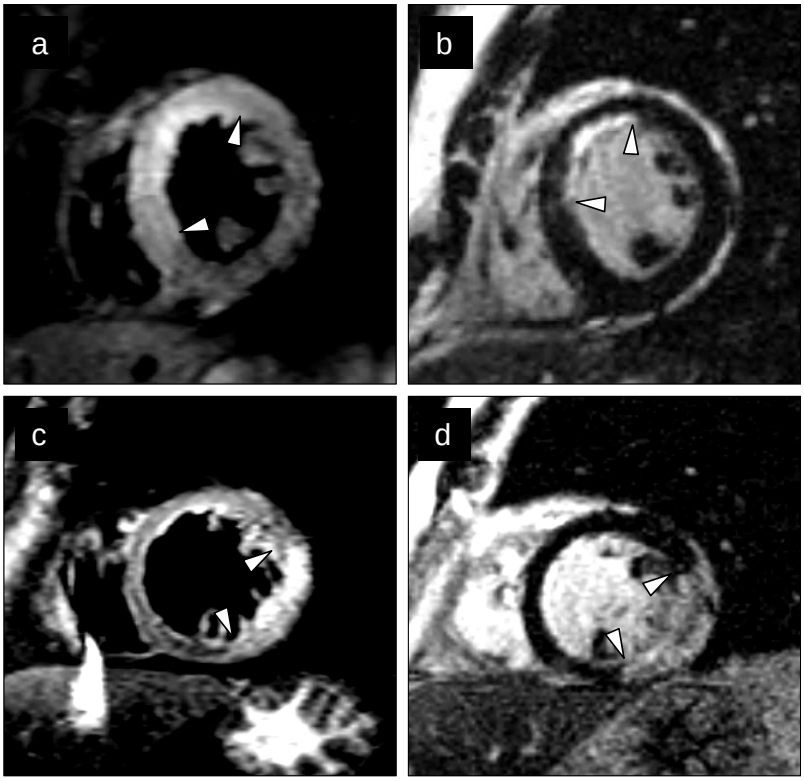

Figure 10. Infarct-related oedema versus infarct size. The upper images show subendocardial anteroseptal infarction (b) with infarct-related oedema (a) that extends beyond the borders of the hyperenhanced area. Lower images show transmural inferolateral infarction (d) with infarct-related oedema (c) that matches the infarct area.

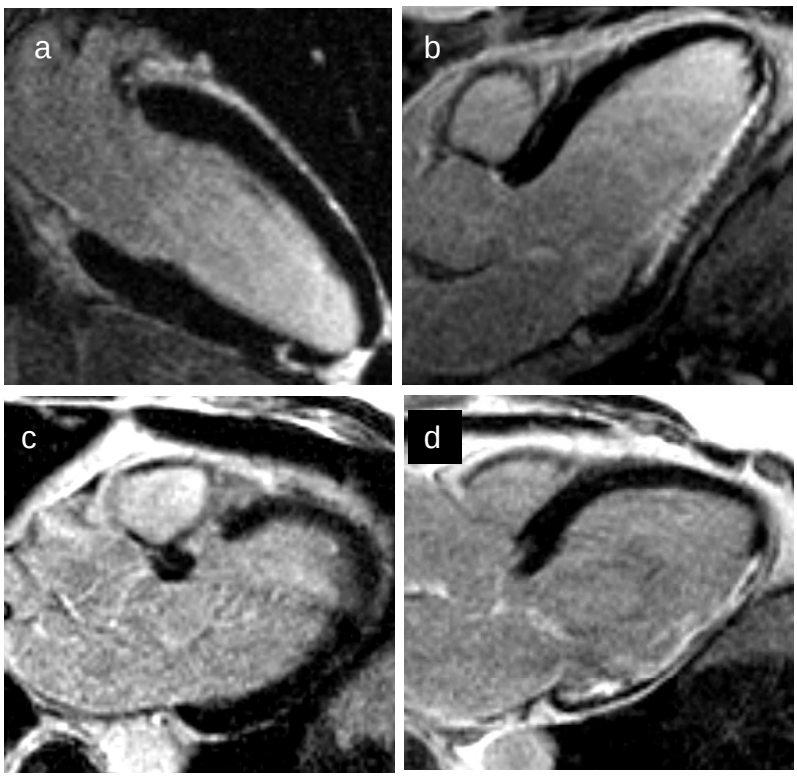

Figure 11. Visualization of infarction using delayed-contrast-enhanced imaging: a. minimal myocardial injury in distal inferior wall after elective percutaneous coronary intervention, b. subendocardial inferolateral infarction, c. limited transmural septal infarction with coronary angiography showing occluded first septal branch, d. inferolateral infarction with wall thinning and largely transmural hyperenhancement.

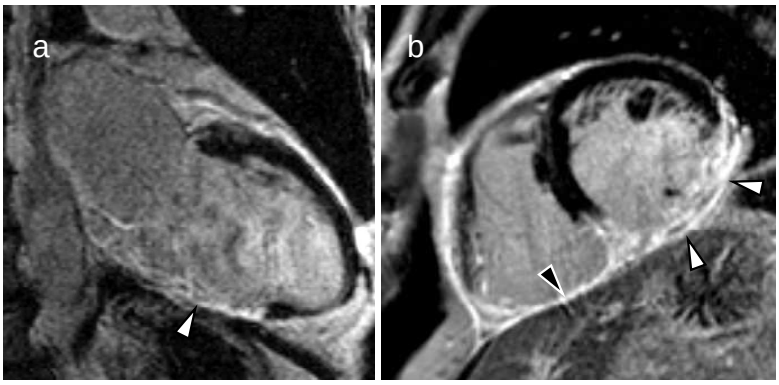

Figure 12. Visualization of infarction using delayed-contrast-enhanced imaging: 2-chamber view (a) and short axis (b) view showing inferolateral infarction (white markers) with right ventricular involvement (black marker).

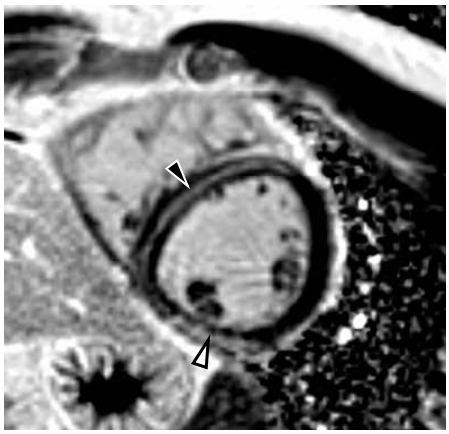

Figure 13. Hyperenhancement in myocarditis. Midventricular short axis showing midwall hyperenhancement in the septum and subepicardial hyperenhancement in the inferior wall in a 40-year old patient presenting with typical chest pain, positive Troponin-T, normal ECG and normal coronary arteries.

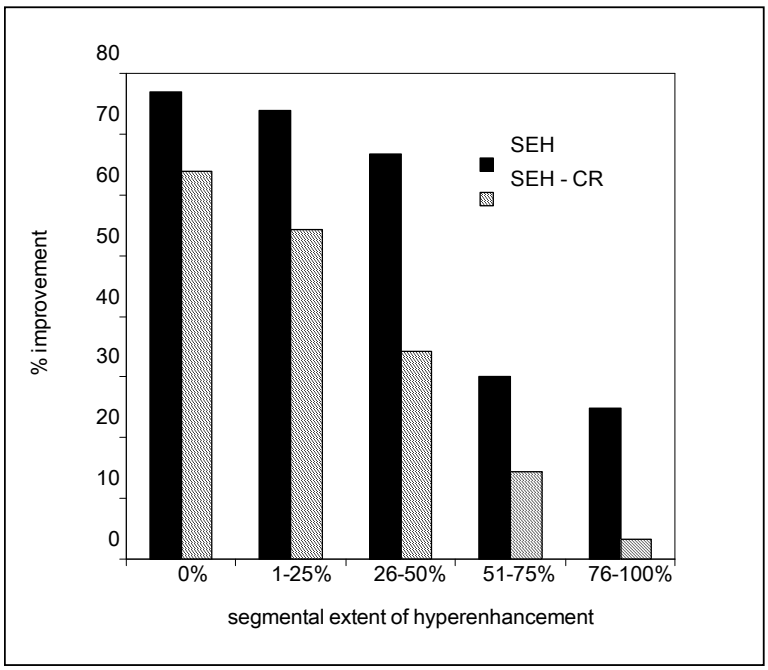

Figure 14. Segmental extent of hyperenhancement versus likelihood of functional recovery 3 months after acute myocardial infarction. Reprinted with permission (ref. 123).

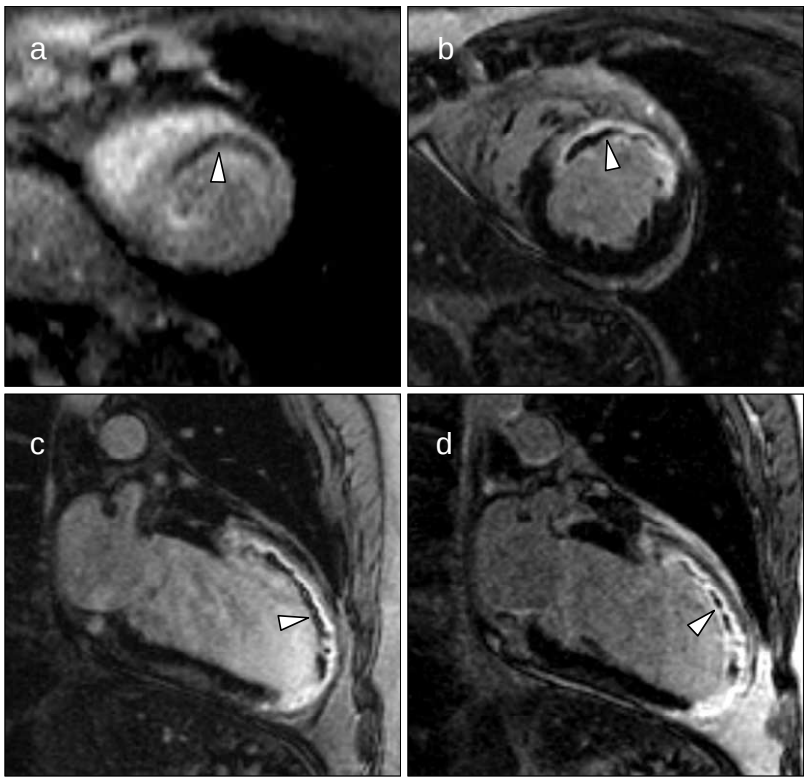

Figure 15. Microvascular obstruction (marker) in a patient with 4-day old reperfused anterior infarction, as seen on midventricular first pass image (a) and on delayed contrast-enhanced images 10 (b,c) and 30 minutes (d) after contrast injection.

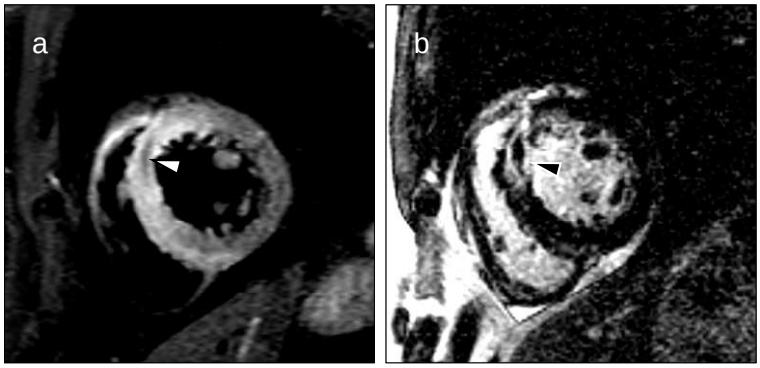

Figure 16. Intramyocardial haemorrhage (white marker) is seen as a central region of low signal within the region of high signal of infarct-related oedema on the T2-weighted spinecho image (a). The corresponding delayed contrast-enhanced image (b) shows a small central hypo-intense region (black marker) corresponding to microvascular obstruction.

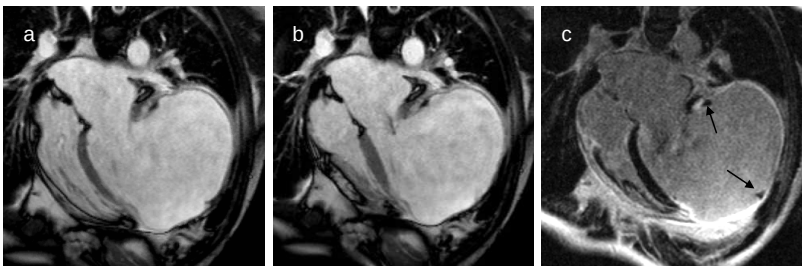

Figure 17. End-diastolic (a) and end-systolic (b) still-frames showing a severely deformed left ventricle with massive aneurysm after inferolateral myocardial infarction. The delayed contrast-enhanced image (c) shows the exact definition of the border between scar and healthy myocardium, as well as 2 small thombi (arrows).

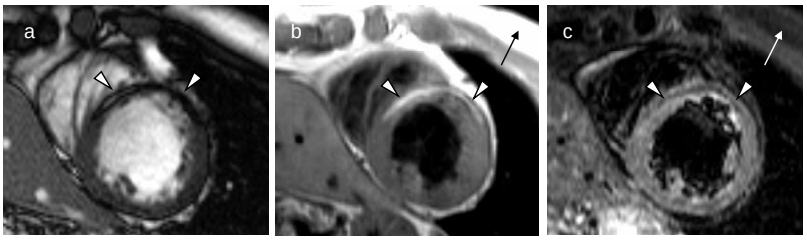

Figure 18. Short axis view in a patient with old anteroseptal infarction. Lipomatous metaplasia (markers) leads to phase cancellation and signal loss in SSFP cine imaging (a), regional high signal intensity in T1-weighted spinecho imaging (b) and very low signal in T2-weighted spinecho imaging with fat suppression (c). See also subcutaneous fat (arrows).

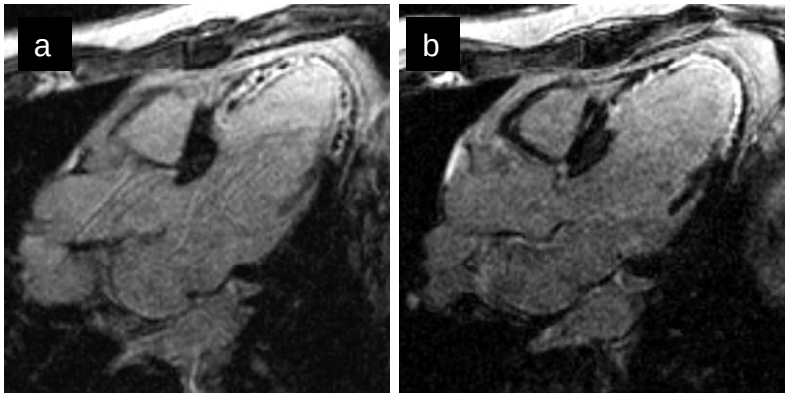

Figure 19. Three-chamber delayed contrast-enhanced view in a patient with anteroseptal infarction acquired 4 days (a) and 4 months (b) after reperfusion, showing infarct regression and disappearance of microvascular obstruction.

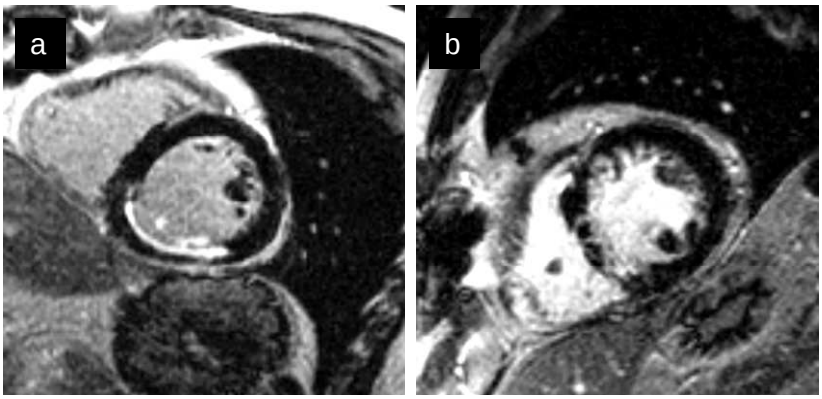

Figure 20. Relatively smooth subendocardial hyperenhancement in a patient with 6-day old reperfused inferolateral infarction (a) and irregularly shaped and patchy enhancement in a patient with a history of coronary artery bypass grafting but no history of infarction (b).

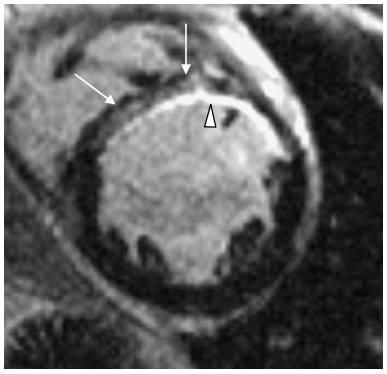

Figure 21. The 'grey' zone. Midventricular short axis view in a patient with old anteroseptal infarction showing an intensely bright subendocardial zone (marker) surrounded by a more patchy midwall and subendocardial enhancement (arrows).

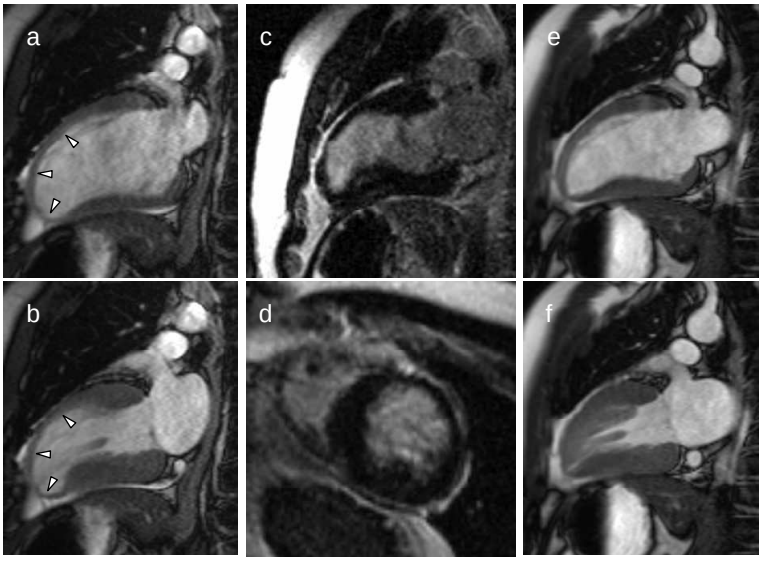

Figure 22. Prediction of functional recovery in a patient presenting with heart failure and proximally occluded left anterior descending artery 1 year after percutaneous angioplasty and stenting. End-diastolic still-frame (a) and end-systolic still-frame (b) in 2-chamber view show marked wall thinning and lack of wall thickening (markers). Delayed contrast-enhanced imaging showed no hyperenhancement (c,d). Follow-up cine 6 months after re-intervention showed normal wall thickness and full recovery of wall thickening with an increase in ejection fraction fraction from 39% to 61%.

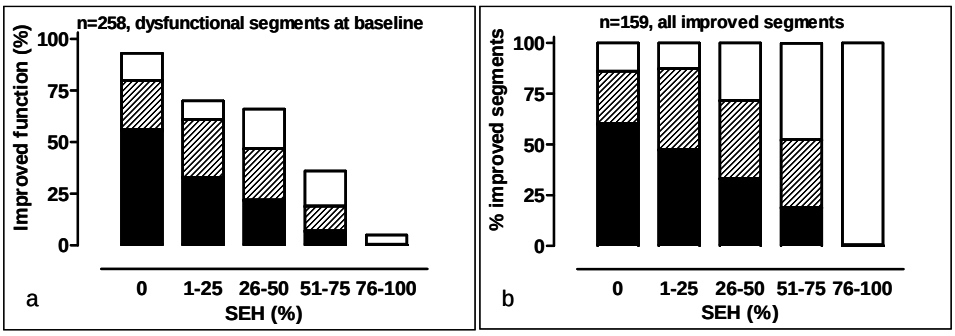

Figure 23. Delayed contrast-enhanced imaging: viability. Reprinted with permission (ref 23).
a. Likelihood of functional improvement after revascularisation in relation to baseline segmental extent of hyperenhancement (SEH), expressed as a percentage of total number of dysfunctional segments, at 3 months (black bars), 6 months (striped bars) and 2 years (white bars) follow-up. All dysfunctional segments are included (n=258).
b. Time course of regional functional improvement in relation to baseline SEH, shown as the relative percentage of improvement at 3 months (black bars), 6 months (striped bars) and 2 years (white bars) follow-up. Only segments with functional improvement are included (n=159).

REFERENCES

1. Marcu CB, Beek AM, van Rossum AC. Clinical applications of cardiovascular magnetic resonance imaging. *CMAJ*. 2006;175:911-7.
2. Pennell DJ, Sechtem UP, Higgins CB, Manning WJ, Pohost GM, Rademakers FE *et al*. Clinical indications for cardiovascular magnetic resonance (CMR): Consensus Panel report. *Eur Heart J* 2004;25:1940-65.
3. Finn JP, Nael K, Deshpande V, Ratib O, Laub G. Cardiac MR Imaging: State of the Technology. *Radiology* 2006;241:338-54.
4. Lohan DG, Saleh R, Saleh RF, Tomasian AF, Krishnam MF, Finn JP. Current status of 3-T cardiovascular magnetic resonance imaging. *Top Magn Reson Imaging* 2008;19.
5. Kanal E, Borgstede JP, Barkovich AJ, Bell C, Bradley WG, Etheridge S *et al*. American College of Radiology White Paper on MR Safety: 2004 Update and Revisions. *Am.J.Roentgenol.* 2004;182:1111-4.
6. Levine GN, Gomes AS, Arai AE, Bluemke DA, Flamm SD, Kanal E *et al*. Safety of Magnetic Resonance Imaging in Patients With Cardiovascular Devices: An American Heart Association Scientific Statement From the Committee on Diagnostic and Interventional Cardiac Catheterization, Council on Clinical Cardiology, and the Council on Cardiovascular Radiology and Intervention: Endorsed by the American College of Cardiology Foundation, the North American Society for Cardiac Imaging, and the Society for Cardiovascular Magnetic Resonance. *Circulation* 2007;116:2878-91.
7. Pohost GM, Kim RJ, Kramer CM, Manning WJ. Task Force 12: Training in Advanced Cardiovascular Imaging (Cardiovascular Magnetic Resonance [CMR]): Endorsed by the Society for Cardiovascular Magnetic Resonance. *J Am Coll Cardiol.* 2008;51:404-8.
8. Griswold MA, Jakob PM, Heidemann RM, Nittka M, Jellus V, Wang J *et al*. Generalized autocalibrating partially parallel acquisitions (GRAPPA). *Magn Reson Med.* 2002;47:1202-10.
9. Pruessmann KP, Weiger M, Scheidegger MB, Boesiger P. SENSE: sensitivity encoding for fast MRI. *Magn Reson Med.* 1999;42:952-62.
10. Wintersperger BJ, Reeder SB, Nikolaou K, Dietrich O, Huber A, Greiser A *et al*. Cardiac CINE MR imaging with a 32-channel cardiac coil and parallel imaging: impact of acceleration factors on image quality and volumetric accuracy. *J Magn Reson Imaging.* 2006;23:222-7.
11. Jahnke C, Paetsch I, Gebker R, Bornstedt A, Fleck E, Nagel E. Accelerated 4D dobutamine stress MR imaging with k-t BLAST: feasibility and diagnostic performance. *Radiology.* 2006;241:718-28.
12. Tsao J, Boesiger P, Pruessmann KP. k-t BLAST and k-t SENSE: dynamic MRI with high frame rate exploiting spatiotemporal correlations. *Magn Reson Med.* 2003;50:1031-42.
13. Kozerke S, Plein S. Accelerated CMR using zonal, parallel and prior knowledge driven imaging methods. *J Cardiovasc Magn Reson* 2008;10:29.
14. Kunz RP, Oellig F, Krummenauer F, et al. Assessment of Left Ventricular unctions by Breath-Hold Cine MR Imaging: Comparison of Different Steady-State Free Precession Sequences. *J Magn Reson Imaging* 2005;21:140-8.
15. Papavassiliu T, Kuhl HP, Schroder M, Suselbeck T, Bondarenko O, Bohm CK *et al*. Effect of endocardial trabeculae on left ventricular measurements and measurement reproducibility at cardiovascular MR imaging. *Radiology.* 2005;236:57-64.
16. Alfakih K, Plein S, Thiele H, Jones T, Ridgway JP, Sivananthan MU. Normal human left and right ventricular dimensions for MRI as assessed by turbo gradient echo and steady-state free precession imaging sequences. *J Magn Reson Imaging.* 2003;17:323-9.
17. Maceira AM, Prasad SK, Khan M, Pennell DJ. Reference right ventricular systolic and diastolic function normalized to age, gender and body surface area from steady-state free precession cardiovascular magnetic resonance. *Eur Heart J.* 2006;27:2879-88.
18. Alfakih K, Plein S, Bloomer T, Jones T, Ridgway J, Sivananthan M. Comparison of right ventricular volume measurements between axial and short axis orientation using steady-state free precession magnetic resonance imaging. *J Magn Reson Imaging.* 2003;18:25-32.

19. Maceira AM, Prasad SK, Khan M, Pennell DJ. Normalized left ventricular systolic and diastolic function by steady state free precession cardiovascular magnetic resonance. *J Cardiovasc Magn Reson.* 2006;8:417-26.
20. Cerqueira MD, Weissman NJ, Dilsizian V, Jacobs AK, Kaul S, Laskey WK *et al*. Standardized myocardial segmentation and nomenclature for tomographic imaging of the heart: a statement for healthcare professionals from the Cardiac Imaging Committee of the Council on Clinical Cardiology of the American Heart Association. *Circulation.* 2002;105:539-42.
21. McGillem MJ, Mancini GB, DeBoe SF, Buda AJ. Modification of the centerline method for assessment of echocardiographic wall thickening and motion: a comparison with areas of risk. *J Am Coll Cardiol.* 1988;11:861-6.
22. van Rugge FP, van der Wall EE, Spanjersberg SJ, de Roos A, Matheijssen NA, Zwinderman AH *et al*. Magnetic resonance imaging during dobutamine stress for detection and localization of coronary artery disease. Quantitative wall motion analysis using a modification of the centerline method. *Circulation.* 1994;90:127-38.
23. Bondarenko O, Beek AM, Twisk JW, Visser CA, van Rossum AC. Time course of functional recovery after revascularization of hibernating myocardium: a contrast-enhanced cardiovascular magnetic resonance study. *Eur Heart J*. 2008;29:2000-5.
24. Bogaert J, Rademakers FE. Regional nonuniformity of normal adult human left ventricle. *Am J Physiol Heart Circ Physiol* 2001;280:H610-H620.
25. Haendchen RV, Wyatt HL, Maurer G, Zwehl W, Bear M, Meerbaum S *et al*. Quantitation of regional cardiac function by two-dimensional echocardiography. I. Patterns of contraction in the normal left ventricle. *Circulation* 1983;67:1234-45.
26. Kramer CM, Rogers WJ, Theobald TM, Power TP, Petruolo S, Reichek N. Remote Noninfarcted Region Dysfunction Soon After First Anterior Myocardial Infarction: A Magnetic Resonance Tagging Study. *Circulation* 1996;94:660-6.
27. Pflugfelder PW, Sechtem UP, White RD, Higgins CB. Quantification of regional myocardial function by rapid cine MR imaging. *Am J Roentgenol* 1988;150:523-9.
28. Rademakers FE, Rogers WJ, Guier WH, Hutchins GM, Siu CO, Weisfeldt ML *et al*. Relation of regional cross-fiber shortening to wall thickening in the intact heart. Three-dimensional strain analysis by NMR tagging. *Circulation* 1994;89:1174-82.
29. Sechtem U, Sommerhoff BA, Markiewicz W, White RD, Cheitlin MD, Higgins CB. Regional left ventricular wall thickening by magnetic resonance imaging: Evaluation in normal persons and patients with global and regional dysfunction. *Am J Cardiol.* 1987;59:145-51.
30. van Rugge FP, Holman ER, van der Wall EE, de Roos A, van der Laarse A, Bruschke AVG. Quantitation of global and regional left ventricular function by cine magnetic resonance imaging during dobutamine stress in normal human subjects. *Eur Heart J* 1993;14:456-63.
31. Gotte MJW, Germans T, Russel IK, Zwanenburg JJM, Marcus JT, van Rossum AC *et al*. Myocardial Strain and Torsion Quantified by Cardiovascular Magnetic Resonance Tissue Tagging: Studies in Normal and Impaired Left Ventricular Function. *J Am Coll Cardiol.* 2006;48:2002-11.
32. Kuijer JP, Marcus JT, Gotte MJ, van Rossum AC, Heethaar RM. Three-dimensional myocardial strains at end-systole and during diastole in the left ventricle of normal humans. *J Cardiovasc Magn Reson.* 2002;4:341-51.
33. Zwanenburg JJM, Gotte MJW, Kuijer JPA, Heethaar RM, van Rossum AC, Marcus JT. Timing of cardiac contraction in humans mapped by high-temporal-resolution MRI tagging: early onset and late peak of shortening in lateral wall. *Am J Physiol Heart Circ Physiol* 2004;286:H1872-H1880.
34. Burke AP, Virmani R. Pathophysiology of acute myocardial infarction. *Med Clin.North Am.* 2007;91:553-72.
35. Higgins CB, Herfkens R, Lipton MJ, Sievers R, Sheldon P, Kaufman L *et al*. Nuclear magnetic resonance imaging of acute myocardial infarction in dogs: alterations in magnetic relaxation times. *Am J Cardiol.* 1983;52:184-8.
36. McNamara MT, Higgins CB, Schechtmann N, Botvinick E, Lipton MJ, Chatterjee K *et al*. Detection and characterization of acute myocardial infarction in man with use of gated magnetic resonance. *Circulation.* 1985;71:717-24.

37. Wesbey G, Higgins CB, Lanzer P, Botvinick E, Lipton MJ. Imaging and characterization of acute myocardial infarction in vivo by gated nuclear magnetic resonance. *Circulation.* 1984;69:125-30.
38. Simonetti OP, Finn JP, White RD, Laub G, Henry DA. "Black blood" T2-weighted inversion-recovery MR imaging of the heart. *Radiology* 1996;199:49-57.
39. Abdel-Aty H, Zagrosek A, Schulz-Menger J, Taylor AJ, Messroghli D, Kumar A *et al*. Delayed Enhancement and T2-Weighted Cardiovascular Magnetic Resonance Imaging Differentiate Acute From Chronic Myocardial Infarction. *Circulation* 2004;109:2411-6.
40. Bogaert J, Dymarkowski S. Delayed contrast-enhanced MRI: use in myocardial viability assessment and other cardiac pathology. *Eur Radiol.* 2005;15 Suppl 2:B52-8.:B52-B58.
41. Marcu CB, Nijveldt R, Beek AM, van Rossum AC. Delayed contrast enhancement magnetic resonance imaging for the assessment of cardiac disease. *Heart Lung Circ.* 2007;16:70-8.
42. Peshock RM, Malloy CR, Buja LM, Nunnally RL, Parkey RW, Willerson JT. Magnetic resonance imaging of acute myocardial infarction: gadolinium diethylenetriamine pentaacetic acid as a marker of reperfusion. *Circulation* 1986;74:1434-40.
43. Schaefer S, Malloy CR, Katz J, Parkey RW, Buja LM, Willerson JT *et al*. Gadolinium-DTPA-enhanced nuclear magnetic resonance imaging of reperfused myocardium: identification of the myocardial bed at risk. *J.Am.Coll.Cardiol.* 1988;12:1064-72.
44. Tscholakoff D, Higgins CB, Sechtem U, McNamara MT. Occlusive and reperfused myocardial infarcts: effect of Gd-DTPA on ECG-gated MR imaging. *Radiology* 1986;160:515-9.
45. Kuo PH, Kanal E, Abu-Alfa AK, Cowper SE. Gadolinium-based MR contrast agents and nephrogenic systemic fibrosis. *Radiology.* 2007;242:647-9.
46. Swaminathan S, Horn TD, Pellowski D, Abul-Ezz S, Bornhorst JA, Viswamitra S *et al*. Nephrogenic systemic fibrosis, gadolinium, and iron mobilization. *N Engl J Med.* 2007;357:720-2.
47. Prakash A, Torres AJ, Printz BF, Prince MR, Nielsen JC. Usefulness of magnetic resonance angiography in the evaluation of complex congenital heart disease in newborns and infants. *Am J Cardiol.* 2007;100:715-21.
48. Schwitter J. Myocardial perfusion imaging by cardiac magnetic resonance. *J Nucl Cardiol.* 2006;13:841-54.
49. Nijveldt R, Beek AM, Hirsch A, Stoel MG, Hofman MB, Umans VA *et al*. Functional recovery after acute myocardial infarction: comparison between angiography, electrocardiography, and cardiovascular magnetic resonance measures of microvascular injury. *J Am Coll Cardiol.* 2008;52:181-9.
50. Schwitter J, Wacker CM, van Rossum AC, Lombardi M, Al Saadi N, Ahlstrom H *et al*. MR-IMPACT: comparison of perfusion-cardiac magnetic resonance with single-photon emission computed tomography for the detection of coronary artery disease in a multicentre, multivendor, randomized trial. *Eur Heart J.* 2008;29:480-9.
51. Elkington AG, Gatehouse PD, Cannell TM, Moon JC, Prasad SK, Firmin DN *et al*. Comparison of hybrid echo-planar imaging and FLASH myocardial perfusion cardiovascular MR imaging. *Radiology.* 2005;235:237-43.
52. Kellman P, Derbyshire JA, Agyeman KO, McVeigh ER, Arai AE. Extended coverage first-pass perfusion imaging using slice-interleaved TSENSE. *Magn Reson Med.* 2004;51:200-4.
53. Wang Y, Moin K, Akinboboye O, Reichek N. Myocardial first pass perfusion: steady-state free precession versus spoiled gradient echo and segmented echo planar imaging. *Magn Reson Med.* 2005;54:1123-9.
54. Giang TH, Nanz D, Coulden R, Friedrich M, Graves M, Al Saadi N *et al*. Detection of coronary artery disease by magnetic resonance myocardial perfusion imaging with various contrast medium doses: first european multi-centre experience. *Eur Heart J* 2004;25:1657-65.
55. Hsu LY, Rhoads KL, Holly JE, Kellman P, Aletras AH, Arai AE. Quantitative myocardial perfusion analysis with a dual-bolus contrast-enhanced first-pass MRI technique in humans. *J Magn Reson Imaging.* 2006;23:315-22.
56. Jerosch-Herold M, Seethamraju RT, Swingen CM, Wilke NM, Stillman AE. Analysis of myocardial perfusion MRI. *J Magn Reson Imaging.* 2004;19:758-70.

57. Judd RM, Lugo-Olivieri CH, Arai M, Kondo T, Croisille P, Lima JA *et al*. Physiological basis of myocardial contrast enhancement in fast magnetic resonance images of 2-day-old reperfused canine infarcts. *Circulation* 1995;92:1902-10.

58. Kim RJ, Chen EL, Lima JA, Judd RM. Myocardial Gd-DTPA kinetics determine MRI contrast enhancement and reflect the extent and severity of myocardial injury after acute reperfused infarction. *Circulation* 1996;94:3318-26.

59. Kim RJ, Fieno DS, Parrish TB, Harris K, Chen EL, Simonetti O *et al*. Relationship of MRI delayed contrast enhancement to irreversible injury, infarct age, and contractile function. *Circulation* 1999;100:1992-2002.

60. Klein C, Schmal TR, Nekolla SG, Schnackenburg B, Fleck E, Nagel E. Mechanism of late gadolinium enhancement in patients with acute myocardial infarction. *J Cardiovasc Magn Reson.* 2007;9:653-8.

61. Lima JA, Judd RM, Bazille A, Schulman SP, Atalar E, Zerhouni EA. Regional heterogeneity of human myocardial infarcts demonstrated by contrast-enhanced MRI. Potential mechanisms. *Circulation* 1995;92:1117-25.

62. Rehwald WG, Fieno DS, Chen EL, Kim RJ, Judd RM. Myocardial magnetic resonance imaging contrast agent concentrations after reversible and irreversible ischemic injury. *Circulation.* 2002;105:224-9.

63. Choi SI, Jiang CZ, Lim KH, Kim ST, Lim CH, Gong GY *et al*. Application of breath-hold T2-weighted, first-pass perfusion and gadolinium-enhanced T1-weighted MR imaging for assessment of myocardial viability in a pig model. *J Magn Reson Imaging.* 2000;11:476-80.

64. Li G, Xiang B, Dai G, Shaw A, Liu H, Yang B *et al*. Tissue oedema does not change gadolinium-diethylenetriamine pentaacetic acid (Gd-DTPA)-enhanced T1 relaxation times of viable myocardium. *J Magn Reson Imaging.* 2005;21:744-51.

65. de Roos A, Doornbos J, van der Wall EE, van Voorthuisen AE. MR imaging of acute myocardial infarction: value of Gd-DTPA. *AJR Am J Roentgenol.* 1988;150:531-4.

66. Rehr RB, Peshock RM, Malloy CR, Keller AM, Parkey RW, Buja LM *et al*. Improved in vivo magnetic resonance imaging of acute myocardial infarction after intravenous paramagnetic contrast agent administration. *Am J Cardiol.* 1986;57:864-8.

67. van Rossum AC, Visser FC, Van Eenige MJ, Sprenger M, Valk J, Verheugt FW *et al*. Value of gadolinium-diethylene-triamine pentaacetic acid dynamics in magnetic resonance imaging of acute myocardial infarction with occluded and reperfused coronary arteries after thrombolysis. *Am J Cardiol* 1990;65:845-51.

68. Nishimura T, Kobayashi H, Ohara Y, Yamada N, Haze K, Takamiya M *et al*. Serial assessment of myocardial infarction by using gated MR imaging and Gd-DTPA. *Am J Roentgenol.* 1989;153:715-20.

69. van der Wall EE, van Dijkman PR, de Roos A, Doornbos J, van der LA, Manger C, V *et al*. Diagnostic significance of gadolinium-DTPA (diethylenetriamine penta-acetic acid) enhanced magnetic resonance imaging in thrombolytic treatment for acute myocardial infarction: its potential in assessing reperfusion. *Br.Heart J.* 1990;63:12-7.

70. van Dijkman PR, van der Wall EE, de Roos A, Matheijssen NA, van Rossum AC, Doornbos J *et al*. Acute, subacute, and chronic myocardial infarction: quantitative analysis of gadolinium-enhanced MR images. *Radiology.* 1991;180:147-51.

71. Fieno DS, Kim RJ, Chen EL, Lomasney JW, Klocke FJ, Judd RM. Contrast-enhanced magnetic resonance imaging of myocardium at risk: distinction between reversible and irreversible injury throughout infarct healing. *J.Am.Coll.Cardiol.* 2000;36:1985-91.

72. Simonetti OP, Kim RJ, Fieno DS, Hillenbrand HB, Wu E, Bundy JM *et al*. An improved MR imaging technique for the visualization of myocardial infarction. *Radiology* 2001;218:215-23.

73. Mahrholdt H, Wagner A, Holly TA, Elliott MD, Bonow RO, Kim RJ *et al*. Reproducibility of chronic infarct size measurement by contrast-enhanced magnetic resonance imaging. *Circulation.* 2002;106:2322-7.

74. Thiele H, Kappl MJE, Conradi S, Niebauer J, Hambrecht R, Schuler G. Reproducibility of Chronic and Acute Infarct Size Measurement by Delayed Enhancement-Magnetic Resonance Imaging. *J Am Coll Cardiol.* 2006;47:1641-5.

75. Wagner A, Mahrholdt H, Thomson L, Hager S, Meinhardt G, Rehwald W *et al*. Effects of Time, Dose, and Inversion Time for Acute Myocardial Infarct Size Measurements Based on Magnetic Resonance

Imaging-Delayed Contrast Enhancement. *Journal of the American College of Cardiology* 2006;47:2027-33.

76. Gupta A, Lee VS, Chung YC, Babb JS, Simonetti OP. Myocardial infarction: optimization of inversion times at delayed contrast-enhanced MR imaging. *Radiology.* 2004;233:921-6.
77. Kellman P, Arai AE, McVeigh ER, Aletras AH. Phase-sensitive inversion recovery for detecting myocardial infarction using gadolinium-delayed hyperenhancement. *Magn Reson.Med.* 2002;47:372-83.
78. Sievers B, Elliott MD, Hurwitz LM, Albert TSE, Klem I, Rehwald WG *et al*. Rapid Detection of Myocardial Infarction by Subsecond, Free-Breathing Delayed Contrast-Enhancement Cardiovascular Magnetic Resonance. *Circulation* 2007;115:236-44.
79. Kuhl HP, Papavasiliu TS, Beek AM, Hofman MB, Heusen NS, van Rossum AC. Myocardial viability: rapid assessment with delayed contrast-enhanced MR imaging with three-dimensional inversion-recovery prepared pulse sequence. *Radiology.* 2004;230:576-82.
80. Nguyen TD, Spincemaille P, Weinsaft JW, Ho BY, Cham MD, Prince MR *et al*. A fast navigator-gated 3D sequence for delayed enhancement MRI of the myocardium: comparison with breathhold 2D imaging. *J Magn Reson Imaging.* 2008;27:802-8.
81. Kim RJ, Wu E, Rafael A, Chen EL, Parker MA, Simonetti O *et al*. The Use of Contrast-Enhanced Magnetic Resonance Imaging to Identify Reversible Myocardial Dysfunction. *N.Engl.J.Med.* 2000;343:1445-53.
82. Bondarenko O, Beek AM, Hofman MB, Kuhl HP, Twisk JW, van Dockum WG *et al*. Standardizing the definition of hyperenhancement in the quantitative assessment of infarct size and myocardial viability using delayed contrast-enhanced CMR. *J Cardiovasc Magn Reson.* 2005;7:481-5.
83. Amado LC, Gerber BL, Gupta SN, Rettmann DW, Szarf G, Schock R *et al*. Accurate and objective infarct sizing by contrast-enhanced magnetic resonance imaging in a canine myocardial infarction model. *J Am Coll Cardiol.* 2004;44:2383-9.
84. Beek AM, Bondarenko O, Afsharzada F, Van Rossum AC. Quantification of late gadolinium enhanced CMR in viability assessment in chronic ischemic heart disease: a comparison to functional outcome. *J Cardiovasc Magn Reson* 2009;11(1):6.
85. Heiberg E, Ugander M, Engblom H, Gotberg M, Olivecrona GK, Erlinge D *et al*. Automated quantification of myocardial infarction from MR images by accounting for partial volume effects: animal, phantom, and human study. *Radiology.* 2008;246:581-8.
86. Hsu LY, Natanzon A, Kellman P, Hirsch GA, Aletras AH, Arai AE. Quantitative myocardial infarction on delayed enhancement MRI. Part I: Animal validation of an automated feature analysis and combined thresholding infarct sizing algorithm. *J Magn Reson Imaging.* 2006;23:298-308.
87. Porto I, Selvanayagam J, Ashar V, Neubauer S, Banning AP. Safety of magnetic resonance imaging one to three days after bare metal and drug-eluting stent implantation. *Am J Cardiol.* 2005;96:366-8.
88. Schroeder AP, Houlind K, Pedersen EM, Thuesen L, Nielsen TT, Egeblad H. Magnetic resonance imaging seems safe in patients with intracoronary stents. *J Cardiovasc Magn Reson.* 2000;2:43-9.
89. White HD, Norris RM, Brown MA, Brandt PW, Whitlock RM, Wild CJ. Left ventricular end-systolic volume as the major determinant of survival after recovery from myocardial infarction. *Circulation.* 1987;76:44-51.
90. Bellenger NG, Davies LC, Francis JM, Coats AJ, Pennell DJ. Reduction in sample size for studies of remodeling in heart failure by the use of cardiovascular magnetic resonance. *J Cardiovasc Magn Reson.* 2000;2:271-8.
91. Grothues F, Smith GC, Moon JC, Bellenger NG, Collins P, Klein HU *et al*. Comparison of interstudy reproducibility of cardiovascular magnetic resonance with two-dimensional echocardiography in normal subjects and in patients with heart failure or left ventricular hypertrophy. *Am J Cardiol.* 2002;90:29-34.
92. Grothues F, Moon JC, Bellenger NG, Smith GS, Klein HU, Pennell DJ. Interstudy reproducibility of right ventricular volumes, function, and mass with cardiovascular magnetic resonance. *Am Heart J.* 2004;147:218-23.
93. McKay RG, Pfeffer MA, Pasternak RC, Markis JE, Come PC, Nakao S *et al*. Left ventricular remodeling after myocardial infarction: a corollary to infarct expansion. *Circulation.* 1986;74:693-702.

94. Epstein AE, DiMarco JP, Ellenbogen KA, Estes NA, III, Freedman RA, Gettes LS *et al*. ACC/AHA/HRS 2008 Guidelines for Device-Based Therapy of Cardiac Rhythm Abnormalities: a report of the American College of Cardiology/American Heart Association Task Force on Practice Guidelines (Writing Committee to Revise the ACC/AHA/NASPE 2002 Guideline Update for Implantation of Cardiac Pacemakers and Antiarrhythmia Devices) developed in collaboration with the American Association for Thoracic Surgery and Society of Thoracic Surgeons. *J Am Coll Cardiol.* 2008;51:e1-62.
95. Lim HS, Lip GY, Tse HF. Implantable cardioverter defibrillator following acute myocardial infarction: the '48-hour' and '40-day' rule. *Europace.* 2008;10:536-9.
96. Kumar A, Abdel-Aty H, Krioedemann I, Schulz-Menger J, Gross CM, Dietz R *et al*. Contrast-enhanced cardiovascular magnetic resonance imaging of right ventricular infarction. *J Am Coll Cardiol.* 2006;48:1969-76.
97. Mollet NR, Dymarkowski S, Volders W, Wathiong J, Herbots L, Rademakers FE *et al*. Visualization of Ventricular Thrombi With Contrast-Enhanced Magnetic Resonance Imaging in Patients With Ischemic Heart Disease. *Circulation* 2002;106:2873-6.
98. Srichai MB, Junor C, Rodriguez LL, Stillman AE, Grimm RA, Lieber ML *et al*. Clinical, imaging, and pathological characteristics of left ventricular thrombus: A comparison of contrast-enhanced magnetic resonance imaging, transthoracic echocardiography, and transesophageal echocardiography with surgical or pathological validation. *Am Heart J* 2006;152:75-84.
99. Schulz-Menger J, Gross M, Messroghli D, Uhlich F, Dietz R, Friedrich MG. Cardiovascular magnetic resonance of acute myocardial infarction at a very early stage. *J Am Coll Cardiol.* 2003;42:513-8.
100. Cury RC, Shash K, Nagurney JT, Rosito G, Shapiro MD, Nomura CH *et al*. Cardiac magnetic resonance with T2-weighted imaging improves detection of patients with acute coronary syndrome in the emergency department. *Circulation.* 2008;%19;118:837-44.
101. Stork A, Muellerleile K, Bansmann PM, Graessner J, Kaul M, Kemper J *et al*. Value of T2-weighted, first-pass and delayed enhancement, and cine CMR to differentiate between acute and chronic myocardial infarction. *Eur Radiol.* 2007;17:610-7.
102. Abdel-Aty H, Cocker M, Friedrich MG. Myocardial oedema is a feature of Tako-Tsubo cardiomyopathy and is related to the severity of systolic dysfunction: Insights from T2-weighted cardiovascular magnetic resonance. *Int.J Cardiol.* 2007.
103. Gagliardi MG, Bevilacqua M, Di Renzi P, Picardo S, Passariello R, Marcelletti C. Usefulness of magnetic resonance imaging for diagnosis of acute myocarditis in infants and children, and comparison with endomyocardial biopsy. *Am J Cardiol.* 1991;68:1089-91.
104. Bouchard A, Reeves RC, Cranney G, Bishop SP, Pohost GM. Assessment of myocardial infarct size by means of T2-weighted 1H nuclear magnetic resonance imaging. *Am Heart J.* 1989;117:281-9.
105. Dymarkowski S, Ni Y, Miao Y, Bogaert J, Rademakers F, Bosmans H *et al*. Value of t2-weighted magnetic resonance imaging early after myocardial infarction in dogs: comparison with bis-gadolinium-mesoporphyrin enhanced T1-weighted magnetic resonance imaging and functional data from cine magnetic resonance imaging. *Invest Radiol.* 2002;37:77-85.
106. Friedrich MG, Abdel-Aty H, Taylor A, Schulz-Menger J, Messroghli D, Dietz R. The salvaged area at risk in reperfused acute myocardial infarction as visualized by cardiovascular magnetic resonance. *J Am Coll Cardiol.* 2008;51:1581-7.
107. Aletras AH, Tilak GS, Natanzon A, Hsu LY, Gonzalez FM, Hoyt RF, Jr. *et al*. Retrospective determination of the area at risk for reperfused acute myocardial infarction with T2-weighted cardiac magnetic resonance imaging: histopathological and displacement encoding with stimulated echoes (DENSE) functional validations. *Circulation.* 2006;113:1865-70.
108. Janssens S, Dubois C, Bogaert J, Theunissen K, Deroose C, Desmet W *et al*. Autologous bone marrow-derived stem-cell transfer in patients with ST-segment elevation myocardial infarction: double-blind, randomised controlled trial. *Lancet.* 2006;367:113-21.
109. Arai AE. Using Magnetic Resonance Imaging to Characterize Recent Myocardial Injury: Utility in Acute Coronary Syndrome and Other Clinical Scenarios. *Circulation* 2008;118:795-6.
110. Keegan J, Gatehouse PD, Prasad SK, Firmin DN. Improved turbo spin-echo imaging of the heart with motion-tracking. *J Magn Reson Imaging.* 2006;24:563-70.

111. Kellman P, Aletras AH, Mancini C, McVeigh ER, Arai AE. T2-prepared SSFP improves diagnostic confidence in oedema imaging in acute myocardial infarction compared to turbo spin echo. *Magn Reson Med.* 2007;57:891-7.

112. Ibrahim T, Bulow HP, Hackl T, Hornke M, Nekolla SG, Breuer M *et al*. Diagnostic value of contrast-enhanced magnetic resonance imaging and single-photon emission computed tomography for detection of myocardial necrosis early after acute myocardial infarction. *J Am Coll Cardiol.* 2007;49:208-16.

113. Ricciardi MJ, Wu E, Davidson CJ, Choi KM, Klocke FJ, Bonow RO *et al*. Visualization of discrete microinfarction after percutaneous coronary intervention associated with mild creatine kinase-MB elevation. *Circulation.* 2001;103:2780-3.

114. Bruder O, Breuckmann F, Jensen C, Jochims M, Naber CK, Barkhausen J *et al*. Prognostic impact of contrast-enhanced CMR early after acute ST segment elevation myocardial infarction (STEMI) in a regional STEMI network: results of the "Herzinfarktverbund Essen". *Herz.* 2008;33:136-42.

115. Choi KM, Kim RJ, Gubernikoff G, Vargas JD, Parker M, Judd RM. Transmural extent of acute myocardial infarction predicts long-term improvement in contractile function. *Circulation.* 2001;104:1101-7.

116. Nijveldt R, Beek AM, Hofman MB, Umans VA, Algra PR, Spreeuwenberg MD *et al*. Late gadolinium-enhanced cardiovascular magnetic resonance evaluation of infarct size and microvascular obstruction in optimally treated patients after acute myocardial infarction. *J Cardiovasc Magn Reson.* 2007;9:765-70.

117. Assomull RG, Lyne JC, Keenan N, Gulati A, Bunce NH, Davies SW *et al*. The role of cardiovascular magnetic resonance in patients presenting with chest pain, raised troponin, and unobstructed coronary arteries. *Eur Heart J.* 2007;28:1242-9.

118. Garcia-Pavia P, Aguiar-Souto P, Silva-Melchor L, Cavero MA, Pastrana M, Goicolea J *et al*. Cardiac magnetic resonance imaging in the diagnosis of myocarditis mimicking myocardial infarction. *Int.J Cardiol.* 2006;%20;112:e27-e29.

119. Friedrich MG, Strohm O, Schulz-Menger J, Marciniak H, Luft FC, Dietz R. Contrast media-enhanced magnetic resonance imaging visualizes myocardial changes in the course of viral myocarditis. *Circulation.* 1998;97:1802-9.

120. Mahrholdt H, Goedecke C, Wagner A, Meinhardt G, Athanasiadis A, Vogelsberg H *et al*. Cardiovascular magnetic resonance assessment of human myocarditis: a comparison to histology and molecular pathology. *Circulation.* 2004;109:1250-8.

121. Mahrholdt H, Wagner A, Deluigi CC, Kispert E, Hager S, Meinhardt G *et al*. Presentation, patterns of myocardial damage, and clinical course of viral myocarditis. *Circulation.* 2006;114:1581-90.

122. Haghi D, Fluechter S, Suselbeck T, Kaden JJ, Borggrefe M, Papavassiliu T. Cardiovascular magnetic resonance findings in typical versus atypical forms of the acute apical ballooning syndrome (Takotsubo cardiomyopathy). *Int.J Cardiol.* 2007;120:205-11.

123. Wu E, Ortiz JT, Tejedor P, Lee DC, Bucciarelli-Ducci C, Kansal P *et al*. Infarct size by contrast enhanced cardiac magnetic resonance is a stronger predictor of outcomes than left ventricular ejection fraction or end-systolic volume index: prospective cohort study. *Heart.* 2008;94:730-6.

124. Braunwald E, Kloner RA. The stunned myocardium: prolonged, postischemic ventricular dysfunction. *Circulation.* 1982;66:1146-9.

125. Beek AM, Kuhl HP, Bondarenko O, Twisk JW, Hofman MB, van Dockum WG *et al*. Delayed contrast-enhanced magnetic resonance imaging for the prediction of regional functional improvement after acute myocardial infarction. *J Am Coll Cardiol.* 2003;42:895-901.

126. Shapiro MD, Nieman K, Nasir K, Nomura CH, Sarwar A, Ferencik M *et al*. Utility of cardiovascular magnetic resonance to predict left ventricular recovery after primary percutaneous coronary intervention for patients presenting with acute ST-segment elevation myocardial infarction. *Am J Cardiol.* 2007;100:211-6.

127. Bowen L. Applied Multilevel Analysis: A Practical Guide. Jos WR Twisk. *Int.J Epidemiol.* 2007.

128. Carlos ME, Smart SC, Wynsen JC, Sagar KB. Dobutamine stress echocardiography for risk stratification after myocardial infarction. *Circulation.* 1997;95:1402-10.

129. Nijland F, Kamp O, Verhorst PM, de Voogt WG, Visser CA. Early prediction of improvement in ejection fraction after acute myocardial infarction using low dose dobutamine echocardiography. *Heart.* 2002;88:592-6.

130. Previtali M, Fetiveau R, Lanzarini L, Cavalotti C, Klersy C. Prognostic value of myocardial viability and ischemia detected by dobutamine stress echocardiography early after acute myocardial infarction treated with thrombolysis. *J Am Coll Cardiol.* 1998;32:380-6.
131. Dendale PA, Franken PR, Waldman GJ, De Moor DG, Tombeur DA, Block PF *et al*. Low-dosage dobutamine magnetic resonance imaging as an alternative to echocardiography in the detection of viable myocardium after acute infarction. *Am Heart J.* 1995;130:134-40.
132. Geskin G, Kramer CM, Rogers WJ, Theobald TM, Pakstis D, Hu YL *et al*. Quantitative assessment of myocardial viability after infarction by dobutamine magnetic resonance tagging. *Circulation.* 1998;98:217-23.
133. Kramer CM, Malkowski MJ, Mankad S, Theobald TM, Pakstis DL, Rogers WJ, Jr. Magnetic resonance tagging and echocardiographic response to dobutamine and functional improvement after reperfused myocardial infarction. *Am Heart J.* 2002;143:1046-51.
134. Kloner RA, Ganote CE, Jennings RB. The "no-reflow" phenomenon after temporary coronary occlusion in the dog. *J Clin.Invest.* 1974;54:1496-508.
135. Reffelmann T, Kloner RA. The "no-reflow" phenomenon: basic science and clinical correlates. *Heart.* 2002;87:162-8.
136. Rochitte CE, Lima JA, Bluemke DA, Reeder SB, McVeigh ER, Furuta T *et al*. Magnitude and time course of microvascular obstruction and tissue injury after acute myocardial infarction. *Circulation.* 1998;98:1006-14.
137. Wu KC, Kim RJ, Bluemke DA, Rochitte CE, Zerhouni EA, Becker LC *et al*. Quantification and time course of microvascular obstruction by contrast-enhanced echocardiography and magnetic resonance imaging following acute myocardial infarction and reperfusion. *J Am Coll Cardiol.* 1998;32:1756-64.
138. Taylor AJ, Al Saadi N, Abdel-Aty H, Schulz-Menger J, Messroghli DR, Friedrich MG. Detection of acutely impaired microvascular reperfusion after infarct angioplasty with magnetic resonance imaging. *Circulation.* 2004;109:2080-5.
139. Bodi V, Sanchis J, Lopez-Lereu MP, Losada A, Nunez J, Pellicer M *et al*. Usefulness of a Comprehensive Cardiovascular Magnetic Resonance Imaging Assessment for Predicting Recovery of Left Ventricular Wall Motion in the Setting of Myocardial Stunning. *J Am Coll Cardiol.* 2005;46:1747-52.
140. Hombach V, Grebe O, Merkle N, Waldenmaier S, Hoher M, Kochs M *et al*. Sequelae of acute myocardial infarction regarding cardiac structure and function and their prognostic significance as assessed by magnetic resonance imaging. *Eur Heart J* 2005;26:549-57.
141. Baks T, van Geuns RJ, Biagini E, Wielopolski P, Mollet NR, Cademartiri F *et al*. Recovery of left ventricular function after primary angioplasty for acute myocardial infarction. *Eur Heart J.* 2005;26:1070-7.
142. Yan AT, Gibson CM, Larose E, Anavekar NS, Tsang S, Solomon SD *et al*. Characterization of microvascular dysfunction after acute myocardial infarction by cardiovascular magnetic resonance first-pass perfusion and late gadolinium enhancement imaging. *J Cardiovasc Magn Reson.* 2006;8:831-7.
143. Lund GK, Stork A, Saeed M, Bansmann MP, Gerken JH, Muller V *et al*. Acute myocardial infarction: evaluation with first-pass enhancement and delayed enhancement MR imaging compared with 201Tl SPECT imaging. *Radiology.* 2004;232:49-57.
144. Haager PK, Christott P, Heussen N, Lepper W, Hanrath P, Hoffmann R. Prediction of clinical outcome after mechanical revascularization in acute myocardial infarction by markers of myocardial reperfusion. *J Am Coll Cardiol.* 2003;%19;41:532-8.
145. Sakuma T, Hayashi Y, Sumii K, Imazu M, Yamakido M. Prediction of short- and intermediate-term prognoses of patients with acute myocardial infarction using myocardial contrast echocardiography one day after recanalization. *J Am Coll Cardiol.* 1998;32:890-7.
146. Sorajja P, Gersh BJ, Costantini C, McLaughlin MG, Zimetbaum P, Cox DA *et al*. Combined prognostic utility of ST-segment recovery and myocardial blush after primary percutaneous coronary intervention in acute myocardial infarction. *Eur Heart J.* 2005;26:667-74.
147. Wu KC, Zerhouni EA, Judd RM, Lugo-Olivieri CH, Barouch LA, Schulman SP *et al*. Prognostic significance of microvascular obstruction by magnetic resonance imaging in patients with acute myocardial infarction. *Circulation.* 1998;97:765-72.

148. Galiuto L, Garramone B, Scara A, Rebuzzi AG, Crea F, La Torre G *et al*. The extent of microvascular damage during myocardial contrast echocardiography is superior to other known indexes of post-infarct reperfusion in predicting left ventricular remodeling: results of the multicenter AMICI study. *J Am Coll Cardiol.* 2008;51:552-9.

149. Fishbein MC, Rit J, Lando U, Kanmatsuse K, Mercier JC, Ganz W. The relationship of vascular injury and myocardial haemorrhage to necrosis after reperfusion. *Circulation.* 1980;62:1274-9.

150. Asanuma T, Tanabe K, Ochiai K, Yoshitomi H, Nakamura K, Murakami Y *et al*. Relationship Between Progressive Microvascular Damage and Intramyocardial Haemorrhage in Patients With Reperfused Anterior Myocardial Infarction: Myocardial Contrast Echocardiographic Study. *Circulation.* 1997;96:448-53.

151. Lotan CS, Bouchard A, Cranney GB, Bishop SP, Pohost GM. Assessment of postreperfusion myocardial haemorrhage using proton NMR imaging at 1.5 T. *Circulation.* 1992;86:1018-25.

152. Parizel PM, Makkat S, Van Miert E, Van Goethem JW, van den HL, De Schepper AM. Intracranial haemorrhage: principles of CT and MRI interpretation. *Eur Radiol.* 2001;11:1770-83.

153. Ochiai K, Shimada T, Murakami Y, Ishibashi Y, Sano K, Kitamura J *et al*. Hemorrhagic myocardial infarction after coronary reperfusion detected in vivo by magnetic resonance imaging in humans: prevalence and clinical implications. *J Cardiovasc Magn Reson.* 1999;1:247-56.

154. Basso C, Corbetti F, Silva C, Abudureheman A, Lacognata C, Cacciavillani L *et al*. Morphologic Validation of Reperfused Hemorrhagic Myocardial Infarction by Cardiovascular Magnetic Resonance. *Am J Cardiol.* 2007;100:1322-7.

155. Beek AM, Nijveldt R, van Rossum AC. Intramyocardial haemorrhage and microvascular obstruction after primary percutaneous coronary intervention. In press *Int J CV. Imag* 2009.

156. Bowers TR, O'Neill WW, Grines C, Pica MC, Safian RD, Goldstein JA. Effect of reperfusion on biventricular function and survival after right ventricular infarction. *N Engl J Med.* 1998;338:933-40.

157. Larose E, Ganz P, Reynolds HG, Dorbala S, Di Carli MF, Brown KA et al. Right ventricular dysfunction assessed by cardiovascular magnetic resonance imaging predicts poor prognosis late after myocardial infarction. *J Am Coll Cardiol.* 2007;49:855-62.

158. Lloyd SG, Buckberg GD. Use of cardiac magnetic resonance imaging in surgical ventricular restoration. *Eur J Cardiothorac Surg.* 2006;29 Suppl 1:S216-24. Epub;%2006 Mar 24.:S216-S224.

159. Nijveldt R, Marcu CB, van Rossum AC. Lipomatous metaplasia in myocardial infarction detected by cardiovascular magnetic resonance. *Heart.* 2006;92:1337.

160. Schmitt M, Samani N, McCann G. Images in cardiovascular medicine. Lipomatous metaplasia in ischemic cardiomyopathy: a common but unappreciated entity. *Circulation.* 2007;116:e5-e6.

161. Baroldi G, Silver MD, De Maria R, Parodi O, Pellegrini A. Lipomatous metaplasia in left ventricular scar. *Can.J Cardiol.* 1997;13:65-71.

162. Baks T, van Geuns RJ, Biagini E, Wielopolski P, Mollet NR, Cademartiri F *et al*. Effects of primary angioplasty for acute myocardial infarction on early and late infarct size and left ventricular wall characteristics. *J Am Coll Cardiol.* 2006;47:40-4.

163. Jugdutt BI. Ventricular remodeling after infarction and the extracellular collagen matrix: when is enough enough? *Circulation.* 2003;108:1395-403.

164. Ertl G, Frantz S. Healing after myocardial infarction. *Cardiovasc Res.* 2005;66:22-32.

165. Moon JC, De Arenaza DP, Elkington AG, Taneja AK, John AS, Wang D *et al*. The pathologic basis of Q-wave and non-Q-wave myocardial infarction: a cardiovascular magnetic resonance study. *J Am Coll Cardiol.* 2004;44:554-60.

166. Asch FM, Shah S, Rattin C, Swaminathan S, Fuisz A, Lindsay J. Lack of sensitivity of the electrocardiogram for detection of old myocardial infarction: a cardiac magnetic resonance imaging study. *Am Heart J.* 2006;152:742-8.

167. Bayes dL, Cino JM, Pujadas S, Cygankiewicz I, Carreras F, Garcia-Moll X *et al*. Concordance of electrocardiographic patterns and healed myocardial infarction location detected by cardiovascular magnetic resonance. *Am J Cardiol.* 2006;97:443-51.

168. Soriano CJ, Ridocci F, Estornell J, Jimenez J, Martinez V, De Velasco JA. Noninvasive diagnosis of coronary artery disease in patients with heart failure and systolic dysfunction of uncertain etiology, using late gadolinium-enhanced cardiovascular magnetic resonance. *J Am Coll Cardiol.* 2005;45:743-8.
169. Mahrholdt H, Wagner A, Judd RM, Sechtem U, Kim RJ. Delayed enhancement cardiovascular magnetic resonance assessment of non-ischaemic cardiomyopathies. *Eur Heart J* 2005;26:1461-74.
170. Kwong RY, Chan AK, Brown KA, Chan CW, Reynolds HG, Tsang S *et al*. Impact of unrecognized myocardial scar detected by cardiac magnetic resonance imaging on event-free survival in patients presenting with signs or symptoms of coronary artery disease. *Circulation.* 2006;113:2733-43.
171. Roes SD, Kelle S, Kaandorp TA, Kokocinski T, Poldermans D, Lamb HJ *et al*. Comparison of myocardial infarct size assessed with contrast-enhanced magnetic resonance imaging and left ventricular function and volumes to predict mortality in patients with healed myocardial infarction. *Am J Cardiol.* 2007;100:930-6.
172. Yokota H, Heidary S, Katikireddy CK, Nguyen P, Pauly JM, McConnell MV *et al*. Quantitative characterization of myocardial infarction by cardiovascular magnetic resonance predicts future cardiovascular events in patients with ischemic cardiomyopathy. *J Cardiovasc Magn Reson.* 2008;10:17.
173. Schmidt A, Azevedo CF, Cheng A, Gupta SN, Bluemke DA, Foo TK *et al*. Infarct tissue heterogeneity by magnetic resonance imaging identifies enhanced cardiac arrhythmia susceptibility in patients with left ventricular dysfunction. *Circulation.* 2007;115:2006-14.
174. Yan AT, Shayne AJ, Brown KA, Gupta SN, Chan CW, Luu TM *et al*. Characterization of the peri-infarct zone by contrast-enhanced cardiac magnetic resonance imaging is a powerful predictor of post-myocardial infarction mortality. *Circulation.* 2006;114:32-9.
175. Bogun F, Desjardins B, Crawford T, Good E, Jongnarangsin K, Oral H *et al*. Post-Infarction Ventricular Arrhythmias Originating in Papillary Muscles. *J Am Coll Cardiol.* 2008;51:1794-802.
176. Allman KC, Shaw LJ, Hachamovitch R, Udelson JE. Myocardial viability testing and impact of revascularization on prognosis in patients with coronary artery disease and left ventricular dysfunction: a meta-analysis. *J Am Coll Cardiol.* 2002;39:1151-8.
177. Camici PG, Prasad SK, Rimoldi OE. Stunning, hibernation, and assessment of myocardial viability. *Circulation.* 2008;117:103-14.
178. Selvanayagam JB, Jerosch-Herold M, Porto I, Sheridan D, Cheng AS, Petersen SE *et al*. Resting myocardial blood flow is impaired in hibernating myocardium: a magnetic resonance study of quantitative perfusion assessment. *Circulation.* 2005;112:3289-96.
179. Baer FM, Theissen P, Schneider CA, Voth E, Sechtem U, Schicha H *et al*. Dobutamine magnetic resonance imaging predicts contractile recovery of chronically dysfunctional myocardium after successful revascularization. *J Am Coll Cardiol.* 1998;31:1040-8.
180. Cwajg JM, Cwajg E, Nagueh SF, He ZX, Qureshi U, Olmos LI *et al*. End-diastolic wall thickness as a predictor of recovery of function in myocardial hibernation: relation to rest-redistribution T1-201 tomography and dobutamine stress echocardiography. *J Am Coll Cardiol.* 2000;35:1152-61.
181. Schinkel AF, Bax JJ, Boersma E, Elhendy A, Vourvouri EC, Roelandt JR *et al*. Assessment of residual myocardial viability in regions with chronic electrocardiographic Q-wave infarction. *Am Heart J.* 2002;144:865-9.
182. Kim RJ, Shah DJ. Fundamental concepts in myocardial viability assessment revisited: when knowing how much is "alive" is not enough. *Heart.* 2004;90:137-40.
183. Baer FM, Voth E, Schneider CA, Theissen P, Schicha H, Sechtem U. Comparison of low-dose dobutamine-gradient-echo magnetic resonance imaging and positron emission tomography with [18F]fluorodeoxyglucose in patients with chronic coronary artery disease. A functional and morphological approach to the detection of residual myocardial viability. *Circulation.* 1995;91:1006-15.
184. Cigarroa CG, deFilippi CR, Brickner ME, Alvarez LG, Wait MA, Grayburn PA. Dobutamine stress echocardiography identifies hibernating myocardium and predicts recovery of left ventricular function after coronary revascularization. *Circulation.* 1993;88:430-6.
185. Bax JJ, Poldermans D, Elhendy A, Boersma E, Rahimtoola SH. Sensitivity, specificity, and predictive accuracies of various noninvasive techniques for detecting hibernating myocardium. *Curr.Probl.Cardiol.* 2001;26:147-86.

186. Bondarenko O, Beek AM, Nijveldt R, McCann GP, van Dockum WG, Hofman MB *et al*. Functional outcome after revascularization in patients with chronic ischemic heart disease: a quantitative late gadolinium enhancement CMR study evaluating transmural scar extent, wall thickness and periprocedural necrosis. *J Cardiovasc Magn Reson.* 2007;9:815-21.
187. Schvartzman PR, Srichai MB, Grimm RA, Obuchowski NA, Hammer DF, McCarthy PM *et al*. Nonstress delayed-enhancement magnetic resonance imaging of the myocardium predicts improvement of function after revascularization for chronic ischemic heart disease with left ventricular dysfunction. *Am Heart J.* 2003;146:535-41.
188. Selvanayagam JB, Kardos A, Francis JM, Wiesmann F, Petersen SE, Taggart DP *et al*. Value of delayed-enhancement cardiovascular magnetic resonance imaging in predicting myocardial viability after surgical revascularization. *Circulation.* 2004;110:1535-41.
189. Bove CM, DiMaria JM, Voros S, Conaway MR, Kramer CM. Dobutamine response and myocardial infarct transmurality: functional improvement after coronary artery bypass grafting--initial experience. *Radiology.* 2006;240:835-41.
190. Knuesel PR, Nanz D, Wyss C, Buechi M, Kaufmann PA, von Schulthess GK *et al*. Characterization of dysfunctional myocardium by positron emission tomography and magnetic resonance: relation to functional outcome after revascularization. *Circulation.* 2003;108:1095-100.
191. Kuhl HP, Lipke CS, Krombach GA, Katoh M, Battenberg TF, Nowak B *et al*. Assessment of reversible myocardial dysfunction in chronic ischaemic heart disease: comparison of contrast-enhanced cardiovascular magnetic resonance and a combined positron emission tomography-single photon emission computed tomography imaging protocol. *Eur Heart J.* 2006;27:846-53.
192. Wellnhofer E, Olariu A, Klein C, Grafe M, Wahl A, Fleck E *et al*. Magnetic resonance low-dose dobutamine test is superior to SCAR quantification for the prediction of functional recovery. *Circulation.* 2004;109:2172-4.
193. Wu YW, Tadamura E, Yamamuro M, Kanao S, Marui A, Tanabara K *et al*. Comparison of contrast-enhanced MRI with (18)F-FDG PET/201Tl SPECT in dysfunctional myocardium: relation to early functional outcome after surgical revascularization in chronic ischemic heart disease. *J Nucl Med.* 2007;48:1096-103.
194. Klein C, Nekolla SG, Bengel FM, Momose M, Sammer A, Haas F *et al*. Assessment of myocardial viability with contrast-enhanced magnetic resonance imaging: comparison with positron emission tomography. *Circulation.* 2002;105:162-7.
195. Kuhl HP, Beek AM, van der Weerdt AP, Hofman MB, Visser CA, Lammertsma AA *et al*. Myocardial viability in chronic ischemic heart disease: comparison of contrast-enhanced magnetic resonance imaging with (18)F-fluorodeoxyglucose positron emission tomography. *J Am Coll Cardiol.* 2003;41:1341-8.
196. Bilchick KC, Dimaano V, Wu KC, Helm RH, Weiss RG, Lima JA, *et al.* Cardiac magnetic resonance assessment of dyssynchrony and myocardial scar predicts function class improvement following cardiac resynchronization therapy. *JACC: Cardiovascular Imaging* 2008 Sep;1(5):561-8.
197. Koos R, Neizel M, Schummers G, Krombach GA, Stanzel S, Gunther RW, *et al.* Feasibility and initial experience of assessment of mechanical dyssynchrony using cardiovascular magnetic resonance and semi-automatic border detection. *J Cardiovasc Magn Reson* 2008;10(1):49.
198. Bleeker GB, Kaandorp TAM, Lamb HJ, Boersma E, Steendijk P, de Roos A, *et al*. Effect of Posterolateral Scar Tissue on Clinical and Echocardiographic Improvement After Cardiac Resynchronization Therapy. *Circulation* 2006 Feb 21;113(7):969-76.
199. White JA, Yee R, Yuan X, Krahn A, Skanes A, Parker M, *et al*. Delayed Enhancement Magnetic Resonance Imaging Predicts Response to Cardiac Resynchronization Therapy in Patients With Intraventricular Dyssynchrony. *J Am Coll Cardiol* 2006 Nov 21;48(10):1953-60.

Chapter 2

Delayed contrast-enhanced magnetic resonance imaging for the prediction of regional functional improvement after acute myocardial infarction

Aernout M. Beek, Harald P. Kühl, Olga Bondarenko, Jos W.R. Twisk, Mark B.M. Hofman, Willem G. van Dockum, Cees A. Visser, Albert C. van Rossum

J Am Coll Cardiol 2003;42:895-901

ABSTRACT

Objectives. We evaluated whether delayed contrast enhanced magnetic resonance imaging (DCE-MRI) using an extracellular contrast agent could predict improvement of dysfunctional but viable myocardium after acute reperfused myocardial infarction (MI).

Background. The transmural extent of hyperenhancement at DCE-MRI has been related to improvement of function in reperfused myocardial infarction. However, evidence is still limited and earlier reports have produced conflicting results regarding the significance of contrast patterns after infarction.

Methods. Thirty patients (mean age 59±11 years, 27 males) underwent cine MRI and DCE-MRI 7±3 days after a first reperfused acute MI and follow-up cine MRI at 13±3 weeks. Segmental wall thickening and segmental extent of hyperenhancement were scored in 1689 segments.

Results. Of 500 dysfunctional segments, 273 (55%) improved at follow-up. There was no difference in likelihood of improvement or complete functional recovery between segments with 0 and 1-25% hyperenhancement. The likelihood of improvement of segments without hyperenhancement was 2.9, 14.3 and 20 times higher than that of segments with 26-50%, 51-75% and >75% hyperenhancement, respectively ($p<0.001$). The likelihood of complete functional recovery of segments without hyperenhancement was 3.8, 11.1 and 50 times higher than that of segments with 26-50%, 51-75% and >75% hyperenhancement, respectively ($p<0.001$).

Conclusions. In patients with recent reperfused MI, functional improvement of stunned myocardium is predicted by delayed contrast enhanced MRI.

Acknowledgements

This study was supported by the Netherlands Heart Foundation (grant 2001.158).

INTRODUCTION

The recognition of stunned myocardium early after acute myocardial infarction has important prognostic and therapeutic implications(1). Using low-dose dobutamine echocardiography and ^{18}F-fluorodeoxyglucose-positron emission tomography a subgroup of patients with residual myocardial viability has been identified that is at high risk for future clinical events(2;3). Contrast-enhanced magnetic resonance imaging (MRI) using an extracellular contrast agent like gadolinium-diethylenetriamine pentaacetic acid (Gd-DTPA) has been applied extensively for the evaluation of myocardial injury after acute myocardial infarction(4-11). In a recent series of studies using canine infarction models, it has been shown that hyperenhancement on T1-weighted delayed contrast-enhanced (DCE-)MRI (originally described as images acquired more than 10 minutes after contrast injection) only occurred in necrotic, irreversibly injured myocardium, irrespective of the age of the infarct(12,13). The high signal intensity is related to a regional increased concentration of the contrast agent, most likely caused by ischemia-related changes in volume of distribution and contrast-kinetics (14-16). The regional extent of hyperenhancement has been shown to predict functional improvement of stunned myocardium, both in a canine model and recently also in patients with reperfused myocardial infarction(10,11,17). However, evidence is still limited and earlier reports have produced conflicting results on the significance of contrast patterns after myocardial infarction. Several investigators have demonstrated that the hyperenhanced region overestimates the actual necrotic region, and that it contains residual viable myocardium that may recover function when adequately reperfused(8,18,19). Comparison between these studies is hampered by considerable methodological differences, including the MRI technique that was used, the contrast dose, and the clinical or experimental setting. The current standard DCE-MRI technique combines optimal image quality, high spatial resolution and contrast-to-noise, and is a promising tool for the transmural evaluation of myocardial viability(10,11,20). We therefore conducted a prospective study to evaluate the role of this DCE-MRI technique in the prediction of functional improvement in patients with first acute myocardial infarction.

METHODS

Patient population. Patients were eligible for the study if admitted with first acute myocardial infarction according to standard electrocardiogram (ECG) and enzymatic criteria. Only patients with direct (coronary catheterization, TIMI (Thrombolysis In Myocardial Infarction) flow grade 3 in the infarct related artery) or indirect (rapid decrease of symptoms and more than fifty % resolution of ST-elevation on ECG, either during or

after thrombolytic therapy or spontaneous) evidence of successful reperfusion were included. Exclusion criteria were hemodynamic instability, failure to give informed consent or any relative or absolute contra-indication for MRI. The study is part of a larger project evaluating the current role of contrast-enhanced MRI in patients with (suspected) ischemic heart disease, that was approved by the Committee on Research Involving Human Subjects of the VU Medical Center. Thirty-nine patients were initially enrolled. Nine patients were excluded from the final analysis: 1 patient had significant valvular disease, 4 patients were lost to follow-up, and 4 patients had insufficient image quality of either baseline or follow-up MRI study. The clinical characteristics of the remaining 30 patients are listed in table 1. Five patients (4 spontaneous symptom and ECG resolution, 1 thrombolysis) were revascularized between the baseline and follow-up MRI study. In three of these, PTCA of the infarct related artery was performed before discharge because of symptomatic ischemia during exercise testing. Two patients were readmitted with unstable angina pectoris with negative cardiac enzymes, and underwent PTCA (of the infarct related artery) and CABG respectively.

MRI. All MRI procedures were performed with the patient in supine position in a 1.5 Tesla clinical scanner (Sonata/Vision, Siemens, Erlangen, Germany) using a 4-elements phased array cardiac receiver coil. ECG-gated images were acquired during repeated breath-holds of varying duration depending on heart rate (~ 10 seconds). Cine images using a segmented gradient-echo sequence (6 mm slice thickness) were obtained in multiple short-axis views every 10 mm covering the whole left ventricle. Ten to fifteen minutes after injection of a gadolinium-based contrast agent (Magnevist, Schering; 0.2 mmol/kg) DCE images were acquired in the same orientation as the cine images using a segmented inversion-recovery gradient-echo pulse sequence (TR/TE 9.6/4.4 ms, FA 25°, matrix 208x256 and a typical voxel size of 1.6x1.3x5.0 mm, TI 250-300 msec). The baseline study was performed 7 ± 3 days after admission, with follow-up at 13±3 weeks. DCE images were acquired only during the baseline study.

Data analysis. All data were analyzed on a separate workstation (Sun Microsystems, Inc., Santa Clara, California) using a dedicated software package (Mass, Medis, Leiden, The Netherlands). Baseline cine images and contrast-enhanced images were matched by using slice position, since both data sets were acquired during the same imaging session. Registration of follow-up to baseline cine images was achieved by consensus of 2 observers using various anatomic landmarks, including the septal insertion sites of the right ventricle, the papillary muscles, and trabecularization patterns in right and left ventricle. Images were then analyzed by consensus of two observers, who were blinded to patient data and the results of the other examinations.

Segmental analysis. For analysis of segmental function and contrast pattern the two most basal and two most distal slices were excluded, because short axis images at these levels preclude a reliable segmental evaluation due to presence of the left ventricular outflow tract and small diameter, respectively. Each short axis was divided in twelve equi-angular segments, starting at the posterior septal insertion of the right ventricle. Segmental wall thickening (SWT) was scored according to the following scale: 1 – normal, 2 – mild hypokinesis, 3 – severe hypokinesis, 4 – akinesis, 5 – dyskinesis. Functional improvement was defined as a decrease in SWT-score of ≥1. Complete recovery was defined as a decrease to SWT-score 1. Interobserver variability (AMB,HPK) was tested in 10 patients (532 segments).

For analysis of the DCE images the segmental extent of hyperenhancement (SEH) was calculated by dividing the hyperenhanced area by the total area of the predefined segment expressed as percentage. Any subendocardial area of hypoenhancement within the hyperenhanced area was considered part of the hyperenhanced area. SEH was then scored as follows: 1 – 0%, 2 – 1-25%, 3 – 25-50%, 4 – 51-75%, 5 – 76-100% hyperenhancement(10). To explore the relation between DCE-MRI and change in ejection fraction, we calculated a viability score in each patient, as: the total number of segments with baseline wall thickening abnormality and SEH-score ≤2, divided by all segments with baseline wall thickening abnormality.

Table 1. Patient characteristics

Number patients	30
Male	28
Age	59±11
Infarct site ECG	
anterior	13
inferior (-lateral)	11
posterior	6
Maximum total CK	2190±1364
Maximum MB-fraction	178±110
Ejection fraction base-line(%)	51±9
Thrombolysis	5
Primary PTCA	18
Days between admission and base-line MRI	7±3
Weeks between admission and follow-up MRI	13±3

CK = creatine kinase; PTCA = percutaneous coronary transluminal angioplasty

The assessment of contrast images and the size of the hyperenhanced areas are sensitive to image window setting. To eliminate the influence of subjective window setting, SEH was scored again after thresholding the images at 6 SD above signal intensity of the opposite, non-infarcted myocardium in the same slice (SEH_{th}). The choice of 6 SD as the cut-off value was based on our own clinical experience and recent literature(21). To test the inter-observer variability (AMB,OB), SEH was scored independently in 5 patients (299 segments), with window setting adjusted to personal preference.

Global analysis. On all short axis cine slices the endocardial and epicardial borders were outlined manually in end-diastolic and end-systolic images, excluding trabeculae and papillary muscles. Ejection fraction was calculated as follows: (end-diastolic volume – end-systolic volume)/end-diastolic volume.

Statistical analysis. The paired sample t-test and the independent samples t-test were used to compare means within the study group or between subgroups. We used kappa values to assess interobserver variability and enhancement score (SEH and SEH_{th}) variability. Since wall thickening scores within one patient are strongly related, we used multilevel logistic regression to evaluate the relation between change in wall thickening and baseline hyperenhancement-score (MlwiN, version 1.02.0002)(22,23). Multilevel analysis can be considered an extension to the commonly used repeated measures ANOVA that has the disadvantage that only a continuous outcome variable can be analyzed. Furthermore, repeated measures ANOVA requires a fully balanced dataset, and only corrects for correlated observations at one level. In this study, two dichotomous outcome variables were analyzed (improvement and complete recovery), with correlated observations at two levels (i.e. slices within patients and segments within slices). A correction was made for baseline wall thickening-scores, and the regression equation was used to calculate odds ratio's that expressed the likelihood of improvement relative to functional outcome of segments without hyperenhancement (SEH-score 1). The relation between change in ejection fraction and various patient variables was evaluated using logistic regression.

RESULTS

A total of 1740 segments (4.8 slices/patient) were available for analysis. During the analysis, 51 (3%) segments were additionally excluded because assessment was considered not reliable on any of the cine or contrast images by at least one of the two observers (e.g. presence of left ventricular outflow tract, localized artifacts).

Cine MRI. Of 1689 segments, 500 (30%) showed a baseline wall thickening abnormality. In these, baseline mean SWT-score was 3.2±0.9. At follow-up, mean SWT-score had decreased to 2.5 ± 1.3 ($p<0.001$ vs. baseline). Fifty-five percent (273 of 500) of segments improved at follow-up, 7% (36) worsened, and 38% (191) remained unchanged.

Interobserver agreement for the assessment of segmental wall thickening was 85% (kappa = 0.69).

DCE-MRI. Twenty-nine patients showed regional hyperenhancement, and in all patients, the area corresponded to the electrocardiographic infarct location. One patient with a small inferior infarction (maximum CK 426) had no regional hyperenhancement. The interobserver agreement for the assessment of segmental extent of hyperenhancement was 87% (kappa=0.76).

Segments that improved had lower mean SEH-score than segments that did not improve (2.4±1.3 vs. 3.7±1.4; $p<0.001$). The functional change according to segmental extent of hyperenhancement is shown in figure 1a and table 2. Of 151 segments with ≤25% hyperenhancement that improved, 119 (79%) had complete functional recovery, 25 (17%) residual mild hypokinesis, and 7 (5%) residual severe hypokinesis. Of the 31 segments with >75% hyperenhancement that improved, only 4 (13%) had complete functional recovery, 9 (29%) residual mild hypokinesis, and 17 (55%) initially akinetic segments and 1 initially dyskinetic segment had residual severe hypokinesis. Figure 2 illustrates the relation between hyperenhancement and change in wall thickening in a patient with recent anterior myocardial infarction (see also electronic data supplement J Am Coll Cardiol 2003;42:895-901).

Table 2. Number of segments with functional improvement and complete recovery (CR) at follow-up according to baseline SEH and SEH_{th}-score.

SEH						
	total	108	92	105	70	125
	improved	83	68	70	21	31
	CR	69	50	36	10	4
SEH_{th}						
	total	120	74	87	55	164
	improved	82	53	65	17	56
	CR	70	39	41	7	12
SEH/SEH_{th}-score		1	2	3	4	5

Also see Figure 2.
CR = complete recovery; SEH = segmental extent of hyperenhancement; SEH_{th} = SEH scored after thresholding the Images at 6 SD above signal intensity of opposite, non-infarcted myocardium in the same slice.

Multilevel analysis showed that the inverse relation between likelihood of improvement and segmental extent of hyperenhancement was highly significant. Functional outcome in relation to contrast-score is shown in table 3. Outcome was comparable in segments with SEH-score 1 and 2. The likelihood of partial or complete functional recovery of segments without hyperenhancement (SEH-score 1) was significantly higher than of segments with

SEH-scores 3, 4 and 5. Segments without hyperenhancement were 20 and 50 times more likely to have partial or complete recovery of function respectively, than segments with >75% hyperenhancement (see table 3).

Analysis using standardized window setting (SEHth). The overall agreement between the SEH-score and the SEHth-score was 85% (kappa=0.70). Agreement was lower when only the 500 segments with abnormal baseline wall thickening were taken into account: 64% (SEH< SEHth in 24% of segments, SEH>SEHth in 12% of segments) (kappa=0.55). The functional change according to baseline SEHth is shown in figure 1b and table 2. Multilevel analysis showed that the likelihood of partial or complete functional recovery was similar for SEHth-scores 1, 2 and 3, and was significantly lower for SEHth-scores 4 and 5 (table 3).

Subendocardial dark zone. Sixty-five segments had a subendocardial zone of low signal intensity within the hyperenhanced region. Mean wall thickening score at baseline in these segments was high (3.8 ± 0.5), and remained high at follow-up (3.8 ± 0.6; p=NS). Only 10 of these (15%) showed improvement: 6 initially akinetic segments had residual severe hypokinesis, 3 akinetic segments had residual mild hypokinesis and only 1 segment had complete recovery. Of the remaining 55 segments, 45 remained akinetic, 1 remained severely hypokinetic, and 9 worsened.

Table 3. Multilevel logistic regression analysis*

		improvement		complete recovery	
		OR	p	OR	p
SEH-score	2	0.63 (0.26-1.55)	0.32	0.81 (0.36-1.82)	0.61
	3	0.35 (0.14-0.88)	0.03	0.26 (0.11-0.59)	0.00
	4	0.07 (0.03-0.20)	0.00	0.09 (0.03-0.26)	0.00
	5	0.05 (0.02-0.13)	0.00	0.02 (0.01-0.11)	0.00
SEH_{th}-score	2	0.66 (0.26-1.55)	0.32	0.70 (0.31-1.61)	0.41
	3	0.79 (0.34-1.86)	0.59	0.52 (0.22-1.23)	0.14
	4	0.12 (0.04-0.34)	0.00	0.10 (0.03-0.37)	0.00
	5	0.09 (0.04-0.23)	0.00	0.03 (0.01-0.11)	0.00

*Odds ratios (95% confidence interval) represent likelihood of improvement or recovery relative to outcome of segments with SEH- and SEH_{th}-score 1.
Odds ratio (OR) = EXP (regression coefficient). Other abbreviations as in Table 2.

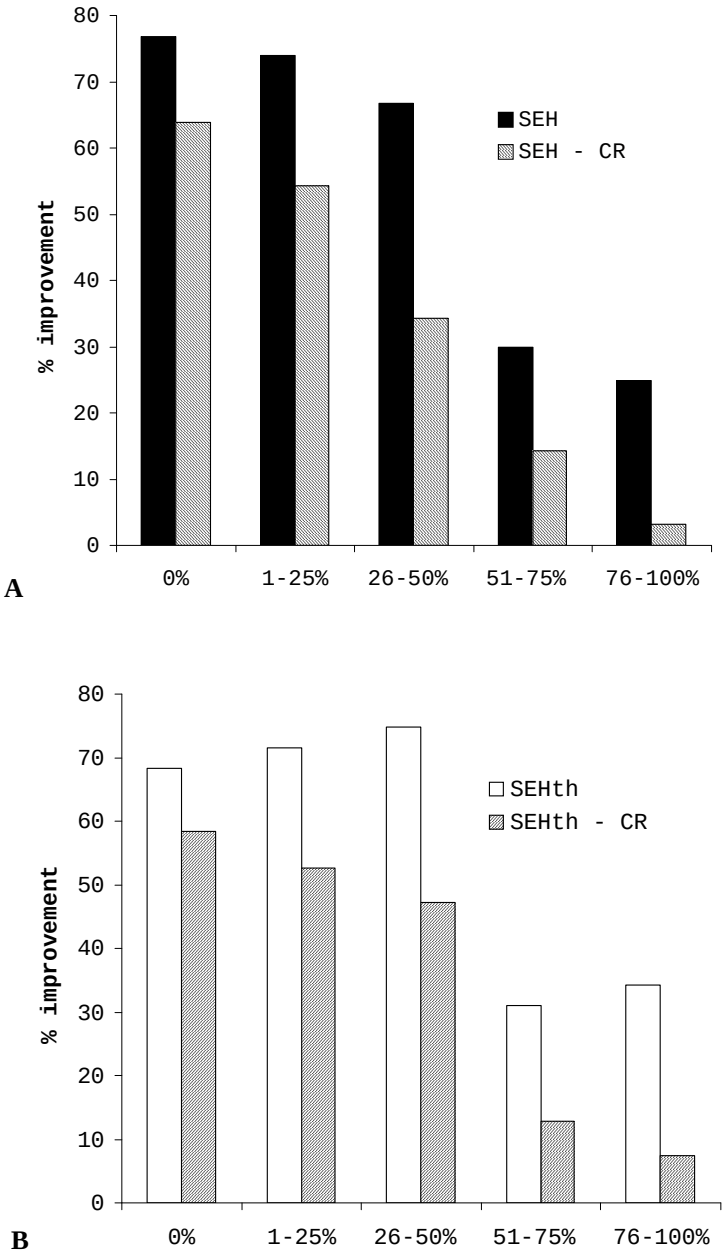

Figure 1. Functional outcome of dysfunctional segments according to baseline segmental extent of hyperenhancement (A: SEH; B: SEH_{th}). CR = complete recovery. Also see table 2.

Left ventricular ejection fraction. Overall ejection fraction did not change at follow-up (0.51±0.09 vs 0.53±0.10, p=NS). Previous studies have reported a significant relation between the percentage dysfunctional but viable myocardium and the change in ejection fraction(10,21). We tested multiple patient- and scan-related variables for their ability to predict the change in ejection fraction at follow-up: age, baseline ejection fraction, maximum CK, maximum CK-MB, the presence of a dark zone, and the viability score. No significant predictors of change in ejection fraction could be identified (table 4). However, the study group was small, and some variables (the viability score, presence of a dark zone) might have reached statistical significance with a larger study group size.

Table 4. Logistic regression analysis for the prediction of the change in ejection fraction

	Odds Ratio	95% confidence interval	p-value
age	1.00	0.93-1.08	0.93
CK	0.86	0.44-1.68	0.65
MB	1.15	0.44-3.00	0.77
presence of dark zone	2.40	0.48-12.13	0.29
viabilityscore (SEH ≤2)	1.40	0.95-2.07	0.10

CK = creatine kinase; SEH = segmental extent of hyperenhancement.

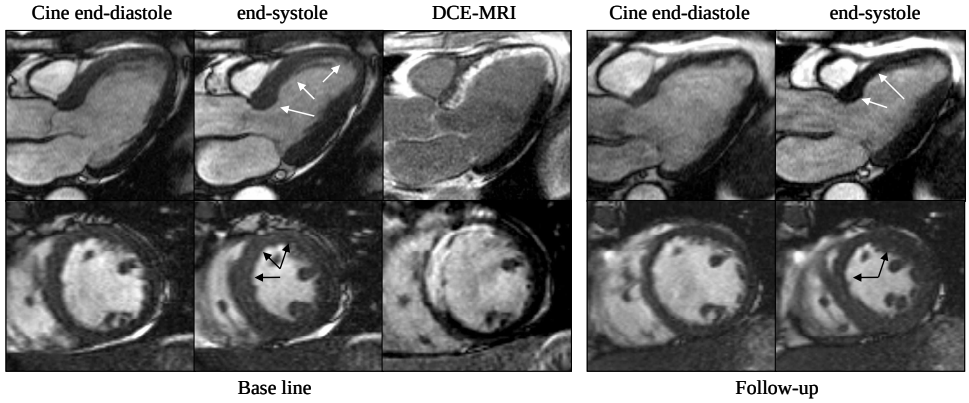

Figure 2. Three chamber view and short axis in a patient 5 days and 12 weeks after primary PTCA plus stenting of the left anterior descending coronary artery for anterior myocardial infarction. Baseline cine (**left**) shows severe wall thickening abnormality (**black arrows**) in the anteroseptal, anterior and apical region. Follow-up cine (**right**) shows partial functional recovery in varying degrees in areas with subendocardial hyperenhancement. The larger part of the area with transmural hyperenhancement remains akinetic, although there is some improvement in the mid-section of the anteroseptum (**white arrows**). To view cines in motion, please see the accompanying videos corresponding to Figure 2 (*J Am Coll Cardiol 2003;42:895-901*).

DISCUSSION

This study shows that DCE-MRI can be used to predict improvement of dysfunctional but viable myocardium in patients with recent reperfused MI. The likelihood of functional improvement decreased with increasing SEH. Multilevel logistic regression analysis, which takes into account the fact that segments within one patient and one slice are strongly correlated, showed that this inverse relation was highly significant.

Hyperenhancement after recent myocardial infarction. High resolution experimental studies that used the current standard DCE-MRI technique have demonstrated that hyperenhanced areas correlate exclusively with irreversibly damaged, necrotic myocardium, at various time intervals after infarction and irrespective of the status of the infarct related artery (12,13). Hillenbrand et al. used a canine infarction model to evaluate functional recovery after various occlusion times, and found that both likelihood of improvement and change in absolute wall thickening were predicted by the transmural extent of hyperenhancement (17). Using electron probe x-ray microanalysis, Rehwald et al. showed that elevations in Gd-DTPA concentration only occur in regions with histologically proven irreversible ischemic damage (16). Our data are in line with these experimental and two recent clinical studies that used the same MRI-technique to evaluate viability after recent myocardial infarction. Choi et al. studied 24 patients one week and 16±6 weeks after infarction and found that the transmural extent of hyperenhancement strongly predicted functional improvement (10). Gerber at al. evaluated 20 patients with contrast-enhanced MRI and myocardial tagging, and found that improvement in circumferential shortening was inversely related to the regional extent of hyperenhancement at delayed imaging (11). Compared with Choi et al., we found that more segments with >75% hyperenhancement improved at follow-up (25% (31/125) versus 5% (3/64)), although the majority of these segments had severe residual dysfunction and only four had complete recovery. Gerber et al. reported the mean functional improvement but did not state the percentage of segments with >75% hyperenhancement that improved. Hillenbrand et al. also found some improvement (12%) in segments with extensive enhancement in their canine experiment (17). Results of the highly detailed experimental studies make it unlikely that Gd-DTPA accumulates in reversibly damaged myocardium, although one cannot entirely exclude the possibility that distribution of Gd-DTPA in human and canine infarcts is different. However, several other factors may have played a role.

An important issue and potential source of error was recently evaluated by Oshinski et al, who found that MRI overestimated infarct size in a rat-model of reperfused infarction when images were acquired too early after contrast injection (24). However, these authors used a different pulse sequence (single slice spin-echo sequence with an acquisition time of 2-3 minutes) with a fixed inversion time and a different contrast dose (0.03 mmol/kg),

interferes with extrapolation of their results to our study (25). In the literature, the time between contrast injection and data acquisition varies considerably, between 5-30 minutes (8,12,13,17,18,20). In our study, DCE-MRI data acquisition was started 10-15 minutes after contrast injection, and we did not notice a decrease in hyperenhanced area over time. However, we did not systematically evaluate time-dependency of size of infarction, and future study is required.

Another possible cause of error is related to the use of qualitative assessment of regional wall thickening. Tethering of (largely) non-viable segments to surrounding viable segments regaining contraction may falsely give the impression of improved function (17). In segments with >75% hyperenhancement, the likelihood of improvement was twice the likelihood of complete recovery, which suggests that it may be more difficult to establish partial recovery with (severe) residual dysfunction than complete recovery. In addition, all studies that use the change in regional wall thickening as the standard of viability require accurate registration of baseline and follow-up images. Despite the use of standard imaging procedures and anatomic landmarks, misregistration may be caused by infarct sequels as scar formation and remodeling.

Definition of hyperenhancement – current limitations of DCE-MRI. During data acquisition, the area of hyperenhancement is defined by suppressing signal of remote myocardium without elevated Gd-DTPA concentrations. DCE-MRI may therefore be less reliable when there is co-existing myocardial disease with diffuse or regional fibrosis. In addition, careful optimization and continuous adjustment of the inversion time (TI) is required, because ongoing wash-out of contrast in remote, non-infarcted myocardium causes continuous change of myocardial relaxation parameters (20). Currently, the correct choice of TI largely depends on the experience of the operator, making it a potential source of error. Newer reconstruction methods that are more operator-independent are being developed (26).

During image analysis, the definition of hyperenhancement is not standardized. Signal intensities and area of enhancement are influenced by window setting, which may inappropriately define segmental viability status. Animal studies have used objective thresholds related to the (nulled) signal of remote, non-enhanced myocardium, defining hyperenhanced as more than 2 or 3 SD above the mean signal intensity of remote (12,13,17,27). Studies in patients have generally not reported the use of an objective definition of (hypo- and) hyperenhancement (8,10,18,28). In our experience, thresholding the images at 2 or 3 SD above remote grossly overestimates the visually determined areas. Signal intensity of remote myocardium is actively suppressed, and is therefore so low that areas that have only marginally higher signal intensity are falsely considered part of the infarcted area. In a group of patients with chronic ischemic heart disease, Kim et al.

reported that signal intensity in regions of interest within the hyperenhanced infarcted area was always more than 6 SD above non-enhanced remote regions, although this was not used in the actual analysis (21). In the subset of segments with baseline abnormal wall thickening, we found that SEH_{th}-scores correlated only moderately with the SEH-scores (agreement 64%, overestimating in 24%, kappa 0.55). Multilevel analysis showed that the discriminative power of SEH_{th} was smaller than of SEH, since only SEH_{th}-scores 4 and 5 had significantly lower likelihood of improvement than SEH_{th}-score 1. In addition, we found that on some occasions the presence of a dark zone could only be recognized on the non-thresholded images. The interobserver agreement between two observers that independently drew myocardial contours and adjusted window setting for non-thresholded SEH in our study was good (87%, kappa=0.76).

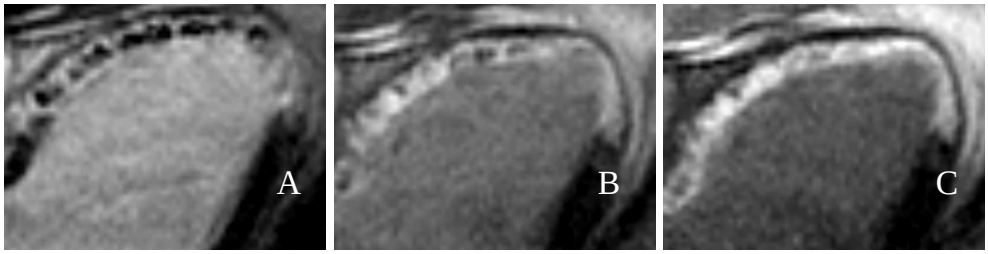

Figure 3. Temporal changes in signal intensity after 0.2 mmol/kg gadolinium-DTPA i.v. in the same patient as Figure 2. Magnified view of 3-chamber view at 2 min (A), 15 min (B), and 30 min (C).

Hypoenhancement at delayed imaging. Low signal intensity (hypoenhancement) during the first two minutes after contrast injection is attributed to microvascular obstruction (7,15). It is associated with greater myocardial damage and identifies patients with worse prognosis (7,28,29). Signal intensity in these dark zones rises slowly in the first 5-10 minutes after contrast injection (7,15). The extent of hypoenhancement may vary with the time after injection, since it is unlikely that the degree of microvascular damage is identical throughout the entire infarct. Some areas may have mild damage, and allow slow contrast wash-in by diffusion from surrounding regions with intact microcirculation (figure 3) (30). Others may have extensive microvascular damage, resulting in persistent hypoenhancement even at late imaging. We found that segments with dark zones within the hyperenhanced areas at delayed imaging had poor function with very low likelihood of improvement at follow-up.

In conclusion, this study shows that delayed contrast-enhanced MRI can be used to predict improvement of dysfunctional but viable segments in patients with recent reperfused myocardial infarction. Future study should focus on further standardization of scan procedures and image analysis.

REFERENCES

1. Lee KS, Marwick TH, Cook SA, et al. Prognosis of patients with left ventricular dysfunction, with and without viable myocardium after myocardial infarction. Relative efficacy of medical therapy and revascularization. *Circulation* 1994;90:2687-94.
2. Smart S, Wynsen J, Sagar K. Dobutamine-atropine stress echocardiography for reversible dysfunction during the first week after acute myocardial infarction: limitations and determinants of accuracy. *J Am Coll Cardiol* 1997;30:1669-78.
3. Schwaiger M, Brunken R, Grover-McKay M, et al. Regional myocardial metabolism in patients with acute myocardial infarction assessed by positron emission tomography. *J Am Coll Cardiol* 1986;8:800-8.
4. De Roos A, Van Rossum AC, van der Wall EE, et al. Reperfused and nonreperfused myocardial infarction: diagnostic potential of Gd-DTPA--enhanced MR imaging. *Radiology* 1989;172:717-20.
5. Van Rossum AC, Visser FC, Van Eenige MJ, et al. Value of gadolinium-diethylene-triamine pentaacetic acid dynamics in magnetic resonance imaging of acute myocardial infarction with occluded and reperfused coronary arteries after thrombolysis. *Am J Cardiol* 1990;65:845-51.
6. van der Wall EE, van Dijkman PR, De Roos A, et al. Diagnostic significance of gadolinium-DTPA (diethylenetriamine penta-acetic acid) enhanced magnetic resonance imaging in thrombolytic treatment for acute myocardial infarction: its potential in assessing reperfusion. *Br Heart J* 1990;63:12-7.
7. Lima JA, Judd RM, Bazille A, et al. Regional heterogeneity of human myocardial infarcts demonstrated by contrast-enhanced MRI. Potential mechanisms. *Circulation* 1995;92:1117-25.
8. Rogers WJJ, Kramer CM, Geskin G, et al. Early contrast-enhanced MRI predicts late functional recovery after reperfused myocardial infarction [see comments]. *Circulation* 1999;99:744-50.
9. Dendale P, Franken PR, Block P, et al. Contrast enhanced and functional magnetic resonance imaging for the detection of viable myocardium after infarction. *Am Heart J* 1998;135:875-80.
10. Choi KM, Kim RJ, Gubernikoff G, et al. Transmural extent of acute myocardial infarction predicts long-term improvement in contractile function. *Circulation* 2001;104:1101-7.
11. Gerber BL, Garot J, Bluemke DA, et al. Accuracy of contrast-enhanced magnetic resonance imaging in predicting improvement of regional myocardial function in patients after acute myocardial infarction. *Circulation* 2002;106:1083-9.
12. Kim RJ, Fieno DS, Parrish TB, et al. Relationship of MRI delayed contrast enhancement to irreversible injury, infarct age, and contractile function. *Circulation* 1999;100:1992-2002.
13. Fieno DS, Kim RJ, Chen EL, et al. Contrast-enhanced magnetic resonance imaging of myocardium at risk: distinction between reversible and irreversible injury throughout infarct healing [In Process Citation]. *J Am Coll Cardiol* 2000;36:1985-91.
14. Kim RJ, Chen EL, Lima JA, et al. Myocardial Gd-DTPA kinetics determine MRI contrast enhancement and reflect the extent and severity of myocardial injury after acute reperfused infarction. *Circulation* 1996;94:3318-26.
15. Judd RM, Lugo-Olivieri CH, Arai M, et al. Physiological basis of myocardial contrast enhancement in fast magnetic resonance images of 2-day-old reperfused canine infarcts. *Circulation* 1995;92:1902-10.
16. Rehwald WG, Fieno DS, Chen EL, et al. Myocardial magnetic resonance imaging contrast agent concentrations after reversible and irreversible ischemic injury. *Circulation* 2002;105:224-9.
17. Hillenbrand HB, Kim RJ, Parker MA, et al. Early assessment of myocardial salvage by contrast-enhanced magnetic resonance imaging. *Circulation* 2000;102:1678-83.
18. Kramer CM, Rogers WJ, Jr., Mankad S, et al. Contractile reserve and contrast uptake pattern by magnetic resonance imaging and functional recovery after reperfused myocardial infarction. *J Am Coll Cardiol* 2000;36:1835-40.
19. Saeed M, Lund G, Wendland MF, et al. Magnetic resonance characterization of the peri-infarction zone of reperfused myocardial infarction with necrosis-specific and extracellular nonspecific contrast media. *Circulation* 2001;103:871-6.
20. Simonetti OP, Kim RJ, Fieno DS, et al. An improved MR imaging technique for the visualization of myocardial infarction. *Radiology* 2001;218:215-23.

21. Kim RJ, Wu E, Rafael A, et al. The Use of Contrast-Enhanced Magnetic Resonance Imaging to Identify Reversible Myocardial Dysfunction. *N Engl J Med* 2000;343:1445-53.
22. Goldstein H. Multilevel Statistical Models. London: Edward Arnold, 1995.
23. Goldstein H, Rashback J, Plewis I et al. A user's guide to MLwiN. London: Institute of Education, 1998.
24. Oshinski, J. N., Yang, Z., Jones, J. R., Mata, J. F., and French, B. A. Imaging time after Gd-DTPA injection is critical in using delayed enhancement to determine infarct size accurately with magnetic resonance imaging. *Circulation* 104, 2838-2842. 4-12-2001.
25. Judd RM, Kim RJ. Imaging time after Gd-DTPA injection is critical in using delayed enhancement to determine infarct size accurately with magnetic resonance imaging. *Circulation* 2002;106:e6.
26. Kellman P, Arai AE, McVeigh ER, et al. Phase-sensitive inversion recovery for detecting myocardial infarction using gadolinium-delayed hyperenhancement. *Magn Reson Med* 2002;47:372-83.
27. Gerber BL, Rochitte CE, Bluemke DA, et al. Relation between Gd-DTPA contrast enhancement and regional inotropic response in the periphery and center of myocardial infarction. *Circulation* 2001;104:998-1004.
28. Wu KC, Zerhouni EA, Judd RM, et al. Prognostic significance of microvascular obstruction by magnetic resonance imaging in patients with acute myocardial infarction. *Circulation* 1998;97:765-72.
29. Gerber BL, Rochitte CE, Melin JA, et al. Microvascular obstruction and left ventricular remodeling early after acute myocardial infarction. *Circulation* 2000;101:2734-41.
30. Mahrholdt H, Wagner A, Judd RM, et al. Assessment of myocardial viability by cardiovascular magnetic resonance imaging. *Eur Heart J* 2002;23:602-19.

Chapter 3

Functional recovery after acute myocardial infarction: A comparison between angiography, electrocardiography and cardiovascular magnetic resonance measures of microvascular injury

Robin Nijveldt, Aernout M. Beek, Alexander Hirsch, Martin G. Stoel, Mark B.M. Hofman, Victor A.W.M. Umans, Paul R. Algra, Jos W.R. Twisk, Albert C. van Rossum

J Am Col Cardiol 2008; 52(3): 181-189

ABSTRACT

Objectives. We examined the relation between angiographic, electrocardiographic and gadolinium-enhanced cardiovascular magnetic resonance (CMR) characteristics of microvascular obstruction (MVO), and their predictive value on functional recovery after acute myocardial infarction (AMI).

Background. MVO on CMR has been shown to predict left ventricular (LV) remodeling, but it is not well known how it compares to commonly used criteria of microvascular injury, and earlier reports have produced conflicting results on the significance and extent of MVO.

Methods. Thrombolysis In Myocardial Infarction (TIMI) flow grade, Myocardial Blush Grade (MBG) and ST-segment resolution were assessed in 60 patients with AMI treated with primary stenting. CMR was performed between 2 and 9 days after revascularization to determine early MVO on first pass perfusion imaging, late MVO on late gadolinium-enhanced imaging, and infarct size and transmural extent. Cine imaging was used to determine LV volumes and global and regional function at baseline and at 4 months follow-up.

Results. Early and late MVO were both related to incomplete ST-segment resolution ($p=0.002$, $p=0.01$ respectively), but not to TIMI flow grade and MBG. Of all angiographic, electrocardiographic, and CMR variables, late MVO was the strongest parameter to predict changes in end-diastolic volume ($\beta=0.53$, $p=0.001$), end-systolic volume ($\beta=8.67$, $p=0.001$) and ejection fraction ($\beta=3.94$, $p=0.006$) at follow-up. Regional analysis showed that late MVO had incremental diagnostic value to transmural extent of infarction (odds ratio 0.18, $p<0.0001$).

Conclusions. In patients after revascularized AMI, late MVO proved a more powerful predictor of global and regional functional recovery than all other characteristics, including transmural extent of infarction.

Acknowledgements

This study was supported by the Netherlands Heart Foundation (grant 2003B126). We thank the technicians, research nurses and staff of the cardiology and radiology departments of the VU University Medical Center and Medical Center Alkmaar for their skilled assistance.

INTRODUCTION

Infarct size is a strong predictor of prognosis after acute myocardial infarction (AMI), and reperfusion therapy has contributed to an important decrease in mortality by limiting myocardial necrosis.[1] However, despite successful recanalization of the infarct-related artery, perfusion of the ischemic myocardium is not or incompletely restored in up to 30% of patients due to microvascular obstruction (MVO), angiographically referred to as the 'no-reflow' phenomenon.[2] The presence of no-reflow in these patients has been found to be a predictor of adverse events, with higher incidence of left ventricular (LV) remodeling, congestive heart failure and death.[3,4] The diagnosis of no-reflow can be made using angiography,[5,6] electrocardiography,[7] nuclear scintigraphy,[8] myocardial contrast echocardiography (MCE)[3] or cardiovascular magnetic resonance (CMR).[4] Both MCE and CMR allow direct visualization of the no-reflow zone.[3,9] MCE using intracoronary contrast agents was the first technique to show that angiographic reflow does not always imply restoration of myocardial flow.[10] Although MCE can be used to predict functional changes and outcome after reperfused AMI, it is still limited by attenuation artifacts and poor visibility of (postero-)lateral segments,[11] and is not capable of quantifying total infarct size. CMR allows accurate assessment of function, transmural extent and total size of infarction, and MVO in all segments of the left ventricle.[12] Two methods have been described for the detection of MVO using gadolinium-enhanced CMR: first pass perfusion[9,13] and late gadolinium enhancement (LGE).[14,15] Both techniques have been shown to predict LV remodeling and outcome, but it is not known how they compare to the commonly used angiographic and electrocardiographic criteria of microvascular injury. Also, evidence is still limited in optimally treated patients, and earlier reports have produced conflicting results on the significance and extent of MVO.[15-18]

The purpose of the present study was, therefore, to explore the relation between angiographic, electrocardiographic, and CMR characteristics of microvascular injury, and to investigate their predictive value on recovery of global and regional LV function after optimal treatment for AMI.

METHODS

Patient population. We screened consecutive patients presenting with a first ST-segment elevation AMI, according to standard electrocardiographic and enzymatic criteria. All patients had undergone primary percutaneous coronary intervention (PCI) with (bare metal) stent implantation within 12 hours of symptom onset. Exclusion criteria were: unsuccessful angiographic reperfusion (Thrombolysis In Myocardial Infarction [TIMI] flow grade <2), haemodynamic instability, left bundle branch block, or (relative) contraindications for

CMR. Sixty-seven patients were prospectively enrolled in the study. Patients were treated with aspirin, heparin, abciximab, clopidogrel, statins, beta-blocking agents and angiotensin-converting enzyme inhibitors, according to ACC/AHA practice guidelines.[19] All of the patients gave informed consent to the study protocol, which was approved by the local ethics committee.

Angiography. Coronary angiography was performed at the end of the PCI procedure for off-line analysis of TIMI flow grade[5] and myocardial blush grade (MBG).[6] Images were assessed by 2 blinded observers, using the following definitions: TIMI flow grade 2, complete filling of the entire vessel, but slower than nonaffected vessels; TIMI flow grade 3, normal flow; MBG 0, no myocardial blush; MBG 1, minimal myocardial blush or contrast density; MBG 2, moderate blush or contrast density, but less than a contralateral or ipsilateral noninfarct-related artery; and MBG 3, normal myocardial blush or contrast density, comparable with a contralateral or ipsilateral noninfarct-related artery. Angiographic incomplete reperfusion was defined as TIMI flow grade 2, or MBG <2.

Electrocardiography. The ST-segment resolution was evaluated on a 12-lead electrocardiogram acquired on admission and 1 hour after PCI. The sum of ST-segment elevation was measured 60 ms after the J point in leads I, aVL and V_1–V_6 for anterior, and leads II, III, aVF and V_5-V_6 for non-anterior AMI. The percent resolution of ST-segment elevation from before to post-PCI was calculated, and categorized as complete (≥70%), partial (30% to <70%), or no (<30%) ST-segment resolution.7 Incomplete reperfusion was defined as <70% ST-segment resolution on electrocardiography.

CMR protocol. CMR examination was performed on a 1.5 T clinical scanner (Sonata/Symphony, Siemens, Erlangen, Germany) using a phased array cardiac receiver coil. Baseline scan was scheduled between 2–9 days after reperfusion and follow-up at 4 months. Electrocardiogram-gated breath-hold cine imaging was performed to determine LV function, using a segmented steady-state free precession pulse sequence in multiple short axis views every 10 mm covering the entire left ventricle. Typical in plane resolution was 1.6 • 1.9 mm2, with slice thickness 5.0–6.0 mm (repetition time/echo time = 3.2/1.6 ms, flip angle 60°, matrix 256 • 156, temporal resolution 35–50 ms). First pass perfusion was performed during administration of a gadolinium-based contrast agent (Magnevist, Schering AG, Berlin, Germany; 0.1 mmol/kg) at a rate of 3.0 ml/sec, using a single shot saturation recovery gradient-echo pulse sequence. Three short axis slices were obtained per heartbeat, every 10 mm, covering the infarct area as seen during cine imaging (90° prepulse, repetition time/echo time = 2.1/1.0 ms, saturation time 120 ms, flip angle 12°, matrix 128x93, in plane resolution 3.0 • 3.3 mm2, slice thickness 8.0 mm, total scan duration ~1.5 min). Immediately after first pass perfusion, an additional 0.1 mmol/kg of gadolinium-based contrast agent was administered (cumulative dose, 0.2 mmol/kg). LGE

images were obtained 12–15 minutes after the second contrast administration,20 using a 2D segmented inversion recovery gradient-echo pulse sequence, with slice position identical to the cine images. Typical in plane resolution was 1.4 • 1.7 mm2, with slice thickness 5.0–6.0 mm. (repetition time/echo time = 9.6/4.4 ms, flip angle 25°, triggering to every other heartbeat). The inversion time was set to null the signal of viable myocardium, and typically ranged from 250–300 ms.

Table 1. Patient characteristics, angiographic and electrocardiographic data.

Number of patients	60
Age	55 ±10
Body mass index (kg/m2)	25.8 ±2.6
Risk factors	
Men	54 (90%)
Diabetes mellitus	2 (3%)
Hyperlipidaemia	17 (28%)
Hypertension	17 (28%)
Smoking	41 (68%)
Time to reperfusion (hr)	3.5 ±3.2
Maximum total creatine kinase (U/L)	3093 ±1851
Medication at discharge	
Aspirin	60 (100%)
Clopidogrel	60 (100%)
Beta-blockade	60 (100%)
Statins	60 (100%)
ACE-inhibitors/ATII-antagonists	49 (82%)
Infarct-related artery	
Left anterior descending artery	39 (65%)
Left circumflex artery	7 (12%)
Right coronary artery	14 (23%)
Platelet glycoprotein IIb/IIIa inhibitors	51 (85%)
TIMI flow post-PCI	
TIMI 2	11 (18%)
TIMI 3	49 (82%)
Myocardial blush grade post-PCI	
MBG 0	2 (3%)
MBG 1	7 (12%)
MBG 2	21 (35%)
MBG 3	30 (50%)
ST-segment resolution (sum of leads)	
incomplete	9 (15%)
partial	27 (45%)
complete	24 (40%)

Values are presented as number (%) or mean ± standard deviation.
ACE = angiotensin-converting enzyme; MBG = myocardial blush grade, PCI = percutaneous coronary intervention, TIMI = Thrombolysis In Myocardial Infarction.

CMR data analysis and definitions. All CMR data were analyzed on a separate workstation using dedicated software (Mass version 2006beta, Medis, Leiden, the Netherlands). Cine, first pass perfusion and LGE images acquired during the same imaging session were matched by using slice position. Registration of follow-up to baseline cine and LGE images was achieved by consensus of two observers using anatomic landmarks, such as papillary muscles and right ventricular insertion sites. On all short axis cine slices, the endocardial and epicardial borders were outlined manually on end-diastolic and end-systolic images. LV volumes and ejection fraction (LVEF) were calculated. Each short axis was divided in 12 equi-angular segments, starting at the posterior septal insertion of the right ventricle. Segmental wall thickening (SWT) was calculated by subtracting end-diastolic from end-systolic wall thickness. Myocardial segments were considered to be dysfunctional if SWT was <3 mm, based on the mean SWT of 4.4±0.7 mm (mean ± 2SD) in a group of 10 healthy volunteers (age 50–75 years). Complete recovery of dysfunctional segments was defined as SWT of ≥3.0 mm at follow-up.

First pass perfusion was evaluated qualitatively. MVO was considered present if a region of hypoperfusion persisted for >1 min after contrast bolus arrival in the left ventricle and was located in the subendocardial layer of the infarct core[9,13] in at least 1 of the slices. To verify that a true perfusion deficit persisted after passage of the contrast agent, all acquired phases were evaluated. MVO on first pass perfusion imaging was termed ‘early MVO’.

The assessment of LGE images and infarct size was done as previously described.[15] Total infarct size was expressed as percentage of LV mass. Transmural extent of infarction was calculated by dividing the hyperenhanced area by the total area of the pre-defined segment (%). A transmurality score was calculated in each patient, expressed as the sum of segments with >75% infarcted myocardium, as a percentage of the total number of segments scored. On LGE images, MVO was defined as any region of hypoenhancement within the hyperenhanced area,[14,15] and was termed ‘late MVO’. MVO was included in the calculation of total infarct size. The extent of late MVO was calculated in each patient, expressed as the sum of the segments with MVO, as a percentage of the number of segments scored.

For analysis of segmental function and transmural extent of infarction, the two most basal and two most distal slices were excluded, because segmental evaluation at these levels is not considered to be reliable due to the LV outflow tract and partial volume effect respectively. All CMR studies were supervised by one operator, and all images were analyzed by two experienced observers who were blinded to patient data. There was no disagreement between both observers regarding the presence of early or late MVO in each patient.

Statistical analysis. Data are expressed as mean ± standard deviation (SD) for continuous variables and as frequency with percentage for categorical variables. Comparison of categorized angiographic and electrocardiographic variables and microvascular injury was done by the Chi-square test, or by the Fisher exact test if an expected cell count was <5. The paired samples t test was used to compare differences in global LV parameters between baseline and follow-up and the independent samples t test to compare means between subgroups. To identify independent predictors of global LV indices at baseline and the change of these parameters between baseline and follow-up, multivariable linear regression analyses with a forward selection procedure were used. Variables entered the model if $p<0.10$. We evaluated four outcome variables of regional myocardial function (change in end-diastolic wall thickness, change in end-systolic wall thickness, change in SWT and complete recovery) in relation to the presence of late MVO. Only dysfunctional segments at baseline were included and outcomes were stratified by the transmural extent of infarction. Because regional function in different segments within one patient are strongly related, outcomes were analyzed using multilevel analyses (linear and logistic regression) with three levels: segments within slices and slices within patients (MLwiN, version 1.02.0002, Centre for Multilevel Modeling, London, United Kingdom).[21] In each analysis, a correction was made for the baseline variable of regional myocardial function in question (i.e., if the dependent variable was change in end-diastolic wall thickness, presence of microvascular injury and baseline end-diastolic wall thickness were included as covariates). All statistical tests were two-tailed and a p-value <0.05 was considered statistically significant.

Table 2. Relation between angiographic/electrocardiographic parameters, and first pass perfusion and late gadolinium-enhanced imaging.

		MVO during first pass perfusion			**MVO on LGE images**		
		No	Yes	p-value	No	Yes	p-value
TIMI	2	2 (18%)	9 (82%)	0.48†	5 (45%)	6 (55%)	1.0†
	3	17 (35%)	32 (65%)		21 (43%)	28 (57%)	
MBG	0-1	3 (33%)	6 (67%)	1.0†	4 (44%)	5 (56%)	1.0†
	2-mrt	16 (31%)	35 (69%)		22 (43%)	29 (57%)	
STres	Incomplete	6 (17%)	30 (83%)	0.002*	11 (31%)	25 (69%)	0.01*
	Complete	13 (54%)	11 (46%)		15 (63%)	9 (37%)	

LGE = late gadolinium enhancement; MBG = myocardial blush grade; MVO = microvascular obstruction; Stres = ST-segment resolution; TIMI = Thrombolysis In Myocardial Infarction.
The p-values are calculated using the Chi-square test (*) or Fisherexact test (†).

RESULTS

Baseline patient characteristics and medication are listed in Table 1. Seven patients did not undergo the follow-up study, and were therefore excluded from CMR analysis (refusal of follow-up CMR in three, claustrophobia in one, cardiac death in two and noncardiac death in one patient). There was no reinfarction, revascularization, or hospitalization for heart failure between baseline and follow-up study in the remaining 60 patients.

Angiography and electrocardiography. All angiographic and electrocardiographic characteristics are listed in Table 1. Of the 11 patients with TIMI flow grade 2, 5 patients had MBG 2 (46%), 4 patients had MBG 1 (36%) and 2 patients had MBG 0 (18%). Of the 49 patients with TIMI flow grade 3, 30 patients had MBG 3 (61%), 16 patients had MBG 2 (33%) and 3 patients had MBG 1 (6%). There was no statistical association between TIMI flow grade or MBG and the time to reperfusion.

The mean sum of total ST-segment elevation was 17.9±10.8 mV before PCI and 7.9±7.3 mV after the procedure, resulting in 10.0±8.6 mV absolute ST-segment resolution. The mean relative ST resolution was 55.7±32.0%. There was a significant relation for ST resolution (categorized as no, partial, or complete) with TIMI flow grade 2–3 (p-value for trend=0.005), and with MBG 0–3 (p-value for trend=0.004). Of the 24 patients with complete ST-segment resolution, 23 had TIMI flow grade 3 (96%), and 21 MBG 2-3 (88%). Of the 36 patients with incomplete ST resolution, 10 had TIMI flow grade 2 (28%), and 6 had MBG 0–1 (17%). There was no statistical relation between ST-segment resolution and the time to reperfusion.

Cardiovascular Magnetic Resonance. The CMR examinations were performed 5±2 days and 116±22 days after primary PCI. The LVEF at baseline was 42.6±9.0%, which significantly improved to 45.0±9.5% at follow-up (p=0.001). There was no statistically significant change in mean global LV volumes between baseline and follow-up in the total group (data not shown). Mean total infarct size was 16.9±9.7% at baseline.

Early MVO was present in 41 patients (68%), and 34 patients (57%) also demonstrated late MVO. Seven patients (12%) had early MVO without late MVO. Both early MVO and late MVO presence were related to incomplete ST segment resolution (p=0.002 and p=0.01 respectively, Chi-square test)(Table 8.2). There was no statistically significant relation between early or late MVO and TIMI flow grade or MBG (Table 2). The time to reperfusion was not different between patients with or without early MVO (3.4±2.5 versus 3.7±4.0 respectively, p=0.73) and between patients with or without late MVO (3.4±2.3 versus 3.8±4.6 respectively, p=0.70).

Table 3A. Univariable and multivariable linear regression analysis for the prediction of baseline ejection fraction and the change in ejection fraction between baseline and follow-up.

Variables	LV ejection fraction at baseline				Δ LV ejection fraction			
	Univariable		Multivariable		Univariable		Multivariable	
	Beta	p-value	Beta	p-value	Beta	p-value	Beta	p-value
Early MVO	-5.50	0.03	-	-	-2.54	0.09	-	-
Late MVO	-5.78	0.01	-	-	-2.84	0.04	-3.94	0.006
Extent of MVO	-0.40	<0.0001	-	-	-0.09	0.17	-	-
TIMI flow 2	-2.71	0.37	-	-	-1.62	0.37	-	-
MBG 0–1	-0.19	0.96	-	-	-1.75	0.37	-	-
Incomplete ST-resolution	-4.64	0.05	-	-	-0.71	0.62	-	-
Infarct size	-0.58	<0.0001	-0.58	<0.0001	-0.05	0.46	-	-
Transmurality	-0.42	<0.0001	-	-	-0.01	0.89	-	-
Age	0.04	0.73	-	-	0.08	0.26	-	-
Baseline LVEF	-	-	-	-	-0.12	0.12	-0.19	0.02

Δ = change, EF = ejection fraction, LGE = late gadolinium enhancement, LV = left ventricular, MBG = myocardial blush grade, MVO = microvascular obstruction, TIMI = Thrombolysis In Myocardial Infarction.

Table 3B. Univariable and multivariable linear regression analysis for the prediction of baseline end-systolic volume and the change in end-systolic volume between baseline and follow-up.

Variables	LV ESV at baseline				Δ LV ESV			
	Univariable		Multivariable		Univariable		Multivariable	
	Beta	p-value	Beta	p-value	Beta	p-value	Beta	p-value
Early MVO	10.53	0.07	–	–	8.26	0.005	–	–
Late MVO	14.57	0.007	–	–	9.83	0.0003	8.67	0.001
Extent of MVO	0.92	<0.0001	–	–	0.42	0.001	–	–
TIMI flow 2	-2.61	0.71	–	–	-0.29	0.94	–	–
MBG 0–1	-5.92	0.44	–	–	1.09	0.78	–	–
Incomplete ST-resolution	4.15	0.46	–	–	4.36	0.13	–	–
Infarct size (% of LV)	1.20	<0.0001	1.20	<0.0001	0.35	0.01	–	–
Transmurality	0.78	0.0004	–	–	0.28	0.02	–	–
Age (years)	-0.21	0.47	–	–	-0.39	0.007	-0.30	0.02
Baseline LV ESV	–	–	–	–	0.02	0.79	–	–

Δ = change; ESV = end-systolic volume; LGE = late gadolinium enhancement; LV = left ventricular; MBG = myocardial blush grade; MVO = microvascular obstruction; TIMI = Thrombolysis In Myocardial Infarction.

Predictors of global function and recovery. Table 3 demonstrates univariable and multivariable linear regression analysis for the prediction of baseline LVEF and LV end-systolic volume, and the change in LVEF and LV end-systolic volume between baseline and follow-up CMR. Infarct size, transmural extent of infarction and the extent of late MVO were all highly significant predictors of LVEF and LV end-systolic volume at baseline. Multivariable analysis revealed LGE infarct size as the strongest and single independent predictor of baseline LVEF (β=-0.58, p<0.0001) and LV end-systolic volume

(β=1.20, p<0.0001). The results of univariable and multivariable regression analysis of LV end-diastolic volume at baseline were comparable to results of LVEF and LV end-systolic volume.

The presence of late MVO was the strongest predictor of change in LVEF and LV end-systolic volume at follow-up (β=-3.94, p=0.006 and β=8.67, p=0.001 respectively). Univariable analysis revealed the presence of late MVO, the extent of late MVO and the transmural extent of infarction as highly significant predictors of change in end-diastolic volume (p<0.005). The extent of late MVO was the strongest significant predictor of change in end-diastolic volume after multivariable analysis (β=0.53, p=0.001).

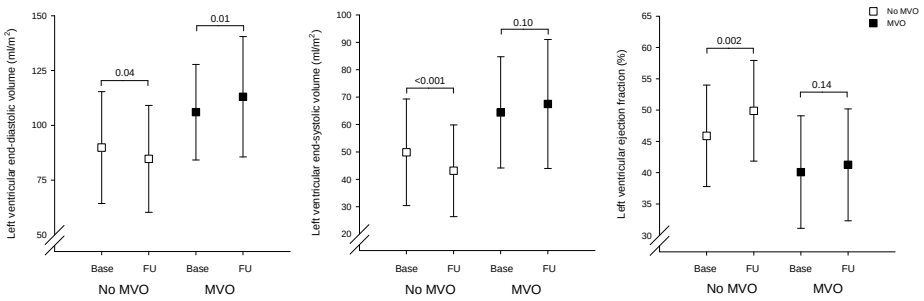

Figure 1. Changes in global left ventricular volumes and function from baseline to follow-up in patients without MVO (-□-) and with MVO (-■-).

The changes in LV volumes and LVEF according to late MVO status are shown in Figure 1. Patients with late MVO showed a significant increase in LV end-diastolic volumes (p=0.01), with a trend towards an increase in LV end-systolic volumes (p=0.10), and absence of improvement in LVEF (p=0.14). Patients without late MVO showed a significant decrease in volumes and a significant improvement in LVEF. Within the group of patients with late MVO, no significant correlation was found between the extent of MVO and the change in LVEF (Pearson's r=0.05, p=0.78), end-systolic volume (Pearson's r=0.19, p=0.29) or end-diastolic volume (Pearson's r=0.21, p=0.24).

Regional function and recovery. A total of 3.924 segments were analyzed, of which 2.158 segments (55%) were dysfunctional at baseline. On the LGE images, 1.709 segments (43.6%) demonstrated hyperenhancement, and 380 segments (9.7%) demonstrated late MVO at baseline. The presence of late MVO significantly increased with infarct transmurality: 0.6%, 17% and 49% in segments with 0–25%, 26–75% and 76–100% extent of infarction, respectively (p<0.001).

Figure 2 shows the observed changes in regional wall thickness and function in dysfunctional segments, according to infarct transmurality and presence of late MVO. Segments with significant hyperenhancement (>25%) and late MVO showed a larger decrease in end-diastolic and end-systolic wall thickness during follow-up than segments without MVO (Figure 8.2A & 8.2B). Also, in segments with >75% hyperenhancement and late MVO, improvement in wall thickening was significantly less than in segments without MVO (p=0.007, Figure 8.2C). Of all dysfunctional segments, 654 segments showed complete recovery at follow-up. The likelihood of complete recovery was highest in segments with no or minimal hyperenhancement without MVO, and lowest in segments with >75% hyperenhancement with MVO (Figure 8.2D). Only 6% (23/372) of dysfunctional segments with late MVO showed complete recovery during follow-up, compared to 35% (631/1.786) of dysfunctional segments without MVO (odds ratio 0.18 (95% CI 0.08–0.38), p<0.0001).

DISCUSSION

The present study is the first to directly compare angiographic, electrocardiographic and gadolinium-enhanced CMR characteristics of microvascular injury, and their predictive value on functional outcome in a homogeneous group of patients after successful primary stenting for AMI. The main findings can be summarized as follows: 1) of all characteristics of microvascular injury, late MVO was the strongest predictor of change in global LV function and volumes at follow-up, 2) ST-segment resolution, but not TIMI flow grade and MBG, correlated with the presence of MVO on first pass perfusion and LGE CMR, and 3) late MVO was a stronger predictor of regional functional outcome than infarct transmurality.

Angiography and electrocardiography. In AMI, restoration of microvascular flow is considered to be a key factor for post-ischemic repair, functional outcome and prognosis. The presence of microvascular injury can be assessed with a multitude of invasive and noninvasive techniques. Despite their proven clinical relevance, there have been few studies on the relative value of these techniques, and to our knowledge there are no studies that have compared CMR characteristics of MVO to TIMI flow grade, MBG or ST-segment resolution. A number of reports have addressed angiographic and electrocardiographic techniques and found that MBG and ST-segment resolution provided prognostic information beyond the standard TIMI flow grading and the (semi-quantitative) TIMI frame count.[22] MBG and ST-segment resolution have each been used as (surrogate) end points in the evaluation of MVO reducing therapies.[23] However, a recent report showed that MBG and ST-segment resolution were discordant in almost 40% of patients,[22] which theoretically limits their use both in daily practice and in research. In our study, ST-segment resolution

was discordant with TIMI flow grade in 38% of the patients, and with MBG in 48% of the patients. Neither TIMI flow grade nor MBG was predictive of functional outcome. Although incomplete ST-segment resolution was related to baseline function, it did not predict changes at follow-up. This finding is probably attributable to the relatively small number of patients.

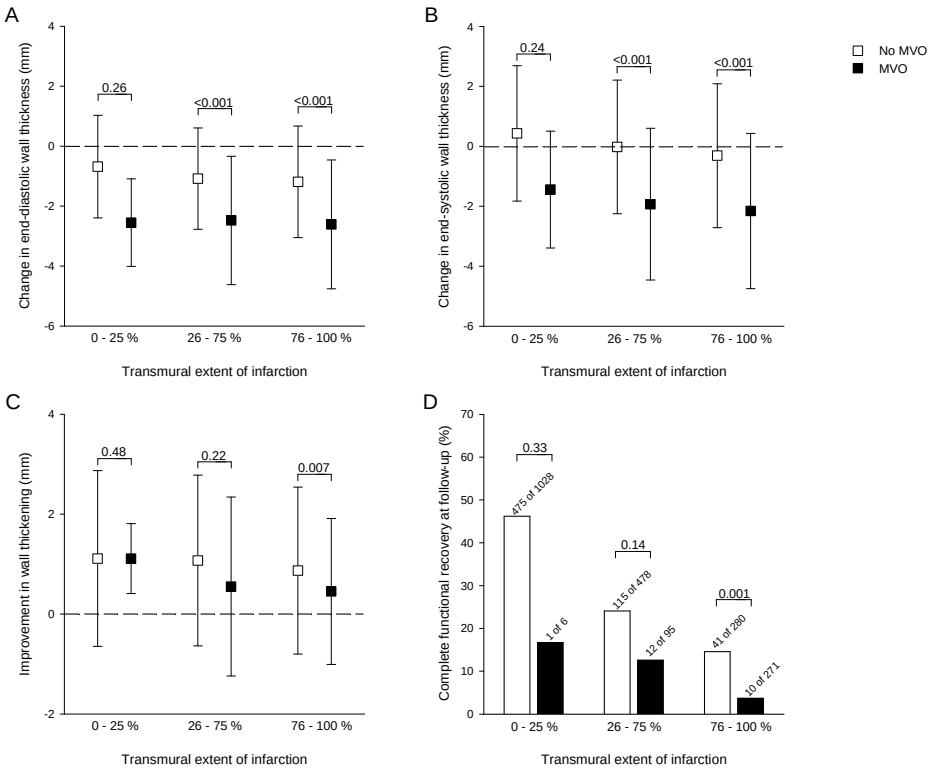

Figure 2. Change of end-diastolic and end-systolic regional wall thickness (A & B) and of wall thickening (C) in dysfunctional segments between baseline and follow-up, according to transmural extent of infarction. D shows complete recovery at follow-up of dysfunctional segments, according to baseline transmural extent of infarction in patients without (-□-) and with MVO (-■-).

Gadolinium-enhanced CMR. By allowing the direct visualization of the non-perfused zone, gadolinium-enhanced CMR has provided new insights in the pathophysiology and prevalence of microvascular obstruction.[4,9,13,24] Current first pass CMR techniques have high sensitivity for the diagnosis of MVO, detecting it in 65–87% of patients with successfully reperfused AMI and TIMI flow grade 3.[16,25,26] The reported prevalence of MVO with LGE imaging is lower: 28-58%.[14,15,17,18,26,27] So far, only two studies have

directly compared early and late MVO, and both showed a higher prevalence of early MVO, but did not assess their relative value for the prediction of outcome.[26,27] The difference in prevalence is attributed to ongoing slow diffusion of contrast into regions with less severe microvascular damage and subsequent smaller areas of hypoenhancement at postponed (late) imaging (Figure 3). The short axis LGE images were acquired between 12–15 minutes after contrast administration.[20] Consequently, we may have missed areas with MVO which had already disappeared due to wash-in of contrast. Late MVO therefore reflects infarcts with a more severely injured microvasculature. Our data extend previous studies by showing that, although first pass imaging was more sensitive in detecting MVO (68% versus 57%), MVO on LGE imaging had greater clinical relevance by identifying patients with worse functional outcome, and was in fact the only predictor of LV volumes and function at follow-up in a multivariable analysis that included all angiographic, electrocardiographic and CMR measures of MVO. Furthermore, the present study documents no statistical relationship between the extent of MVO and LV remodeling over time in patients with presence of late MVO. This finding is in line with our previous results, where we reported no difference in LV indices between patients with small or large areas of MVO,[15] suggesting that the size and extent of MVO may be clinically less important than its mere presence.

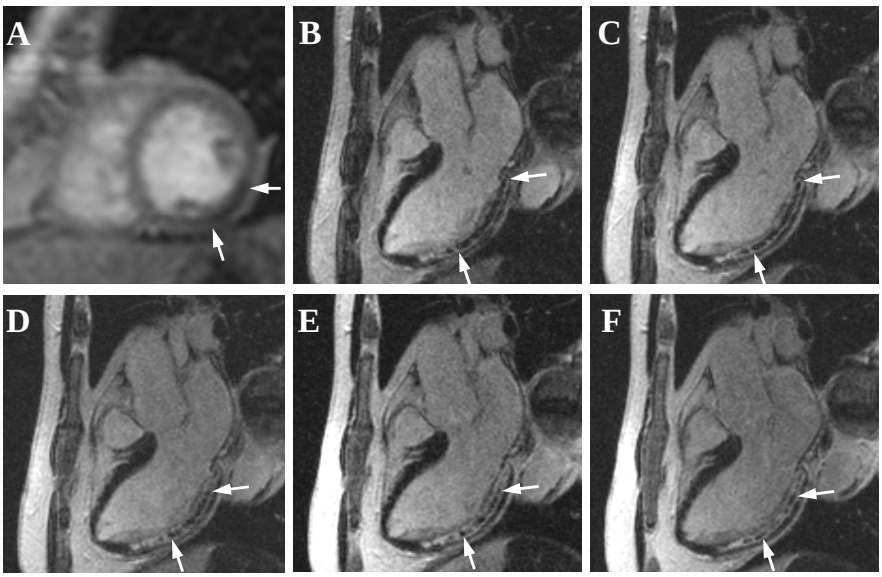

Figure 3. Example of gadolinium-enhanced images of the same patient with presence of MVO at different time points after contrast administration, showing the decline of the MVO region. A shows a short axis first pass perfusion image 1.5 minute after contrast injection, with transmural hypoenhancement in the inferolateral region (arrows). Panel B to F are corresponding three-chamber LGE images which transect A at the dotted line, acquired 10 minutes (B), 15 minutes (C), 20 minutes (D), 30 minutes (E), and 40 minutes (F) after contrast administration.

MVO versus infarct size and transmurality. This study also demonstrates that late MVO has diagnostic value beyond infarct transmurality, which is an established predictor of functional recovery of stunned or hibernating myocardium.[28,29] Several studies have compared MVO (either by first pass or by LGE imaging) to LGE infarct size or transmural extent, but results have not been conclusive, with some reports favoring MVO and others infarct size or transmurality as the best predictor of outcome.[4,14,16,18,25] Although infarct size was the only independent predictor of baseline volumes and function in the present study, late MVO was a better predictor of the changes at follow-up. Regional analysis showed that late MVO was associated with increased wall thinning and less improvement of wall thickening, regardless of the degree of infarct transmurality. These results strongly suggest that, in the acute setting, MVO might be more relevant than infarct size or transmural extent.

Methodological considerations. CMR assessment of MVO and infarction is typically performed between 2 and 9 days after reperfusion, because the extent of both MVO and infarction is stable within that period and has been shown to increase in the first 48 h.[24,30] Thus, we assured a fixed infarct and MVO size, although we may have underestimated the full potential of CMR (and other parameters) to predict functional recovery. Additionally, because we performed LGE imaging between 12–15 min in order to optimally analyze infarct size and extent, we cannot exclude that earlier or later acquisition would have influenced the predictive value of late MVO.

Angiographic and electrocardiographic parameters of no-reflow are obtained in the acute setting of myocardial infarction, immediately or very early after reperfusion. The difference in timing may explain the relatively poor correlation between CMR and the other parameters. However, all parameters have been effectively used for the prediction of outcome after MVO, which justifies their comparison despite the difference in timing.

Clinical implications. Our findings may become relevant for selecting patients that may benefit from adjunctive (e.g., cell) therapy to promote the repair of infarcted myocardium. In addition, because gadolinium-enhanced CMR accurately visualizes both infarct and MVO, it should be strongly recommended as principal imaging technique in trials evaluating new therapeutic strategies to limit microvascular injury in the setting of AMI.

In conclusion, we found late MVO to be the most powerful predictor of functional outcome after AMI when directly comparing angiographic, electrocardiographic and gadolinium-enhanced CMR characteristics of microvascular injury in a homogeneous group of patients after successful PCI. Its predictive value exceeded that of early MVO and assessment of transmural extent of infarction.

REFERENCES

1. Grines CL, Browne KF, Marco J, Rothbaum D, Stone GW, O'Keefe J, Overlie P, Donohue B, Chelliah N, Timmis GC. A comparison of immediate angioplasty with thrombolytic therapy for acute myocardial infarction. The Primary Angioplasty in Myocardial Infarction Study Group. *N Engl J Med*. 1993;328(10):673-679.
2. Kloner RA, Ganote CE, Jennings RB. The ‘no-reflow’ phenomenon after temporary coronary occlusion in the dog. *J Clin Invest*. 1974;54(6):1496-1508.
3. Ito H, Maruyama A, Iwakura K, Takiuchi S, Masuyama T, Hori M, Higashino Y, Fujii K, Minamino T. Clinical implications of the 'no reflow' phenomenon. A predictor of complications and left ventricular remodeling in reperfused anterior wall myocardial infarction. *Circulation*. 1996;93(2):223-228.
4. Wu KC, Zerhouni EA, Judd RM, Lugo-Olivieri CH, Barouch LA, Schulman SP, Blumenthal RS, Lima JA. Prognostic significance of microvascular obstruction by magnetic resonance imaging in patients with acute myocardial infarction. *Circulation*. 1998;97(8):765-772.
5. The TIMI Study Group. The Thrombolysis In Myocardial Infarction (TIMI) trial. *N Engl J Med*. 1985;312(14):932-936.
6. Van 't Hof AW, Liem A, Suryapranata H, Hoorntje JC, de Boer MJ, Zijlstra F. Angiographic assessment of myocardial reperfusion in patients treated with primary angioplasty for acute myocardial infarction: myocardial blush grade. Zwolle Myocardial Infarction Study Group. *Circulation*. 1998;97(23):2302-2306.
7. Schroder R, Dissmann R, Bruggemann T, Wegscheider K, Linderer T, Tebbe U, Neuhaus KL. Extent of early ST segment elevation resolution: a simple but strong predictor of outcome in patients with acute myocardial infarction. *J Am Coll Cardiol*. 1994;24(2):384-391.
8. Kondo M, Nakano A, Saito D, Shimono Y. Assessment of "microvascular no-reflow phenomenon" using technetium-99m macroaggregated albumin scintigraphy in patients with acute myocardial infarction. *J Am Coll Cardiol*. 1998;32(4):898-903.
9. Judd RM, Lugo-Olivieri CH, Arai M, Kondo T, Croisille P, Lima JA, Mohan V, Becker LC, Zerhouni EA. Physiological basis of myocardial contrast enhancement in fast magnetic resonance images of 2-day-old reperfused canine infarcts. *Circulation*. 1995;92(7):1902-1910.
10. Ito H, Tomooka T, Sakai N, Yu H, Higashino Y, Fujii K, Masuyama T, Kitabatake A, Minamino T. Lack of myocardial perfusion immediately after successful thrombolysis. A predictor of poor recovery of left ventricular function in anterior myocardial infarction. *Circulation*. 1992;85(5):1699-1705.
11. Choi EY, Seo HS, Park S, Kim HJ, Ahn JA, Ko YG, Choi BW, Kang SM, Choi D, Ha JW, Rim SJ, Jang Y, Chung N. Prediction of transmural extent of infarction with contrast echocardiographically derived index of myocardial blood flow and myocardial blood volume fraction: comparison with contrast-enhanced magnetic resonance imaging. *J Am Soc Echocardiogr*. 2006;19(10):1211-1219.
12. Kim RJ, Chen EL, Lima JA, Judd RM. Myocardial Gd-DTPA kinetics determine MRI contrast enhancement and reflect the extent and severity of myocardial injury after acute reperfused infarction. *Circulation*. 1996;94(12):3318-3326.
13. Lima JA, Judd RM, Bazille A, Schulman SP, Atalar E, Zerhouni EA. Regional heterogeneity of human myocardial infarcts demonstrated by contrast-enhanced MRI. Potential mechanisms. *Circulation*. 1995;92(5):1117-1125.
14. Hombach V, Grebe O, Merkle N, Waldenmaier S, Hoher M, Kochs M, Wohrle J, Kestler HA. Sequelae of acute myocardial infarction regarding cardiac structure and function and their prognostic significance as assessed by magnetic resonance imaging. *Eur Heart J*. 2005;26(6):549-557.
15. Nijveldt R, Beek AM, Hofman MB, Umans VA, Algra PR, Spreeuwenberg MD, Visser CA, van Rossum AC. Late gadolinium-enhanced cardiovascular magnetic resonance evaluation of infarct size and microvascular obstruction in optimally treated patients after acute myocardial infarction. *J Cardiovasc Magn Reson*. 2007;9(5):765-770.
16. Baks T, van Geuns RJ, Biagini E, Wielopolski P, Mollet NR, Cademartiri F, Boersma E, van der Giessen WJ, Krestin GP, Duncker DJ, Serruys PW, de Feyter PJ. Recovery of left ventricular function after primary angioplasty for acute myocardial infarction. *Eur Heart J*. 2005;26(11):1070-1077.

17. Choi CJ, Haji-Momenian S, Dimaria JM, Epstein FH, Bove CM, Rogers WJ, Kramer CM. Infarct involution and improved function during healing of acute myocardial infarction: the role of microvascular obstruction. *J Cardiovasc Magn Reson*. 2004;6(4):917-925.
18. Tarantini G, Razzolini R, Cacciavillani L, Bilato C, Sarais C, Corbetti F, Marra MP, Napodano M, Ramondo A, Iliceto S. Influence of transmurality, infarct size, and severe microvascular obstruction on left ventricular remodeling and function after primary coronary angioplasty. *Am J Cardiol*. 2006;98(8):1033-1040.
19. Ryan TJ, Antman EM, Brooks NH, Califf RM, Hillis LD, Hiratzka LF, Rapaport E, Riegel B, Russell RO, Smith EE, III, Weaver WD, Gibbons RJ, Alpert JS, Eagle KA, Gardner TJ, Garson A, Jr., Gregoratos G, Smith SC, Jr. 1999 update: ACC/AHA Guidelines for the Management of Patients With Acute Myocardial Infarction: Executive Summary and Recommendations: A report of the American College of Cardiology/American Heart Association Task Force on Practice Guidelines (Committee on Management of Acute Myocardial Infarction). *Circulation*. 1999;100(9):1016-1030.
20. Kim RJ, Shah DJ, Judd RM. How we perform delayed enhancement imaging. *J Cardiovasc Magn Reson*. 2003;5(3):505-514.
21. Goldstein H. Multilevel statistical models. 2nd ed. *London: Edward Arnold*; 1995.
22. Sorajja P, Gersh BJ, Costantini C, McLaughlin MG, Zimetbaum P, Cox DA, Garcia E, Tcheng JE, Mehran R, Lansky AJ, Kandzari DE, Grines CL, Stone GW. Combined prognostic utility of ST-segment recovery and myocardial blush after primary percutaneous coronary intervention in acute myocardial infarction. *Eur Heart J*. 2005;26(7):667-674.
23. Silva-Orrego P, Colombo P, Bigi R, Gregori D, Delgado A, Salvade P, Oreglia J, Orrico P, de BA, Piccalo G, Bossi I, Klugmann S. Thrombus aspiration before primary angioplasty improves myocardial reperfusion in acute myocardial infarction: the DEAR-MI (Dethrombosis to Enhance Acute Reperfusion in Myocardial Infarction) study. *J Am Coll Cardiol*. 2006;48(8):1552-1559.
24. Rochitte CE, Lima JA, Bluemke DA, Reeder SB, McVeigh ER, Furuta T, Becker LC, Melin JA. Magnitude and time course of microvascular obstruction and tissue injury after acute myocardial infarction. *Circulation*. 1998;98(10):1006-1014.
25. Gerber BL, Garot J, Bluemke DA, Wu KC, Lima JA. Accuracy of contrast-enhanced magnetic resonance imaging in predicting improvement of regional myocardial function in patients after acute myocardial infarction. *Circulation*. 2002;106(9):1083-1089.
26. Yan AT, Gibson CM, Larose E, Anavekar NS, Tsang S, Solomon SD, Reynolds G, Kwong RY. Characterization of microvascular dysfunction after acute myocardial infarction by cardiovascular magnetic resonance first-pass perfusion and late gadolinium enhancement imaging. *J Cardiovasc Magn Reson*. 2006;8(6):831-837.
27. Lund GK, Stork A, Saeed M, Bansmann MP, Gerken JH, Muller V, Mester J, Higgins CB, Adam G, Meinertz T. Acute myocardial infarction: evaluation with first-pass enhancement and delayed enhancement MR imaging compared with 201Tl SPECT imaging. *Radiology*. 2004;232(1):49-57.
28. Kim RJ, Wu E, Rafael A, Chen EL, Parker MA, Simonetti O, Klocke FJ, Bonow RO, Judd RM. The use of contrast-enhanced magnetic resonance imaging to identify reversible myocardial dysfunction. *N Engl J Med.* 2000;343(20):1445-1453.
29. Beek AM, Kuhl HP, Bondarenko O, Twisk JW, Hofman MB, van Dockum WG, Visser CA, van Rossum AC. Delayed contrast-enhanced magnetic resonance imaging for the prediction of regional functional improvement after acute myocardial infarction. *J Am Coll Cardiol*. 2003;42(5):895-901.
30. Wu KC, Kim RJ, Bluemke DA, Rochitte CE, Zerhouni EA, Becker LC, Lima JA. Quantification and time course of microvascular obstruction by contrast-enhanced echocardiography and magnetic resonance imaging following acute myocardial infarction and reperfusion. *J Am Coll Cardiol*. 1998;32(6):1756-1764.

Chapter 4

Intramyocardial hemorrhage and microvascular obstruction after primary percutaneous coronary intervention

Aernout M. Beek, Robin Nijveldt, Albert C. van Rossum

In press Int J CV Imaging

ABSTRACT

Purpose. Reperfusion may cause intramyocardial hemorrhage (IMH) by extravasation of erythrocytes through severely damaged endothelial walls. The purpose of the study was to evaluate the clinical significance of IMH in relation to infarct size, microvascular obstruction (MVO) and function in patients after primary percutaneous intervention.

Methods. Forty-five patients underwent cardiovascular MR imaging (CMR) one week and 4 months after primary stenting for a first acute myocardial infarction. T2-weighted spin-echo imaging (T2W) was used to assess infarct related edema and IMH, and delayed enhancement (DE) was used to assess infarct size and MVO. Cine CMR was used to assess left ventricular volumes and function at baseline and at 4 months follow-up.

Results. In 22 (49%) patients, IMH was detected as areas of attenuated signal in the core of the high signal intensity region on T2W images. Patients with IMH had larger infarcts, higher left ventricular volumes and lower ejection fraction. Contrast-to-noise ratio (CNR) between hyperintense periphery and the hypo-intense core of the T2W ischemic area correlated to peak CKMB, total infarct size and MVO size. Using univariable analysis, CNR predicted ejection fraction at baseline (β=-0.62, $p = 0.003$) and follow-up (β=-0.84, $p < 0.001$). However, after multivariable analysis, baseline ejection fraction and presence of MVO were the only parameters that predicted functional changes at follow-up.

Conclusion. IMH was found in the majority of patients with MVO after reperfused myocardial infarction. It was closely related to markers of infarct size, MVO and function, but did not have prognostic significance beyond MVO.

Acknowledgements

This study was supported by the Netherlands Heart Foundation (grant 2003B126). The authors would like to thank Paul Algra, MD, PhD (department of Radiology, Medical Center, Alkmaar, The Netherlands), Victor Umans, MD, PhD (department of Cardiology Medical Center, Alkmaar, The Netherlands) and Mary Belderok (department of Cardiology, VU University Medical Center, Amsterdam) for their contribution to the patient group collection and the data acquisition.The authors would also like to thank Hans Niessen, MD, PhD (department of Pathology, VU University Medical Center, Amsterdam, The Netherlands) for providing Figure 2.

INTRODUCTION

Timely reperfusion is the only way to preserve ischemic myocardium in acute myocardial infarction. However, reperfusion also induces new pathological changes that were not seen in the pre-interventional era [1]. Microvascular obstruction (MVO) or no-reflow refers to the small vessel changes that prevent adequate tissue perfusion despite a revascularized and patent epicardial coronary artery [2,3]. Although MVO is related to infarct size, it is an independent and powerful predictor of adverse outcome [4,5]. Reperfusion may also cause intramyocardial hemorrhage (IMH) by extravasation of erythrocytes through severely damaged endothelial walls [6,7]. IMH can be visualized by T2-weighted CMR because breakdown products of hemoglobin are paramagnetic and influence regional magnetic tissue properties [8,9]. Previous studies found IMH in about one third of patients and suggested a relation with more severe myocardial injury and MVO [10,11]. However, the exact significance of IMH and its relation to MVO remain unclear.

This study was undertaken to further evaluate presence and clinical significance of IMH by exploring its relation to infarct size, MVO and function in patients after primary coronary angioplasty for acute myocardial infarction.

METHODS

Patients. All patients gave informed consent to the study protocol, which was approved by the local ethics committee. Patients were considered study candidates when admitted with a first ST-elevation acute myocardial infarction treated with successful primary coronary angioplasty (PCI) with stent implantation, defined as Thrombolysis In Myocardial Infarction (TIMI) flow grade 2 or 3. Patients with hemodynamic instability or (relative) contraindications for CMR were excluded.

Cardiac Magnetic Resonance imaging protocol. All examinations were performed on a 1.5-T clinical scanner (Sonata/Symphony, Siemens, Erlangen, Germany) using a phased array cardiac receiver coil. The baseline scan was scheduled between 2 to 9 days after reperfusion and follow-up at 4 months. ECG-gated images were acquired during end-expiration breath holding. Segmented steady state free precession cine imaging (average voxel size 1.6x1.9x5 mm3, temporal resolution 47 ms) was used to evaluate left ventricular function in long axis views and full coverage short axis views (interslice gap 5 mm). Prior to contrast injection, breath-hold, segmented T2-weighted spin-echo imaging (T2W) (STIR, TR = 2 x RR-interval, TE 64 ms, average voxel size 1.4x1.9x7 mm3) was performed to visualize infarct related edema and hemorrhage. Three long axis views and a short axis view at the core of the infarct, defined as the short axis slice position with the largest circumferential amount of wall motion abnormalities were acquired [12]. An image

normalisation filter was used to correct for coil inhomogeneity. Delayed enhancement (DE) images were acquired using a segmented inversion recovery gradient-echo pulse sequence (average voxel size 1.4x1.7x5 mm3, trigger pulse 2, inversion time 250-300 ms) 12 to 15 minutes after i.v. administration of 0.2 mmol/kg gadolinium-DTPA in short axis views with slice positions copied from the cine series.

Analysis. All CMR data were analysed on a separate workstation using dedicated software (Mass version 2006beta, Medis, Leiden, the Netherlands). Cine, T2W and contrast images were analysed separately, and, during analysis of one technique, the observers were blinded to results of the other techniques as well as to other clinical patient data.

Endocardial and epicardial contours were manually drawn on all end-diastolic and end-systolic cine images to calculate normalised (body surface area) left ventricular end-diastolic (EDV) and end-systolic volumes (ESV), mass and ejection fraction.

T2W images were assessed qualitatively for the presence of regional high signal intensity. IMH was considered present on T2W if regions of low (attenuated) signal were seen within the high signal area. Using the short axis view, the high signal intensity area (T2W infarct area) was quantified after windowing the images at mean + 2 SD of the signal intensity (SI) of remote, normal myocardium, and expressed as a percentage of total slice area. IMH was included in the calculation of T2W infarct area. An ellipsoid region of interest (0.2-0.3 cm2) was placed in the central part (core) of the T2W infarct, covering the region with attenuated signal when present, and placed in the middle of the hyperintense region in patients without IMH. Regions of interest were also drawn in the peripheral part (peri) of the T2W infarct area and in remote, normal myocardium (Fig. 1). Signal-to-noise ratio (SNR) was calculated as SNRcore = SIcore / SDnoise, and SNRperi = SIperi / SDnoise and SNRnorm = SInorm / SDnoise, respectively. Since no parallel imaging was used, noise was calculated as the standard deviation of a region of interest in background air, divided by 0.7, taking into account the number of effective radiofrequency coils [13]. Contrast-to-noise ratio (CNR) between the infarct periphery and core was calculated as CNR = (SIperi - SIcore) / SDnoise.

DE images were analysed as previously described [14]. Total infarct size was expressed as percentage of total left ventricular mass. MVO was defined as any region of hypoenhancement within the hyperenhanced, infarcted area, and was included in the calculation of total infarct size. MVO size was calculated by subtraction of the hyperenhanced area from the total infarct size, and expressed as a percentage of left ventricular mass (%). For direct comparison of infarct extent with T2W images, infarct area in the same slice position was quantified and expressed as percentage of total slice area.

Table 1. Baseline characteristics acoording to absence (IMH -) or presence (IMH +) of intramyocardial hemorrhage on T2W images.

	IMH -	IMH +	p-value
Number	23	22	NS
Age (sd)	59 ± 10	54 ± 10	NS
Male	21	19	NS
Diabetes	2	0	NS
Hypercholesterolemia	5	8	NS
Hypertension	6	6	NS
Smoking	14	14	NS
Infarct related artery			NS
LAD	13	16	NS
LCx	3	3	NS
RCA	7	3	NS
Time to reperfusion (hrs)	3.6 ± 3.8	3.5 ± 3.0	NS
Abciximab	19	20	NS
TIMI flow post-PCI			NS
TIMI 2	4	3	NS
TIMI 3	19	19	NS
Peak CK	188 ± 102	378 ± 156	<0.001
Time to baseline CMR	4.3 ± 2.1	5.7 ± 2.0	0.03
Total infarct size (% of LV)	11.3 ± 7.3	24.4 ± 7.0	<0.001
MVO	5	22	<0.001
MVO (% of total infarct)	0.3 ± 1.1	12.3 ± 8.9	<0.001
EDV (ml/m2)	89 ± 22	104 ± 22	0.02
ESV (ml/m2)	49 ± 17	64 ± 19	0.007
Ejection fraction (%)	46.4 ± 8.4	38.9 ± 8.1	0.004

Values are presented as numbers or as mean ± standard deviation.
LAD = left anterior descending artery, LCx = circumflex artery, RCA = right coronary artery. TIMI = Thrombolysis in Myocardial Infarction. PCI = percutaneous coronary intervention.

Statistical analysis. Data are expressed as mean ± SD for continuous variables. The independent samples T-test and Chi-square test were used to compare subgroups. The paired samples T-test was used to evaluate changes in left ventricular global parameters between baseline and follow-up. Pearson's correlation coefficients (r) were calculated for the relation between CNR, peak CKMB, total infarct size, MVO size and ejection fraction. Univariable and multivariable linear regression analysis was used to evaluate the relation of clinical (age, CKMB) and CMR parameters (total infarct size, MVO, CNR) to ejection fraction and their ability to predict changes at follow-up.

RESULTS

Fifty consecutive patients were included in the study protocol. T2W image quality was non-diagnostic in both short axis and long axis views in 5 (10%) because of artifacts or regional signal loss caused by cardiac or respiratory motion. The remaining 45 patients had an uncomplicated clinical course between both CMR examinations. Mean time between admission and baseline CMR was 5.1±2.1 days. Mean total infarct size was 17.6±10.0% of total left ventricular mass. MVO was identified on contrast images in 27 patients (60%), and mean MVO size was 6.0±8.4% of total infarct size. Mean ejection fraction was 42±10%, and increased to 45±10% at follow-up (p = 0.004).

Edema, hemorrhage and MVO. In all patients, T2W revealed a region of high signal intensity in the distribution area of the infarct related artery (Fig. 1). In almost half (22 of 45), areas of varying size of lower signal intensity could be identified in the central part of the area of high signal intensity (Fig. 1). Baseline characteristics according to presence of IMH are summarized in Table 1.

All patients with IMH had MVO on contrast images and only 5 patients with MVO did not have IMH on T2W. At baseline, patients with IMH had higher peak CKMB, larger total infarct size, larger volumes and lower ejection fraction. At follow-up, patients without IMH showed a significant improvement in EDV (89±22 vs 83±22 ml/m2, p = 0.05), ESV (49±17 vs 43±15 ml/m2, p = 0.003) and ejection fraction (46.4±8.4 vs 49.6±8.0 %, p = 0.04). Patients with IMH showed a non-significant increase in EDV (104±22 vs 111±29 ml/m2, p = 0.076) and ESV (65±19 vs 67±24 ml/m2, p = 0.310), and a small, non-significant increase in ejection fraction (38.9±8.1 vs 40.6±8.5 %, p = 0.72).

SNR and CNR analysis. Five additional patients were excluded from further signal intensity analysis because the short axis images were of insufficient quality to calculate T2W infarct area or SNR. In the remaining 40 patients, there was a significant correlation between mean infarct area on T2W images and on DE images (r = 0.73, p < 0.001), although the area was larger on T2W images: 49.3±15% vs 28.9±15.7%, p < 0.001 (Fig 1). SNRperi was significantly higher than SNRcore in the patients with MVO (29.4 vs 20.6, p

< 0.001) but not in patients without MVO (29.9 vs 30.2, p = 0.68). As a result, CNR was higher in patients with MVO than in patients without MVO (8.8±5.5 vs 0.3±3.5, p < 0.001). CNR correlated significantly with peak CKMB (r = 0.51, p = 0.001), total infarct size (r = 0.57, p < 0.001), and size of the MVO area (r = 0.52, p < 0.001).

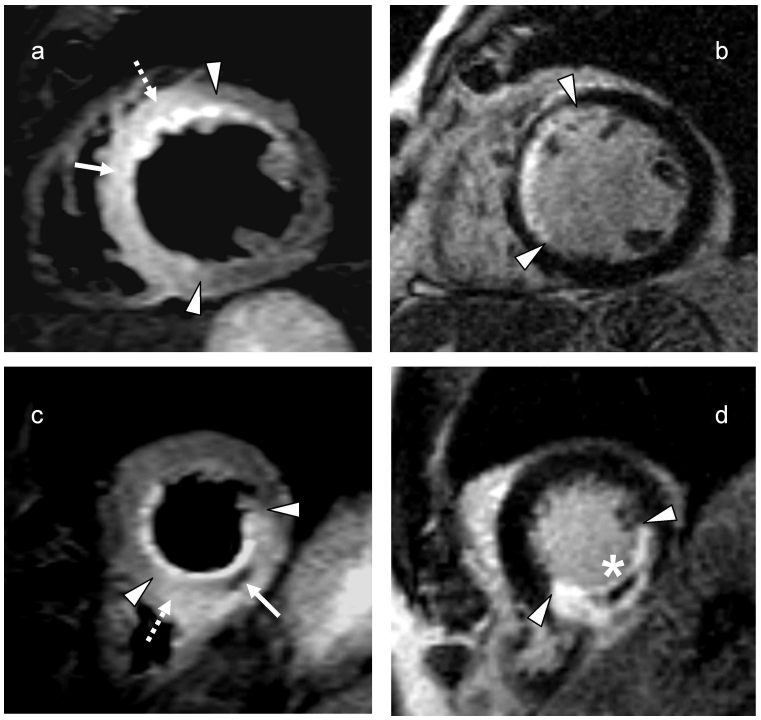

Figure 1. Edema, hemorrhage, infarct and microvascular obstruction. High and homogeneous T2W signal (a) in a patient with subendocardial anteroseptal infarction without MVO (b). Attenuated T2W signal corresponding to hemorrhage in the infarct core (c) in a patient with transmural inferoposterior infarction with MVO (d). Infarct area on T2W images is larger than on DE images in both patients. Borders of the infarcted areas are indicated by triangles, T2W core by solid arrow, T2W periphery by interrupted arrow and MVO by asterisk.

Hemorrhage and ejection fraction. Using univariable analysis, CNR strongly predicted ejection fraction at baseline (β=-0.62, p = 0.003) and follow-up (β=-0.84, p < 0.001), but not the change over time (β=-0.22, p = 0.11). After multivariable analysis, infarct size remained the single independent predictor of ejection fraction at baseline (β=-0.69, p < 0.001) and follow-up (β=-0.73, p < 0.001), whereas baseline ejection fraction and presence

of MVO were the only predictors of change in ejection fraction (β=-0.29 and β=-4.99 respectively, $p < 0.01$).

DISCUSSION

Our study showed that intramyocardial hemorrhage can be found in almost half of patients with successfully revascularized acute myocardial infarction. The presence of IMH was associated with larger infarcts, presence of MVO, higher left ventricular volumes and lower ejection fraction, and the lack of improvement at follow-up. Contrast-to-noise ratio between (attenuated) core and (high) peripheral T2W signal intensity was strongly related to markers of infarct size, MVO and function. However, in our study, it was not an independent predictor of functional changes at follow-up.

T2-weighted imaging, edema and hemorrhage. Normal myocardium has low to intermediate signal on T2W images, but increased regional water content, such as infarct related edema, causes an increase in the T2-relaxation time and T2W signal intensity [15]. Hemorrhage and the breakdown of oxygenated hemoglobin also influence magnetic properties of the surrounding tissue. The effects of hemoglobin degradation have been extensively studied in patients with cerebral hemorrhage; they are complex and strongly dependent on the age of the hematoma and the integrity of the erythrocyte membrane [8]. T2W signal is high in the very early, hyperacute phase, but then falls because of the paramagnetic effects of deoxyhemoglobin and intracellular methemoglobin [8]. Especially in the core of the hematoma, where there is marked hypoxia, signal may remain very low for a prolonged period of time [16]. Lotan et al studied IMH in a canine myocardial infarction model using ex-vivo T2W [9]. They found areas of low signal within the zone of increased signal that accurately matched the location of macroscopic hemorrhage in all animals but one (with a very small hemorrhage), and no hypointense T2W regions in the animals without hemorrhage. Hemorrhage size according to CMR correlated closely to size determined from tissue slices and according to labeled red blood cells. Basso et al recently compared in-vivo and ex-vivo CMR to histopathological findings in 2 patients that had died 12 and 24 days after percutaneous revascularization, respectively [17]. Both patients had hemorrhagic infarcts, with massive bleeding at the core of the infarct. Both in-vivo and ex-vivo T2W showed areas of low signal intensity within areas of high signal intensity that corresponded to hemorrhage and edema, respectively. Thus, although we have no direct proof of the presence of hemorrhage in our patients, we believe that these studies sufficiently show that hemorrhage and hemoglobin breakdown leads to T2W signal attenuation as documented in our study. Our results are roughly in line with the results from previous studies that used T2*('star')-weighted gradient-echo techniques to visualize IMH [10,11]. Asanuma et al found IMH in 9 of 24 (38%) patients with reperfused anterior MI

[10]. Patients with IMH had larger enzymatic infarct size, more Q-wave infarctions and less improvement in echocardiographic wall motion score. Ochiai et al showed IMH in 13 of 39 (33%) patients with reperfused infarction, and also found an association between IMH, infarct severity and less improvement of ventriculographic ejection fraction [11]. There are no studies comparing T2W spinecho imaging to T2*-weighted gradient-echo imaging for the assessment of IMH, and, at this point, it is not clear which is the optimal technique for its visualisation. Cardiac application of both techniques has been validated in a limited number of experimental and pathological studies [9,11,18]. Although T2*-weighted gradient-echo imaging is very sensitive to the paramagnetic effects of the deoxyhemoglobin and methemoglobin, it requires relatively long echo times that may degrade image quality during cardiac imaging [8]. T2W spinecho imaging has the advantage that it also depicts infarct related edema, which has been shown to correspond to the area at risk [19,20]. In line with a recent report by Friedrich et al, we found that mean (single slice) T2W infarct area was (approximately 70%) larger than DE infarct area [20].

Clinical implications. Hemorrhagic myocardial infarction was rarely seen in autopsy studies in the pre-reperfusion era, but its reported incidence markedly increased after the introduction of thrombolytic therapy [6,21]. Later studies showed that it also occurred after primary PCI [10,11]. The appearance of hemorrhage therefore depends on the coexistence of myocardial reperfusion and microvascular damage in the setting of severe myocardial ischemia [7,17]. The large majority (81%) of our patients with MVO also had IMH, and MVO size in the 5 patients without IMH was very small (<1% of total infarct size). Further more, our results suggest that hemorrhage severity, as reflected by the degree of T2W signal attenuation as contrast-to-noise ratio, is related to infarct and MVO extent, but does not have prognostic value beyond MVO. In early studies in the mid-seventies, Kloner et al already demonstrated that extravasation of erythrocytes is one of the morphological features found in areas of no-reflow [22]. This close relation between MVO and IMH might explain the lack of additional prognostic significance as seen in our study. Figure 2 illustrates the co-existence of edema, IMH and MVO in a patient who died 3 days after inferoposterior myocardial infarction (patient was not included in the study group).

The non-invasive assessment of IMH by CMR might be used to indicate infarct severity and underlying microvascular injury, e.g. in patients with (moderate to severe) renal insufficiency, who have a relative contra-indication against the use of gadolinium compounds [23]. However, further study is needed to define the optimum CMR technique to assess IMH, and to determine the exact role of IMH in the myocardial healing process.

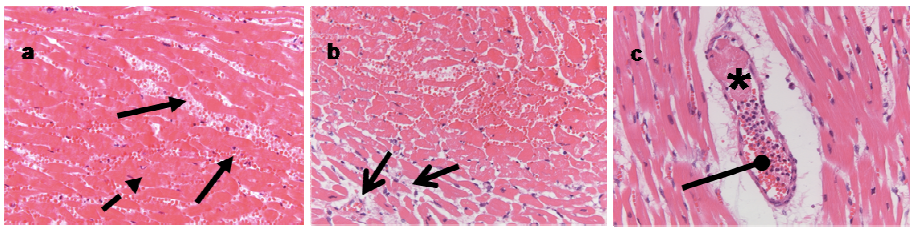

Figure 2. Microscopic slides at 200x magnification after standard hematoxylin and eosin staining of 3 samples of the heart of a 44-year old man who died 3 days after admission with acute inferoposterior infarction (patient not included in the study group). (a) infarct core with necrotic cardiomyocytes (interrupted arrow) and abundant erythrocytes (solid arrows), (b) infarct border zone with edema (open arrow), (c) capillary vessel with thrombus (asterisk) and plugged polymorphonuclear cells (circled arrow). To view image in colour see original citation.

Study limitations. Spatial coverage of the T2W images was limited as we focused on the identification of hemorrhage in the core of the infarct. As a result, we may have missed regions of signal attenuation in adjacent slices in the 5 patients with MVO but without IMH. Signal-to-noise ratios are related to scan parameters such as voxel size, and therefore our results may not be directly applicable when other scanners are used. The current breath-hold T2W spin-echo imaging technique is limited by its sensitivity to artifacts caused by cardiac or respiratory motion, as illustrated by the considerable number of non-diagnostic images in our study group (10% of long axis images, 20% of short axis images). A recently proposed adaptation of the technique to optimize performance has not yet been evaluated in a clinical setting [24].

In conclusion, intramyocardial hemorrhage was found in the majority of patients with microvascular obstruction after percutaneous revascularization for acute myocardial infarction. It was closely related to markers of infarct size, MVO and function, but, in this study, did not have prognostic significance beyond MVO.

REFERENCES

1. Pasotti M, Prati F, Arbustini E. The pathology of myocardial infarction in the pre- and post-interventional era. Heart 2006;92:1552-6.
2. Ambrosio G, Weisman HF, Mannisi JA, et al. Progressive impairment of regional myocardial perfusion after initial restoration of postischemic blood flow. Circulation 1989;80:1846-61.
3. Reffelmann T, Kloner RA. The "no-reflow" phenomenon: basic science and clinical correlates. Heart 2002;87:162-8.
4. Wu KC, Zerhouni EA, Judd RM, et al. Prognostic significance of microvascular obstruction by magnetic resonance imaging in patients with acute myocardial infarction. Circulation 1998;97:765-72.
5. Nijveldt R, Beek AM, Hirsch A, et al. Functional recovery after acute myocardial infarction: A comparison between angiography, electrocardiography and cardiovascular magnetic resonance measures of microvascular injury. J Am Coll Cardiol 2008;52:181-9.
6. Fujiwara H, Onodera T, Tanaka M, et al. A clinicopathologic study of patients with hemorrhagic myocardial infarction treated with selective coronary thrombolysis with urokinase. Circulation 1986;73:749-57.
7. Basso C, Thiene G. The pathophysiology of myocardial reperfusion: a pathologist's perspective. Heart 2006;92:1559-62.
8. Bradley WG, Jr. MR appearance of hemorrhage in the brain. Radiology 1993 Oct 1;189(1):15-26.
9. Lotan CS, Bouchard A, Cranney GB, et al. Assessment of postreperfusion myocardial hemorrhage using proton NMR imaging at 1.5 T. Circulation 1992;86:1018-25.
10. Asanuma T, Tanabe K, Ochiai K, et al. Relationship between progressive microvascular damage and intramyocardial hemorrhage in patients with reperfused anterior myocardial infarction: Myocardial contrast echocardiographic study. Circulation 1997;96:448-53.
11. Ochiai K, Shimada T, Murakami Y, et al. Hemorrhagic myocardial infarction after coronary reperfusion detected in vivo by magnetic resonance imaging in humans: prevalence and clinical implications. J Cardiovasc Magn Reson 1999;1:247-56.
12. Simonetti OP, Finn JP, White RD, et al. "Black blood" T2-weighted inversion-recovery MR imaging of the heart. Radiology 1996;199:49-57.
13. Constantinides CD, Ergin A, McVeigh E. Signal-to-noise measurements in magnitude images from NMR phased arrays. Magn Reson Med 1997;38:852-7.
14. Nijveldt R, Beek AM, Hofman MBM, et al. Late gadolinium-enhanced cardiovascular magnetic resonance evaluation of infarct size and microvascular obstruction in optimally treated patients after acute myocardial infarction. J Cardiovasc Magn Reson 2007;9:765-70.
15. Higgins CB, Herfkens R, Lipton MJ, et al. Nuclear magnetic resonance imaging of acute myocardial infarction in dogs: alterations in magnetic relaxation times. Am J Cardiol 1983;52:184-8.
16. Parizel PM, Makkat S, Van Miert E, et al. Intracranial hemorrhage: principles of CT and MRI interpretation. Eur Radiol. 2001;11:1770-83.
17. Basso C, Corbetti F, Silva C, et al. Morphologic validation of reperfused hemorrhagic myocardial infarction by cardiovascular magnetic resonance. Am J Cardiol 2007;100:1322-7.
18. van den Bos EJ, Baks T, Moelker AD, et al. Magnetic resonance imaging of hemorrhage within reperfused myocardial infarcts: possible interference with iron oxide-labelled cell tracking? Eur Heart J 2006;27:1620-6.
19. Aletras AH, Tilak GS, Natanzon A, et al. Retrospective Determination of the area at risk for reperfused acute myocardial infarction with T2-weighted cardiac magnetic resonance imaging: Histopathological and displacement encoding with stimulated echoes (DENSE) functional validations. Circulation 2006;113:1865-70.
20. Friedrich MG, Abdel-Aty H, Taylor A, et al. The salvaged area at risk in reperfused acute myocardial infarction as visualized by cardiovascular magnetic resonance. J Am Coll Cardiol 2008;51:1581-7.

21. Mathey DG, Schofer J, Kuck KH, et al. Transmural, hemorrhagic myocardial infarction after intracoronary streptokinase. Clinical, angiographic, and necropsy findings. Br Heart J 1982 Dec 1;48(6):546-51.
22. Kloner RA, Ganote CE, Jennins RB et al. Demonstration of the “no-reflow” phenomenon in the dog heart after temporary ischemia. Recent Adv Stud Cardiac Struct Metab 1975;10:463-74.
23. Kuo PH, Kanal E, Abu-Alfa AK, et al. Gadolinium-based MR contrast agents and nephrogenic systemic fibrosis. Radiology 2007;242:647-9.
24. Keegan J, Gatehouse PD, Prasad SK, et al. Improved turbo spin-echo imaging of the heart with motion-tracking. J Magn Res Imaging 2006;24:563-70.

Chapter 5

Myocardial viability in chronic ischemic heart disease: Comparison of contrast-enhanced magnetic resonance imaging with ^{18}F-fluorodeoxyglucose positron emission tomography

Harald P. Kühl, Aernout M. Beek, Arno P. van der Weerdt, Mark B. M. Hofman, Cees A. Visser, Adriaan A. Lammertsma, Nicole Heussen, Frans C. Visser and Albert C. van Rossum

J Am Coll Cardiol 2003;41;1341-8

ABSTRACT

Objectives. We sought to compare contrast-enhanced magnetic resonance imaging (ceMRI) with nuclear metabolic imaging for the assessment of myocardial viability in patients with chronic ischemic heart disease and left ventricular (LV) dysfunction.

Background. Contrast-enhanced MRI has been shown to identify scar tissue in ischemically damaged myocardium.

Methods. Twenty-six patients with chronic coronary artery disease and LV dysfunction (mean ejection fraction 31 ± 11%) underwent ^{18}F-fluorodeoxyglucose (FDG) positron emission tomography (PET), technetium-99m tetrofosmin single-photon emission computed tomography (SPECT), and ceMRI. In a 17-segment model, the segmental extent of hyperenhancement (SEH) by ceMRI, defined as the relative amount of contrast-enhanced tissue per myocardial segment, was compared with segmental FDG and tetrofosmin uptake by PET and SPECT.

Results. In severely dysfunctional segments (n = 165), SEH was 9 ± 14%, 33 ± 25% ($p < 0.05$), and 80 ± 23% ($p < 0.05$) in segments with normal metabolism/perfusion, metabolism/perfusion mismatch, and matched defects, respectively. Segmental glucose uptake by PET was inversely correlated to SEH ($r = -0.86$, $p < 0.001$). By receiver operator characteristic curve analysis, the area under the curve was 0.95 for the differentiation between viable and non-viable segments. At a cutoff value of 37%, SEH optimally differentiated viable from non-viable segments defined by PET. Using this threshold, the sensitivity and specificity of ceMRI to detect non-viable myocardium as defined by PET were 96% and 84%, respectively.

Conclusions. Contrast-enhanced MRI allows assessment of myocardial viability with a high accuracy, compared with FDG-PET, in patients with chronic ischemic heart disease and LV dysfunction.

Acknowledgements

This work was supported by the Netherlands Heart Foundation (grant no. 2001.158). Dr. H. P. Kühl was supported in part by grants from the Faculty of Medicine of the Rheinisch-Westfälische Technische Hochschule, Aachen, and by the Grimmke-Stiftung, Düsseldorf, Germany.

INTRODUCTION

Assessment of residual myocardial viability in patients with chronic coronary artery disease and left ventricular (LV) dysfunction is of great clinical importance [1, 2, 3 and 4]. Several techniques analyzing the morphologic [5], functional [6], cellular [7], or metabolic [8] integrity of the myocardium have been introduced into clinical medicine. Each of these methods has specific advantages for the diagnosis of myocardial viability, but none allows direct visualization of the transmural extent of viable and non-viable tissue. Recently, contrast-enhanced magnetic resonance imaging (ceMRI) has been proposed as an alternative imaging modality for the assessment of myocardial viability. In several experimental studies, the relationship between hyperenhanced myocardium at ceMRI and myocardial necrosis determined by histology has been investigated [9, 10, 11, 12, 13 and 14]. Using high spatial resolution techniques, the size and shape of hyperenhanced areas at ceMRI were identical to areas of irreversible injury defined by tetrazolium staining [15]. Moreover, ceMRI allows one to distinguish between regions with reversible and irreversible myocardial injury, depending on the transmural extent of hyperenhancement [14 and 15]. Furthermore, the transmural extent of hyperenhancement has been shown to be predictive of recovery of segmental contractile function after myocardial revascularization in experimental studies [16] and in patients with acute myocardial infarctions and chronic ischemic heart disease [17 and 18].

The aim of this study was to compare ceMRI with nuclear metabolic imaging using ^{18}F-fluorodeoxyglucose (FDG) positron emission tomography (PET) for the detection of myocardial viability in patients with chronic ischemic heart disease and LV dysfunction.

METHODS

Patient population. Twenty-six consecutive patients with LV dysfunction scheduled for myocardial viability assessment were scanned with both PET and ceMRI within three weeks of each other. All patients were in a stable clinical condition, and there were no ischemic events or mechanical interventions in the period between the different examinations. Three patients were scanned within two weeks after an acute myocardial infarction and were excluded from the final analysis. The baseline characteristics of the patient population are given in Table 1. The Committee on Research Involving Human Subjects of the Vrije Universiteit Medical Center, Amsterdam, approved the study protocol, and all subjects gave written, informed consent.

Table 1. Baseline Characteristics of the Patient Population

Mean age in yrs (range)	65 (41-81)
Males/females	18/5
History of myocardial infarction	18 (78%)
Time interval between infarction and viability studies (months)	150 ± 83
Q waves on ECG	15 (65%)
Coronary angiography	21 (91%)
Single-vessel disease	4
Two-vessel disease	5
Three-vessel disease	12
Previous revascularization	14 (61%)
CABG	2
PTCA	7
CABG and PTCA	5
Mean ejection fraction (%)	31 ± 11

Data are presented as the mean value ± SD or number (%) of subjects. CABG = coronary artery bypass grafting; ECG = electrocardiogram; MRI = magnetic resonance imaging; PTCA = percutaneous transluminal coronary angioplasty.

IMAGING PROTOCOLS

Magnetic resonance imaging. Images were acquired on a 1.5-tesla whole-body scanner (Magnetom Sonata by Siemens, Erlangen, Germany) with the patient in a supine position using a four-element, phased-array cardiac coil. Scout images were acquired in long-axis and short-axis orientations for planning of the final double-oblique long-axis and short-axis views. Electrocardiographically gated cine images were acquired using a segmented steady-state free precession sequence (true FISP; echo time/repetition time [TE/TR] of 1.2/3.2 ms; resolution of 1.3 × 1.8 × 5 mm). Three long-axis views and seven to 11 short-axis views 1 cm apart, covering the whole LV, were obtained during repeated breath-holds. A gadolinium-based contrast agent (Magnevist 0.2 mmol/kg; Schering AG, Berlin, Germany) was then administered intravenously using an automated injection at a rate of 3 ml/s. After 15 to 20 min, contrast-enhanced images were acquired in the same orientation as the cine images, using a segmented inversion-recovery, gradient-echo pulse sequence triggered to end diastole [19]. The inversion time was set to null the signal of normal myocardium after contrast administration (typically 250 to 300 ms) and was adjusted in the course of the investigation if necessary. Other parameters of the sequence were TR/TE of 9.6/4.4 ms, flip angle 25°, matrix 208 × 256, and a typical voxel size of 1.6 × 1.3 × 5.0 mm.

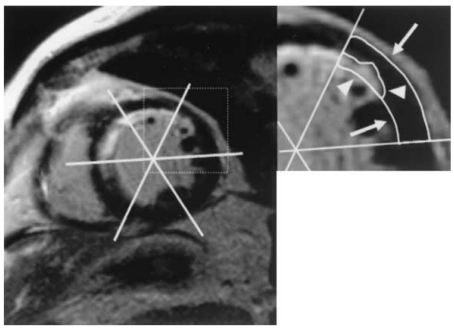

Figure 1. Analysis of contrast-enhanced images. (Large panel) The posterior insertion of the right ventricular wall into the left ventricle served as a landmark for the definition of sectors in the short-axis slices. (Small panel) Total myocardial area per sector (outer white line, arrows) and contrast-enhanced area per sector (inner white line, arrowheads) were traced manually, and the amount of hyperenhancement was expressed as the percentage relative to total myocardial area.

FDG-PET imaging. All patients underwent hyperinsulinemic-euglycemic clamping [20]. Scans were performed in a two-dimensional mode, using an ECAT EXACT HR+ (Siemens/CTI, Knoxville, Tennessee), after an intravenous injection of 370 MBq of FDG. The dynamic scan consisted of 39 frames with variable frame lengths for a total time of 60 min. All dynamic scan data were corrected for physical decay of ^{18}F and for dead time, scatter, and random and measured photon attenuation. The images were reconstructed using filtered backprojection with a Hanning filter at the Nyquist frequency. This resulted in a transaxial spatial resolution of ~7 mm full width at half maximum. Additionally, each patient underwent technetium-99m-tetrofosmin single-photon emission computed tomography (SPECT) for assessment of rest blood flow.

Table 2. Results of Magnetic Resonance Imaging Parameters and uptake by Positron Emission Tomography, According to Wall Motion

Wall Motion	No. of Segments	EDWT (mm)	Wall Thickening (mm)	SEH (%)	FDG Uptake (%)
Normal	156	7.8 ± 1.7	4 ± 1	2 ± 8	86 ± 12
Mild to moderate hypokinesia	70	7.1 ± 1.6	2 ± 1*	9 ± 13*	82 ± 15
Severe hypokinesia	65	6.7 ± 2.0*	1 ± 0.7*	14 ± 20*	75 ± 17*
Akinesia/dyskinesia	100	5.5 ± 1.6*	0.2 ± 0.3*	50 ± 38*	54 ± 22*

*$p < 0.05$ vs. normal. Data are presented as the mean value ± SD.
EDWT = end-diastolic wall thickness; FDG= ^{18}F-fluorodeoxyglucose; SEH = segmental extent of hyperenhancment.

DATA ANALYSIS

Segmental model. For each imaging modality, an identical 17-segment model was used dividing the LV into six basal, six midventricular, and four distal segments, and the apex

[21]. The basal, midventricular, and distal segments were evaluated in short-axis images, whereas the apical cap was evaluated in the two-chamber long-axis view with ceMRI and in the vertical long-axis view with PET and SPECT. By convention, the most basal short-axis slice used for analysis was located just below and exclusive of the LV outflow tract.

Magnetic resonance imaging. All MRI images were first previewed on a personal computer work station, using commercial software (Radworks version 5.0, Applicare Medical Imaging, Zeist, The Netherlands). To compose the basal, midventricular, and distal segments, MRI data of a maximum of three short-axis slices were averaged. All short-axis slices were projected on the two-chamber long-axis view and were allocated to the different positions according to their relationship to the papillary muscles: the midventricular slices at the level of the papillary muscles and the basal and distal slices above or below the papillary muscles. Each basal and midventricular slice was divided into six equidistant sectors angulated 60° apart starting from the posterior insertion of the right ventricular free wall into the LV myocardium. The distal slices were segmented into four equidistant sectors angulated at 90°.

Evaluation of contrast-enhanced images. The MASS software (Medis, Leiden, The Netherlands) was used for quantitative analysis. Each myocardial sector was evaluated for the presence of hyperenhancement, defined as an area of signal enhancement ≥3 SD of the signal of non-enhanced myocardium. The total myocardial area and contrast-enhanced area per sector were traced manually. The extent of contrast enhancement was expressed as a percentage of the total myocardial area ($A_{hyperenhanced}/A_{myocardium} \times 100$, where A denotes area) (Fig. 1). The MRI data of corresponding sectors on different short-axis slices used to compose one myocardial segment were averaged to give one final value for the segmental extent of hyperenhancement (SEH).

Assessment of segmental function. Wall motion was assessed by visual interpretation for each myocardial sector on each cross section using a five-point scale: 1 = normal contractility; 2 = mild to moderate hypokinesia; 3 = severe hypokinesia; 4 = akinesia; and 5 = dyskinesia. The results of different sectors composing the different myocardial segments were averaged. Additionally, segmental end-diastolic wall thickness (EDWT) and wall thickening were determined by manual tracing of endocardial and epicardial borders in end-diastolic and end-systolic stop-frame images, excluding trabeculations and papillary muscles.

FDG-PET. Data were analyzed blinded to the MRI results and patient data, using a SUN work station (SUN Microsystem, Inc.) with Siemens/CTI software. Transaxial images were reoriented according to the anatomic axis of the heart. Reconstructed slices were displayed as short-axis slices and horizontal as well as vertical long-axis slices. Short-axis slices were oriented in the same way as described for ceMRI, using the posterior insertion of the right

ventricular wall with the LV as a landmark. Regions of interest (ROIs) were defined manually on each of the short-axis slices using the same segmentation model as for ceMRI. Corresponding ROIs from a variable number of slices were grouped in each patient to compose the 17 segments. For each segment, mean tracer uptake was calculated. Uptake of FDG in each segment was normalized to the myocardial segment with maximal tetrofosmin uptake.

Table 3. Magnetic Resonance Imaging parameters in severely dysfunctional segments (n = 165) according to the viability status by Positron Emission Tomography

	MRI Parameters		
Viability Status by PET	**SEH (%)**	**EDWT (mm)**	**Wall Thickening (mm)**
Normal (n = 78)	9 ± 14	7 ± 2	1 ± 0.7
Mismatch (n = 38)	33 ± 25*	6 ± 2	0.6 ± 0.6
Non-viable (n = 49)	80 ± 23*†	4 ± 1*†	0.1 ± 0.4*†

*$p < 0.05$ vs. viable segments. †$p < 0.05$ vs. mismatched segments. Data are presented as the mean value ± SD.

MRI = magnetic resonance imaging; PET = positron emission tomography; other abbreviations as in Table 2.

Definition of viability by PET. Segments with normal perfusion (tetrofosmin uptake ≥50%) and metabolism (FDG uptake ≥50%) and segments with reduced perfusion (tetrofosmin uptake <50%) and normal or increased metabolism (mismatch) were considered viable. Segments with reduced perfusion and reduced metabolism (matched defect) were considered non-viable [22, 23, 24 and 25]. In two patients with a left bundle branch block, dysfunctional segments in the septum demonstrating FDG uptake <50% were considered viable if tetrofosmin uptake exceeded 50%, as FDG-PET may underestimate viability in the septal region in the presence of left bundle branch block [26].

Statistics. Data are expressed as the mean value ± SD. To compare the segmental results for EDWT, wall thickening, SEH, and FDG uptake by PET, depending on cardiac function, and to compare the segmental results for EDWT, wall thickening, and SEH, depending on the viability status as defined by PET, the unpaired Student t test at the Bonferroni-adjusted individual significance level (0.05/24; number of comparisons = 24) was performed. Recently described non-parametric analysis of overall sensitivities and specificities, as well as areas under the receiver operator characteristic (ROC) curves, were applied [27 and 28]. The area under the ROC curve (AUC) was considered as a measure of accuracy of ceMRI to discriminate between viable and non-viable myocardium, as defined by PET. The ROC

curve analysis was also used to assess the optimal cutoff point of the increase of SEH, as determined by ceMRI for the detection of segments with myocardial non-viability. Sensitivity and specificity were determined for viability or non-viability, as defined by PET. Computations were performed using SAS version 8.02 for Windows.

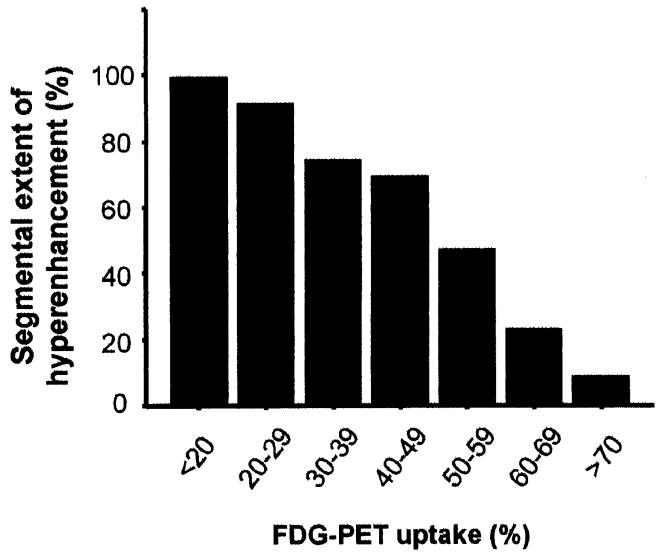

Figure 2. Bar graph showing mean segmental extent of hyperenhancement by contrast-enhanced magnetic resonance imaging categorized according to 18F-fluorodeoxyglucose (FDG) uptake by positron emission tomography (PET).

RESULTS

A total of 391 segments in 23 patients were analyzed. Table 2 summarizes the results for EDWT, wall thickening, SEH, and FDG uptake by PET, depending on segmental cardiac function. Segments with normal wall motion or mild to moderate dysfunction showed normal metabolism and perfusion in 225 (99%) of 226 segments; of these, 169 segments demonstrated no hyperenhancement and 57 segments revealed subendocardial enhancement only (mean SEH 15 ± 11%). Segments with severe dysfunction (n = 165) showed normal metabolism/perfusion in 78 segments, a metabolism/perfusion mismatch in 38 segments, and a matched defect in 49 segments. Table 3 summarizes the results for SEH, EDWT, and wall thickening, depending on the viability status defined by nuclear imaging. Of 78 dysfunctional segments with normal perfusion and metabolism, 50 segments (64%) showed no hyperenhancement and 28 segments (36%) demonstrated subendocardial hyperenhancement (25 ± 13% SEH). In 38 mismatched segments, there were six segments (16%) without hyperenhancement and 32 segments with hyperenhancement (40 ± 23%

SEH). In 49 segments with a matched defect, only one segment (2%) demonstrated no hyperenhancement, whereas 48 segments showed a large extent of hyperenhancement (82 ± 20% SEH). A strong inverse correlation was found between FDG uptake by PET and SEH by ceMRI ($r = -0.86$, $p < 0.001$). The correlation between FDG uptake and EDWT ($r = -0.51$, $p < 0.001$) or wall thickening ($r = -0.41$, $p < 0.001$) was lower than that with ceMRI. Figure 2 shows mean SEH by ceMRI categorized according to FDG uptake by PET.

Table 4. Sensitivity and Specificity of Different Thresholds of Segmental Extent of Hyperenhancement for the Detection of Non-Viable Myocardium by 18F-Fluorodeoxyglucose–Positron Emission Tomography.

SEH Threshold (%)	Sensitivity (%)	Specificity (%)
30	96	76
35	96	80
40	94	85
45	92	88
50	90	89
55	84	91
60	84	93
65	80	95
70	76	96

SEH = segmental extent of hyperenhancement.

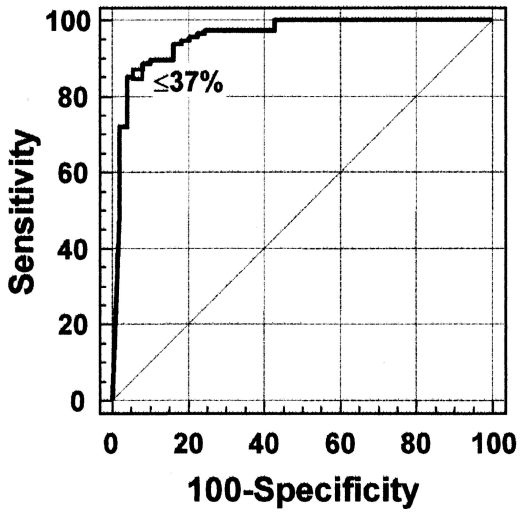

Figure 3. The receiver operator characteristic analysis of the differentiation between viable and non-viable segments by contrast-enhanced magnetic resonance imaging using 18F-fluorodeoxyglucose-positron emission tomography as a reference standard.

Accuracy of ceMRI to predict viability by FDG-PET. To assess the ability of ceMRI to discriminate between viable and non-viable segments, as defined by FDG-PET, ROC analysis was performed on all segments with severe dysfunction. The AUC of ceMRI to predict myocardial viability defined by FDG-PET was 0.95 (95% confidence interval 0.93 to 0.97) (Fig. 3). A threshold of ≤37% SEH was identified to yield optimal sensitivity and specificity for the differentiation of viable and non-viable segments defined by FDG-PET. Using this cutoff value, 100 segments were assessed as viable and 65 segments as non-viable by ceMRI. Compared with FDG-PET, the sensitivity and specificity of ceMRI for the identification of non-viable myocardium were 96% and 84%, respectively. Table 4 displays different sensitivity and specificity levels derived from the ROC curve for the detection of non-viable myocardium, as defined by PET, according to different thresholds of SEH, as assessed by ceMRI.

Relationship of viability status by ceMRI and FDG-PET. Table 5 relates the viability by ceMRI to the viability status by FDG-PET. Concordance between the techniques was high for segments with normal metabolism/perfusion (95%) or a matched defect (96%). Mismatched segments demonstrated SEH ≤37% in 24 segments (63%). Uptake of FDG was lower in the mismatched segments with SEH >37% compared with the mismatched segments with SEH ≤37% (54 ± 3% vs. 71 ± 9%; $p < 0.001$).

Figure 4 shows representative images of a patient with akinesia of the inferior wall, subendocardial hyperenhancement on ceMRI, and a metabolism/perfusion mismatch by PET and SPECT. Complete agreement between PET and ceMRI was present in 11 patients. Figure 5 shows an example of a patient with a match between ceMRI and PET. In the remaining 12 patients, the methods differed by one segment in four patients, two segments in five patients, and three segments in three patients.

Table 5. Viability by Contrast-Enhanced Magnetic Resonance Imaging According to Viability Status by Positron Emission Tomography

Viability Status by PET	Viability by ceMRI	
	SEH ≤37%	SEH >37%
Normal (n = 78)	74	4
Mismatch (n = 38)	24	14
Non-viable (n = 49)	2	47

ceMRI = contrast-enhanced magnetic resonance imaging; PET = positron emission tomography; SEH = segmental extent of hypersensitivity.

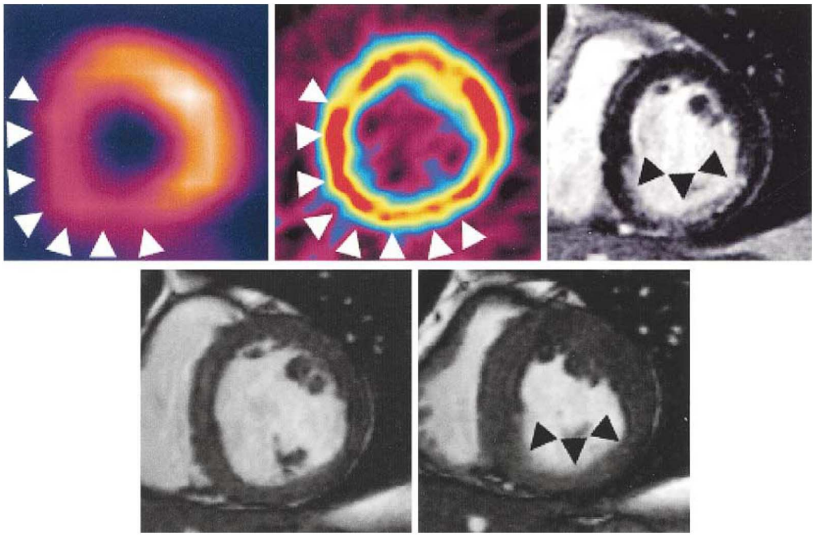

Figure 4. (Top row) Representative tetrofosmin SPECT (left panel), FDG-PET (middle panel), and contrast-enhanced magnetic resonance imaging (ceMRI) (right panel) images of the basal myocardial segments of the same patient. The SPECT image shows a perfusion defect extending from the septum to the inferior wall (white arrowheads). FDG-PET demonstrates preserved glucose metabolism in the same region (white arrowheads). On the ceMRI image, a subtle subendocardial area of hyperenhancement is seen extending from the inferoseptal to posterolateral myocardium (black arrowheads). (Bottom row) End-diastolic (left panel) and end-systolic (right panel) frames of the corresponding cine images. An area of akinesia extends along the same region as the hyperenhancement area. This area corresponds to non-contracting but viable myocardium. SPECT = single photon emission computed tomography. Other definitions are defined in Figure 2. To view image in colour see original citation.

DISCUSSION

Previous studies have suggested that myocardial hyperenhancement by ceMRI represents irreversible myocardial injury, thus allowing determination of myocardial viability. The aim of this study was to compare assessment of myocardial viability by ceMRI with metabolic imaging using FDG-PET, which is considered the in vivo reference standard for viability determination. For this purpose, we quantitatively analyzed the segmental extent of scar tissue by ceMRI and compared it with segmental FDG uptake by PET. The results demonstrate that non-viable segments by FDG-PET demonstrate a significantly larger extent of hyperenhancement compared with segments identified as viable by FDG-PET. Moreover, we found a progressive increase of scar among segments with normal perfusion/metabolism, reduced perfusion but preserved metabolism representing hibernating myocardium, and a matched perfusion/metabolism defect (Table 3). Using ROC analysis, the AUC was 0.95 for the discrimination of viable myocardium from scar, as defined by FDG-PET, reflecting high diagnostic accuracy. A cutoff value of 37% SEH was identified from the ROC curve to differentiate non-viable from viable myocardium with

optimal sensitivity and specificity. Thus, ceMRI allows accurate assessment of myocardial viability in patients with ischemic heart disease and severely reduced LV function.

Comparison with previous studies. The results of the present study compare favorably with previous reports relating the extent of fibrosis to FDG-PET findings. Maes et al. [29] observed a similar extent of percentage volume fibrosis assessed on the basis of myocardial biopsy data (35 ± 25%) in segments showing non-viability by PET. Dakik et al. [30] demonstrated that ~30% of transmural scarring correlated with a lack of improvement in function after revascularization. In a recent animal experiment studying the relationship between ceMRI and regional inotropic response, Gerber et al. [31] demonstrated that only segments with <33% transmural extent of CE had inotropic reserve during dobutamine infusion, whereas segments with a higher (>33%) transmural extent of CE did not. The results of the present study are also in close agreement with a recent report by Klein et al. [32], who evaluated ceMRI and FDG-PET for viability assessment in a similar patient population. In their study, the AUC was 0.93, with a sensitivity of 86% and a specificity of 94% for the detection of non-viability by FDG-PET. Additionally, a high correlation was reported between semiquantitative estimates of scar severity by ceMRI and PET ($r = 0.91$). Similarly, we observed a strong correlation between the segmental extent of scar by ceMRI and FDG uptake by PET ($r = -0.86$). This finding closely agrees with the results of a previous study relating the amount of fibrosis at histologic examination with regional thallium-201 activity ($r = -0.85$) in patients with chronic ischemic heart disease [33]. Other functional parameters that have been useful for the characterization of myocardial viability, such as regional wall thickness and wall thickening [5], correlated less well with FDG-PET, which is in line with the results reported by Klein et al. [32].

A high concordance was found between ceMRI and PET for assessment of the viability status of dysfunctional segments with normal perfusion/metabolism or a matched defect (Table 3). In segments with preserved metabolism but reduced perfusion (mismatch), reflecting hibernating myocardium, the results were less explicit. Sixty-three percent of segments scored viable and 37% of segments scored non-viable by ceMRI, using the threshold value of 37% SEH. The amount of enhancement averaged 33 ± 25% in this group of segments (Table 3). A similar extent of volume fibrosis at histologic examination in segments with hibernating myocardium of >6 months duration (41.9 ± 22.1%) has been reported in a previous study [34]. It should be considered that myocardial viability is a gradual phenomenon and that the dichotomous definition of viability used in the present study for ceMRI is related to the dichotomous definition of viability for FDG-PET. Thus, a segment with 50% SEH, although scored non-viable by ceMRI in the present study, demonstrates a large rim of viable myocardium. Even if recovery of function after revascularization is unlikely, restoration of blood flow may contribute to prevent further

ischemic injury and improve the clinical status and prognosis of the patient [34 and 35]. Moreover, while the cutoff value of 37% SEH is mathematically the best threshold, one might wish to choose a different cutoff value to minimize the chances of missing viable myocardium. Thus, as demonstrated in Table 4, a threshold of 50% would increase the specificity of detecting non-viable myocardium, thereby increasing the amount of segments scored viable by ceMRI.

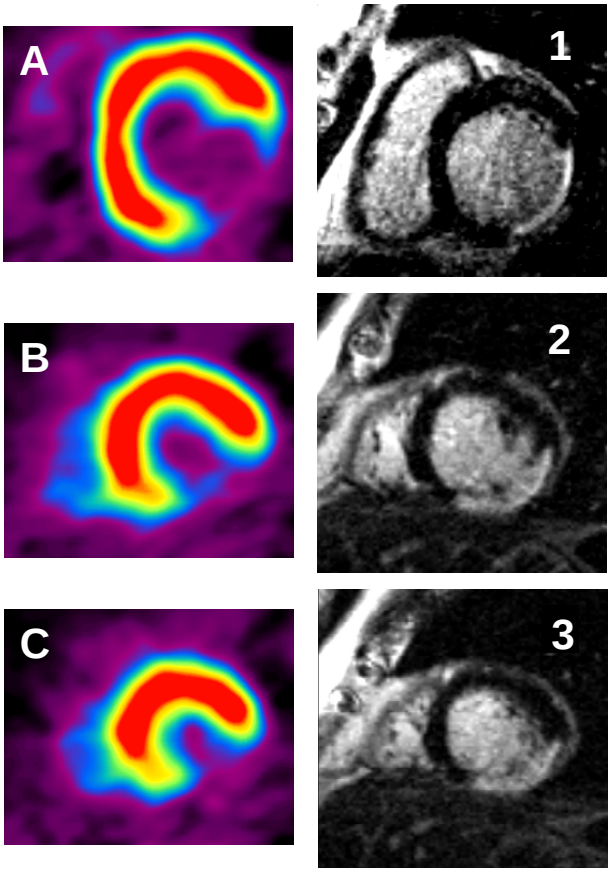

Figure 5. Example of a patient with a 36-month-old posterolateral myocardial infarction. The 18F-fluorodeoxyglucose-positron emission tomography images (left) reveal a defect in the posterolateral wall extending to the inferior wall at the basal (A), mid (B) and distal (C) ventricular level. Contrast-enhanced magnetic resonance imaging (right) shows transmural enhancement of a similar size in the same location (1,2,3). (Adapted from *J Am Coll Cardiol 2003;41;p1347, fig 5).* To view image in colour see original citation.

Study limitations. As in all studies comparing different imaging modalities, there is the possibility of image misalignment, which may account for some of the discrepancies between the FDG-PET and ceMRI results. Moreover, variability may be associated with averaging of MRI as well as PET and SPECT data, which was performed in order to compose the 17 myocardial segments. The MRI sequence used is susceptible to artifacts associated with patient movement or imperfect breath-holding, which can be erroneously interpreted as areas of hyperenhancement. Recovery of myocardial function after revascularization was not assessed in the present study. Thus, conclusions on the functional recovery of dysfunctional segments deemed viable by ceMRI cannot be drawn from the present study. Others have shown that recovery of function after revascularization is related to the transmural extent of hyperenhancement in patients with ischemic cardiomyopathy [17], with a gradual decrease in functional recovery paralleled by an increasing transmurality of hyperenhancement. In the study of Kim et al. [17], 73% (44/60) of segments with no hyperenhancement or with <50% transmural hyperenhancement improved function after revascularization. Based on these results, one might speculate that most of the dysfunctional segments assessed as viable by ceMRI in our study might have recovered function after restoration of adequate blood flow. Nevertheless, determination of contractile function after revascularization would be helpful to establish the relative importance of ceMRI and FDG-PET to predict functional recovery, which is considered an important outcome variable. Another limitation is that although the prognostic relevance of FDG-PET to predict morbidity and mortality is well established [2 and 36], data on ceMRI are scarce [37]. Thus, the prognostic relevance of ceMRI needs to be established in future studies.

In conclusion, in patients with chronic ischemic heart disease and LV dysfunction, ceMRI allows detection of myocardial viability with a high accuracy, as compared with FDG-PET. Therefore, ceMRI should be considered as an alternative technique for assessment of myocardial viability in patients with chronic coronary artery disease and may be an alternative imaging modality in centers where FDG-PET is unavailable or less economical. Future studies should be directed at assessing the prognostic value of ceMRI to predict morbidity and mortality in patients with chronic ischemic heart disease and LV dysfunction.

REFERENCES

1. Allman KC, Shaw LJ, Hachamovitch R, et al. Myocardial viability testing and impact of revascularization on prognosis in patients with coronary artery disease and left ventricular dysfunction: a meta-analysis. *J Am Coll Cardiol* 39 (2002), pp. 1151–1158.
2. Pagley PR, Beller GA, Watson DD, et al. Improved outcome after coronary bypass surgery in patients with ischemic cardiomyopathy and residual myocardial viability. *Circulation* 1997; 96:793-800.
3. Haas F, Haenel CJ, Picker W. Preoperative positron emission tomographic viability assessment and perioperative and postoperative risk in patients with advanced ischemic heart disease. *J Am Coll Cardiol* 1997; 30:1693-1700.
4. Chaudhry FA, Tauke JT, Alessandrini RS, et al. Prognostic implications of myocardial contractile reserve in patients with coronary artery disease and left ventricular dysfunction. *J Am Coll Cardiol* 1999; 32:912-920.
5. Baer FM, Voth E, Schneider CA, et al. Comparison of low-dose Dobutamine-gradient-echo magnetic resonance imaging and positron emission tomography with 18F-fluourodeoxyglucose in patients with chronic coronary artery disease. A functional and morphological approach to the detection of residual myocardial viability. *Circulation* 1995; 91:1006-1015.
6. Pierard LA, De Landsheere CM, Berthe C, et al. Identification of viable myocardium by echocardiography during Dobutamine infusion in patients with myocardial infarction after thrombolytic therapy: comparison with positron emission tomography. *J Am Coll Cardiol* 1990; 15(5):1021-1031.
7. Dilsizian V, Rocco TP, Freddman NMT, et al. Enhanced detection of ischemic but viable myocardium by the reinjection of thallium after stress-redistribution imaging. *N Engl J Med* 1990; 323:141-146.
8. Tillisch JH, Brunke R, Marshall R, et al. Reversibility of cardiac wall-motion abnormalities predicted by positron tomography. *N Engl J Med* 1986; 314:884-888.
9. Wesbey GE, Higgins CB, McNamara MT, et al. Effect of gadolinium-DTPA on the magnetic relaxation times of normal and infarcted myocardium. *Radiology* 1984; 153:165-169.
10. McNamara MT, Tscholakoff D, Revel D, et al. Differentiation of reversible and irreversible myocardial injury by MR imaging with and without gadolinium-DTPA. *Radiology* 1986; 158:765-769.
11. Schaefer S, Malloy CR, Katz J, et al. Gadolinium-DTPA-enhanced nuclear magnetic resonance imaging of reperfused myocardium: identification of the myocardial bed at risk. *J Am Coll Cardiol* 1988; 12:1064-1072.
12. Saeed M, Wendland MF, Masui T, et al. Reperfused myocardial infarctions on T1- and susceptibility-enhanced MRI: evidence of loss of compartimentalization of contrast media. *Magn Reson Med* 1994; 31:31-39.
13. Judd RM, Lugo-Olivieri CH, Arai AE, et al. Physiological basis of myocardial contrast enhancement in fast magnetic resonance images of 2-day-old reperfused canine infarcts. *Circulation* 1995;92:1902-1910.
14. Kim RJ, Fieno DS, Parrish TB, et al. Relationship of MRI delayed contrast enhancement to irreversible injury, infarct age and contractile function. *Circulation* 1999; 100:1992-2002.
15. Fieno DS, Kim RJ, Chen EL, et al. Contrast-enhanced magnetic resonance imaging of myocardium at risk: distinction between reversible and irreversible injury throughout infarct healing. *J Am Coll Cardiol* 2000; 36:1985-1991.
16. Hillenbrand HB, Kim RJ, Parker MA, et al. Early assessment of myocardial salvage by contrast-enhanced magnetic resonance imaging. *Circulation* 2000; 102:1678-1683.
17. Kim RJ, Wu E, Rafael A, et al. The use of contrast-enhanced magnetic resonance imaging to identify reversible myocardial dysfunction. *N Engl J Med* 2000; 343:1445-1453.
18. Choi KM, Kim RJ, Gubernikoff G, et al. Transmural extent of acute myocardial infarction predicts long-term improvement in contractile function. *Circulation* 2001; 104:1101-1107.
19. Simonetti OP, Kim RJ, Fieno DS, et al. An improved MR imaging technique for the visualization of myocardial infarction. *Radiology* 2001; 218:215-223.
20. DeFronzo RA, Tobin JD, Andres R. Glucose clamp technique: a method for quantifying insulin secretion and resistance. *Am J Physiol* 1979; 237(3):E214-E223.

21. Cerqueira MD, Weissman NJ, Dilsizian V, et al. Standardized myocardial segmentation and nomenclature for tomographic imaging of the heart: a statement for healthcare professionals from the Cardiac Imaging Committee of the Council on Clinical Cardiology of the American Heart Association. *Circulation* 2002; 105:539-542.
22. Maes AF, Borgers M, Flameng W, et al. Assessment of myocardial viability in chronic coronary artery disease using technetium-99m sestamibi SPECT: correlation with histologic and positron emission tomographic studies and functional follow-up. *J Am Coll Cardiol* 29 (1997), pp. 62–68.
23. Matsunari I, Fujino S, Taki J, et al. Quantitative rest technetium-99m tetrofosmin imaging in predicting functional recovery after revascularization: comparison with rest-redistribution thallium-201. *J Am Coll Cardiol* 29 (1997), pp. 1226–1233.
24. Melon PG, De Landsheere CM, Degueldre C, et al. Relation between contractile reserve and positron emission tomographic patterns of perfusion and glucose utilization in chronic ischemic left ventricular dysfunction: implications for identification of myocardial viability. *J Am Coll Cardiol* 1997; 30:1651-1659.
25. Gerber BL, Ordoubadi FF, Wijns W, et al. Positron emission tomography using(18)F-fluoro-deoxyglucose and euglycaemic hyperinsulinaemic glucose clamp: optimal criteria for the prediction of recovery of post-ischaemic left ventricular dysfunction. Results from the European Community Concerted Action Multicenter study on use of(18)F-fluoro-deoxyglucose Positron Emission Tomography for the Detection of Myocardial Viability. *Eur Heart J* 2001; 22:1691-1701.
26. Zanco P, Desideri A, Mobilia G, et al. Effects of left bundle branch block on myocardial FDG PET in patients without significant coronary artery stenoses. *J Nucl Med* 41 (2000), pp. 973–977.
27. Obuchowski NA. Nonparametric analysis of clustered ROC curve data. *Biometrics* 53 (1997), pp. 567–578.
28. Rao JN and Scott AJ. A simple method for the analysis of clustered binary data. *Biometrics* 48 (1992), pp. 577–585.
29. Maes A, Flameng W, Nuyts J, et al. Histological alterations in chronically hypoperfused myocardium: correlation with PET findings. *Circulation* 90 (1994), pp. 735–745.
30. Dakik HA, Howell JF, Lawrie GM, et al. Assessment of myocardial viability with 99mTc-sestamibi tomography before coronary artery bypass surgery: correlation with histopathology and postoperative improvement in cardiac function. *Circulation* 1997; 96:2892-2898.
31. Gerber BL, Rochitte CE, Bluemke DA, et al. Gelation betwee Gd-DTPA contrast enhancement and regional inotropic response in the periphery and center of myocardial infarction. *Circulation* 2001; 104:998-1004.
32. Klein C, Nekolla SG, Bengel FM, et al. Assessment of myocardial viability with contrast-enhanced magnetic resonance imaging: comparison with positron emission tomography. *Circulation* 2002; 105:162-167.
33. Zimmermann R, Mall G, Rauch B, et al. Residual 201Tl activity in irreversible defects as a marker of myocardial viability: clinicopathological study. *Circulation* 91 (1995), pp. 1016–1021.
34. Schwarz ER, Schoendube FA, Kostin S, et al. Prolonged myocardial hibernation exacerbates cardiomyocyte degeneration and impairs recovery of function after revascularization. J Am Coll Cardiol 31 (1998), pp. 1018–1026.
35. Samady H, Elefteriades JA, Abbott BG, et al. Failure to improve left ventricular function after coronary revascularization for ischemic cardiomyopathy is not associated with worse outcome. *Circulation* 100 (1999), pp. 1298–1304.
36. vom Dahl J, Altehoefer C, Sheehan FH, et al. Effect of myocardial viability assessed by technetium-99m-sestamibi SPECT and fluorine-18-FDG PET on clinical outcome in coronary artery disease. *J Nucl Med* 38 (1997), pp. 742–748.
37. Wu KC, Zerhouni EA, Judd RM, et al. Prognostic significance of microvascular obstruction by magnetic resonance imaging in patients with Acute myocardial infarction. *Circulation* 97 (1998), pp. 765–772.

Chapter 6

Time course of functional recovery after revascularisation of hibernating myocardium: a contrast-enhanced CMR study

Olga Bondarenko, Aernout M. Beek, Jos W.R. Twisk, Cees A. Visser, Albert C. van Rossum

Eur Heart J 2008;29(16):2000-5

ABSTRACT

Background. We sought to evaluate the relation between long-term functional outcome after revascularisation in patients with chronic ischemic LV dysfunction and baseline extent of myocardial fibrosis.

Methods. Thirty five patients underwent cine and delayed contrast-enhanced (de)CMR for the quantitative assessment of regional and global LV function and segmental extent of hyperenhancement (SEH). Function was assessed 1 month before, and 3, 6 and 24±12 months after revascularisation, and temporal changes were related to baseline extent of hyperenhancement.

Results. The likelihood of functional improvement was inversely related to the SEH during the entire follow-up: at the end of the study period, segments with 1-25%, 26-50%, 51-75% and 76-100% SEH were 2, 5, 11 and 86 times less likely to have functional improvement than segments without hyperenhancement (multilevel analysis, $p<0.001$). Although improvement continued over the whole study period in all SEH-groups, the time course was significantly more delayed in segments with more extensive hyperenhancement at baseline (multilevel analysis, $p<0.001$).

Conclusions: In patients with chronic ischemic LV dysfunction, improvement of dysfunctional but viable myocardium can be considerably delayed. Both the likelihood and the time course of long-term functional improvement are related to the baseline amount of scar, as visualised by deCMR.

Acknowledgements

This work was supported by the Netherlands Heart Foundation (grant N° 2001.158). Mary Belderok is kindly acknowledged for her contribution to the organization of the study and the data collection.

INTRODUCTION

Functional outcome after revascularisation of chronic ischemic dysfunctional myocardium is related to the preoperative regional extent of fibrosis and the presence of a sufficient number of residual viable myocytes (1;2). However, functional recovery is often incomplete even in regions assessed as viable by a variety of techniques. Several studies using delayed contrast enhanced cardiovascular MRI (deCMR) have shown that up to 22% of regions with little or no fibrosis do not improve (1;3;4). Although this may be partly attributed to incomplete revascularisation, or early or late graft failure, it may also be explained by the timing of the follow-up functional study. Functional recovery of hibernating regions, especially those with more advanced structural damage, may be considerably delayed. Functional outcome after revascularisation is generally assessed after 3-6 months, whereas a longer interval would be more appropriate. So far, few reports have explored the time course of functional recovery in relation to baseline markers of viability (5-7).

To address this issue, we used cine and deCMR to study a group of patients with chronic ischemic dysfunction before and 3, 6, and 24 ± 12 months after revascularisation. Using quantitative analysis of left ventricular function and regional extent of hyperenhancement, long-term functional outcome and time course of functional changes were related to baseline extent of fibrosis.

METHODS

Patients. All patients with known coronary artery disease and regional wall motion abnormalities on echocardiography or left ventricular (LV) angiography, without CMR contraindications, who were scheduled to undergo surgical or percutaneous revascularisation between April 2001 and February 2004, were study candidates. The Committee on Research Involving Human Subjects of the VU University Medical Centre, Amsterdam, approved the study protocol. All patients gave written informed consent.

Initially, 120 study candidates were prospectively earmarked as potential study candidates from the CABG and PCI waiting lists at our hospital. Patients were initially contacted by phone and were offered study information by mail. Ten patients could not be reached in time before the revascularisation, 12 patients refused to participate directly without giving any reason, 14 patients were already participating in another study and 5 other patients spoke neither Dutch nor English. The remaining 79 patients received the study information.

Table 1. Patients characteristics

Males/females	29/6
Age (yrs)	63 ± 11
Risk factors, %	
Systemic hypertension	45
Diabetes mellitus	17
Hypercholesterolemia	31
Smoking	41
Positive family history	12
Coronary angiography, %	
Single-vessel disease	14
Two-vessel disease	14
Three-vessel disease	72
History of myocardial infarction, %	59
Previous revascularisation, %	
CABG	7
PTCA	3
Ejection fraction at baseline (%)	39 ± 11
Months between infarction and baseline CMR (range)	53 (2-177)

CABG = coronary artery bypass grafting; PTCA = percutaneous transluminal coronary angioplasty

They were contacted by phone again a week later and asked whether they would like to participate in the study. Seventeen patients refused to give their consent. Six patients were willing but could not participate for logistical reasons, e.g. scanner availability. One patient forgot his first MRI appointment 3 times in a row and was excluded by us from further participation. Another 2 patients appeared claustrophobic at the very beginning of the first examination and were not able to complete the study. Fifty-three patients completed CMR examination 4 ± 2 weeks before revascularisation. Three of them appeared not to be suitable for the study due to absence of wall motion abnormalities in 2 cases and no revascularisation in 1 case. CMR was repeated 3, 6 and 24 ± 12 months (median 26 months, range 13 – 44 months) after revascularisation in 45, 41, and 35 patients, respectively. No patient died. Six patients were excluded from the study: in 1 patient the coronary artery bypass surgery (CABG) was accompanied by LV aneurysmectomy, 4 patients had electrocardiographic and/or biochemical evidence of peri-procedural myocardial infarction, and 1 patient had a permanent pacemaker implanted. Two patients suffered a cerebrovascular accident. Follow-up was incomplete in the remaining 7 patients: no follow-up in 4 patients ((newly developed) claustrophobia in 2, fear of needles in 1, lack of motivation in 1), and 2 patients declined to return after the 3-month study, and 1 for the

3- and the 6-month study. The baseline characteristics of the 35 patients, who underwent all 4 CMR examinations, are listed in Table 1.

CABG was performed in 25 patients and percutaneous transluminal coronary angioplasty (PTCA) in 10. All patients were in stable clinical condition at the time of the CMR examinations and there was no clinical evidence of ischemic events in the period between the CMR examinations and revascularisation. Complete revascularisation was defined as revascularisation of all major epicardial vessels or first generation side branches with >50% diameter stenosis. For patients in whom revascularisation was incomplete, only segments in revascularised coronary artery territories were considered (8).

CMR. All scans were performed on a 1.5T scanner (Sonata, Siemens, Erlangen, Germany) with the patient in a supine position using a four-element phased array cardiac receiver coil. ECG-gated cine images were acquired using a breath-hold segmented steady-state free precession sequence (true FISP; echo time/repetition time of 1.2/3.2ms; resolution of 1.3 x 1.8 x 5mm). Per patient eight to ten short-axis views were obtained every 10mm starting from the mitral valve insertion and covering the entire left ventricle. A gadolinium-based contrast agent (Magnevist, Schering AG, Berlin, Germany; 0,2mmol/kg) was then administrated intravenously with a power injector through a peripheral vein. After 10 to 15 minutes contrast-enhanced images were acquired in the same orientation as the cine images using a 2D-segmented inversion recovery gradient-echo pulse sequence triggered to end-diastole (repetition time/echo time = 9.6/4.4 ms, flip angle 25˚, matrix 208x256 and a typical voxel size of 1.6 x 1.3 x 5.0).

Data analysis. All data were analysed on a separate workstation (Sun Microsystems, Inc., Santa Clara, California) using a dedicated software package (MASS 5.1, Medis, Leiden, The Netherlands).

Segmental function. Segmental wall thickness was measured at end-systole and end-diastole after manual tracing of endocardial end epicardial borders in stop-frame images, excluding trabeculations and papillary muscles. The contours were drawn blinded to patient identity, clinical history and scan time point. The analysis program used the modified centreline method (9) along 100 chords per short axis slice, and allowed the automatic segmentation, in which the number of chords per segment depended on the number of segments chosen (nr chords per segment = 100/nr of segments). Segmental wall thickness was calculated as the average of the chords within one segment. Segmental wall thickening (SWT) in millimetres was calculated as: end systolic wall thickness minus end diastolic wall thickness. The normal range of SWT was defined in a group of 10 healthy volunteers (age 50 – 75 years): 4.4 ± 0.7 mm. Segments with SWT < 3 mm (mean – 2SD) were considered dysfunctional. Registration of follow-up cine images was achieved using standard imaging procedure and various anatomical landmarks such as right ventricle septal insertion sites,

papillary muscle location, and trabecularisation patterns in the right and left ventricles. Functional improvement was defined as an increase in SWT of ≥ 1.5 mm compared to baseline, based on the in-plane spatial resolution of the cine sequence. The results of intraobserver and interobserver (by 2 observers) variability of SWT were determined in 10 randomly chosen patients. The time period between the repeated readings was 2 weeks.

Images were evaluated using a 16-segment model (8). Using the full coverage cine short-axis data set, six basal, six midventricular and four distal segments were composed by averaging the data of a maximum of three short-axis slices. The most basal short-axis slice used for composition of the basal segments was located just below the LV outflow tract. The two most apical slices were excluded, because short-axis images at this level preclude a reliable segmental evaluation due to small diameter.

Global function. Left ventricular end-diastolic and end-systolic volumes (LVEDV and LVESV, respectively) were determined by planimetry of all short-axis images in each patient. Left ventricular ejection fraction (LVEF, in %) was calculated as (LVEDV – LVESV)/LVEDV.

Segmental hyperenhancement. Hyperenhanced regions were quantified after standardisation by thresholding signal intensity contrast-enhanced images as previously described (10). Areas of hyperenhancement were quantified by computer-assisted planimetry on each of the short axis images and segmental extent of hyperenhancement (SEH) was expressed as percentage of segmental area. Images were evaluated according to the same 16-segment model as described above. All segments were assigned to one of the following SEH groups: 1 - 0%, 2 – 1 to 25%, 3 – 26 to 50%, 4 – 51 to 75%, and 5 – 76 to 100% hyperenhancement.

Statistical analysis. All values are expressed as mean ± SD. The paired sample t test and the independent samples t test were used to compare means within the study group or between subgroups. We used multilevel logistic regression (MlwiN, version 1.02.0007, Centre for Multilevel Modelling, London, United Kingdom) (11;12) to adjust for the nonindependence of the data, to evaluate the relation between baseline extent of hyperenhancement and change in segmental wall thickening. In this analysis we added a random intercept and we estimated the regression coefficients (as fixed effects and transformed them into the odds ratio’s) for the dummy variables, reflecting the different groups of hyperenhancement. We used the 0% SEH group as a reference, so all other groups were related to this one. The dummy variables for SEH were in the model as fixed effects. Because we only had two levels (segments clustered within patients) and no random slopes, there was no covariance of the random effects, so no particular structure was chosen. The regression equation was used to calculate odds ratios, which expressed the likelihood of improvement relative to functional outcome of segments without any hyperenhancement. The multilevel logistic regression was also used to evaluate time course

of regional functional improvement in relation to segmental extent of myocardial fibrosis. ANOVA for repeated measurements (using univariate estimation approach with the Greenhouse Geisser adjustment and testing the difference between baseline and post-baseline measurements) was applied to analyse changes in global ventricular function. We used linear regression analysis to assess the relation between viability at baseline and changes in ejection fraction at late follow-up. Intraclass correlation coefficients were used for assessment of intra- and interobserver variability. All statistical tests were two-tailed, and p values of less than 0.05 were considerate to indicate statistical significance.

RESULTS

Regional function. At baseline 560 segments (35 patients x 16 segments) were available for analysis. 518 segments were successfully revascularised. Almost 50% of these segments (n=258) had a baseline SWT of less than 3 mm (mean 1.2 ± 1.0 mm) and were considered dysfunctional. The interobserver variability for SWT was 0.1 ± 0.7 mm (mean difference between values of observer 1 (OB) and 2 (AMB); intraclass correlation coefficient = 0.89, 95% confidence interval 0.55–0.98). The intra-observer variability for SWT was 0.0 ± 0.4 mm (mean difference between 2 measurements (OB); intraclass correlation coefficient = 0.97, 95% confidence interval 0.86 – 0.99).

Table 2. Regional functional improvement

	SEH				
	0%	1 - 25%	26 - 50%	51 -75%	76 - 100%
baseline	62	57	59	59	21
3 months	35 (56%)	19 (33%)	13 (22%)	4 (7%)	0
6 months	15 (24%)	16 (28%)	15 (25%)	7 (12%)	0
24 months	8 (13%)	5 (9%)	11 (19%)	10(17%)	1
total	58 (93%)	40 (70%)	39 (66%)	21 (36%)	1 (5%)

Regional functional improvement, expressed in absolute numbers of improved segments and a percentage of baseline, for every MRI examination according to segmental extent of hyper-enhancement (SEH); n = number of dysfunctional segments at baseline.

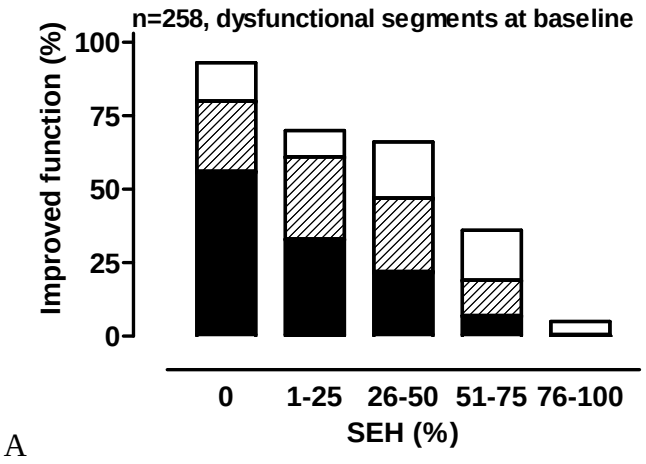

A

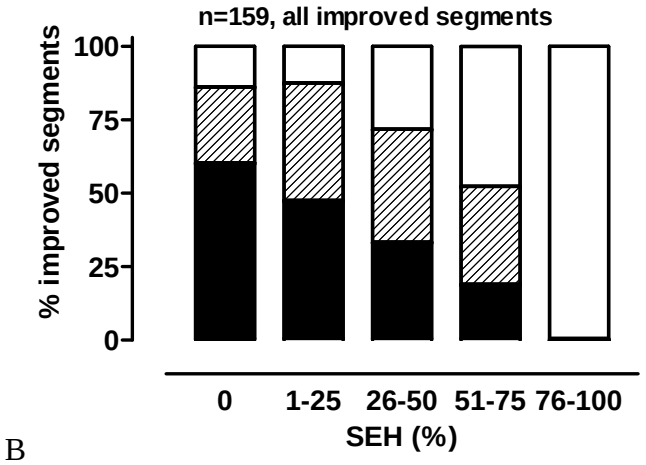

B

Figure 1. A. Likelihood of functional improvement after revascularisation in relation to baseline segmental extent of hyperenhancement (SEH), expressed as a percentage of total number of dysfunctional segments, at 3 months (black bars), 6 months (striped bars) and 2 years (white bars) follow-up. All dysfunctional segments are included (n=258). B. Time course of regional functional improvement in relation to baseline SEH, shown as the relative percentage of improvement at 3 months (black bars), 6 months (striped bars) and 2 years (white bars) follow-up. Only segments with functional improvement are included (n=159).

Functional improvement. At the end of the study period, functional improvement was seen in: 93%, 70%, 66%, 36% and 5% of segments with no, 1-25%, 26-50%, 51-75%, and 75-100% SEH, respectively (table 2, figure 1a). The likelihood of functional improvement was inversely related to the segmental extent of hyperenhancement during the entire follow-up: at the end of the study period, segments with 1-25%, 26-50%, 51-75% and 76-100% SEH were 2 (1.1 - 3.6), 5 (2.5 – 8.6), 11 (5.0 – 20.1) and 86 (11.0 – 682.0) times less

likely to have functional improvement than segments without hyperenhancement (multilevel analysis, $p < 0.001$). Similar results were found when analysing the data with different cut-offs for segmental functional improvement (2, 2.5 and 3 mm SWT change), although the odds ratio's were lower due to the lower number of improving segments at these higher cut-offs.

Time course. The time course of functional improvement was considerably protracted: at 3 months, improvement was seen in less than half of all segments that eventually improved (71 of 159; 45%). Although improvement continued over the whole study period in all SEH-groups, the time course was significantly more delayed in segments with more extensive hyperenhancement at baseline (multilevel logistic regression, $p < 0.001$; figure 1b). At 3 months, the major part (54/98, 55%) of improvement in segments with no or minimal (≤25%) hyperenhancement was found in the first 3 months, versus only 28% (17/61) of improvement in segments with >25% hyperenhancement. Conversely, more than 1/3 (22/61, 36%) of total improvement in segments with >25% hyperenhancement occurred between 6 months and the final follow-up, versus only a small fraction (13/98, 13%) in segments with no or minimal hyperenhancement.

A total of 75 segments became dysfunctional at late follow-up. Twenty-two (18%) of 124 segments that initially improved (mean SWT at baseline 1.8 ± 0.8 mm, 3 months follow-up 3.2 ± 1.3 mm, 6 months follow-up 3.3 ± 1.8 mm) showed a decrease in SWT >1.5 mm at late follow-up ending up as dysfunctional (mean SWT 1.4 ± 1.0 mm). At baseline, 10 of these showed no hyperenhancement, and 9, 2 and 1 segments had 1 – 25%, 26 – 50% and 51 – 75% SEH, respectively. A similar proportion of revascularised segments with normal SWT at baseline (49 of 260 (19%)) became dysfunctional 2 years after revascularisation (mean SWT 4.4 ± 0.9 mm at baseline vs. 1.7 ± 0.9 mm at late follow-up). The long-term follow-up also revealed worsening of regional function in 4 of 25 (16%) initially normokinetic, non-revascularised segments (mean SWT 4.1 ± 1.0 mm vs. 2.6 ± 0.4 mm).

Global left ventricular function. Both end-diastolic and end-systolic LV volumes showed small but significant improvements at 3 months follow-up, with no additional changes at 6 months and 2 years. The ejection fraction showed a small increase at all follow-up time points, which reached statistical significance only at 6 months. There were no statistically significant changes in LV mass. Data are summarised in figure 2a-c.

For each patient we calculated a viability index by adding the number of dysfunctional segments with SEH ≤ 50 % and then dividing this by the total number of dysfunctional segments in the left ventricle. There was a significant, positive relation between the viability index and improvement in ejection fraction at late follow-up (regression coefficient $r = 0.47$, $p = 0.005$).

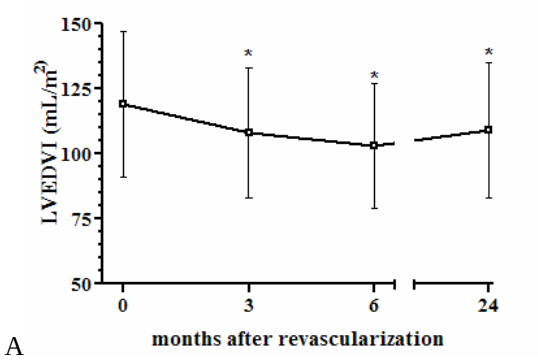

A

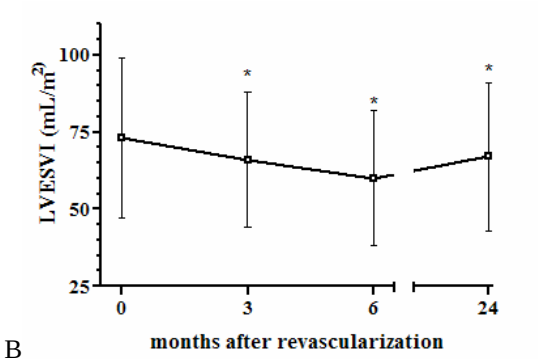

B

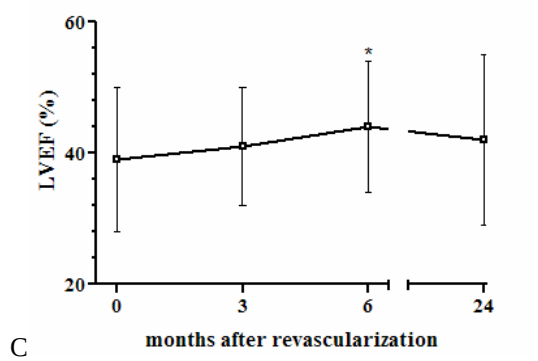

C

Figure 2. Changes in global left ventricular parameters. A. LVEDVI = left ventricular end-diastolic volume index, B. LVESVI = left ventricular end-systolic volume index, C. LVEF = left ventricular ejection fraction.
* Indicates statistically significant difference compared to baseline value. Bars represent standard deviation. P values are given for linear trend over time analysis.

DISCUSSION

This is the first study that used cardiovascular magnetic resonance imaging to evaluate long-term follow-up after revascularisation in patients with chronic ischemic myocardial

dysfunction. Our results showed that both likelihood and time course of functional improvement were related to the amount of baseline myocardial scar.

Long-term functional outcome after revascularisation. Previous studies have shown a variety of degenerative changes at cellular and subcellular level in histological assessment of targeted biopsies taken at the time of CABG (13;14). Increased extracellular matrix, with replacement of cardiomyocytes by fibrosis, is considered to have a central role in the likelihood and time course of functional recovery after restoration of blood flow. Although the exact mechanism of hibernation is still not fully understood, several investigators have found a relation between functional outcome after revascularisation and the degree of these morphological changes (7;13-17). Delayed contrast enhanced CMR allows the accurate visualisation and quantification of regional scar, and is of proven value in the assessment of myocardial viability (1;3;18;19).

Extending previous work, our results showed that functional outcome was inversely related to the baseline segmental extent of hyperenhancement at every time point of the study. Compared to earlier studies using deCMR, we found a relatively low improvement rate at 3 months; for example, only 56% of segments without hyperenhancement improved versus 78% reported by Kim et al (1). However, at the end of the study period, improvement rate was higher than previously reported in all groups with less than transmural (<75%) enhancement. For example, after 2 years, almost all segments without hyperenhancement (93%) showed functional improvement.

Time course of recovery. Our results clearly show that delayed recovery is common in successfully revascularised hibernating myocardium, and that this was not limited to regions with more extensive structural damage, but that it also occurred in regions with no hyperenhancement. In all SEH-groups, a comparable number of segments continued to show improvement throughout the study period. However, the relative time course differed considerably, and, in fact, was inversely related to the segmental extent of hyperenhancement. Thus, both long-term likelihood and time course of functional improvement were predicted by the degree of morphological changes at baseline.

Previous reports have shown that morphological changes are paralleled by metabolic alterations: regional scar extent was inversely related to FDG-uptake by PET (2;20). Outcome was best in segments with both a thick viable rim > 4.5 mm (indicating limited scar extent) and preserved FDG-uptake, whereas segments with impaired FDG-uptake (indicating more severe metabolic disturbance) had low likelihood of recovery despite the presence of thick viable rim (2). However, follow-up in this study was shorter (11 ± 2 months) and our data suggest that segments with a higher degree of metabolic disturbance may require a longer time to recover.

In line with previous studies, we found that the negative predictive value of (almost) transmural hyperenhancement was high: only 1 segment with >75% SEH improved after revascularisation. Apparently, extensive morphological changes preclude functional improvement, although technically we cannot rule out the possibility that some improvement would have occurred at an even longer follow-up time in segments with only little residual non-enhancing myocardium (>75-<100% transmurality).

Significant improvement in global LV function after revascularisation requires a substantial amount of viable myocardium (21). Long-term data are scarce, since most viability studies have focused on short term (≤6 months after revascularisation) changes in regional function. In our study group there was a significant positive relation between the amount of dysfunctional but viable myocardium at baseline, estimated per patient, and improvement in the ejection fraction at late follow-up. However, we only found small changes in mean global LV function after revascularisation, even at late follow-up, which suggests that the improvement in regional function may not have been enough for global improvement. Alternatively, the regional improvement may have been partly offset by the 72 newly dysfunctional segments (13% of total) at late follow-up. Changes in global function are also influenced by several other factors, such as baseline volumes and ejection fraction, periprocedural ischemic accidents, and long-term graft failure or restenosis.

Limitations. Only 35 patients completed the whole study protocol, however this sample size is comparable with previously published studies that used deCMR and cine imaging in patients with chronic ischemic heart disease and a revascularisation procedure (1;2). We chose a 16-segment model for the regional evaluation of LV function, because this can be directly translated into clinical practice. Transforming the CMR data into a limited number of segments involves averaging information of several slices. Although averaging data has the obvious disadvantage that some detail may be lost, it may at the same time help to prevent misregistration of follow-up scans, which is an important potential limitation in any long-term follow-up study of regional function. Although observers were unaware of patient identity during analysis of the cine data, follow-up studies could be identified by the presence of sternal wire or stent artefacts. It was not possible to differentiate between the various post procedural time points.

In conclusion, in patients with chronic ischemic left ventricular dysfunction, improvement of dysfunctional but viable myocardium after revascularisation can be considerably delayed. Both the likelihood and the time course of long-term functional improvement are related to the baseline amount of scar, as visualised by deCMR.

REFERENCES

1. Kim RJ, Wu E, Rafael A, Chen EL, Parker MA, Simon-etti O, Klocke FJ, Bonow RO, Judd RM. The use of contrast-enhanced magnetic resonance imaging to identify reversible myocardial dysfunction. *N Engl J Med.* 2000;343:1445-1453.
2. Knuesel PR, Nanz D, Wyss C, Buechi M, Kaufmann PA, von Schulthess GK, Luscher TF, Schwitter J. Characterization of dysfunctional myo-cardium by positron emission tomography and magnetic resonance: relation to functional outcome after revascularization. *Circulation*. 2003;108:1095-1100.
3. Selvanayagam JB, Kardos A, Francis JM, Wiesmann F, Petersen SE, Taggart DP, Neubauer S. Value of delayed-enhancement cardiovascular mag-netic resonance imaging in predicting myocardial viability after surgical revascularization. *Circulation*. 2004;110:1535-1541.
4. Wellnhofer E, Olariu A, Klein C, Grafe M, Wahl A, Fleck E, Nagel E. Magnetic resonance low-dose dobutamine test is superior to SCAR quan-tification for the prediction of functional recovery. *Circulation*. 2004;109:2172-2174.
5. Bax JJ, Visser FC, Poldermans D, Elhendy A, Cornel JH, Boersma E, van Lingen A, Fioretti PM, Visser CA. Time course of functional recovery of stunned and hibernating segments after surgical revascularization. *Circulation*. 2001;104:I314-I318.
6. Haas F, Augustin N, Holper K, Wottke M, Haehnel C, Nekolla S, Meisner H, Lange R, Schwaiger M. Time course and extent of improvement of dysfunctioning myocardium in patients with coronary artery disease and severely depressed left ventricular function after revascularization: correlation with positron emission tomo-graphic findings. *J Am Coll Cardiol*. 2000;36:1927-1934.
7. Shivalkar B, Maes A, Borgers M, Ausma J, Scheys I, Nuyts J, Mortelmans L, Flameng W. Only hibernating myocardium invariably shows early recovery after coronary revascularization. *Circulation*. 1996;94:308-315.
8. Cerqueira MD, Weissman NJ, Dilsizian V, Jacobs AK, Kaul S, Laskey WK, Pennell DJ, Rumberger JA, Ryan T, Verani MS. Standardized myo-cardial segmentation and nomenclature for tomographic imaging of the heart: a statement for healthcare professionals from the Cardiac Imaging Committee of the Council on Clinical Cardiology of the American Heart Association. *Circulation*. 2002;105:539-542.
9. van Rugge FP, van der Wall EE, Spanjersberg SJ, de Roos A, Matheijssen NA, Zwinderman AH, van Dijkman PR, Reiber JH, Bruschke AV. Magnetic resonance imaging during dobutamine stress for detection and localization of coronary artery disease. Quantitative wall motion analysis using a modification of the cen-terline method. *Circulation*. 1994;90:127-138.
10. Bondarenko O, Beek AM, Hofman MB, Kuhl HP, Twisk JW, van Dockum WG, Visser CA, van Rossum AC. Standardizing the definition of hyperenhancement in the quantitative assessment of infarct size and myocardial viability using delayed contrast-enhanced CMR. *J Cardiovasc Magn Reson*. 2005;7:481-485.
11. Goldstein H. Multilevel statistical models. 2003. Edward Arnold, London.
12. Twisk JWR. Applied multilevel analysis. A practical guide. 2005. Cambridge University Press, Cambridge, UK..
13. Elsasser A, Schlepper M, Klovekorn WP, Cai WJ, Zimmermann R, Muller KD, Strasser R, Kostin S, Gagel C, Munkel B, Schaper W, Schaper J. Hibernating myocardium: an incomplete adaptation to ischemia. *Circulation*. 1997;96:2920-2931.
14. Schwarz ER, Schoendube FA, Kostin S, Schmiedtke N, Schulz G, Buell U, Messmer BJ, Morrison J, Hanrath P, vom DJ. Prolonged myocardial hibernation exacerbates cardiomyocyte degeneration and impairs recovery of function after revascularization. *J Am Coll Cardiol*. 1998;31:1018-1026.
15. Depre C, Vanoverschelde JL, Melin JA, Borgers M, Bol A, Ausma J, Dion R, Wijns W. Structural and metabolic correlates of the reversibility of chronic left ventricular ischemic dysfunction in humans. *Am J Physiol*. 1995;268:H1265-H1275.
16. Haas F, Jennen L, Heinzmann U, Augustin N, Wottke M, Schwaiger M, Lange R. Ischemically compromised myocardium displays different time-courses of functional recovery: correlation with morphological alterations? *Eur J Cardiothorac Surg*. 2001;20:290-298.

17. Vanoverschelde JL, Depre C, Gerber BL, Borgers M, Wijns W, Robert A, Dion R, Melin JA. Time course of functional recovery after coronary artery bypass graft surgery in patients with chronic left ventricular ischemic dysfunction. *Am J Cardiol*. 2000;85:1432-1439.
18. Beek AM, Kuhl HP, Bondarenko O, Twisk JW, Hofman MB, van Dockum WG, Visser CA, van Rossum AC. Delayed contrast-enhanced magnetic resonance imaging for the prediction of regional functional improvement after acute myo-cardial infarction. *J Am Coll Cardiol*. 2003;42:895-901.
19. Kim RJ, Fieno DS, Parrish TB, Harris K, Chen EL, Simonetti O, Bundy J, Finn JP, Klocke FJ, Judd RM. Relationship of MRI delayed contrast enhancement to irreversible injury, infarct age, and contractile function. *Circulation*. 1999;100:1992-2002.
20. Kuhl HP, Beek AM, van der Weerdt AP, Hofman MB, Visser CA, Lammertsma AA, Heussen N, Visser FC, van Rossum AC. Myocardial viability in chronic ischemic heart disease: comparison of contrast-enhanced magnetic resonance imaging with (18)F-fluorodeoxyglucose positron emission tomography. *J Am Coll Cardiol*. 2003;41:1341-1348.
21. Bax JJ, Poldermans D, Elhendy A, Boersma E, Rahim-toola SH. Sensitivity, specificity, and predictive accuracies of various noninvasive tech-niques for detecting hibernating myocardium. *Curr Probl Cardiol.* 2001;26:147-186.

Chapter 7

Quantitative regional left ventricular wall thickening in healthy volunteers using cine magnetic resonance imaging

Aernout M. Beek, Tjeerd Germans, Robin Nijveldt, Albert C. van Rossum

Submitted

ABSTRACT

The assessment of regional left ventricular function provides important diagnostic and prognostic information. Reports that have systematically evaluated the normal range are scarce and outdated. In this study we used state-of-the-art cine cardiovascular MRI and the centerline method in 36 healthy volunteers to assess regional wall thickness and wall thickening in a 16-segment model. Data were presented in graphic format and in tables. Regional end-diastolic and end-systolic wall thickness and percent systolic wall thickening showed significant heterogeneity that was in line with previous reports. Regional percent systolic wall thickening was significantly related to regional circumferential strain. There was no difference in parameters between individuals younger than and older than 40 years. This study provides the normal range of regional left ventricular wall thickness and thickening using cine cardiovascular MRI and myocardial tagging.

INTRODUCTION

Global left ventricular function determines prognosis and management in a great variety of cardiovascular diseases, and its assessment plays a central role in the diagnostic work-up [1]. Although the assessment of regional function per se has less prognostic significance, it provides important information about the origin of the underlying disorder, its relation to the coronary arteries, and, importantly, it may detect abnormalities while global parameters are still well within the normal range. The quantitative assessment of regional thickening is challenged by through-plane motion and myocardial deformation in other than the radial direction, such as circumferential or longitudinal shortening. Regional function is therefore ideally quantified using cardiovascular magnetic resonance (CMR) myocardial tagging and subsequent strain analysis [2]. In daily practice, strain analysis is seldom used, because it requires additional post processing tools and time and the majority of clinical questions can be answered using a qualitative (eye-balling) approach. However, on some occasions, e.g. with longitudinal follow-up examinations, or for research purposes when tagging sequences or analysis tools are not available, a more objective measure would be preferable. Regional wall thickening can be quantified using the centerline method that was introduced in the early 1980's for use with contrast ventriculography, and was later modified for echocardiography and cine CMR [3-5]. The centerline method is based on the concept that systolic wall motion and thickening proceed in a multicentric fashion rather than directed at a single central point or axis in the left ventricular chamber [6]. Cine CMR is ideally suited for the centerline method, because both epicardial and endocardial borders can be reliably detected throughout the cardiac cycle.

Compared to the number of reports on global function, there are surprisingly few CMR studies that have addressed quantitative regional wall thickening in healthy volunteers, all using older cine sequences and generally presenting the data in graphs, which is impractical for clinical use. The currently available, segmented, steady state free precession (SSFP) cine CMR sequence allows a sharper definition of the blood-myocardium border than previously used sequences. In addition, most scanners now routinely use retrospective ECG gating which leads to slightly though significantly larger end-diastolic ventricular endocardial contours [7]. The resulting changes in normal values of wall thickness, systolic wall thickening, volumes and mass have been addressed in recent publications on global parameters [8,9]. Data for regional function are still lacking which is illustrated by the use of old echocardiographic reference values even in CMR studies [10].

In the present study we therefore sought to provide normal values for quantitative regional myocardial function using state-of-the-art cine CMR including retrospective ECG-gating. To evaluate the relation between (simple) regional systolic wall thickening and the

current golden standard of quantitative regional function (myocardial tagging), data were additionally compared to circumferential strain analysis.

METHODS

Patients. Thirty-six healthy volunteers (mean age 43±13 yrs, range 24-62, 56% male, blood pressure 124/73 ± 12/7) without known cardiac disease or cardiac risk factors, with normal physical examination and electrocardiogram, and without contra-indications to CMR (intra-cranial clips, claustrophobia, etc) were included in the study.

CMR. All images were acquired on a 1.5 T MR-scanner (Sonata, Siemens, Erlangen) with patients in supine position, using a six-element phased array surface coil, and mild expiration breath holding. After localizing scouts, long axis views and multiple short axis views (every 10 mm, covering the entire left ventricle) were acquired using a retrospectively gated SSFP cine pulse sequence (average voxel size 1.3x1.6x5 mm3, TR/TE 1.5/3.0, temporal resolution 38-45 msec). Myocardial tagging images with a high temporal resolution of 14.1 ms were obtained with multiple breath-hold, retrospectively gated, SSFP imaging (average voxel size 1.6x3.8x6 mm3,TR/TE 4.7/2.3, tag spacing 7 mm) using the linearly increasing start-up angle (LISA) approach [11]. Complementary tagging (complementary spatial modulation of magnetization, CSPAMM) was used for improved tag contrast and strain analysis [11]. Three left ventricular (LV) short axis slices were acquired at 25%, 50% and 75% of the distance between the mitral valve annulus and the apex on a LV 4-chamber view in end-systole to avoid inclusion of the LV outflow tract, with 4 image series per slice: horizontally and vertically tagged images with both positive and negative sinusoidal tagging for CSPAMM. Total imaging time per slice was ~4 minutes.

Image analysis. Images were analyzed on a separate workstation (Sun Microsystems, Inc., Santa Clara, California) using a dedicated software package (Mass, Medis, Leiden, The Netherlands).

Cine CMR. Epicardial and endocardial contours were drawn semi-automatically on end-diastolic and end-systolic views. In the endocardial contour, only compacted myocardium was considered, and papillary muscles and trabecularization were carefully excluded, both in the end-diastolic and the end-systolic images (figure 1). Regional end-diastolic wall thickness (EDWT, mm), end-systolic wall thickness (ESWT, mm), systolic wall thickening (SWT = ESWT – EDWT, mm) and percent systolic wall thickening (%SWT = ESWT – EDWT / EDWT, %) were subsequently calculated using the modified centerline method [4,5]. Inter- (AMB, TG) and intraobserver (TG) variability of systolic wall thickening analysis were defined in 10 randomly chosen subjects.

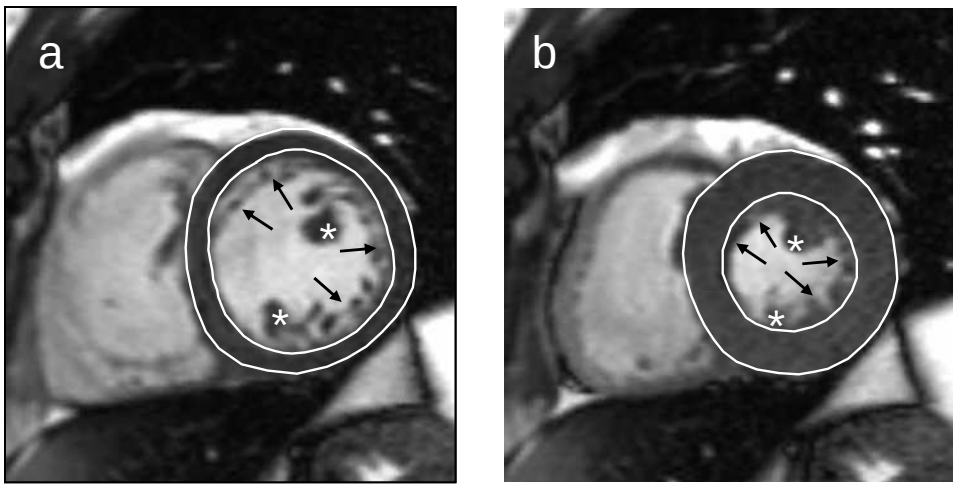

Figure 1. Example of contours on midventricular end-diastolic (a) and end-systolic (b) image. Note that trabecularizations (arrows) and papillary muscles (asterisks) were excluded in both phases.

Strain analysis. Strain analysis was performed using the harmonic phase method, as described previously [13]. Circumferential strain (Ecc) was calculated from the Lagrangian strain tensor as the percent change in length of a small line segment in the circumferential direction and was averaged per segment. Because the fibers at the midwall are mainly oriented in the circumferential direction, only strain data from the mid-50% of the myocardial wall were used [14].

Segmentation. A standard 16-segment model was used to analyse regional function in the 3 short axis tagging views and 3 matching cine views at basal (6 segments: anterior (ant); anteroseptal (as); inferoseptal (is); inferior (inf); inferolateral (il); anterolateral (al)), mid (6 segments: ant; as; is; inf; il; al) and apical (4 segments: ant; septal (sep); inf; lateral (lat)) left ventricular level [15]. Mean segmental values were compared within each slice and between slices. For comparison between slices, results of segments 2 and 3 (basal septal), 5 and 6 (basal lateral), 8 and 9 (mid septal) and 11 and 12 (mid lateral) were averaged to allow comparison to the apical segment.

Statistical analysis. Results are presented as mean ± SD. Since segments are clustered at multiple levels, we used Mixed Models Analysis to compare segmental parameters EDWT, SWT, %SWT and Ecc within slices, and between slice levels and age groups (SPSS for Windows, version 14.01). Correlation between %SWT and Ecc were explored using Pearson's correlation and the F-test for equality of variances.

RESULTS

Mean end-diastolic volume was 185±39 g (94±14 ml/m2), end-systolic volume 74±20 g (37±8 ml/m2), ejection fraction 61±4%, and mass 105±28 g (54±11 g/m2). Mean segmental and total values, as well as lower limits of normal are listed in tables 1 and 2, and are graphically presented in figures 2 and 3. Inter- and intraobserver variability of systolic wall thickening analysis were 0.1 ± 0.7 and 0.0 ± 0.4, respectively (mean difference ± SD in mm).

End-diastolic wall thickness. Mean EDWT was 5.2±1.3 mm (range 2.1-9.7). It was largest in the septum at all levels, and significantly decreased in apical direction ($p<0.001$).

Systolic wall thickening. Mean SWT was 4.4±1.3 mm (range 1.4-9.1) and, as EDWT, significantly decreased in apical direction: 4.7±1.4 vs 4.3±1.2 vs 3.9±1.2 mm in the basal, mid and apical slice, respectively ($p<0.001$).

Percent systolic wall thickening. Mean %SWT was 89±29% (range 22-180), and higher in the apical slice: 86±30 vs 86±27 vs 96±30% ($p<0.001$ vs basal and mid). %SWT was lowest in the septal segments and highest in the lateral segments at every slice level ($p<0.001$). There was a fair correlation between SWT and %SWT (Pearson's correlation 0.652, $p<0.001$).

Circumferential strain. Mean Ecc was –17.4±3.5% (range –26.2 - –9.7), and was lowest in the apical slice: -17.7±3.3 vs –17.8±3.5 vs –16.2±3.7% ($p<0.001$ vs basal and mid). Ecc was highest in the lateral segments at every slice level ($p<0.001$).

There was a significant correlation between %SWT and Ecc (Pearson correlation -0.111, $p<0.01$). Segmental Ecc was significantly less dispersed than segmental %WT: coefficient of variation (SD/mean * 100): 20% vs 33% ($p<0.001$). We found no correlation between SWT and Ecc.

Age. There was no significant difference in segmental EDWT, SWT, %SWT or Ecc between individuals younger than and older than 40 years.

DISCUSSION

Regional left ventricular wall thickening can be studied with a variety of imaging techniques: contrast- or radionuclide ventriculography, echocardiography, computed tomography, and cine CMR. 2D-echocardiography provides a bedside and fast qualitative assessment of regional wall motion, and is the method of choice in acute clinical settings. However, it does not allow a reliable quantification of wall thickening, despite increasing technology (3D) and the use of contrast. In this study we sought to provide normal values for regional systolic wall thickening for state of the art SSFP cine CMR imaging, using the centerline method in a 16-segment model.

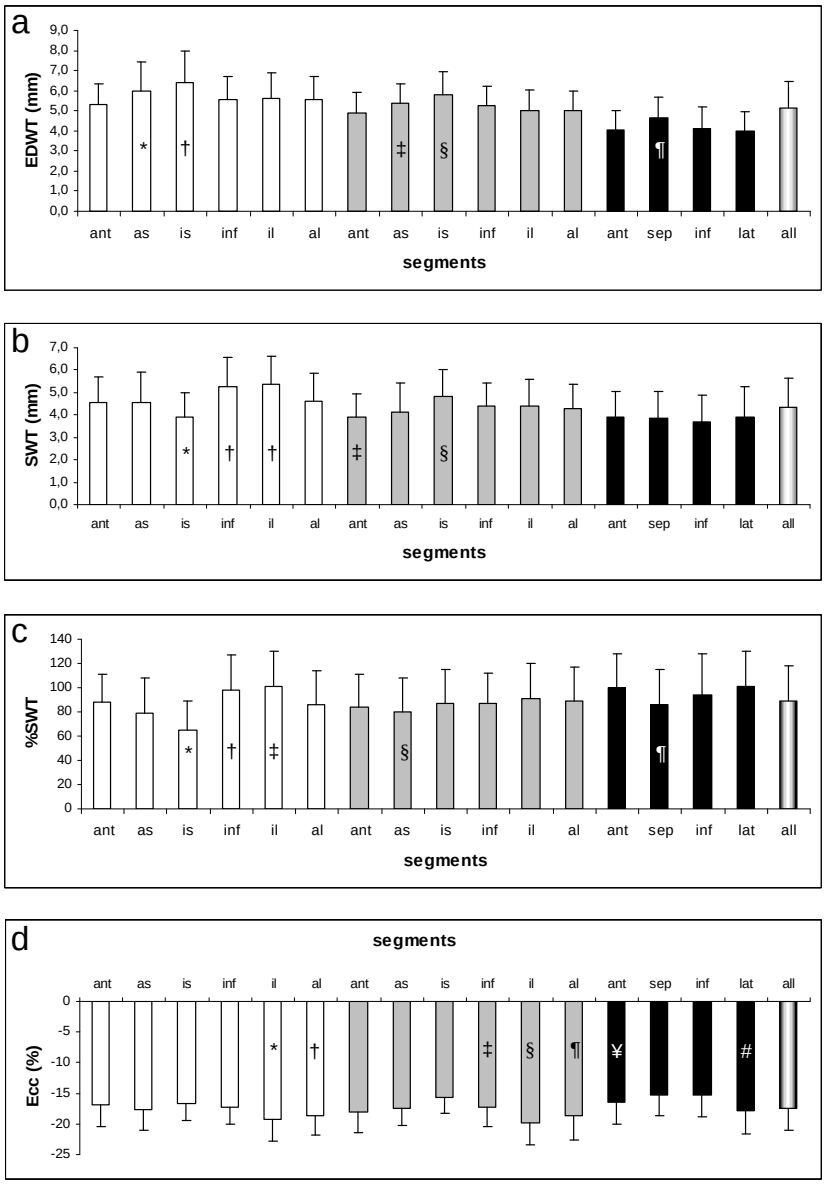

Figure 2. Segmental EDWT (a), SWT (b), %SWT (c) and Ecc (d) in basal □, mid ▒ and apical ■ slices. P-values reflect comparison within slices only. Abbreviations see text.

a. * p<0.05 vs ant, is, inf, il, al; † p<0.01 vs ant, inf, il, al; ‡ p<0.05 vs ant, is, il, al; p<0.01 vs ant, inf, il, al; ¶ vs ant, inf, lat

b. * p<0.01 vs all; † p<0.05 vs ant, as, al; ‡ p<0.01 vs is, inf, il, <0.05 vs al; § p<0.01 vs inf, il, al

c. * p<0.01 vs all; † p<0.01 vs as, al; ‡ p<0.01 vs ant, as, al; § p<0.05 vs il, al; ¶ p<0.01 vs ant, lat

d. * p<0.01 vs ant, as, is, inf; † p<0.05 vs ant, is, inf; ‡ p<0.01 vs all; § p<0.01 vs ant, as, inf, al; ¶ p<0.05 vs as, inf; ¥ p<0.05 vs all; # p<0.01 vs sep, inf

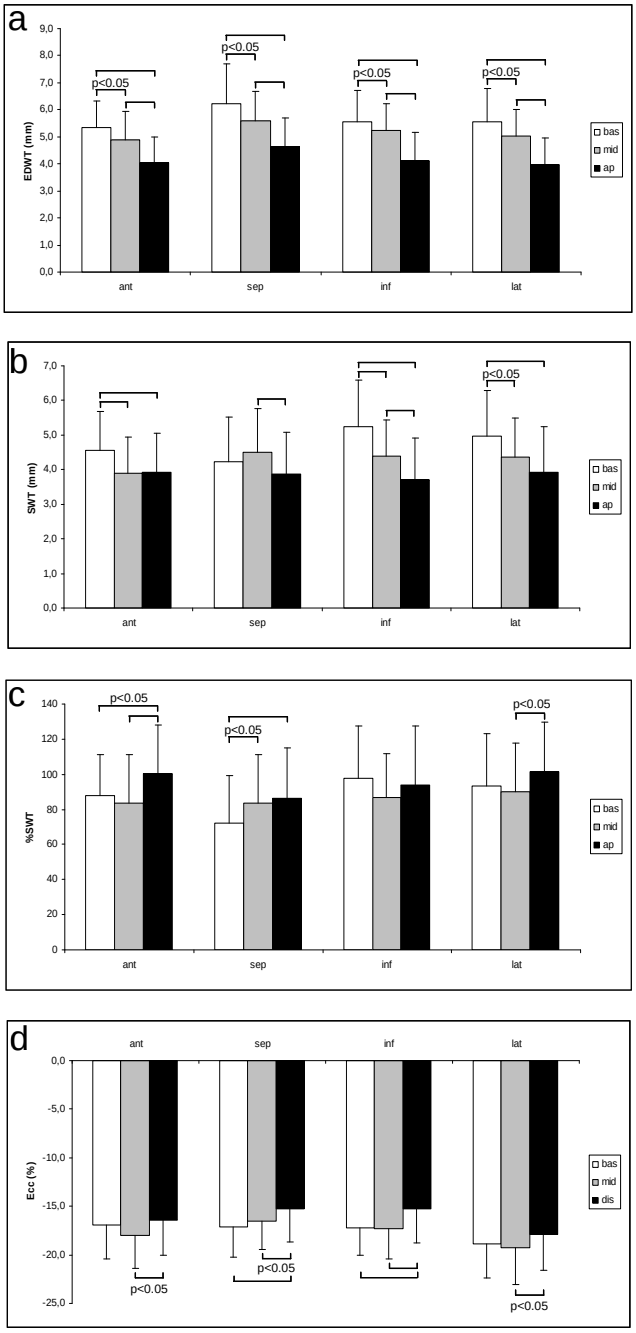

Figure 3. Segmental EDWT (a), SWT (b), %SWT (c) and Ecc (d) per slice. Septal and lateral segments at basal and mid level were averaged to allow comparison to apical slice. Abbreviations see text. P<0.01 unless stated otherwise.

SSFP cine CMR is ideal for the assessment of both global and regional function, because of the excellent spatial resolution and the high contrast between the blood pool and the myocardium. In line with previous studies, our data show heterogeneity of regional function, both within and between slices [16-19]. %SWT was significantly related to Ecc, and both showed a comparable regional variation with lower values in the septum and higher values in the free wall. However, the correlation was low, with discrepancies most obvious in the basal and mid septum. %SWT in the basal septum was exceptionally low, compared to other regions, and also to Ecc. This may be partly explained by the effects of through-plane motion caused by shortening along the left ventricular long axis, which is most prominent in the basal slice [20]. This results in different parts of the myocardium scanned in end-diastole and end-systole, and could have led to falsely low thickening values because the left ventricular outflow tract partly replaced the basal septum in the fixed scan position. Correction for this systolic shift by choosing a more apical slice as end-systolic image is not possible because of regional differences, which range from 15 mm in the inferior wall to 10 mm in the septum. Selective presaturation and suppression of slice-adjacent tissue with the use of a thick systolic slice has been suggested as a possible solution [20].

%SWT and Ecc were relatively homogenous in the basal and mid slice but showed a different pattern in the apical slice: %SWT was highest, and Ecc was lowest. Previous studies have demonstrated greater %SWT in the apical slices, whereas reports on Ecc have produced conflicting results [19,21-23]. Lower Ecc and higher %SWT may be explained by the fibre architecture in the apical parts of the left ventricle. These lack the midwall circumferentially arranged fibres that are found in the basal and mid parts, which may favor radial thickening over circumferential shortening [14].

Götte et al previously showed that strain analysis is superior to wall thickening for the detection of myocardial infarction associated regional dysfunction [24]. However, in this study, the standard deviation of %SWT (using FLASH gradient-echo cine CMR in 13 age-matched volunteers) was so high that the lower limit of normal (defined as mean–2SD) was zero or even negative in almost all regions. Although we still saw considerable spread in %SWT, the average mean–2SD in our study was 30%, which seems a more realistic value.

Mean EDWT in our group of healthy volunteers was 5.2±1.3 mm, with upper limits of normal (mean + 2 SD) in the basal septum and in the lateral wall 9.2 and 8 mm, respectively. Both are considerably lower than the traditional cut-off for regional hypertrophy in echocardiography textbooks (12 mm) [25]. This can be explained by the accurate visualization of the blood-myocardial border. This allows the reliable exclusion of myocardial trabeculations and papillary muscles from wall thickness measurements and assessment of the true change in myocardial wall thickness (figure 1). However, myocardial

mass calculated in this way will not correspond to the pathological-anatomic assessment of mass that will include both trabeculations and papillary muscles. Future studies will have to explore the effect of these findings on the definitions of hypertrophy and viability.

Expressing wall thickening in (absolute) millimeters makes the parameter independent of base line end-diastolic wall thickness. Although we found a fair correlation between SWT and %SWT, there was no correlation between SWT and Ecc, suggesting that SWT may not be suitable for the assessment of regional function.

In our study group, age did not influence any of the regional parameters. However, the study group was relatively small and we only examined morphological and systolic parameters. Previous work suggested that, in otherwise healthy subjects, parameters of diastolic function do show significant age-related changes [26,27].

Quantifying regional function with the centerline method has distinct limitations. It only provides a planar view of the radial component of myocardial deformation, does not take into account the circumferential, longitudinal or rotational motion. In addition to the effects of through-plane motion that are most important in the basal slice, the apical slice crosses the curved myocardial wall in an oblique fashion. Although our slice thickness of only 5 mm (compared to 10 mm in most previous studies) minimizes this potential error, it may still result in some overestimation of wall thickness. Methods to overcome these effects have been described, but significantly complicate the calculation of SWT, thus making them unsuitable for clinical use [28,29].

Despite its limitations, %SWT remains a valuable parameter of regional left ventricular function because it is naturally appealing and directly relates to the visual assessment of the imaging cardiologist. Further more, analysis of %SWT using the centerline method is quick and can be processed on-line at the scanner, simultaneously with the analysis of global left ventricular parameters.

In this study, we provided the normal range for percent segmental systolic wall thickening with state-of-the-art cine CMR imaging, and compared the data to the golden standard of regional function, circumferential strain analysis. Our results showed the normal heterogeneity of %SWT, and a low but significant correlation between %SWT and Ecc. Future studies are required to evaluate the performance of our dataset in patients with (suspected) myocardial disease.

REFERENCES

1. Sanz G, Castaner A, Betriu A (1982) Determinants of prognosis in survivors of myocardial infarction: a prospective clinical angiographic study. *N Engl J Med* 306:1065-70
2. Gotte MJW, Germans T, Russel IK, Zwanenburg JJM, Marcu JT, van Rossum AC, Veldhuisen DJ (2006) Myocardial Strain and Torsion Quantified by Cardiovascular Magnetic Resonance Tissue Tagging: Studies in Normal and Impaired Left Ventricular Function. *J Am Coll Cardiol* 48:2002-11
3. Sheehan FH, Mathey DG, Schofer J, Krebber HJ, Dodge HT (1983) Effect of interventions in salvaging left ventricular function in acute myocardial infarction: A study of intracoronary streptokinase. *Am J Cardiol* 52:431-8
4. McGillem MJ, Mancini GB, DeBoe SF, Buda AJ (1988) Modification of the centerline method for assessment of echocardiographic wall thickening and motion: a comparison with areas of risk. *J Am Coll Cardiol* 11:861-6
5. van Rugge FP, van der Wall EE, Spanjersberg SJ, de Roos A, Matheijssen NAA, Zwindeman AH, van Dijkman PRM, Reiber JHC, Bruschke AVG (1994) Magnetic resonance imaging during dobutamine stress for detection and localization of coronary artery disease. Quantitative wall motion analysis using a modification of the centerline method. *Circulation* 90:127-38
6. Goodyer AV, Langou RA (1982) The multicentric character of normal left ventricular wall motion. Implications for the evaluation of regional wall motion abnormalities by contrast angiography. *Cathet Cardiovasc Diagn* 8:225-232
7. Sievers B, Addo M, Kirchberg S, Baken A, John-Puthenveettil B, Franken U, Trappe HJ (2005) Impact of the ECG gating method on ventricular volumes and ejection fractions assessed by cardiovascular magnetic resonance imaging. *J Cardiovasc Magn Reson* 7:441-6
8. Maceira AM, Prasad SK, Khan M, Pennell DJ (2006) Normalized Left Ventricular Systolic and Diastolic Function by Steady State Free Precession Cardiovascular Magnetic Resonance. *J Cardiovasc Magn Reson* 8:417-26
9. Hudsmith LE, Petersen SE, Francis JM, Robson MD, Neubauer S (2005) Normal human left and right ventricular and left atrial dimensions using steady state free precession magnetic resonance imaging. *J Cardiovasc Magn Reson* 7:775-82
10. Taylor W, Al-Saadi N, Abdel-Aty H, Schulz-Menger J, Messroghli DR, Friedrich MG (2004) Detection of acutely impaired microvascular reperfusion after infarct angioplasty with magnetic resonance imaging. *Circulation* 109:2080-2085
11. Zwanenburg JJ, Kuijer JPA, Marcus JT, Heethaar RM (2003) Steady-state free precession with myocardial tagging: CSPAMM in a single breathhold. *Magn Reson Med* 49:722-30
12. Kuijer JPA, Jansen E, Marcus JT, van Rossum AC, Heethaar RM (2001) Improved harmonic phase myocardial strain maps. *Magn Reson Med* 46:993-9
13. Zwanenburg JJM, Gotte MJW, Kuijer JPA, Heethaar RM, van Rossum AC, Marcus JT (2004) Timing of cardiac contraction in humans mapped by high-temporal-resolution MRI tagging: early onset and late peak of shortening in lateral wall. *Am J Physiol Heart Circ Physiol* 286:H1872-H1880
14. Greenbaum RA, Ho SY, Gibson DG, Becker AE, Anderson RH (1981) Left ventricular fibre architecture in man. *Br Heart J* 45:248-63
15. Cerqueira MD, Weissman NJ, Dilsizian V, Jacobs AK, Kaul S, Laskey WK, Pennell DJ, Rumberger JA, Ryan T, Verani MS (2002) Standardized Myocardial Segmentation and Nomenclature for Tomographic Imaging of the Heart: A Statement for Healthcare Professionals From the Cardiac Imaging Committee of the Council on Clinical Cardiology of the American Heart Association. *Circulation* 105:539-42
16. Haendchen RV, Wyatt HL, Maurer G, Zwehl W, Bear M, Meerbaum S, Corday E (1983) Quantitation of regional cardiac function by two-dimensional echocardiography. I. Patterns of contraction in the normal left ventricle. *Circulation* 67:1234-45
17. Pflugfelder PW, Sechtem UP, White RD, Higgins CB (1988) Quantification of regional myocardial function by rapid cine MR imaging. *Am J Roentgenol* 150:523-9

18. Sechtem U, Sommerhoff BA, Markiewicz W, White RD, Cheitlin MD, Higgins CB (1987) Regional left ventricular wall thickening by magnetic resonance imaging: Evaluation in normal persons and patients with global and regional dysfunction. *Am J Cardiol* 59:145-51
19. van Rugge FP, Holman ER, van der Wall EE, de Roos A, van der Laarse A, Bruschke AVG (1993) Quantitation of global and regional left ventricular function by cine magnetic resonance imaging during dobutamine stress in normal human subjects. *Eur Heart J* 14:456-63
20. Rogers WJ, Jr., Shapiro EP, Weiss JL, Buchalter MB, Rademakers FE, Weisfeldt ML, Zerhouni EA (1991) Quantification of and correction for left ventricular systolic long- axis shortening by magnetic resonance tissue tagging and slice isolation. *Circulation* 84:721-31
21. Kramer CM, Rogers WJ, Theobald TM, Power TP, Petruolo S, Reichek N (1996) Remote Noninfarcted Region Dysfunction Soon After First Anterior Myocardial Infarction: A Magnetic Resonance Tagging Study. *Circulation* 94:660-6
22. Bogaert J, Rademakers FE (2001) Regional nonuniformity of normal adult human left ventricle. *Am J Physiol Heart Circ Physiol* 280:H610-H620
23. Rademakers FE, Rogers WJ, Guier WH, Hutchins GM, Siu CO, Wiesfeldt ML, Weiss JL, Shapiro EP (1994) Relation of regional cross-fiber shortening to wall thickening in the intact heart. Three-dimensional strain analysis by NMR tagging. *Circulation* 89:1174-82
24. Gotte MJW, van Rossum AC, Twisk JWR, Kuijer JPA, Marcus JT, Visser CA (2001) Quantification of regional contractile function after infarction: strain analysis superior to wall thickening analysis in discriminating infarct from remote myocardium. *J Am Coll Cardiol* 37:808-17
25. Otto C (2004) Textbook of clinical echocardiography, 3rd ed. Elsevier, Philadelphia.
26. Germans T, Gotte MJW, Nijveldt R, Beek AM, Bronzwaer JGF, Paulus WA, van Rossum AC (2007) Effects of Aging on Left Atrioventricular Coupling and Left Ventricular Filling Assessed Using Cardiac Magnetic Resonance Imaging in Healthy Subjects. *Am J Cardiol* 100:122-7
27. Fonseca CG, Oxenham HC, Cowan BR, Occleshaw CJ, Young AA (2003) Aging alters patterns of regional nonuniformity in LV strain relaxation: a 3-D MR tissue tagging study. *Am J Physiol Heart Circ Physiol* 285:H621-H630
28. Beyar R, Shapiro EP, Graves WL, Rogers WJ, Guier WH, Carey GA, Soulen RL, Zerhouni EA, Weisfeldt ML, Weiss JL (1990) Quantification and validation of left ventricular wall thickening by a three-dimensional volume element magnetic resonance imaging approach. *Circulation* 81:297-307
29. Holman ER, Buller VGM, de Roos A, van der Geest RJ, Baur LHB, van der Laarse A, Bruschke AVG, Reiber JHC, van der Wall EE (1997) Detection and Quantification of Dysfunctional Myocardium by Magnetic Resonance Imaging: A New Three-dimensional Method for Quantitative Wall-Thickening Analysis. *Circulation* 95:924-31

Chapter 8

Quantification of late gadolinium-enhanced CMR in viability assessment in chronic ischemic heart disease: a comparison to functional outcome

Aernout M. Beek, Olga Bondarenko, Farshid Afsharzada, Albert C. van Rossum

J Cardiovasc Magn Reson 2009;11(1):6.

ABSTRACT

Background. Quantification of late gadolinium enhanced cardiovascular MRI (LGE) by objective window setting increases reproducibility and facilitates multicenter comparison and cooperation. So far, quantification methods or models have only been validated to postmortem animal studies. This study was undertaken to evaluate quantification of LGE in relation to the clinical standard of viability, i.e. functional outcome after revascularization.

Methods. Thirty-eight patients with chronic ischemic myocardial dysfunction underwent cine and LGE 1 month before and cine CMR 6 months after coronary revascularization. Hyperenhancement was quantified by thresholding window setting at: 2-8SD above mean signal intensity of a remote normal region, and according to the full width at half maximum method (FWHM). Dysfunctional segments were divided in 5 groups according to segmental extent of hyperenhancement (SEH): SEH 1 – no hyperenhancement to SEH 5 – 76-100% with each quantification method.

Results. Quantification methods had a strong influence on SEH and total infarct size. Multilevel analysis showed that thresholding contrast images at 6SD best predicted segmental functional outcome after revascularization, but the difference with other methods was small and non-significant.

Conclusions. Simple thresholding techniques strongly influence global and segmental extent of hyperenhancement, but have relatively little influence on the accuracy to predict segmental functional improvement after revascularization.

Acknowledgements

This work was supported by the Netherlands Heart Foundation (grant 2001.158).

Prof. Jos W.R. Twisk, PhD, Department of Clinical Epidemiology and Biostatistics is kindly acknowledged for his contribution to the statistical analysis. Mary Belderok is kindly acknowledged for her contribution to the organization of the study and the data collection.

INTRODUCTION

Revascularization of dysfunctional but viable myocardium may lead to reversed remodelling, improved regional and global function and better prognosis in patients with chronic ischemic heart disease [1]. The diagnostic accuracy of imaging modalities to predict functional outcome is influenced by the definition of disease (what is viable). Although visual or qualitative analysis may provide satisfactory results, standardization and quantification of these definitions increases reproducibility and reliability in follow-up studies, and facilitates comparison between different centers.

Late gadolinium-enhanced cardiovascular magnetic resonance imaging (LGE) accurately visualizes the transmural extent of ischemia-related scar and has been shown to predict the likelihood of functional improvement after revascularization [2,3]. Several methods have been proposed to differentiate hyperenhanced, non-viable from non-enhancing, viable myocardium, all using the in-slice signal intensity of infarcted or remote myocardium, and ranging from simple thresholding to more complex computer algorithms. We have previously shown that the use of common thresholds based on the suppressed signal of remote myocardium may lead to considerable overestimation of the infarct size [4]. However, in this study, we used visual estimation as the reference standard. Although a number of experimental studies have used ex-vivo imaging or 2,3,5-triphenyltetrazolium choride (TTC) staining to determine the optimal threshold of hyperenhancement, so far, no study has used the clinically useful standard of viability i.e. functional outcome after revascularization [5-7].

Therefore, the aim of this study was to evaluate the relation between quantification of LGE and functional outcome after revascularization in patients with chronic ischemic myocardial dysfunction. To quantify LGE, we chose simple thresholding techniques that are easily applicable in any clinical or research situation.

METHODS

Patients. All patients with known coronary artery disease and regional wall motion abnormalities on echocardiography or left ventricular (LV) angiography, without CMR contraindications, who were scheduled to undergo surgical or percutaneous revascularisation, were study candidates. The Committee on Research Involving Human Subjects of the VU University Medical Centre, Amsterdam, approved the study protocol. All patients gave written informed consent.

Forty-seven patients were initially included in this study protocol. After revascularization, 7 patients were excluded because of left ventricular aneurysmectomy (1), electrocardiographic and/or biochemical evidence of peri-procedural myocardial infarction

(defined as post procedural peak CK-MB >3 upper limit of normal) (4), pacemaker implantation (1), and incomplete data (1). During analysis, 2 more patients were excluded because of absence of wall motion abnormalities at baseline and non-diagnostic image quality, leaving 38 patients as the final study group. All patients were in stable clinical condition at the time of both CMR examinations without clinical evidence of ischemic events during the study period.

CMR. CMR scans were acquired at 4±4 weeks before and 30±4 weeks after revascularisation. All scans were performed on a 1.5T scanner (Sonata, Siemens, Erlangen, Germany) with the patient in a supine position using a four-element phased array cardiac receiver coil. ECG-gated cine images were acquired using a breath-hold segmented steady-state free precession sequence (true FISP; echo time/repetition time of 1.2/3.2ms; resolution of 1.3 x 1.8 x 5mm). Per patient eight to ten short-axis views were obtained every 10mm starting from the mitral valve insertion and covering the entire left ventricle. Ten to 15 minutes after injection of a gadolinium-based contrast agent (Magnevist, Schering AG, Berlin, Germany; 0,2mmol/kg) contrast-enhanced images were acquired in the same orientation as the cine images using a 2D-segmented inversion recovery gradient-echo pulse sequence triggered to end-diastole (repetition time/echo time = 9.6/4.4 ms, flip angle 25˚, inversion time set to suppress signal from remote myocardium, matrix 208x256 and a typical voxel size of 1.6 x 1.3 x 5.0).

Data analysis. All data were analysed on a separate workstation using a dedicated software package (MASS v15, 2008, Medis, Leiden, The Netherlands).

Segmental function. Segmental wall thickness was measured at end-systole and end-diastole after manual tracing of endocardial end epicardial borders in stop-frame images, carefully excluding trabeculations and papillary muscles. The observer (OB) was blinded to other patient or imaging data such as extent of coronary artery disease, use of medication and results of the LGE analysis. Baseline and follow-up slices were analysed separately after registration using the scanner slice position and various anatomical landmarks such as right ventricle septal insertion sites, papillary muscle location, and trabecularization patterns in the right and left ventricles. Although the observer was unaware of the timing of the study, blinding to pre-/postoperative status was impossible because of the artifacts related to sternal wires. For segmental analysis, the 2 most basal and apical slices were excluded because of the left ventricular outflow tract and partial volume effects, respectively. The remaining slices were divided into 6 segments each, starting at the inferior insertion of the right ventricle to the septum. Segmental wall thickening (SWT) in millimetres was calculated as: end systolic wall thickness minus end diastolic wall thickness. Segments with SWT <3 mm (mean – 2SD) were considered dysfunctional [4]. Functional improvement was defined as an increase in SWT of ≥1.5 mm compared to baseline. Intraobserver and

interobserver variability of SWT were 0.0 ± 0.4 mm (mean difference between 2 measurements (OB); intraclass correlation coefficient = 0.97, 95% confidence interval 0.86 – 0.99), and 0.1 ± 0.7 mm (mean difference between values of observer 1 (OB) and 2 (AMB); intraclass correlation coefficient = 0.89, 95% confidence interval 0.55–0.98), as reported previously [3].

Global function. Left ventricular end-diastolic volume (EDV) and end-systolic volumes (ESV) were determined by planimetry of all short-axis images in each patient and indexed to body surface area. Left ventricular ejection fraction (EF, %) was calculated as (LVEDV – LVESV)/LVEDV * 100%.

Hyperenhancement. Endocardial and epicardial contours were manually traced, again avoiding papillary muscles and trabecularizations. Hyperenhanced regions were then determined in the following ways:

I. After thresholding signal intensity at 2-8 standard deviations (SD) above the mean signal intensity of remote normal myocardium in the same slice. A region of interest of 0.5-1 cm^2 was manually drawn and placed in remote normal myocardium (defined as normal function without hyperenhancement on visual assessment). If a slice contained no remote normal myocardium, mean and SD of the nearest slice with normal remote myocardium was used; if the 2 neighbouring slices contained normal myocardium, mean and SD were averaged.

II. After thresholding signal intensity using the full-width at half-maximum (FWHM) method that defines the hyperenhanced area by using 50% of the maximum signal found within the hyperenhanced area. The maximum signal was found by computer-assisted window thresholding of the hyperenhanced area. If no hyperenhancement was found in a slice, the maximum signal of the nearest slice with hyperenhancement was used; if the 2 neighbouring slices showed hyperenhancement, maximum signals were averaged.

All areas of hyperenhancement were quantified by computer-assisted planimetry on each of the short axis images and segmental extent of hyperenhancement (SEH) was expressed as percentage of segmental area. Obvious artifacts such as caused by motion were excluded by highlighting them using a tool from the software package. Other small isolated regions of hyperenhancement that were clearly not of ischemic origin (like small subepicardial spots) were also excluded from analysis. Total infarct size was calculated by summation of all slice volumes of hyperenhancement, i.e. including the slices that were excluded for segmental analysis.

Statistical analysis. The paired sample t test (with Bonferroni correction) and the independent samples t test were used to compare means within the study group or between subgroups. To account for the non-independence of the data, we used multilevel logistic regression (MlwiN, version 1.02.0007, Centre for Multilevel Modelling, London, United

Kingdom) to analyse the relation between SEH and the likelihood of improvement. Details of the multilevel analysis have been published previously [3]. All dysfunctional segments were assigned to one of the following groups according to SEH: 1 - 0%, 2 – 1 to 25%, 3 – 26 to 50%, 4 – 51 to 75%, and 5 – 76 to 100% hyperenhancement. The regression coefficients were used to calculate odds ratios that express the likelihood of improvement of SEH-groups 2-5 relative to SEH-group 1. To compare the different quantification methods, multilevel analysis was repeated assuming a linear correlation between SEH and likelihood of improvement, which generates one regression coefficient per method. Receiver operating characteristics (ROC) analysis was used to find the SEH cut-off with highest diagnostic accuracy to predict segmental functional improvement.

Improvement in ejection fraction was defined as an increase from baseline to follow-up of $\geq$ 5%. Since the number of viable segments per patient is not normally distributed, the Mann-Whitney test was used to compare these between patients with and without improved ejection fraction.

All values are expressed as mean ± SD. P-values <0.05 were considered statistically significant.

Table 1. Patient characteristics.

Number of patients	38
Age (sd)	62 (10)
Men	33 (87%)
Diabetes	10 (26%)
Hypercholesterolemia	7 (18%)
Hypertension	8 (21%)
Smoking	13 (34%)
1-vessel disease	4 (11%)
2-vessel disease	10 (26%)
3-vessel disease	24 (63%)
Medication	
aspirin	22 (58%)
acenocoumarol	16 (42%)
betablockers	29 (76%)
statins	29 (76%)
ace-inhibitors	20 (53%)
PCI*	9 (24%)
CABG**	30 (76%)
mean nr grafts (sd)	3,6 (1,1)

* percutaneous coronary intervention.

** coronary artery bypass grafting.

RESULTS

Patient characteristics are provided in table 1.

Extent of hyperenhancement. The extent of hyperenhancement according to quantification method is shown in table 2. Both total infarct size and segmental extent of hyperenhancement were strongly correlated between all methods ($p<0.001$), except total infarct size between FWHM and 2SD and 3SD (non-significant after Bonferroni correction). Total infarct size decreased with increasing number of SD's (all steps $p<0.001$). Total infarct size according to FWHM differed significantly from 2-4 SD ($p<0.001$). Mean SEH decreased with increasing number of SD's and FWHM (all $p<0.001$).

Table 2. Global and segmental extent of hyperenhancement according to quantification method.

	2SD	3SD	4SD	5SD	6SD	7SD	8SD	FWHM
TIS	31.3 (12.1)	23.6 (11.6)	18.7 (11.5)	15.7 (11.1)	12.6 (9.1)	10.4 (8.9)	7.9 (6.8)	14.1 (6.8)
SEH*	36.2 (31.9)	29.2 (31.0)	24.3 (29.5)	20.9 (27.9)	17.9 (25.8)	15.8 (24.4)	14.1 (23.3)	15.4 (22.4)

TIS = mean (sd) total infarct size. SEH = mean (sd) segmental extent of hyperenhancement. * = dysfunctional segments only.
Statistical analysis see text.

Table 3. Likelihood of improvement versus quantification method.

	SEH 1	SEH 2	SEH 3	SEH 4	SEH 5
2SD	1	0,7	1,2	2,0	2,5
3SD	1	1,6	3,8	3,8	5,2
4SD	1	1,3	1,5	3,4	4,5
5SD	1	1,5	3,1	4,3	6,1
6SD	1	2,9	4,7	5,2	14,8
7SD	1	2,0	4,4	3,9	10,8
8SD	1	2,1	4,1	3,2	9,6
FWHM	1	2,4	3,5	4,7	5,5

SEH = segmental extent of hyperenhancement. Numbers represent odds ratios of likelihood of improvement of SEH 2-5 versus SEH 1, which is set at 1.

Functional improvement. A total of 1122 segments were analysed (29.6±5.5/patient). Of these, 628 were dysfunctional (mean SWT 1.1±1.1mm). Segmental function improved in 174 segments (mean SWT 0.9±1.2 to 3.5±1.5 mm). The likelihood of improvement was inversely related to the SEH according to all quantification methods. The results of the multilevel analysis are displayed in table 3. The odds ratios were inverted so that they reflect the number of times that a certain SEH group is less likely to improve compared to SEH group 1 in that category. Quantifying hyperenhancement using 6SD best predicted segmental functional improvement at follow-up: segments in SEH-groups 2, 3, 4 and 5 were 2.7, 4.7, 5.2 and 14.8 less likely to improve than segments in SEH-group 1 (table 3).

Multilevel analysis was repeated assuming a linear relationship between SEH-groups and likelihood of improvement. This analysis generates one odds ratio that represents the likelihood of improvement from one SEH-group to the next. 6SD had the highest predictive power: SEH-group x was 2.04 (95% confidence intervals 1.62-2.58) less likely to improve than the SEH-group x-1. 2SD had the lowest power with (inverted) odds ratio 1.66 (1.31-2.08). Figure 1 shows 95%-confidence intervals for each method, demonstrating that there is considerable overlap.

Left ventricular EDV and ESV were 123±36 ml/m2 and 79±35 ml/m2 at baseline, and decreased significantly to 108±36 ml/m2 ($p<0.001$) and 68±35 ml/m2 ($p=0.002$), respectively. Mean EF improved from 38.2±11.4% at baseline to 40.4±12% at follow-up ($p=0.067$).

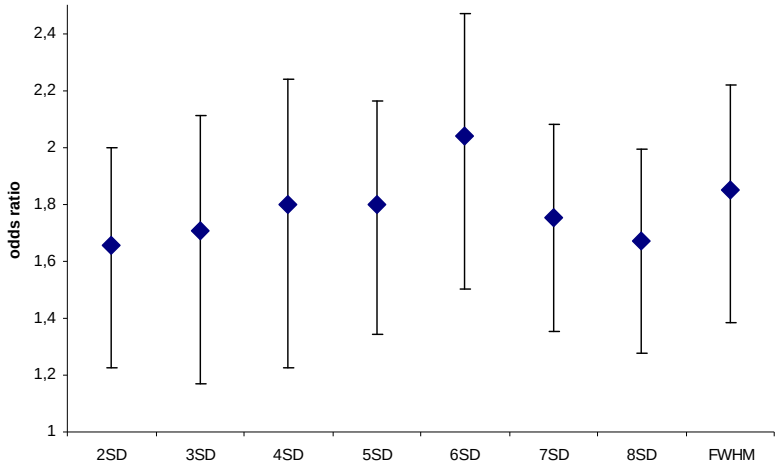

Figure 1. Multilevel analysis assuming linear relation between likelihood of improvement according and quantification method. (Inverted) odds ratios and 95%-confidence intervals according to quantification method. See text for further explanation.

Table 4. Sensitivity and specificity according to quantification method.

	sens	spec	SEH*
2SD	0,72	0,55	28
3SD	0,72	0,57	21
4SD	0,64	0,65	25
5SD	0,68	0,64	14
6SD	0,70	0,65	9
7SD	0,65	1,00	9
8SD	0,65	1,00	7
FWHM	0,61	0,66	9

* = segmental extent of hyperenhancement (%) at optimal sensitivity and specificity.

ROC analysis showed that the 6SD method optimally predicted segmental improvement at < 10% SEH (AUC 0.700 (0.654-0.746), sensitivity 70%, specificity 65%) (table 4). Twenty-two patients showed significant (≥5%) improvement in EF. Although the number of dysfunctional segments with < 10% SEH-6SD was higher in patients with improved ejection fraction compared to patients without improvement (median 7.5, range 1-24, vs 4.0, range 0-14), there was considerable overlap, and no significant difference could be found (Mann-Whitney-test, p = 0.251).

DISCUSSION

Our results show that quantification methods have a strong influence on total and regional infarct extent. Although analysis using 6SD above signal intensity of a remote normal region resulted in the best prediction of segmental functional improvement after revascularization, differences with the other methods were small and non-significant.

LGE quantification. Both SD- and FWHM-methods are based on experience rather than on firm pathophysiological evidence. SD uses the (purposely suppressed) signal of a remote normal region, whereas FWHM uses the peak signal within the hyperenhanced region. FWHM has been suggested on theoretical grounds to be less sensitive to partial volume effects. Amado et al compared total infarct size according to the SD- and FWHM-thresholding methods and postmortem data in an animal occlusion-reperfusion study [5]. They found that FWHM correlated best with TTC-staining with a small overestimation (significance not reported), whereas no significant correlation and considerable overestimation was found with 6SD. Heiberg et al recently proposed a quantification method to compensate for partial volume effects in thicker (8-10) mm) slices by weighting

pixels according to their signal intensity [7]. The standard LGE protocol in our institution uses 5 mm slice thickness, which maintains excellent image quality while minimizing partial volume effects.

Hsu et al developed a computer algorithm based on feature analysis and combined thresholding involving sequential use of the 2SD- and FWHM-method [6]. The algorithm was validated in a canine study, and compared to visual assessment and 2SD- and FWHM-thresholding using ex-vivo and in-vivo LGE. The authors found that infarct size measured by their model showed no difference with TTC-staining, and was more accurate than the other methods, that all overestimated the histopathological infarct size. The algorithm was subsequently tested in 20 patients with acute or chronic infarction, and resulted in significantly lower values for both regional and global infarct size when compared to visual assessment, although this study lacked a reference standard [9]. Hsu et al used phase-sensitive reconstruction in both studies and also used 8 mm slice thickness, which makes comparison of their findings to our study difficult and again stresses the importance of standardization.

In a previous study we quantified hyperenhancement in 15 patients with chronic ischemic heart disease. In comparison to visual assessment, we found significant overestimation with 2-4SD of both segmental extent and total infarct size [4]. The use of 6SD led to a significant underestimation, whereas 5SD showed no difference.

In the current study we used functional outcome after revascularisation as the clinical reference standard of viability. We found that, although the extent of hyperenhancement was profoundly influenced by the quantification method used, there was no significant difference in their accuracy to predict segmental functional improvement at follow-up. 6SD showed the highest accuracy, followed closely by FWHM, 4SD and 5SD. Thresholding at 2SD and 3SD above remote signal intensity was less accurate, but there was still considerable overlap of confidence intervals with 6SD. Our data suggest that simple thresholding methods using the signal intensity of remote or of the hyperenhanced area have relatively little effect on the assessment of regional viability and the prediction of likelihood of improvement. The lack of a clear difference may seem surprising considering the large differences that the use of the various methods caused in total infarct size and segmental extent of hyperenhancement. However, with each method the inverse relation between SEH and likelihood of improvement remains intact, which makes it hard to detect small differences in predictive power. A larger study group and longer follow-up may be required to strengthen the statistical position of 6SD [3].

Limitations. All current LGE quantification methods are limited by the fact that essential steps like the delineation of myocardial contours, the drawing a region of interest in remote myocardium and the exclusion of artifacts are all (still) done manually. The applicability of

our results is limited to patients with chronic ischemic heart disease, although they are probably valid in acute myocardial infarction, since both animal and clinical studies have shown that hyperenhancement reflects necrosis at all stages after infarction [10-12]. However, this remains to be established. Also, our results cannot be extrapolated to other techniques (e.g. 3D-acquisition) or scanner types (especially with different magnetic field strengths).

In conclusion, in this study we evaluated the relation between simple thresholding techniques to quantify LGE images and functional outcome after revascularization in patients with chronic ischemic myocardial dysfunction. Although quantitative analysis with window setting thresholded at mean + 6SD of the signal of a remote normal region best predicted segmental functional improvement, there was no significant difference with the other SD or FWHM methods. Further study is needed to evaluate SD and FWHM in larger groups with a longer follow-up and compare them to the more complex algorithms that have not yet been tested in human viability studies.

REFERENCES

1. Camici PG, Prasad SK, Rimoldi OE. Stunning, Hibernation, and Assessment of Myocardial Viability. *Circulation*. 2008;117:103-114.
2. Kim RJ, Wu E, Rafael A et al. The Use of Contrast-Enhanced Magnetic Resonance Imaging to Identify Reversible Myocardial Dysfunction. *N Engl J Med*. 2000;343:1445-1453.
3. Bondarenko O, Beek AM, Twisk JWR et al. Time course of functional recovery after revascularization of hibernating myocardium: a contrast-enhanced cardiovascular magnetic resonance study. *Eur Heart J*. 2008;29:2000-5.
4. Bondarenko O, Beek AM, Hofman MBM et al. Standardizing the Definition of Hyperenhancement in the Quantitative Assessment of Infarct Size and Myocardial Viability Using Delayed Contrast-Enhanced CMR. *J Cardiovasc Magn Reson*. 2005;7:481-485.
5. Amado LC, Gerber BL, Gupta SN et al. Accurate and objective infarct sizing by contrast-enhanced magnetic resonance imaging in a canine myocardial infarction model. *J Am Coll Cardiol*. 2004;44:2383-2389.
6. Hsu LY, Natanzon A, Kellman P et al. Quantitative myocardial infarction on delayed enhancement MRI. Part I: Animal validation of an automated feature analysis and combined thresholding infarct sizing algorithm. *J Magn Reson Imaging*. 2006;23:298-308.
7. Heiberg E, Ugander M, Engblom H et al. Automated Quantification of Myocardial Infarction from MR Images by Accounting for Partial Volume Effects: Animal, Phantom, and Human Study. *Radiology*. 2008;246:581-588.
8. Simonetti OP, Kim RJ, Fieno DS et al. An improved MR imaging technique for the visualization of myocardial infarction. *Radiology*. 2001;218:215-223.
9. Hsu LY, Ingkanisorn WP, Kellman P et al. Quantitative myocardial infarction on delayed enhancement MRI. Part II: Clinical application of an automated feature analysis and combined thresholding infarct sizing algorithm. *J Magn Reson Imaging*. 2006;23:309-314.
10. Beek AM, Kuhl HP, Bondarenko O et al. Delayed contrast-enhanced magnetic resonance imaging for the prediction of regional functional improvement after acute myocardial infarction. *J Am Coll Cardiol*. 2003;42:895-901.
11. Fieno DS, Kim RJ, Chen EL et al. Contrast-enhanced magnetic resonance imaging of myocardium at risk: distinction between reversible and irreversible injury throughout infarct healing. *J Am Coll Cardiol. 2000*;36:1985-1991.
12. Selvanayagam JB, Kardos A, Francis JM et al. Value of Delayed-Enhancement Cardiovascular Magnetic Resonance Imaging in Predicting Myocardial Viability After Surgical Revascularization. *Circulation*. 2004;110:1535-1541.

Summary

Samenvatting (met wat meer toelichting)

SUMMARY

This thesis addresses the clinical applications of Cardiovascular Magnetic Resonance imaging (CMR) in patients with myocardial infarction. The introduction of steady state free-precession (SSFP) cine imaging and delayed contrast-enhanced (DCE) imaging around the turn of the century has triggered a major step forward in the position of CMR in the field of cardiac imaging. CMR is now the definitive reference technique for the non-invasive evaluation of left and right ventricular function, mass and regional scar. Other CMR techniques are T2-weighted spin-echo (T2W) imaging and first pass myocardial perfusion imaging. T2W imaging is sensitive to regional high water content and can therefore be used to visualise infarct-related myocardial oedema. First pass perfusion imaging is used to assess myocardial perfusion and microvascular obstruction. The latest developments of these techniques in both the acute and the chronic phase of myocardial infarction are reviewed in chapter 1.

Chapters 2-4 focus on the use of CMR in patients with acute myocardial infarction. Regions that are severely dysfunctional early after infarction may show (partial) recovery of function when the occluded coronary artery is timely reperfused. The likelihood of recovery depends on the local extent of irreversibly damaged tissue, which can be visualised as areas of high signal intensity (hyperenhancement) on DCE images. In Chapter 2, we showed that DCE can be used to predict functional recovery of stunned myocardium after acute infarction. We evaluated 30 patients after a first reperfused acute myocardial infarction using cine imaging and DCE at one week and follow-up cine at 3 months. The likelihood of improvement of dysfunctional segments was strongly and inversely related to the segmental extent of hyperenhancement.

Microvascular obstruction (MVO), or no-reflow, refers to the fact that, in acute myocardial infarction, successful revascularisation of the epicardial coronary artery is not always followed by the restoration of myocardial perfusion. MVO is a well-known predictor of poor functional recovery and less favourable outcome. On DCE images, it can be seen as regions of low signal intensity within the hyperenhanced infarction. Coronary angiography, electrocardiography and echocardiography can also be used to assess MVO. In chapter 3, we directly compared angiographic, electrocardiographic and CMR measures of microvascular obstruction in 60 patients after primary stenting for a first acute myocardial infarction. We found that DCE imaging was a very sensitive marker of MVO and that it was the strongest predictor of changes in left ventricular volumes and ejection fraction at follow-up.

Microvascular obstruction may lead to intramyocardial haemorrhage by extravasation of erythrocytes through severely damaged endothelial walls. It is not known whether haemorrhage has additional unfavourable impact or whether it is a mere side effect. In

chapter 4, we used non-enhanced T2W imaging to assess the clinical significance of infarct-related intramyocardial haemorrhage in relation to infarct size, microvascular obstruction, baseline function and functional outcome. Regional infarct-related oedema normally causes high-intensity areas on T2W images, but the high signal is attenuated by the presence of haemorrhage, which alters regional magnetic properties. Haemorrhage was detected in 22 of 45 patients, and its presence was related to a larger infarct size, the presence of MVO and lower ejection fraction. The best predictor of functional changes, however, was MVO, and, in this study, the presence of haemorrhage was of no additional value.

Chapters 5 and 6 focus on the use of CMR in patients with chronic ischemic heart disease. In these patients, left ventricular systolic dysfunction may result from infarction and irreversibly scarred myocardium or from chronic hypoperfusion in which the function may recover after restoration of flow. As in acute myocardial infarction, the likelihood of functional recovery depends on the regional scar extent, which can be visualised by DCE imaging. In Chapter 5, we showed that DCE imaging correlated well to the current reference imaging standard of viability, ^{18}F-fluorodeoxyglucose positron emission tomography (PET). In 26 patients with chronic coronary artery disease and left ventricular dysfunction, segmental extent of hyperenhancement was inversely related to segmental glucose uptake by PET. At 37% segmental extent of hyperenhancement, DCE imaging optimally differentiated viable from non-viable segments defined by PET (sensitivity 96%, specificity 84%). After successful revascularisation, chronically ischemic, dysfunctional myocardium does not always improve despite proven viability. This may be explained by a delayed time course of recovery and premature follow-up imaging. This issue was addressed in Chapter 6. We assessed functional outcome and temporal changes in relation to baseline extent of hyperenhancement in 35 patients with chronic ischemic LV dysfunction 1 month before, and 3, 6 and 24±12 months after revascularisation. The study showed that improvement of dysfunctional but viable myocardium can be considerably delayed and that both likelihood and time course of long-term functional improvement were related to the baseline amount of scar.

Both cine images and DCE images are generally assessed in a qualitative way (‘eyeballing’). However, quantitative assessment is preferable for comparison within patients, between patients and between different centers. Chapters 7 and 8 address the quantitative analysis of cine images and DCE images. Regional left ventricular function can be quantified as systolic wall thickening which is the difference between regional end-diastolic wall thickness and end-systolic wall thickness and is expressed in absolute millimetres or as a percentage of end-diastolic wall thickness. Although systolic wall thickening is widely used in the literature, there is a surprising scarcity of systematic reports

on its normal range, and even prominent CMR publications use normal values from old echocardiographic reports. In Chapter 7, we therefore used cine imaging and the centerline method to provide the normal range for regional wall thickness and wall thickening in 36 healthy volunteers. Regional end-diastolic and end-systolic wall thickness and percent systolic wall thickening showed significant heterogeneity that was in line with previous reports. The results in this study further suggested that the traditionally used definition of myocardial hypertrophy may not be valid when using current high resolution cine CMR sequences. DCE images can easily be quantified, but the resulting regional and global infarct extent strongly depend on image window setting, which generally reflects the personal preference of the observer and may differ considerably especially between the various centers. A range of quantification methods of varying complexity has been proposed, but their value remains unsure because of the lack of an in-vivo, human standard of regional scar. In Chapter 8, we therefore used functional outcome after revascularisation, which is considered the clinical standard of viability, to evaluate two DCE quantification methods in 38 patients with chronic ischemic myocardial dysfunction. Hyperenhancement was quantified by thresholding window setting at: 2-8 standard deviations above mean signal intensity of a remote normal region, and according to the full-width-at-half-maximum method. We found that, although the quantification method had a strong impact on the quantified global and segmental extent of hyperenhancement, it had relatively little influence on the accuracy to predict segmental functional improvement after revascularization.

CONSIDERATIONS

When considering the studies presented in this thesis, along with many others published so far, it can be safely concluded that CMR is a valuable technique in patients with myocardial infarction. The advantages of CMR compared to other techniques as echocardiography and radionuclide perfusion imaging of CMR are clear: wide field-of-view, high resolution, high quality, one-stop (function-perfusion-viability) examination, and simple quantification without geometrical assumptions. In addition, as a unique feature, it allows the in-vivo demonstration of oedema, haemorrhage, microvascular obstruction and acute or chronic infarct extent. It is this tissue characterisation that has created new possibilities in the management of patients with myocardial infarction that will be addressed in the coming years: e.g. oedema as a marker of area at risk; microvascular obstruction and haemorrhage as markers of infarct and prognostic markers, and as endpoints in reperfusion studies; infarct heterogeneity as a marker of ventricular arrhythmia. So, the cardiac imager is happy, and so is the researcher, but what about the clinician, the referring cardiologist, and the patient with myocardial infarction? Are the advantages of CMR translated into improved

diagnosis and management? In the early phase after myocardial infarction, echocardiography is adequate to answer most clinical questions, especially in patients with an uncomplicated course. CMR has additional value when diagnosis is unsure, when complications are suspected but cannot be adequately depicted, when prediction of functional recovery is relevant and, importantly, in the quantification of LV function in ICD candidates. In the chronic phase of infarction, management critically depends on quantification of ventricular function and the assessment of viability, and CMR should be strongly considered in any patient with (suspected) chronic infarction or (ischemic) cardiomyopathy. However, the ultimate impact of CMR on management and outcome of patients with myocardial infarction is hard to define because current availability is still limited compared to other techniques. Put in other words: the list of publications favouring its use is growing considerably quicker than the number of CMR imaging centres. This may be explained by a variety of potential hurdles, such as the need for collaboration between cardiologists and radiologists, the lack of a clear reimbursement that acknowledges the contribution of all those involved and the need for training and credentialing of technical and medical staff. CMR is about to make its final growth spurt, but only after these issues are solved.

SAMENVATTING (met wat meer toelichting)

Hoewel behandeling en prognose van het acute hartinfarct de afgelopen jaren sterk verbeterd zijn, is coronaire of ischemische hartziekte nog steeds de belangrijkste doodsoorzaak in de westerse wereld. Bij de diagnose en behandeling worden techieken gebruikt die informatie verschaffen over functie van de hartspier en de hartkleppen, de doorbloeding en de schade ten gevolge van het hartinfarct. Bekende en veelgebruikte technieken zijn o.a. echocardiografie (vooral voor de afbeelding van functie) en nucleaire scans (vooral voor de afbeelding van de doorbloeding van de hartspier). *Cardiovascular Magnetic Resonance imaging* (CMR) is een nieuwere techniek die gebruikt kan worden voor de afbeelding van het hart. CMR werd aanvankelijk met name gebruikt voor onderzoeksdoeleinden, maar het heeft de laatste jaren een grote ontwikkeling doorgemaakt en is nu een waardevol diagnostisch hulpmiddel geworden voor de dagelijkse cardiologische praktijk. In dit proefschrift wordt een aantal van de toepassingsmogelijkheden van CMR bij patiënten met een hartinfarct nader onderzocht.

Hoofdstuk 1 geeft een overzicht van de CMR-technieken die gebruikt kunnen worden bij patiënten met een hartinfarct. De twee belangrijkste technieken zijn *cine* CMR en *delayed contrast-enhanced (DCE)* CMR. Cine imaging wordt vooral gebruikt voor de afbeelding van functie van hartspier en kleppen en is de gouden standaard voor de kwantificering van functie van linker en rechter hartkamer. Het littekenweefsel van een hartinfarct kan nauwkeurig worden gevisualiseerd na contrast toediening met behulp van DCE imaging. Litteken is zichtbaar als regionale contrastaankleuring (hoge signaal intensiteit) binnen de niet aankleurende niet-geïnfarceerde delen van de hartspier. Ander veel gebruikte CMR technieken zijn *T2-gewogen spin-echo (T2W)* CMR en *first-pass perfusie* CMR. Met behulp van de T2W techniek kunnen gebieden met een hoog watergehalte gedetecteerd worden. Hiermee kan in de eerste fase na het infarct infarct-gerelateerd oedeem zichtbaar worden gemaakt. De doorbloeding van de hartspier kan worden beoordeeld met behulp van first-pass perfusie CMR. De laatste ontwikkelingen van deze technieken, alsmede de toepassingen ervan in zowel de acute en de chronische fase van het hartinfarct worden in de rest van Hoofdstuk 1 besproken.

In de hoofdstukken 2-4 wordt het gebruik van CMR bij patiënten met een acuut hartinfarct bestudeerd. Als een hartinfarct tijdig is behandeld door het openen van de infarct-gerelateerde kransslagader, kan de functie (deels) weer herstellen. De kans hierop hangt af van de lokale uitgebreidheid van de infarctschade. In Hoofdstuk 2 wordt aangetoond dat de kans op dit functieherstel kan worden voorspeld met behulp van DCE imaging. In dit onderzoek ondergingen 30 patiënten met een behandeld acuut hartinfarct een CMR onderzoek op 1 week en 3 maanden na opname. Hieruit bleek dat de kans op

functieverbetering sterk afhankelijk was van de mate van regionale schade: hoe meer infarcering, hoe kleiner de kans op herstel.

Het openmaken van een kransslagader is niet altijd voldoende om de doorbloeding van de hartspier weer te herstellen. Soms treedt bij een infarct tijdens en direct na de behandeling een complicatie op waardoor de kleinste vertakkingen van de grotere kransslagaderen verstopt raken: ‘microvasculaire obstructie’. De reden hiervoor is nog niet geheel duidelijk, maar als dit optreedt, is de kans op herstel van functie laag en wordt de prognose van de patiënt minder gunstig. Op DCE CMR beelden is microvasculaire obstructie te zien als uitsparingen binnen het aankleurende infarctgebied (zie bijvooorbeeld Hoofdstuk 2, figuur 3). Er zijn verschillende andere manieren om dit fenomeen te onderzoeken, zoals met behulp van invasieve (angiografische) metingen direct na de dotterbehandeling, het electrocardiogram en echocardiografie. In Hoofdstuk 3 zijn de belangrijkste hiervan met elkaar en met CMR vergeleken in 60 patiënten die een dotterbehandeling hadden ondergaan in verband met een acuut hartinfarct. Hieruit bleek dat de aanwezigheid van microvasculaire obstructie op DCE CMR verreweg de beste voorspeller was van functieveranderingen na het hartinfarct en dus de beste manier was om microvasculaire obstructie te onderzoeken.

De bij microvasculaire obstructie beschadigde haarvaten kunnen ook plaatselijke bloedingen in de hartspier veroorzaken. Het is niet duidelijk of zulke bloedingen een extra risico vormen, bovenop het al bestaan van microvasculaire obstructie. In Hoofdstuk 4 is dit onderzocht door T2W imaging, waarmee bloedingen zichtbaar gemaakt kunnen worden door gebruik te maken van het feit dat de afbraak van bloed de plaatselijke magnetische eigenschappen verandert. Bloedingen werden aangetroffen bij 22 van de 45 patiënten, die in vergelijking met de patiënten zonder bloeding een groter infarct hadden met een slechtere pompfunctie. Veranderingen van functie op 4 maanden na het infarct werden echter het beste voorspeld door de aanwezigheid van microvasculaire obstructie, en de aanwezigheid van bloeding voegde hier niets aan toe. De voorlopige conclusie luidt dat bloedingen in de hartspier kort na een (behandeld) acuut hartinfarct weliswaar de ernst van de beschadiging aangeven, maar dat ze zelf waarschijnlijk geen aanvullende klinische betekenis hebben.

Een verminderde pompfunctie van het hart kan leiden tot hartfalen. Bij sommige patiënten bestaat deze pompfunctiestoornis op basis van een chronische doorbloedingsstoornis waarbij vaak ernstige afwijkingen in alle kransslagaderen aanwezig zijn. De hartspier heeft dan aanpassingsmechanismen ingeschakeld waarbij de functie en wanddikte belangrijk afgenomen kunnen zijn zonder dat de hartspier daadwerkelijk afsterft (eng. ‘hibernation’ - winterslaap). Indien de doorbloeding hersteld wordt door bijvoorbeeld een bypass operatie of dotterbehandeling, kan dit leiden tot functieherstel en verbetering of

zelfs verdwijnen van hartfalen. Functieherstel zal echter alleen maar optreden als er voldoende vitaliteit (eng. ‘viability’ - levensvatbaarheid) aanwezig is. Om de kans op functieherstel in te schatten en te voorkomen dat een patiënt onnodig wordt blootgesteld aan het risico van een operatie wordt daarom meestal eerst vitaliteitsonderzoek gedaan. Hiervoor bestaan meerdere technieken, zoals echocardiografie, nucleaire technieken en sinds een aantal jaren ook DCE CMR. Net zoals na het acute infarct correspondeert de hoeveelheid contrastaankleuring op DCE beelden met de hoeveelheid littekenweefsel: veel aankleuring betekent veel littekenweefsel, ofwel weinig vitaliteit met een lage kans op functieherstel, en vice versa. Hoofdstuk 5 en 6 gaan over het gebruik van DCE CMR bij patiënten met chronische ischemische hartziekte. In Hoofdstuk 5 werd in 26 patiënten aangetoond dat DCE CMR imaging uitstekend overeenkwam met de techniek die nog steeds geldt als de referentie techniek voor de afbeelding van vitaliteit, ^{18}F-fluorodeoxyglucose positron emissie tomografie (PET). Hierbij bleek dat een waarde van 37% littekenweefsel volgens DCE imaging betrouwbaar kon differentiëren tussen aanwezigheid (<37% littekenweefsel) en afwezigheid (>37% littekenweefsel) van vitaliteit volgens de PET-techniek.

Ondanks bewezen ‘vitaliteit’ lijkt verbetering van functie toch vaak niet op te treden. Eén van de mogelijke verklaringen hiervoor is dat het lang kan duren voordat herstel optreedt. Onderzoek naar verbetering van functie na herstel van doorbloeding vindt vaak al na 3-4 maanden plaats, en dit is wellicht nog te vroeg. Dit werd onderzocht in Hoofdstuk 6. Bij 35 patiënten met een gestoorde functie op basis van een chronische doorbloedingsstoornis werd de functie beoordeeld op 1 maand vóór en op 3, 6 en 24±12 maanden na herstel van de doorbloeding. Vooraf werd tevens de mate van littekenvorming m.b.v. DCE imaging bepaald. Hoewel het belangrijkste deel van functieherstel in de eerste 3 maanden plaats vond, bleek zelfs tot op het allerlaatste meetpunt nog verdere verbetering mogelijk. Net zoals na het acute infarct bleek dat op elke tijdstip de kans op functieverbetering sterk afhankelijk was van de mate van littekenvorming: hoe meer littekenweefsel, hoe kleiner de kans op herstel. Bovendien bleek dat ook de snelheid van herstel afhankelijk was van de hoeveelheid littekenweefsel vooraf: delen met meer litteken herstelden trager dan delen met weinig of geen littekenweefsel.

Afbeeldingen van het hart kunnen op 2 manieren worden beoordeeld: kwalitatief, waarbij de beoordelaar zijn subjectieve inschatting geeft; en kwantitatief, waarbij de beoordelaar, al dan niet met behulp van een (semi-)automatisch software programma, een getalswaarde geeft. Een kwantitatieve beoordeling heeft in het algemeen de voorkeur als een vergelijking tussen opeenvolgende onderzoeken plaats vindt, of bij vergelijking van onderzoeken verricht in verschillende klinieken. In de hoofdstukken 7 en 8 wordt de kwantitatieve analyse van functionele en contrastbeelden nader bestudeerd.

Regionale functie kan worden gekwantificeerd als systolische wandverdikking, waarbij het verschil in wanddikte aan het eind van de vullingsfase (diastole) van het hart en de uitdrijvingsfase (systole) wordt berekend en kan worden uitgedrukt als een absoluut getal of als een percentage. Hoewel dit een veel gebruikte maat is in de literatuur, zijn er geen recente gegevens over normaalwaarden. In Hoofdstuk 7 werden met behulp van cine CMR en de zgn. centerline methode normaalwaarden bepaald voor regionale wanddikte en wandverdikking in 36 gezonde vrijwilligers. Zoals al eerder beschreven bleek er een aanzienlijke regionale variatie te bestaan in zowel wanddikte als systolische wandverdikking. De resultaten in deze studie suggereerden verder dat de traditioneel gebruikte en vanuit de echocardiografie stammende definitie van wanddikte niet toepasbaar is bij het gebruik van de huidige hoge resolutie cine CMR-techniek.

DCE beelden worden voor onderzoeksdoeleinden vaak kwantitatief geanalyseerd, waarbij de regionale of totale infarctgrootte wordt uitgedrukt als absolute eenheid (gram) of als percentage van regionale of totale kamer massa. De kwantificering gebeurt met behulp van speciaal ontwikkelde software en is eenvoudig en reproduceerbaar, maar de pitfall zit bij deze analyse in de wijze van de beeldinstelling: de beoordelaar doet dit zelf al naar gelang zijn eigen voorkeur, en die kan (vooral tussen verschillende centra) aanzienlijk verschillen. Standaardisatie van deze instelling is mogelijk met behulp van diverse in complexiteit wisselende methoden. Het is niet duidelijk welke van deze het meest betrouwbaar is, ook al omdat een ‘gouden standaard’ ontbreekt (de daadwerkelijke hoeveelheid littekenweefsel is alleen onder de microscoop vast te stellen, geen optie voor rondlopende patiënten). In Hoofdstuk 8 is daarom onderzocht of de wijze van kwantificering invloed had op de mogelijkheid om functieherstel na revascularisatie te voorspellen. Dit wordt wel de klinische standaard van vitaliteit genoemd. De hoeveelheid contrastaankleuring werd gekwantificeerd door de beeldinstelling te standaardiseren volgens verschillende methodes gebaseerd op de signaalintensiteit van een normaal gebied en op die van het geïnfarceerde gebied. De studie toonde aan dat de gekozen methode weliswaar een sterke invloed had op de berekende hoeveelheid contrastaankleuring (en dus regionale en totale infarctgrootte), maar dat deze slechts een beperkte invloed had op de nauwkeurigheid om functieherstel te voorspellen. Kwantificering lijkt dus met name van belang voor vergelijking van infarctgrootte en –uitbreiding, binnen één individu, tussen patiënten of tussen verschillende centra.

OVERWEGINGEN

Uit dit proefschrift en de vele andere publicaties uit recente jaren blijkt ontegenzeggelijk de aanvullende waarde van CMR in de diagnostiek en behandeling van patiënten met een hartinfarct. De opvallendste eigenschap van CMR ten opzichte van andere technieken is dat

het de diverse componenten van het infarct zichtbaar kan maken: het oedeem, de microvasculaire schade, bloeding, en, in groot detail, de mate van infarctschade zowel in de acute als in de chronische fase van het infarct. Verder heeft het als belangrijkste voordeel dat de pompfunctie van het hart eenvoudig en betrouwbaar kan worden gekwantificeerd. Moet dus nu bij iedere patiënt met een hartinfarct een CMR worden verricht, en doen we hem tekort als hij 'alleen' met een echocardiogram wordt bekeken? Het antwoord hierop is enigszins afhankelijk van de fase van het hartinfarct en de gewenste informatie. In het acute stadium, bij een patiënt met een ongecompliceerd, tijdig en succesvol behandeld hartinfarct, met een goede restfunctie is een echo een uitstekende en snelle manier om het hart te beoordelen, en zijn de aanvullende kwaliteiten van CMR niet nodig. CMR heeft dan alleen meerwaarde als onduidelijkheid bestaat over de diagnose of de uitbreiding, als de afbeelding onvoldoende is, als beoordeling van de kans op functieherstel gewenst is, of voor de kwantificering van de pompfunctie indien deze verminderd is. In de chronische fase zijn informatie over functie en vitaliteit cruciaal voor de behandeling, zodat CMR bij elke patiënt met (verdenking op) een doorgemaakt hartinfarct of een verminderde pompfunctie belangrijke informatie zou geven. Of CMR daadwerkelijk impact heeft op de behandeling en prognose van patiënten met een hartinfarct en overwaarde heeft ten opzichte van andere technieken, valt op dit moment moeilijk te bezien, omdat CMR weliswaar in toenemende maar nog in beperkte mate beschikbaar is. Met andere woorden: de toename van het aantal publicaties over het nut van CMR is beduidend groter dan de toename van het aantal ziekenhuizen met een CMR afdeling. Niet geheel onbegrijpelijk, want, hoewel het enthousiasme voor CMR vaak groot is, zijn er wel degelijk hindernissen te nemen. Zo is lokale samenwerking tussen cardiologen en radiologen noodzakelijk maar niet altijd eenvoudig. Verder bestaat er onduidelijkheid over de vergoeding voor een 'MRI hart'. Tenslotte is training en certificering van laboranten, technici en medisch specialisten een absolute vereiste. De echte groeispurt van CMR komt eraan, maar pas als deze hordes genomen zijn.

DANKWOORD

Mijn oprechte dank gaat uit naar allen die, op enigerlei directe of indirecte wijze, hebben bijgedragen aan de totstandkoming van dit proefschrift. Dat zijn er velen, verzameld in de 12½ jaar die ik mij al bezig houd met cardiale MRI, patiënten, verpleegkundigen van de Eerste Harthulp, de hartbewaking en de afdelingen, medewerkers van de poli, nieuw en oud, van de functie-afdeling, de echo-afdeling, het cath lab, de elektriek, de arts-assistenten, MRI laboranten, secretaresses van secint en seccar, arts-onderzoekers, stafleden van cardiologie en radiologie, administratieve krachten (letterlijk) van MRI, en alle andere die ik vergeten ben, en die ervoor hebben gezorgd dat ik dat heb kunnen doen wat ik leuk vind, namelijk een smeuiige combinatie van klinisch werk, onderwijs, en, jawel, wetenschap.

Als ‘imager’ is het soms nodig om even in te zoomen.

Bert, grondlegger van de cardiale MRI in het VUMC. De afgelopen vaak onstuimige afdelingsjaren hebben jou weliswaar steeds meer naar de rand van k-space geduwd, maar zeg eens eerlijk, ook in jou gaan nog steeds de protonen kriebelen bij het zien van (weer) een mooi plaatje! Jij staat aan de basis van het succes van onze CMR afdeling, dank voor je besmettelijk enthousiasme, en je volhardendheid waarmee je ook mij naar dit boekje hebt gestuwd.

Mary, wat kan ik nog zeggen, je bent al zo vaak de moeder van cardiale MR genoemd, wat kan ik daar nou nog aan toevoegen, nou vooruit dan: ‘When I find myself in times of trouble…’. Dank voor je fantastische ondersteuning en gezelligheid in al die jaren.

De arts-onderzoekers die de afgelopen jaren mee hebben geholpen cardiale MRI te vernieuwen en te verbeteren, en, niet in het minst, het dagelijkse leven te verlevendigen en mijn taken te verlichten: Willemijn, Willem, Olga (dank voor je samenwerking in ons prachtige EHJ stuk), Robin (en jij voor de jouwe in dat fraaie JACC MVO paper, en in ons prikkelende, maar toch enigszins verguisde haemorrhage stuk), Tjeerd (en jij voor je hulp bij de SWT: we moeten geduldig zijn, men gaat vanzelf weer inzien dat verdikking ook aantrekkelijk kan zijn), en de huidige generatie scanners Jan, Wessel en Farshid.

Special thanks to our foreign fellows that chose to spend part of their lives with us to learn CMR, Harald (Prof Kühl! many thanks for working together in our two JACC papers), Theano (Greece lightning), Bogdan (Roumanian-American-(and now)Dutch, looking forward to working with you again!), Gerry (the only one who spoke better Dutch than (Scottish) English - ahtuhmin, ahtuhmahdoh; our lives will never be the same, one day, Madeleine wíll be found), Nicola, and Simon: it was great working with you all.

Een MRI hart is iets anders dan een doorsnee ‘breintje’ of ‘knietje’: je hebt niet alleen die absurde vlakken en sequenties, en niet te vergeten adenosine en de daarmee samenhangende ‘stress’ voor patient én laborant, maar ook nog eens een onrust zaaiende Beek in je nek; laboranten die dat leuk vinden en kunnen volhouden zijn bijzonder: Milan

(onze centrale man achter de knoppen, ook voor al uw filmpjes en andere IT-werk), op de voet gevolgd door José, Michael, Jantien, Joost, en de laatste tijd ook Adri en Aukje, en van vroeger maar niet te vergeten Karin (en Willy): dankzij jullie kunnen we de kwaliteit leveren waarom wij bekend staan, zowel in patiëntenzorg als in onderzoek, hulde aan jullie allen!
I am greatly indebted to dr. Cor Allaart, prof.dr. Emile Comans, dr. Francisca Nijland, dr. Jürg Schwitter and prof.dr. Ernst van der Wall for their careful assessment of this thesis and their participation in its defence.
De (rest van de) staf van de afdeling cardiologie: Yolande, Jean, Carel, Otto, Michiel, Koen, Jan, Gerrit, roommate Stijn en buurvrouwen Karin en Koningstra, en Ankie. En Marco (hoe bevallen de Haagse protonen?), Mark (dank voor je samenwerking mn ook in de HOC, die staat als een huis).
Mijn Paranimfen, inderdaad met een hoofdletter, Alex (bbb) en George (715680), kijk zo hoort het nou, jullie naast me om me hierdoor heen te slepen! En verder: Dino (precíes 10 jaar later!! finally returning the honour, het blijven mooie, herfstige herinneringen), Eric C (dank voor je steun tijdens editing), en, in herinnering, griezelen-met-grootmoeder oma Lies (dit had je eigenlijk moeten zien!), en natuurlijk Schoof (eigenlijk toch bijna een Beek..), Stibbe (die bokaal staat dus voorlopig mooi bij mij!) en Joost (de nederlandse ‘Van’, wanneer gaan we weer??), en alle andere dierbaren in mijn leven.
Lieve mam, wat zou het heerlijk geweest zijn om samen met jou verder te hebben kunnen beleven en genieten, ook dit. Lieve pa, wat een enthousiasme toen ik je vertelde over een komende promotie (nu nog een échte baan!?), en wat ben je lekker aan het leven, met Herma, sorry voor mijn als altijd slordige planning waardoor ik jullie van je vakantie terug moest roepen, maar zonder jullie is helaas géén optie! En de rest van ons gezin, Wiek én Jeroen, en Roosmarijn, en MDFRKS, ik kijk écht heel erg uit naar onze volgende (ski?)vakantie samen!

En dan, hoezo promotie!? Ha!! Mijn twee schatten, Gabriela en Lorenzo, ik omarm jullie als niet te voren, zo veel hivj, nee nee ik ben nog lang niet klaar, ik houd jullie nog steeds vast!, kus pap.
En dan. Wat resteert, ben jij, ADMV, Marcia, míjn hart is van jou, jou beleef ik, bemin ik, bezing ik, walking through the streets (of Ste Gemme)…

CURRICULUM VITAE

Aernout Michiel Beek was born exactly 3 minutes after his brother Alexander Robert on September 21st, 1960, in The Hague. After graduating secondary school (Gymnasium Celeanum, Zwolle), he studied medicine at the VU faculty of Geneeskunde in Amsterdam. After having finished his basic medical training, he spent several years abroad (UK, The Hague) acquiring life and working experience. He returned to Amsterdam to start his cardiology training at the department of Cardiology of the VU medical center and joined the staff in 1999. He is now an imaging cardiologist specialised in Cardiovascular Magnetic Resonance imaging. He is married to Marcia and they have two children, Gabriela (1995) and Lorenzo (1999).

LIST OF PUBLICATIONS

1. Beek AM, Bondarenko O, Afsharzada F, van Rossum AC. Quantification of late gadolinium enhanced CMR in viability assessment in chronic ischemic heart disease: a comparison to functional outcome. J Cardiovasc Magn Reson. 2009 Mar 9;11(1):6.
2. Beek AM, Kühl HP, Bondarenko O, Twisk JW, Hofman MB, van Dockum WG, Visser CA, van Rossum AC. Delayed contrast-enhanced magnetic resonance imaging for the prediction of regional functional improvement after acute myocardial infarction. J Am Coll Cardiol. 2003 Sep 3;42(5):895-901.
3. Beek AM, Nijveldt R, van Rossum AC. Intramyocardial haemorrhage and microvascular obstruction after primary percutaneous coronary intervention. Int J CV Imag 2009, in press.
4. Beek AM, van Rossum AC. Cardiovascular MRI in patients with acute myocardial infarction – a review. Heart 2009, in press.
5. Beek AM, Verheugt FW, Meyer A. Usefulness of electrocardiographic findings and creatine kinase levels on admission in predicting the accuracy of the interval between onset of chest pain of acute myocardial infarction and initiation of thrombolytic therapy. Am J Cardiol. 1991 Nov 15;68(13):1287-90.
6. Bondarenko O, Beek AM, Twisk JW, Visser CA, van Rossum AC. Time course of functional recovery after revascularization of hibernating myocardium: a contrast-enhanced cardiovascular magnetic resonance study. Eur Heart J. 2008 Aug;29(16):2000-5.
7. Bondarenko O, Beek AM, Nijveldt R, McCann GP, van Dockum WG, Hofman MB, Twisk JW, Visser CA, van Rossum AC. Functional outcome after revascularization in patients with chronic ischemic heart disease: a quantitative late gadolinium enhancement CMR study evaluating transmural scar extent, wall thickness and periprocedural necrosis. J Cardiovasc Magn Reson. 2007;9(5):815-21.
8. Bondarenko O, Beek AM, Hofman MB, Kühl HP, Twisk JW, van Dockum WG, Visser CA, van Rossum AC. Standardizing the definition of hyperenhancement in the quantitative assessment of infarct size and myocardial viability using delayed contrast-enhanced CMR. J Cardiovasc Magn Reson. 2005;7(2):481-5.
9. Groothuis JGJ, Beek AM, Brinckman SL, Meijerink MR, Koestner SC, Nijveldt R, Götte MJ, Hofman MBM, van Kuijk C, van Rossum AC. Comparison of computed coronary angiography to first pass myocardial perfusion magnetic resonance imaging in patients with low to intermediate probability coronary artery disease. Radiology 2009, in press.
10. Kühl HP, Beek AM, van der Weerdt AP, Hofman MB, Visser CA, Lammertsma AA, Heussen N, Visser FC, van Rossum AC. Myocardial viability in chronic ischemic heart disease: comparison of contrast-enhanced magnetic resonance imaging with (18)F-fluorodeoxyglucose positron emission tomography. J Am Coll Cardiol. 2003 Apr 16;41(8):1341-8.
11. Marcu CB, Beek AM, van Rossum AC. Chagas' heart disease diagnosed on MRI: the importance of patient "geographic" history. Int J Cardiol. 2007 Apr 25;117(2):e58-60.
12. Marcu CB, Beek AM, Van Rossum AC. Cardiovascular magnetic resonance imaging for the assessment of right heart involvement in cardiac and pulmonary disease. Heart Lung Circ. 2006 Dec;15(6):362-70.
13. Marcu CB, Beek AM, van Rossum AC. Clinical applications of cardiovascular magnetic resonance imaging. CMAJ. 2006 Oct 10;175(8):911-7.
14. Marcu CB, Beek AM, van Rossum AC. Unusual variation in upper-body venous anatomy found with cardiovascular MRI. CMAJ. 2006 Jul 4;175(1):27.
15. McCann GP, Beek AM, Vonk-Noordegraaf A, van Rossum AC. Delayed contrast-enhanced magnetic resonance imaging in pulmonary arterial hypertension. Circulation. 2005 Oct 18;112(16):e268.
16. Nijveldt R, Beek AM, Hirsch A, Stoel MG, Hofman MB, Umans VA, Algra PR, Twisk JW, van Rossum AC. Functional recovery after acute myocardial infarction: comparison between angiography, electrocardiography, and cardiovascular magnetic resonance measures of microvascular injury. J Am Coll Cardiol. 2008 Jul 15;52(3):181-9.
17. Nijveldt R, Beek AM, Hirsch A, Hofman MB, Umans VA, Algra PR, van Rossum AC. 'No-reflow' after acute myocardial infarction: direct visualisation of microvascular obstruction by gadolinium-enhanced CMR. Neth Heart J. 2008 May;16(5):179-81.
18. Nijveldt R, Beek AM, Germans T, Bondarenko O, van Rossum AC. Arrhythmogenic right ventricular cardiomyopathy with evidence of biventricular involvement. CMAJ. 2007 Jun 19;176(13):1819-21.

19. Nijveldt R, Beek AM, Hofman MB, Umans VA, Algra PR, Spreeuwenberg MD, Visser CA, van Rossum AC. Late gadolinium-enhanced cardiovascular magnetic resonance evaluation of infarct size and microvascular obstruction in optimally treated patients after acute myocardial infarction. J Cardiovasc Magn Reson. 2007;9(5):765-70.
20. Nijveldt R, Beek AM, van Gorp JM, van Rossum AC. Pericardial cyst. Lancet. 2005 Jun 4-10;365(9475):1960. Erratum in: Lancet. 2005 Sep 17-23;366(9490):984. Nijveldtl, Robin [corrected to Nijveldt, Robin]; Beekl, Aernout M [corrected to Beek, Aernout M].
21. van Dockum WG, Beek AM, ten Cate FJ, ten Berg JM, Bondarenko O, Götte MJ, Twisk JW, Hofman MB, Visser CA, van Rossum AC. Early onset and progression of left ventricular remodeling after alcohol septal ablation in hypertrophic obstructive cardiomyopathy. Circulation. 2005 May 17;111(19):2503-8.
22. Knaapen P, Bondarenko O, Beek AM, Götte MJ, Boellaard R, van der Weerdt AP, Visser CA, van Rossum AC, Lammertsma AA, Visser FC. Impact of scar on water-perfusable tissue index in chronic ischemic heart disease: Evaluation with PET and contrast-enhanced MRI. Mol Imaging Biol. 2006 Jul-Aug;8(4):245-51.
23. Knaapen P, Bondarenko O, Beek AM, Götte MJ, Boellaard R, van der Weerdt AP, Visser CA, van Rossum AC, Lammertsma AA, Visser FC. Impact of Scar on Water-Perfusable Tissue Index in Chronic Ischemic Heart Disease : Evaluation with PET and Contrast-Enhanced MRI. Mol Imaging Biol. 2006 Apr 28.
24. Kühl HP, Papavasiliu TS, Beek AM, Hofman MB, Heusen NS, van Rossum AC. Myocardial viability: rapid assessment with delayed contrast-enhanced MR imaging with three-dimensional inversion-recovery prepared pulse sequence. Radiology. 2004 Feb;230(2):576-82.
25. Kühl HP, van de Weert AP, Beek AM, Visser FC, van Rossum AC. Myocardial viability by contrast enhanced MRI in a patient with left bundle branch block showing a severe defect on FDG-PET. Heart. 2002 Apr;87(4):319.
26. Marcu CB, Versteeg KS, Beek AM, Van Rossum AC. Prognostic value of delayed gadolinium enhancement MRI in patients with ischemic cardiomyopathy. Conn Med. 2009 Apr;73(4):197-203.
27. Marcu CB, Nijveldt R, Beek AM, Van Rossum AC. Delayed contrast enhancement magnetic resonance imaging for the assessment of cardiac disease. Heart Lung Circ. 2007 Apr;16(2):70-8.
28. McCann GP, Beek AM, Vonk-Noordegraaf A, van Rossum AC. Delayed contrast-enhanced magnetic resonance imaging in pulmonary arterial hypertension, Circulation 2005 Oct 18;112(16):e268.
29. McCann GP, Van Dockum WG, Beek AM, Nijveldt R, Ten Cate FJ, Ten Berg JM, Van Rossum AC. Extent of myocardial infarction and reverse remodeling assessed by cardiac magnetic resonance in patients with and without right bundle branch block following alcohol septal ablation for obstructive hypertrophic cardiomyopathy. Am J Cardiol. 2007 Feb 15;99(4):563-7.
30. McCann GP, Gan CT, Beek AM, Niessen HW, Vonk Noordegraaf A, van Rossum AC. Extent of MRI delayed enhancement of myocardial mass is related to right ventricular dysfunction in pulmonary artery hypertension. AJR Am J Roentgenol. 2007 Feb;188(2):349-55.
31. Nijveldt R, Kilner PJ, Beek AM. Anomalies of ventricular septation and apical formation. Cardiol Young. 2008 Feb;18(1):117-8.
32. Nijveldt R, Germans T, Beek AM, Götte MJ, van Rossum AC. Double aortic arch. Neth Heart J. 2007;15(6):229-30.
33. Said SA, Hofman MB, Beek AM, van der Werf T, van Rossum AC. Feasibility of cardiovascular magnetic resonance of angiographically diagnosed congenital solitary coronary artery fistulas in adults. J Cardiovasc Magn Reson. 2007;9(3):575-83.
34. Whitteveen AG, Wirds JW, Beek AM, Boon ES, van der Spoel JI. [Heart tamponade: a life-threatening complication of a central venous catheter]. Ned Tijdschr Geneeskd. 1997 Nov 15;141(46):2249-51.
35. Hirsch A, Nijveldt R, Haeck JD, Beek AM, Koch KT, Henriques JP, van der Schaaf RJ, Vis MM, Baan J Jr, de Winter RJ, Tijssen JG, van Rossum AC, Piek JJ. Relation between the assessment of microvascular injury by cardiovascular magnetic resonance and coronary Doppler flow velocity measurements in patients with acute anterior wall myocardial infarction. J Am Coll Cardiol. 2008 Jun 10;51(23):2230-8.
36. Nijveldt R, Hofman MB, Hirsch A, Beek AM, Umans VA, Algra PR, Piek JJ, van Rossum AC. Assessment of microvascular obstruction and prediction of short-term remodeling after acute myocardial

infarction: cardiac MR imaging study. Radiology. 2009 Feb;250(2):363-70. Epub 2009 Jan 22. Erratum in: Radiology. 2009 May;251(2):615.

37. Nijveldt R, Germans T, McCann GP, Beek AM, van Rossum AC. Semi-quantitative assessment of right ventricular function in comparison to a 3D volumetric approach: a cardiovascular magnetic resonance study. Eur Radiol. 2008
38. Nijveldt R, Hirsch A, Hofman MB, Beek AM, Spijkerboer AM, Piek JJ, van Rossum AC. 3.0 T cardiovascular magnetic resonance in patients treated with coronary stenting for myocardial infarction: evaluation of short term safety and image quality. Int J Cardiovasc Imaging. 2008 Mar;24(3):283-91.
39. van Dockum WG, ten Cate FJ, ten Berg JM, Beek AM, Twisk JW, Vos J, Hofman MB, Visser CA, van Rossum AC. Myocardial infarction after percutaneous transluminal septal myocardial ablation in hypertrophic obstructive cardiomyopathy: evaluation by contrast-enhanced magnetic resonance imaging. J Am Coll Cardiol. 2004 Jan 7;43(1):27-34.
40. Germans T, Götte MJ, Nijveldt R, Spreeuwenberg MD, Beek AM, Bronzwaer JG, Visser CA, Paulus WJ, van Rossum AC. Effects of aging on left atrioventricular coupling and left ventricular filling assessed using cardiac magnetic resonance imaging in healthy subjects. Am J Cardiol. 2007 Jul 1;100(1):122-7.
41. Kremers FPPJ, Hofman MBM, Groothuis JGJ, Jerosch-Herold M, Beek AM, Zuehlsdorff S, Nielles-Vallespin S, van Rossum AC, Heethaar RM. Improved correction of spatial inhomogeneities of surface coils in quantitative analysis of first-pass myocardial perfusion. JMRI 2009, in press.
42. van Dockum WG, Kuijer JP, Götte MJ, Ten Cate FJ, Ten Berg JM, Beek AM, Twisk JW, Marcus JT, Visser CA, van Rossum AC. Septal ablation in hypertrophic obstructive cardiomyopathy improves systolic myocardial function in the lateral (free) wall: a follow-up study using CMR tissue tagging and 3D strain analysis. Eur Heart J. 2006 Dec;27(23):2833-9.
43. Mannaerts HF, Van Der Heide JA, Kamp O, Papavassiliu T, Marcus JT, Beek AM, Van Rossum AC, Twisk J, Visser CA. Quantification of left ventricular volumes and ejection fraction using freehand transthoracic three-dimensional echocardiography: comparison with magnetic resonance imaging. J Am Soc Echocardiogr 2003 February;16(2):101-9.
44. Knaapen P, van Dockum WG, Bondarenko O, Kok WE, Götte MJ, Boellaard R, Beek AM, Visser CA, van Rossum AC, Lammertsma AA, Visser FC. Delayed contrast enhancement and perfusable tissue index in hypertrophic cardiomyopathy: comparison between cardiac MRI and PET. J Nucl Med. 2005 Jun;46(6):923-9.
45. van Dockum WG, Knaapen P, Hofman MB, Kuijer JP, ten Cate FJ, ten Berg JM, Beek AM, Twisk JW, van Rossum AC. Impact of alcohol septal ablation on left anterior descending coronary artery blood flow in hypertrophic obstructive cardiomyopathy. Int J Cardiovasc Imaging. 2009 Jun;25(5):511-8.
46. Vermeltfoort IA, Bondarenko O, Raijmakers PG, Odekerken DA, Kuijper AF, Zwijnenburg A, van der Vis-Melsen MJ, Twisk JW, Beek AM, Teule GJ, van Rossum AC. Is subendocardial ischaemia present in patients with chest pain and normal coronary angiograms? A cardiovascular MR study. Eur Heart J. 2007 Jul;28(13):1554-8.